Chapter 10: Detection and Attribution of Climate Change: from Global to Regional

Coordinating Lead Authors: Nathaniel Bindoff (Australia), Peter Stott (UK)

Lead Authors: Krishna Mirle AchutaRao (India), Myles Allen (UK), Nathan Gillett (Canada), David Gutzler (USA), Kabumbwe Hansingo (Zambia), Gabriele Hegerl (UK), Yongyun Hu (China), Suman Jain (Zambia), Igor Mokhov (Russia), James Overland (USA), Judith Perlwitz (USA), Rachid Sebbari (Morocco), Xuebin Zhang (Canada)

Contributing Authors: Beena Balan Sarojini, Pascale Braconnot, Oliver Browne, Ping Chang, Nikolaos Christidis, Tim DelSole, Catia M. Domingues, Paul J. Durack, Alexey Eliseev, Kerry Emanuel, Chris Forest, Hugues Goosse, Jonathan Gregory, Isaac Held, Greg Holland, Jara Imbers Quintana, Gareth S. Jones, Johann Jungclaus, Georg Kaser, Tom Knutson, Reto Knutti, James Kossin, Mike Lockwood, Fraser Lott, Jian Lu, Irina Mahlstein, Damon Matthews, Seung-Ki Min, Daniel Mitchell, Thomas Moelg, Simone Morak, Friederike Otto, David Pierce, Debbie Polson, Andrew Schurer, Tim Osborn , Joeri Rogelj, Vladimir Semenov, Dmitry Smirnov, Peter Thorne, Muyin Wang, Rong Zhang

Review Editors: Judit Bartholy (Hungary), Robert Vautard (France), Tetsuzo Yasunari (Japan)

Date of Draft: 5 October 2012

Notes: TSU Compiled Version

Table of Contents

Executive Summary

Evidence of the effects of human influence on the climate system has continued to accumulate and strengthen since the AR4. The consistency of observed and modeled changes across the climate system, including regional temperatures, the water cycle, global energy budget, cryosphere and oceans, points to a large-scale warming resulting primarily from anthropogenic increases in greenhouse gas concentrations.

Progress Since AR4

Since AR4, evidence has emerged more clearly from across the climate system that anthropogenic forcings have warmed the climate and produced consequent changes in the global water cycle, the cryosphere, and circulation patterns. The evidence is stronger that climate change has affected climate regionally as well as globally.

Observational uncertainty has been explored much more thoroughly than previously and fingerprints of human influence deduced from a new generation of climate models. An assessment of the very likely range of the greenhouse gas contribution to observed warming of about 0.6K since 1951 is now possible (0.6–1.4 K). Better understanding of pre-instrumental data shows that warming since the mid-20th century is far outside the range of internal climate variability estimated from such records. There is improved understanding of ocean changes including better understanding of ocean temperature variability, which supports it being very likely that more the half of the observed ocean warming since the 1970s is caused by external forcing. We now have a better understanding of ocean salinity change. The salinity changes are consistent with large scale intensification of the hydrological cycle predicted by climate models. There has been a strengthening of the evidence for human influence on temperature extremes since AR4 and it is now judged very likely that human influence has contributed to the observed changes in temperature extremes since the mid-20th century.

In some aspects, including changes in drought, changes in tropical cyclone activity, Antarctic warming and Antarctic mass balance confidence in attribution remains low due to remaining observational and modelling uncertainties. However, changes in near surface temperatures, free atmosphere temperatures, ocean temperatures, and the northern hemisphere snow cover and sea ice extent, when taken together, show, not just global mean changes, but distinctive regional patterns consistent with the expected fingerprints of change from anthropogenic forcings. We conclude that it is *extremely likely* that human activities have caused most of (at least 50%) the observed increase in global average temperatures since the 1950s and that it is *virtually certain* that this warming is not due to internal variability alone.

Evidence for Warming

The anthropogenic fingerprints in the surface temperature (including over land and water), in the free atmosphere (cooling in the stratosphere and warming in the troposphere) and in the ocean (warming spreading from the surface to depth) are expected to be distinct in their patterns in space and time from the dominant modes of decadal variability and the expected response to changes in solar output and explosive volcanic eruptions. Quantification of the contributions of anthropogenic and natural forcing using multi-signal detection and attribution analyses show that it is *extremely likely* that human activities have caused most of (at least 50%) the observed increase in global average temperatures since the 1950s. The greenhouse gas contribution to the observed warming of approximately 0.6 K over 1951–2010 was very likely greater than the total observed warming with a range between 0.6 and 1.4 K. Other forcings, including variability in tropospheric and stratospheric aerosols, stratospheric water vapour, and solar output, as well as internal modes of variability, have also contributed to the year to year and decade to decade variability of the climate system. It is *very likely* that early 20th century warming is due in part to external forcing. While the trend in global mean temperature since 1998 is not significantly different from zero, it is also consistent with natural variability superposed on the long-term anthropogenic warming trends projected by climate models.

More than 90% of the earth's radiative imbalance is currently taken up by the oceans through increased subsurface temperatures. It is *very likely* that more than half of the ocean warming observed since the 1970s is caused by external forcing. This ocean warming is also causing thermal expansion and it is *extremely likely* that there is an anthropogenic influence on the global steric sea level rise for this period.

It is *likely* that anthropogenic forcings, dominated by greenhouse gases have contributed to the warming of the troposphere since 1960 and *very likely* that anthropogenic forcings, dominated by ozone depleting substances, have contributed to the cooling of the lower stratosphere since 1960.

The Hydrological Cycle

New evidence has emerged for the detection of anthropogenic influence on aspects of the water cycle, the consistency of the evidence from both atmosphere and ocean pointing to anthropogenic influence on the water cycle since 1950. This is seen in the detection of human influence on zonal patterns of global precipitation changes, on high northern latitude precipitation changes, and on atmospheric humidity in multiple datasets, together with expectations from theoretical considerations and systematic changes observed and detected in oceanic surface and sub-surface salinity. These patterns are consistent with an intensified global water cycle. There is *medium confidence* that there is an anthropogenic contribution to observed increases in atmospheric moisture content and to global scale changes in precipitation patterns over land, including reductions in low latitudes and increases in northern hemisphere mid to high latitudes. Remaining observational uncertainties and, the large effect of natural variability on observed precipitation, preclude a more confident assessment at this stage. An anthropogenic contribution to increases in tropospheric specific humidity is found with *medium confidence*. It is *likely* that observed changes in ocean surface and sub-surface salinity are due in part to the changes in the hydrological cycle caused by anthropogenic increases in greenhouse gases.

The Cryosphere

It is *likely* that anthropogenic forcings have contributed to Arctic sea ice retreat (high confidence) 1950 and the increased surface melt of Greenland since 2000. The small net increase in Antarctic sea ice extent since 1990 is consistent with internal variability (medium confidence). It is *likely* that there has been an anthropogenic component to observed reductions in snow cover and permafrost since 1970. It is *likely* that glaciers have diminished significantly due to human influence since the 1960s. Due to a low level of scientific understanding there is *low confidence* that anthopogenic forcing is a significant factor observed loss of Antarctic ice sheet mass balance since 1990.

Climate Extremes

It is *very likely* that anthropogenic forcing has contributed to the observed changes in temperature extremes since the mid-20th century. It is *likely* that human influence has substantially increased the probability of some observed heatwaves. There is *medium confidence* that anthropogenic forcing has contributed to a trend towards increases in the frequency of heavy precipitation events over the second half of the 20th century over land regions with sufficient observational coverage to make the assessment. There is *low confidence* in attribution of changes in tropical cyclone activity to human influence due to insufficient observational evidence and limited evidence and low level of agreement between studies.

From Global to Regional

Further evidence has accumulated on the detection and attribution of anthropogenic influence on climate change in different parts of the world. Over every continent except Antarctica, anthropogenic influence has *likely* made a substantial contribution to surface temperature increases since the mid-20th century. There is low *confidence* in attribution of warming in Antarctica due to the large observational uncertainties in estimating Antarctic temperatures. It is *likely* that there has been significant anthropogenic warming in Arctic land surface temperatures over the past 50 years. Detection and attribution at regional scales due to greenhouse gases is complicated by the greater role played by dynamical factors (circulation changes), a greater range of forcings that may be regionally important, and the greater difficulties of modelling relevant processes at regional scales. Nevertheless, human influence has likely contributed to temperature in many sub-continental regions.

Changes in atmospheric circulation are important for local climate change since they could lead to greater or smaller changes in climate in a particular region than elsewhere. It is *likely* that human influence has altered

sea level pressure patterns globally. There is *medium confidence* that stratospheric ozone depletion has contributed to the observed poleward shift of the souther Hadley Cell border during Austral summer. It is *likely* that stratospheric ozone depletion has contributed to the positive trend in the Southern Annular Mode seen in Austral summer since 1951 which corresponds to sea level pressure reductions over the high latitudes, an increase in the subtropics, and a southward shift of the storm tracks.

A Millennia to Multi-Century Perspective

Taking a longer term perspective shows the substantial role played by external forcings in driving climate variability on hemispheric scales, even in pre-industrial times. While internal variability of the climate system, with its ability to move heat around the climate system, is important at hemispheric scales, it is *very unlikely* that reconstructed temperatures since 1400 can be explained by natural internal variability alone. Climate model simulations that include only natural forcings can explain a substantial part of the pre-industrial inter-decadal temperature variability since 1400 on hemispheric scales. However such simulations fail to explain more recent warming since 1950 without the inclusion of anthropogenic increases in greenhouse gas concentrations. The warming since 1950 is far outside the range of similar length trends estimated in residual internal variability estimated from reconstructions of the past millennium.

Implications for Climate System Properties and Projections

More observational data have allowed a better characterisation of basic properties of the climate system which have implications for the rate of future warming. New evidence from 21st century observations and stronger evidence from a wider range of models have strengthened the observational constraint on the transient climate response (TCR) which is estimated to be *very likely* greater than 1°C, and *very unlikely* greater than 3ºC. The global warming response to carbon dioxide emissions has been found to be determined primarily by total cumulative emissions of carbon dioxide, irrespective of the timing of those emissions over a broad range of scenarios. The ratio of warming to cumulative carbon emissions, the Transient Response to Cumulative Emissions (TRCE) is estimated to be *very likely* between 1°C TtC^{-1} and 3°C TtC^{-1} based on observational constraints. Estimates based on observational constraints continue to indicate that it is *very likely* that the equilibrium climate sensitivity (ECS) is larger than 1.5°C. Evidence from observations also supports the overall assessment (box 12.1) that ECS is *likely* in the range from 2°C–4.5°C and that an ECS greater than about 6°Ç–7°C is *very unlikely*.

Remaining Uncertainties

Robustness of detection is subject to climate models correctly simulating internal variability. While comparison with observations indicates that climate models have an adequate simulation of multi-decadal scale variability it is difficult to estimate multi-decadal variability directly from the observational record. However variability would have to be underestimated by a factor of about two for detection of atmospheric and ocean warming to be lost and in any case over the past six centuries residual variability in 50-year trends estimated from paleo data is reasonably close to that in climate model control simulations. At regional scales considerable challenges remain in attributing observed change to external forcing. Modelling uncertainties related to model resolution and incorporation of relevant processes become more important at regional scales, and the effects of internal variability become more significant in masking or enhancing externally forced changes. Observational uncertainties for climate variables, uncertainties in forcings such as aerosols, and limits in process understanding continue to hamper attribution of changes in many aspects of the climate system, making it more difficult to discriminate between natural internal variability and externally forced changes. Increased understanding of uncertainties in radiosonde and satellite records makes assessment of causes of observed trends in the upper troposphere less confident than an assessment of overall atmospheric temperature changes. Changes in the water cycle remain less reliably modelled in both their changes and their internal variability, limiting confidence in attribution assessments. The ability to simulate changes in frequency and intensity of extreme events is limited by the limited observational information on extreme events and the ability of models to reliably simulate mean changes in key features of circulation such as blocking and to simulate soil moisture feedbacks.

10.1 Introduction

This chapter assesses the causes of observed changes assessed in Chapters 2 to 5 using physical understanding, climate models and statistical approaches . The chapter adopts the terminology proposed by the IPCC good practice guidance paper on attribution (Hegerl et al., 2010). The chapter assesses whether changes in climate can be detected as being significantly outside the range expected from internal variability (ie variability resulting from processes internal to the climate system) and assesses to what extent observed changes can be attributed to external drivers of climate change, both human induced and naturally occurring. Methodological approaches to detection and attribution are evaluated in Section 10.2. The chapter assesses changes right across the climate system, from the upper atmosphere to beneath the surface of the ocean. Its remit goes beyond temperature (Section 10.3.1) to assess also changes in the water cycle (10.3.2), circulation and climate phenomena (Section 10.3.3), ocean properties, including ocean temperature and salinity and sea level (Section 10.4), and the cryosphere, including sea ice, ice sheets, ice shelves and glaciers, and snow cover and permafrost (Section 10.5). The chapter considers not just how mean climate has changed but also how extremes are changing (Section 10.6) and, while it has a particular focus on the period for which instrumental data are available it also takes a multi-century perspective, including using non-instrumental data from paleoclimate archives (Section 10.7). It also considers the implications of new understanding of observed changes for climate projections both on the near-term and the long-term (Section 10.8).

There is increased focus on the extent to which the climate system as a whole is responding in a coherent way across a suite of climate indices such as surface mean temperature, temperature extremes, ocean heat content, river run off and precipitation change. Section 10.9 presents a synthesis of the evidence across the chapter for human and natural influences on climate. Detection and attribution of impacts of climate changes are assessed by Working Group II

The chapter also takes a regional perspective in assessing why changes differ from place to place across the planet. There are additional challenges for detection and attribution in proceeding from global to regional scales. Distinguishing signals of externally forced climate changes from the noise of natural internal variability generally becomes more difficult as spatial scale reduces. There is decreasing observational coverage of climate going back in time and observational uncertainties can be a greater problem for some regions than others. Models need to be assessed for their reliability at representing climate variability and change in the particular region in question, and local forcings such as changes in land use, that have little effect on large scales, may be important on regional scales. Extremes may be infrequently observed and dynamical or statistical models may be required to characterise the underlying variability of such rare events.

Evidence of a human influence on climate has progressively accumulated during the period of the four previous assessment reports of the IPCC. There was little observational evidence for a detectable human influence on climate at the time of the first IPCC Assessment Report. By the time of the second report there was sufficient additional evidence for it to conclude that “the balance of evidence suggests a discernible human influence on global climate”. The third Assessment Report found that a distinct greenhouse gas signal was robustly detected in the observed temperature record and that “most of the observed warming over the last fifty years is *likely* to have been due to the increase in greenhouse gas concentrations.”

With the additional evidence available by the time of the fourth Assessment Report, the conclusions were strengthened. This evidence included a wider range of observational data, a greater variety of more sophisticated climate models including improved representations of forcings and processes, and a wider variety of analysis techniques. This enabled the report to conclude that “most of the observed increase in global average temperatures since the mid-20th century is *very likely* due to the observed increase in anthropogenic greenhouse gas concentrations”. The AR4 also concluded that “discernible human influences now extend to other aspects of climate, including ocean warming, continental-average temperatures, temperature extremes and wind patterns.”

A number of uncertainties remained at the time of AR4. It noted that difficulties remained in attributing temperatures on smaller than continental scales and over timescales of less than 50 years. Evidence for significant anthropogenic warming on continental scales excluded Antarctica for which no detection and attribution studies were available at that time. Temperatures of the most extreme hot nights, cold nights and cold days were assessed to have likely increased due to anthropogenic forcing, but human influence on

temperatures of the hottest day had not been detected. A detectable volcanic influence on mean precipitation had been found, a result supported by theoretical understanding, but the result was not robust between model fingerprints, and an anthropogenic fingerprint on global precipitation changes had not been detected. While observed increases in heavy precipitation were assessed to be qualitatively consistent with expectations of the response to anthropogenic forcings, detection and attribution studies had not been carried out. Whereas there was a clear identification of an anthropogenic fingerprint in the observed pattern of tropospheric warming and stratospheric cooling, differential warming of the tropical free troposphere and surface was significantly larger in models than in some observational datasets, though this discrepancy was assessed to be most probably due to residual observational errors. The observed changes in sea level pressure in the NH were also substantially larger than those simulated, although the pattern of reduced pressure over the very high Northern latitudes was qualitatively consistent between models and observations. The observed variability of ocean temperatures appeared inconsistent with climate models, thereby reducing the confidence with which observed ocean warming could be attributed to human influence.

Since the AR4, improvements have been made to observational datasets, taking more complete account of systematic biases and inhomogeneities in observational systems, further developing uncertainty estimates, and correcting detected data problems (Chapter 2). A new set of simulations from a greater number of AOGCMs have been performed as part of the Fifth Coupled Model Intercomparison project (CMIP5). These new simulations have several advantages over the CMIP3 simulations assessed in the AR4 (Hegerl et al., 2007b). They incorporate some moderate increases in resolution, improved parameterisations (Chapter 9) and the set of forcings included in the historical simulations is in general more complete, with many models including an interactive sulphur cycle, and thus able to simulate the indirect aerosol effect, an important forcing missing from many of the CMIP3 simulations. In addition most models include tropospheric and stratospheric ozone changes, black carbon aerosols and changes in land use. Many historical simulations have been continued to 2010 (making some assumptions about emissions post 2005) allowing comparison between simulations and observations from the first decade of the 21st century. Most importantly for attribution, most models include simulations of the response to natural forcings only, and the response to increases in well mixed greenhouse gases only. The advances enabled by this greater wealth of observational and model data are assessed in this chapter.

10.2 Evaluation of Detection and Attribution Methodologies

Detection and attribution methods have been discussed in previous assessment reports (Hegerl et al., 2007b) and the IPCC Good Practice Guidance Paper (Hegerl et al., 2010), to which we refer. This section reiterates key points and discusses new developments and challenges.

10.2.1 The Context of Detection and Attribution

In IPCC Assessments, detection and attribution involves quantifying the evidence for a causal link between external drivers of climate change and observed changes in climatic variables. It provides the central, although not the only, line of evidence that has supported statements such as “the balance of evidence suggests a discernible human influence on global climate” or “most of the observed increase in global average temperatures since the mid-20th century is very likely due to the observed increase in anthropogenic greenhouse gas concentrations.”

There are four core elements to any detection and attribution study:

1. Observations of climate indicators, such as surface temperature, understood, on physical grounds, to be relevant to the process in question;
2. An estimate of how external drivers of climate change have evolved before and during the period under investigation, including both the driver whose influence is being investigated (such as rising greenhouse gas levels) and other external drivers which may have a confounding influence (such as solar activity);
3. A quantitative physically-based understanding, normally encapsulated in a model, of how these external drivers might affect these climate indicators;
4. An estimate, often but not always derived from a physically-based model, of the characteristics of variability expected in those indicators due to random, quasi-periodic and chaotic fluctuations generated in the climate system that are not due to externally-driven climate change.

Detection and attribution is about testing physically-based hypotheses, not just statistical correlations.

The Earth's atmosphere-land-ice-ocean system is chaotic, generating unpredictable variability on all time-scales (HASSELMANN, 1976). An apparent change or trend in a climate-related variable does not necessarily call for an explanation in terms of an external driver: it may simply be a manifestation of chaotic variability. Therefore, a warming trend within a decade, or the occurrence of a single very warm year, is not by itself sufficient evidence for attribution to a particular external driver. Likewise, the absence of warming in the short term, or the occurrence of cold year or season, does not in itself prevent the attribution of a long-term warming trend. Hence, in contrast to the statement that the world has warmed, no statement of why it is warming will ever be entirely unequivocal. Detection and attribution statements can only be made at some confidence level, always less than 100%.

External forcings of climate can be either anthropogenic (for example increases in well-mixed greenhouse gases) or natural. Natural forcings external to the climate system, for example changes in solar irradiance or explosive volcanic eruptions, are therefore distinct from natural variability internal to the climate system. While a coupled climate model is not expected to replicate the observed evolution of internal variability, an important test of any model is its ability to capture the statistics of this "noise". The reliability of forecasts of short-term variability is also a useful test, but forecast skill is not necessary for attribution: attribution generally applies to timescales over which forecast skill arising from initial conditions is negligible.

The definition of detection and attribution used here follows the terminology in the IPCC guidance paper (Hegerl et al., 2010), and is similar to that used in previous assessments. '*Detection* of change is defined as the process of demonstrating that climate or a system affected by climate has changed in some defined statistical sense without providing a reason for that change. An identified change is detected in observations if its likelihood of occurrence by chance due to internal variability alone is determined to be small' (Hegerl et al., 2010). The guidance note defines attribution as 'the process of evaluating the relative contributions of multiple causal factors to a change or event with an assignment of statistical confidence'.

This definition of attribution potentially includes antecedent conditions and natural variability among the multiple causal factors contributing to an observed change or event. Understanding the relative importance of internal versus external factors is important in the analysis of individual weather events (section 10.6.2), but, consistent with previous assessments, the primary focus of this chapter will be on attribution to factors external to the climate system, such as greenhouse gas emissions or solar variability.

In previous assessments, the response to an external driver is attributable to that driver if it can be detected despite allowing for uncertainty in potentially confounding factors and if the observed response is consistent with the expected response (Allen and Tett, 1999; Hasselmann, 1997). The guidance note introduced some new flexibility by proposing that 'the process of attribution requires the detection of a change in the observed variable *or closely associated variables*' (Hegerl et al., 2010). For example, it is impossible in principle to detect a trend in the frequency of one-in-100-year events in a 100-year record, yet if the risk of these events is physically related to large-scale temperatures, and we detect and attribute a large-scale warming, then the new guidance allows attribution of a change in risk before such a change can be detected. This more flexible terminology was introduced to allow attribution statements to be made about a broader range of indicators than time-averaged temperatures. "Closely associated variables" refers to a well-understood physical association, not simply a statistical correlation.

Attribution of observed changes is not possible without some kind of model of the relationship between external climate drivers and observable quantities. We cannot observe a world in which either anthropogenic or natural forcing is absent, so some kind of model is needed to frame quantitative hypotheses: to provide estimates of how we would expect such a world to behave and to respond to anthropogenic and natural forcings (Hegerl and Zwiers, 2011). Models may be very simple, just a set of statistical assumptions, or very complex, complete global climate models: they do not need to be correct in all respects, but they must be physically coherent. Results based on an incoherent model are meaningless, however statistically significant.

One of the simplest approaches to detection and attribution is to compare observations with model simulations of internal variability alone, simulations driven with natural forcings alone, and simulations

driven with all known relevant forcings. If observed changes are consistent with simulations that include human influence, and inconsistent with those that do not, this would be sufficient for attribution providing there were no other confounding influences and no cancelling errors. Fortuitous cancellation of errors in model simulations cannot be avoided, but attribution studies are designed to ensure it does not affect their conclusions. For example, a possible cancellation of errors between climate sensitivity and the magnitude of the sulphate forcing may have led to an underestimated spread of simulated warming over the 20th century in the models used for the IPCC Fourth Assessment (Kiehl, 2007; Knutti, 2008). This cancellation of errors did not, however, affect core conclusions on the cause of recent global-scale surface temperature warming because the detection and attribution studies on which these conclusions were based estimated the responses to greenhouse and sulphate forcing separately from the observations (Hegerl et al., 2011b) rather than assuming the model-simulated responses were correct.

Specifically, so-called 'fingerprint' detection and attribution studies obtain a best estimate and uncertainty range for 'scaling factors' by which the model-simulated responses to individual forcings can be scaled up or scaled down while still remaining consistent with the observations, accounting for similarities ('degeneracy') between the patterns of response to different forcings and uncertainty due to internal climate variability. If a scaling factor is significantly larger than zero (at some significance level), then the response to that forcing, as simulated by that model and given that estimate of internal variability and other potentially confounding responses, is detectable in these observations, while if the scaling factor is consistent with unity, then that model-simulated response is consistent with observed changes. Scaling factors are estimated by fitting model-simulated responses to observations, so it does not matter if the model has a transient climate response that is too low or high, or an aerosol forcing whose *magnitude* is not correct. Conversely, if the spatial or temporal *pattern* of forcing or response is wrong, results can be affected – an uncertainty that is addressed by using multiple models and estimates of forcing, although it is more difficult to address errors in the pattern of response that are common to all models or forcing estimates: see Box 10.1 and further discussion in Section 10.3.1.1 and (Hegerl and Zwiers, 2011); Hegerl et al. (2011b).

The simplest way of fitting model-simulated responses to observations is to assume that the responses to different forcings add linearly, and that internal climate variability is independent of the response to external forcing, so the response to any one forcing can be scaled up or down without affecting any of the others. Under these conditions, attribution can be expressed as a variant of linear regression. The additivity assumption has been tested and found to hold for large-scale temperature changes, but it might not hold for other variables like precipitation (Hegerl et al., (2007b); Hegerl and Zwiers, (2011); Shiogama et al. (2012)). Additivity is not required by other methods, such as neural networks, but these have not yet been found to be needed for attribution studies.

The estimated properties of internal climate variability play a central role in this assessment. These are either estimated empirically from the observations (Sections 10.2.2 and 10.7.6) or derived from control simulations of coupled models (Section 10.2.3). Detection and attribution studies routinely assess if the residual variability from observations is consistent with estimates of internal variability used (Allen and Tett, 1999)

[START BOX 10.1 HERE]

Box 10.1: How Attribution Studies Work

This box presents an idealized demonstration of the concepts underlying most current approaches to detection and attribution and how they relate to conventional linear regression. Coloured dots in panel (a) in Box 10.1, Figure 1 show observed annual global mean temperatures from 1861–2010. The red line shows an estimate of the global mean temperature response to anthropogenic (greenhouse gas and aerosol) forcing obtained from the mean of the CMIP-5 ensemble, while the green line shows the CMIP-5 ensemble mean response to natural (solar and volcanic) forcing. Black dotted line shows the scaled combination of anthropogenic and natural responses that best fits the data.

Panel (b) shows graphically how this fit is obtained: observed temperatures are plotted against the model-simulated response to anthropogenic forcings in one direction and natural forcings in the other. Time increases from left to right following the thick black line on the base of the box. Note how observed temperatures increase with both natural and anthropogenic model-simulated warming: a flat surface obtained

by a least-squares fit through all 150 points slopes up away from the viewer in both directions. Coloured lines indicate where this surface intersects the walls of the box. Its gradient indicates how model-simulated responses to natural and anthropogenic forcing need to be scaled to reproduce the observations: the slope in the anthropogenic direction (visible on the rear left face of the box) is close to unity, indicating the magnitude of the observed response to anthropogenic forcing is close to that of the model-simulated response, while the slope in the natural direction (visible on the rear right face) is 0.76, indicating the best-fit observed response to natural forcing is 76% of the model-simulated response.

Panel (c) shows how uncertainties in these estimated scaling factors are computed: Black diamonds show the magnitude of best-fit natural and anthropogenic responses appearing by chance in 150-year segments of internal variability simulated by control integrations of the CMIP-5 ensemble, with the black ellipse showing the region in which 90% of the points in the underlying distribution would be expected to lie. Assuming that internal variability in global temperature simply adds to the response to external forcing, the same distribution provides an estimate of uncertainty in the scaling required to reproduce the observations, shown by the red diamond and ellipse. The magnitude of the observed response is consistent with the model-simulated response to anthropogenic forcing (scaling factor close to unity) and somewhat lower than the model-simulated response to natural forcing (best-fit scaling factor 0.76, but still consistent with unity at the 5% level). The fact that the red ellipse is well separated from zero in both directions and encloses the (1,1) point means that we can confidently detect both anthropogenic and natural influence, as simulated by the CMIP-5 ensemble, in the observed global mean temperature record. Omitting either signal significantly increases the scatter of points about the best-fit surface in panel (b).

The top axis in panel (c) indicates the attributable anthropogenic warming over 1951–2010 estimated by applying these scaling factors to the warming in the CMIP-5 anthropogenic ensemble (the gradient of the red line in panel (a) over this period). Because the model-simulated responses are scaled to fit the observations, the attributable anthropogenic warming of 0.6°C–0.9°C does not depend on the magnitude of the raw model-simulated changes. Hence an attribution statement based on such an analysis, such as "most of the warming over the past 50 years is attributable to anthropogenic drivers", does not depend on the size of the model-simulated warming.

This demonstration assumes, for visualization purposes, there are only two candidate contributors to the observed warming, anthropogenic or natural, and that only global mean temperatures are available. More complex attribution problems, such as separating the response to greenhouse gases from other anthropogenic factors and including spatial information require, in effect, a higher-dimensional version of panel (b), but the principle is the same.

[INSERT FIGURE BOX 10.1, FIGURE 1 HERE]

Box 10.1, Figure 1: Schematic of detection and attribution. a) Observed global annual mean temperatures relative to 1880–1920 (coloured dots) compared with CMIP-5 ensemble-mean response to anthropogenic forcing (red), natural forcing (green) and best-fit linear combination (black dotted); b) Observed temperatures versus model-simulated anthropogenic and natural temperature changes, with best-fit plane shown by coloured square. c) Gradient of best-fit plane in panel (b), or scaling on model-simulated responses required to fit observations (red diamond) with uncertainty estimate (red ellipse and cross) based on CMIP-5 control integrations (black diamonds). Implied anthropogenic warming 1951–2010 indicated by the top axis. Anthropogenic and natural responses noise-reduced with 5-point and 3-point running means respectively.

[END BOX 10.1 HERE]

10.2.2 Time-Series Methods, Causality and Separating Signal from Noise by Time or Spatial Scale

Some attempts to distinguish between externally driven climate change and changes due to internal variability have attempted to avoid or minimize the use of climate models, for example, by separating signal and noise by timescale (e.g., (Schneider and Held, 2001), spatial pattern (Thompson et al., 2009) or both. Other studies use model control simulations to identify patterns of maximum predictability and contrast these with the forced component in climate model simulations (DelSole et al., 2011): see Section 3. Conclusions are generally consistent with those based on fingerprint detection and attribution, while using a different set of assumptions (see review in Hegerl and Zwiers, 2011).

A number of studies have applied methods developed in the econometrics literature to assess the evidence for a causal link between external drivers of climate and observed climate change using the observations themselves to estimate the expected properties of internal climate variability (e.g., Kaufmann and Stern, 1997). The advantage of these approaches is that they do not depend on the accuracy of any particular climate model, but the price is that some kind of statistical model of variability must be assumed.

Time-series methods applied to the detection and attribution problem can generally be cast in the overall framework of testing for Granger causality (Kaufmann et al., 2011). One variable is said to "Granger cause" another if the omission of the first variable significantly increases the magnitude of the estimated noise required in a statistical model of the relationship between them. This is similar in principle to regression-based approaches (see box). Lockwood (2008) uses a similar approach, following (Douglass et al., 2004; Lean, 2006; Stone and Allen, 2005a).

Time-series methods ultimately depend on the structural adequacy of the Granger causality model. Many such studies use a simple first-order autoregressive, or AR(1), model of residual variability, which implies an exponential decay of correlation between successive fluctuations with lag time. This can lead to an over-emphasis on short-term fluctuations. Smirnov and Mokhov (2009) propose an alternative characterisation that allows them to distinguish between conventional Granger causality and a "long-term causality" that focuses on low-frequency changes. Trends that appear significant when tested against an AR(1) model may not be significant when tested against a process which supports this "long-range dependence" (Franzke, 2010). Hence it is generally desirable to explore sensitivity of results to the specification of the statistical model, and also to other methods of estimating the properties of internal variability, such as climate models, discussed next. For example, (Imbers et al., 2012a) demonstrate that the detection of the influence of increasing greenhouse gases in the global temperature record is robust to the assumption of a Fractional Differencing (FD) model of internal variability, which supports long-range dependence.

10.2.3 Methods Based on General Circulation Models and Optimal Fingerprinting

Fingerprinting methods use climate model simulations to provide more complete information about the expected response to different external drivers, including spatial information, and the properties of internal climate variability. This can help to separate patterns of forced change both from each other and from internal variability.

When the signal of a particular external forcing is strong relative to the noise of internal variability, results are not particularly sensitive to the precise specification of variability. When the signal-to-noise ratio is low, however, as is often the case with regional or non-temperature indicators, the accuracy of the specification of variability becomes a central factor in the reliability of any detection and attribution study. Many studies of such variables inflate the variability estimate from models to determine if results are sensitive to, for example, doubling of variance in the control (for example, (Zhang et al., 2007b), although Imbers et al (2012) note that the possibility of errors in the spectral properties of simulated variability is also important.

A full description of optimal fingerprinting is provided in Appendix 9.A of Hegerl et al. (2007b) and further discussion is to be found in Hasselmann (1997), Allen and Tett (1999) and Hegerl and Zwiers (2011). The box provides a simple example of "fingerprinting" based on global mean temperature alone. In a typical fingerprint analysis, model-simulated spatio-temporal patterns of response to different combinations of external forcings, including segments of control integrations with no forcing, are "observed" in a similar manner to the historical record (masking out times and regions where observations are absent). The magnitudes of the model-simulated responses are then estimated in the observations using a variant of linear regression, possibly allowing for signals being contaminated by internal variability (Allen and Stott, 2003) and inter-model (Huntingford et al, 2006) noise.

In 'optimal' fingerprinting, model-simulated responses and observations are normalized by internal variability to improve the signal-to-noise ratio. This requires an estimate of the inverse noise covariance, conventionally based on a truncated pseudo-inverse estimated from the sample covariance matrix of a set of unforced (control) simulations (Hasselmann, 1997; Allen and Tett, 1999). Ribes et al. (2009) use a regularized estimate of the covariance matrix, meaning a linear combination of the sample covariance matrix and a unit matrix which has been shown (Ledoit and Wolf, 2004) to provide a more accurate estimate of the

true inverse covariance thereby avoiding dependence on truncation. Key attribution results do not, however, depend on optimisation, and uncertainty analysis does not require the covariance matrix to be inverted, so while regularisation may help in some cases, it is not essential. Ribes et al. (2010) also propose a hybrid of the model-based optimal fingerprinting and time-series approaches, referred to as "temporal optimal detection", under which each signal is assumed to consist of a single spatial pattern (estimated from a climate model) modulated by a smoothly-varying time-series (see also Santer et al., 1994).

The final step in an attribution study is to check that the residual variability, after the responses to external drivers have been estimated and removed, is consistent with the expected properties of internal climate variability, and that the estimated magnitude of the externally-driven responses are consistent between model and observations (equivalent to the slopes of the best-fit plane through the scatter plot in panel (b) of the Box being consistent with unity). If either of these checks fails, the attribution result is treated with caution. However, 'passing' the test is not a safeguard against unrealistic variability assumptions, which is why estimates of internal variability are discussed in detail in this chapter and Chapter 9.

10.2.4 Single-Step and Multi-Step Attribution

Attribution studies have traditionally involved explicit simulation of the response to external forcing of an observable variable, such as surface temperature, and comparison with corresponding observations of that variable. Attribution is claimed when the simulated response is consistent with the observations at some confidence level, not consistent with internal variability and not consistent with any plausible alternative response. This, so-called single-step attribution, has the advantage of simplicity, but restricts attention to variables for which long and consistent time-series of observations are available and which can be simulated explicitly in current models, or in a sequence of several models driven solely with external climate forcing.

To address attribution questions for variables for which these conditions are not satisfied, Hegerl et al. (2010) introduced the notation of multi-step attribution, formalising existing practice in a number of studies (Stott et al., 2004a). In a multi-step attribution study, the attributable change in a variable such as large-scale surface temperature is estimated with a single-step procedure, along with its associated uncertainty, and the implications of this change are then explored in a further (physically- or statistically-based) modelling step. Overall conclusions can only be as robust as the least certain link in the multi-step procedure. Furthermore, as the focus shifts towards more noisy regional changes, it can be difficult to separate the effect of different external forcings. In such cases, it can be useful to detect the response to all external forcings in the variable in question, and then determine the most important factors underlying the attribution results by reference to a closely related variable for which a full attribution analysis is available (see e.g., Morak et al., 2011b).

10.2.5 Linking Detection and Attribution to Model Evaluation and Prediction: Bayesian and Frequentist Approaches and the Role of the Null-Hypothesis

Attribution results are typically derived from conventional "frequentist" hypothesis tests that minimise reliance on prior assumptions: when it is reported that the response to anthropogenic greenhouse gas increase is very likely greater than half the total observed warming, it means that the null-hypothesis that the greenhouse-gas-induced warming is less than half the total can be rejected with the data available at the 10% significance level. It may well be the case that all available models, and the prior knowledge of practicing climate scientists, indicate a higher greenhouse-induced warming, but this information is deliberately set aside to provide a conservative assessment. Tighter uncertainty estimates can be obtained if prior knowledge is incorporated using a Bayesian approach. The price of this reduced uncertainty is that results then depend on those prior assumptions in addition to the evidence provided by the observations: see Hegerl et al. (2007b).

Expert judgment is still required in frequentist attribution assessments. However, its role is to assess whether internal variability and potential confounding factors have been adequately accounted for, and to downgrade nominal significance levels to account for remaining uncertainties. Hence it may be the case that prediction statements, which combine expert judgment explicitly with observations, appear more confident than attribution statements, even when they refer to the same variable on successive decades. This is not a contradiction, and simply reflects the relative weight given the expert judgment in the two cases.

The specification of the null-hypothesis plays an important role in any attribution assessment (Curry, 2011a; Hegerl et al., 1997; Hegerl et al., 2007b) (Curry, 2011). Studies conventionally use the null-hypothesis of no or negligible human influence on any particular climate variable. It should be noted that this conservative approach means that positive attribution results will tend to be biased towards well-observed, well-modelled variables and regions, which should be taken into account in the compilation of global impact assessments (Allen, 2011b; Trenberth, 2011b)

10.3 Atmosphere and Surface

This section assesses causes of change in the atmosphere and at the surface over land and ocean.

10.3.1 Temperature

Temperature is first assessed near the surface of the earth and then in the free atmosphere.

10.3.1.1 Surface (Air Temperature and SST)

10.3.1.1.1 Observations of surface temperature change

Global mean temperatures warmed strongly over the period 1900–1940 (Figure 10.1), followed by a period with little trend, and strong warming since the mid-1970s (Section 2.2.3, Figure 10.3). Almost the whole global has seen warming since 1901while over the satellite period since 1979 some regions have seen cooling (Section 2.2.3; Figure 10.3). While this picture is supported by all available global near-surface temperature datasets, there are some differences in detail between them, but these are much smaller than both inter-annual variability and the long-term trend (Section 2.2.3). Regarding the evolution of global temperatures since 1998, Knight et al. (2009) and Hansen et al. (2010) find smaller warming in HadCRUT3 than in the GISTEMP and NCDC records over periods of 4–14 years ending in 2008, and HadCRUT4 contains more warming over this period due in part to the inclusion of stations in Asia and the Arctic (Morice et al., 2012) (see Sections 2.2.3, 10.3.1.1.3). Urbanisation likely caused less than 10% of the centennial trend in land mean surface temperature (Section 2.2.1.2), although the influence may have been larger in some regions.

10.3.1.1.2 Simulations of surface temperature change

As discussed in Section 10.1, the CMIP5 simulations have several advantages compared to the CMIP3 simulations assessed by Hegerl et al. (2007b) for the detection and attribution of climate change. Figure 10.1 (top row) shows that when the effects of anthropogenic and natural external forcings are included in the CMIP5 simulations the spread of simulated global mean temperature anomalies broadly spans the observational estimates of global mean temperature anomaly whereas this is not the case for simulations in which only natural forcings are included (Figure 10.1, second row). Simulations with greenhouse gas changes only, and no changes in aerosols or other forcings, tend to simulate more warming than observed (Figure 10.1, third row), as expected. Anomalies are shown relative to 1880–1919 rather than as absolute temperatures. Showing anomalies is reasonable since climate sensitivity is not a strong function of the bias in global mean temperature in the CMIP5 models (Section 9.7.2.1; Figure 9.43). Better agreement between models and observations when the models include anthropogenic forcings is also seen in the CMIP3 and CMIP5 simulations (Figure 10.1, grey lines), although some individual models including anthropogenic forcings overestimate the warming trend, while others underestimate it (Fyfe et al., 2010). Radiative forcing in the simulations including anthropogenic and natural forcings differs considerably among models (Figure 10.1, top right), suggesting that forcing differences explain some of the differences in temperature response between models. Differences between observed global mean temperature based on four observational datasets are small compared to forced changes (Figure 10.1).

[INSERT FIGURE 10.1 HERE]

Figure 10.1: Left hand column: Four observational estimates of global mean temperature (black lines) from HadCRUT4, GISTEMP, and NOAA NCDC, JMA, compared to model simulations [both CMIP3 – thin blue lines and CMIP5 models – thin yellow lines] with greenhouse gas forcings only (bottom panel), natural forcings only (middle panel) and anthropogenic and natural forcings (upper panel). Thick red and blue lines are averages across all available CMIP3 and CMIP5 simulations respectively . Ensemble members are shown by thin yellow lines for CMIP5, thin blue lines for CMIP3 All simulated and observed data were masked using the HadCRUT4 coverage, and global average anomalies are shown with respect to 1880–1919, where all data are first calculated as anomalies relative to 1961–1990

in each grid box. Inset to middle panel shows the four observational datasets distinguished by different colours. Right hand column: Net forcings for CMIP3 and CMIP5 models estimated using the method of Forster and Taylor (2006). Ensemble members are shown by thin yellow lines for CMIP5, CMIP5 multi-model means are shown as thick red lines.

As discussed in Section 10.2 results from detection and attribution are more robust if they consider more than simple consistency arguments. Analyses that allow for the possibility that models might be consistently over- or under- estimating the magnitude of the response to climate forcings are assessed in Section 10.3.1.1.3, the conclusions from which are not affected (see Section 10.2) by evidence that model spread in global mean temperature, at least for CMIP3, is smaller than implied by the uncertainty in radiative forcing (Schwartz et al., 2007). While there is evidence that CMIP3 models with a larger magnitude of sulphate forcing tend to have a higher climate sensitivity (Kiehl et al. (2007), Knutti (2008) Huybers (2010)), there is no such relationship found in CMIP5 (Forster et al., 2012) which may explain the wider spread of the CMIP5 ensemble compared to the CMIP3 ensemble (Figure 10.1). Climate model parameters are typically chosen primarily to reproduce features of the mean climate and variability (Box 9.1), and CMIP5 aerosol emissions are standardised across models and based on historical emissions (Hegerl et al., 2007; Chapter 7), rather than being determined by inverse calculations in order to fit observed temperature changes (Curry and Webster, 2011; Hegerl et al., 2011c).

The top left panel of Figure 10.2 shows the pattern of temperature trends observed over the period 1901–2010, based on the HadCRUT4 dataset. Warming has been observed almost everywhere, with the exception of only a few regions. Rates of warming are generally higher over land areas compared to oceans, mainly due to differences in local feedbacks and a net anomalous heat transport from oceans to land under greenhouse gas forcing, rather than differences in thermal inertia (e.g., Boer, 2011). The second panel down on the left of Figure 10.2 demonstrates that a similar pattern of warming is simulated in the CMIP5 simulations with natural and anthropogenic forcing over this period. Over most regions, observed trends fall between the 5th and 95th percentiles of simulated trends: Exceptions are parts of Asia, and the Southern Hemisphere mid-latitudes, where the simulations warm less than the observations, and parts of the tropical Pacific, where the simulations warm more than the observations. Trends simulated in response to natural forcings only are generally close to zero, and inconsistent with observed trends in most locations. Trends simulated in response to greenhouse gas changes only over the 1901–2010 period are in most cases larger than those observed, and in many cases significantly so. This is expected since these simulations do not include the cooling effects of aerosols (Figure 10.2, bottom row).

[INSERT FIGURE 10.2 HERE]

Figure 10.2: Trends in observed and simulated temperatures (K over the period shown) over the 1901–2010, 1901–1950, 1951–2010 and 1979–2010 periods (as labelled). Trends in observed temperatures for the HadCRUT4 dataset (first row), model simulations including anthropogenic and natural forcings (second row), model simulations including natural forcings only (third row) and model simulations including GHG forcings only (fourth row). Trends are shown only where observational data are available in the HadCRUT4 dataset. Boxes in the 2nd, 3rd and 4th rows show where the observed trend lies outside the 5th to 95th percentile range of simulated trends.

Over the period 1979–2010 (right column, Figure 10.2) the observed trend pattern is similar to that over the 1901–2010 period, except that much of the eastern Pacific and Southern Ocean cooled over this period. These differences are not reflected in the simulated trends over this period in response to anthropogenic and natural forcing (Figure 10.2, second panel down on the right), which show significantly more warming in much of these regions. This reduced warming in observations over the Southern mid-latitudes over the 1979–2010 period can also be seen in the zonal mean trends (Figure 10.3, bottom panel), which also shows that the models appear to warm too much in this region over this period. However, examining Figure 10.3, top panel, we see that there is no discrepancy in zonal mean temperature trends over the longer 1901–2010 period in this region, suggesting that the discrepancy over the 1979–2010 period may either be an unusually strong manifestation of internal variability or relate to regionally-important forcings over the past three decades which are not included in the simulations, such as sea salt aerosol increases due to strengthened high latitude winds (Korhonen et al., 2010).With the exception of three high-latitude bands, zonal mean trends over the 1901-2010 period in all three datasets are inconsistent with naturally-forced trends, indicating a detectable anthropogenic signal in most zonal means over this period (Figure 10.3, top panel).

[INSERT FIGURE 10.3 HERE]

Figure 10.3: Zonal mean temperature trends per period shown. Solid lines show HadCRUT4 (black), GISTEMP (green), NCDC (blue), JMA (yellow) observational datasets, red shading represents the 90% central range of simulations with anthropogenic and natural forcings, blue shading represents the 90% central range of simulations with natural forcings only. All model and observations data are masked to have the same coverage as HadCRUT4.

The year to year variability of global mean temperatures simulated by the CMIP3 models compares reasonably well with that of observations as can be seen from a quantitative evaluation of model variability by comparing the power spectra of observed and and modeled global mean and continental scale temperatures (Hegerl et al., 2007). CMIP5 models also generally exhibit realistic variability in global mean temperature on decadal to multi-decadal timescales (Jones et al., 2012), although it is difficult to evaluate internal variability on multi-decadal timescales in observations given the shortness of the observational record and the presence of external forcing. The observed change in global mean temperature since 1950 is very large compared to model estimates of internal variability (Mitchell et al., 2012b) and to estimates of internal variability derived from a simple model of the effects of forcings and observational estimates of temperatures from 1500–2010 (Brown and Cordero, 2012).

10.3.1.1.3 Attribution of observed global scale temperature changes

The evolution of temperature since the start of the global instrumental record

Since AR4, detection and attribution studies (Christidis et al., 2010; Gillett et al., 2012a; Gillett et al., 2012b; Jones et al., 2010; Jones et al., 2012; Stott and Jones, 2011) applied to a new generation of models that samples a wider range of forcing, modelling and observational uncertainty than assessed in AR4, support previous studies that concluded that greenhouse gases are the largest contributor to global mean temperature increases since the mid 20th century.

The results of multiple regression analyses of observed temperature changes onto the simulated responses to greenhouse gas, other anthropogenic, and natural forcings, exploring modelling and observational uncertainty and sensitivity to choice of analysis period are shown in Figure 10.4 (Gillett et al., 2012b; Jones and Stott, 2011; Jones et al., 2012). The results, based on HadCRUT4 and a multi-model average, show robustly detected responses to greenhouse gas in the observational record whether data from 1851–2010 or only from 1951–2010 are analysed (Figure 10.4a,c). The advantage of analysing the longer period is that more information on observed and modelled changes is included, the disadvantage is that it is more difficult to verify climate models' estimates of internal variability over such a long period. While individual model results produces some spread among scaling factors, results are broadly consistent from analyses over 1851–2010 and 1951–2010 (Gillett et al., 2012b; Jones et al., 2012) (Figure 10.4a,c) lending confidence to these findings although (Jones et al., 2012) found when they analysed 1901–2010 a greater spread of results across models than they found for 1951–2010 or was found for 1861–2010 by (Gillett et al., 2012b). Over the 1951–2010 period, greenhouse-gas-attributable warming at 0.6–1.4 K is significantly larger than the observed warming of approximately 0.6 K, and is compensated by an aerosol-induced cooling of between 0 and –0.8 K (Figure 10.4b) (Jones et al., 2012). These results are supported by a complementary analysis in which a simple climate model was constrained using observations of near-surface temperature and ocean heat content, as well as prior information on the magnitudes of forcings, and which concluded that greenhouse gases have caused 0.6°C–1.1°C warming since the mid-20th century (Huber and Knutti, 2012).

The inclusion of additional data to 2010 (AR4 analyses stopped at 1999) helps to better constrain the magnitude of the greenhouse-gas attributable warming (Drost et al., 2011; Gillett et al., 2011a; Stott and Jones, 2011), as does the inclusion of spatial information (Stott et al., 2006).While Hegerl et al. (2007b) found a significant cooling of about 0.2 K attributable to natural forcings over the 1950–1999 period, the temperature trend attributable to natural forcings over the 1951–2010 period is very small (<0.1 K). This is because, while Pinatubo cooled the 1990s, there have been no large volcanic eruptions since, resulting in small simulated trends in response to natural forcings over the 1951–2010 period (Figure 10.1). Detection of anthropogenic influence is found to be robust to observational uncertainty which is found to be comparably important to internal climate variability as a source of uncertainty in greenhouse-gas attributable warming and aerosol-attributable cooling (Figure 10.4e,f) (Jones and Stott, 2011). Robust detection of anthropogenic influence is also found if a new optimal detection methodology, the Regularised Optimal Fingerprint (see Section 10.2; Ribes et al., 2012), is applied (Ribes and Terray, 2012). A detectable influence of greenhouse gases is robustly seen in HadGEM2-ES (Stott and Jones, 2011), CanESM2 (Gillett et al., 2011a), and in all other CMIP5 models except for GISS-E2-H (Gillett et al., 2012b; Jones et al., 2012). However the influence

of other anthropogenic forcings is only detected in some CMIP5 models. This lack of detection of other anthropogenic forcings compared to detection of an aerosol response using four CMIP3 models over the period 1900–1999 (Hegerl et al., 2007b) does not relate to the use of data to 2010 rather than 2000 (Gillett et al., 2011a; Stott and Jones, 2011). Whether it is associated with a cancellation of aerosol cooling by ozone and black carbon warming making the signal harder to detect, or by some aspect of the response to other anthropogenic forcings which is less realistic in these models remains to be determined.

There are some inconsistencies in the simulated and observed magnitudes of responses to forcing for some CMIP5 models (Figure 10.4a,c); for example CanESM2 has a greenhouse gas regression coefficient significantly less than one (Gillett et al., 2011a; Gillett et al., 2012b) indicating that it overestimates the magnitude of the response to greenhouse gases, and CSIRO has a greenhouse gas regression coefficient significantly greater than one indicating it underestimates the magnitude of the response to greenhouse gases (Gillett et al., 2012a; Jones et al., 2012). Inconsistencies between simulated and observed trends in global mean temperature were also identified in several CMIP3 models by Fyfe et al. (2010) after removing volcanic, ENSO, and COWL (Cold Ocean/Warm Land pattern) signals from global mean temperature, although uncertainties may have been underestimated because residuals were modelled by a first order autoregressive processes. A longer observational record and a better understanding of the temporal changes in forcing should make it easier to identify discrepancies between the magnitude of the observed response to a forcing, and the magnitude of the response simulated in individual models.

In conclusion, the detection of the global temperature response to greenhouse gas increases is robust to model and observational uncertainty, and methods applied to detect it. It is supported by basic physical arguments. Furthermore, the spatial patterns of warming from simulations forced with increases in greenhouse gases and other anthropogenic forcings agree well with observations but differ from warming patterns associated with internal variability and those due to natural forcings (Sedlacek and Knutti, 2012). We conclude that the greenhouse gas contribution to the observed warming of approximately 0.6 K over 1951–2010 was very likely between 0.6 and 1.4 K.

[INSERT FIGURE 10.4 HERE]

Figure 10.4: Estimated contributions from greenhouse gas (red), other anthropogenic (green) and natural (blue) components to observed global surface temperature changes a) from HadCRUT4 (Morice et al., 2011) showing 5–95% uncertainty limits on scaling factors estimated using eight climate models and a multi-model average (multi) and based on an analysis over the 1951–2010 period and b) The corresponding estimated contributions of forced changes to temperature trends over the 1951–2010 period (Jones et al., 2012). c) and d) As for a) and b) but estimated using seven climate models, a multi-model average (multi), and an estimate taking account of model uncertainty (eiv; Huntingford et al., 2006) based on an analysis over 1861–2010 period (Gillett et al., 2012b) e) and f) as for a) and b) but for the 1900–1999 period, for the HadCM3 model and for five different observational datasets; (HadCRUT2v, HadCRUT3v, GISTEMP, NCDC, JMA. (Jones and Stott, 2011).

The influence of black carbon aerosols (from fossil and bio fuel sources) has been detected in the recent global temperature record in one analysis, although the warming attributable to black carbon is small compared to that attributable to greenhouse gas increases (Jones et al., 2010). This warming is simulated mainly over the Northern Hemisphere with a sufficiently distinct spatio-temporal pattern that it can be separated from the response to other forcings in the regression.

Several recent studies have used techniques other than regression-based detection and attribution analyses to address the causes of recent global temperature changes. Drost et al. (2011) demonstrated that observed global mean temperature and land-ocean temperature contrast exhibited trends over the period 1961–2010 which were outside the 5–95% range of simulated internal variability, based on three different observational datasets. Hemispheric temperature contrast, meridional temperature gradient and annual cycle amplitude exhibited trends which were close to the 5% significance level. (Drost and Karoly, 2012) compare the same indices from observations with CMIP5 models and find that natural forcings cannot explain observed changes in these indices which are only explained when models include changes in anthropogenic forcings. By comparing observed global mean temperature with simple statistical models, Zorita et al. (2008) concluded that the clustering of very warm years in the last decade is very unlikely to have occurred by chance. Smirnov and Mokhov (2009), adopting an approach that allows them to distinguish between conventional Granger causality and a “long-term causality” that focuses on low-frequency changes (see Section 10.2) find that increasing CO_2 concentrations are the principle determining factor in the rise of global

mean surface temperature over recent decades. (McKitrick and Tole, 2012) apply a Bayesian Model Averaging method to surface and lower tropospheric temperatures from 1979–2002 and find that data contamination induced by regional socioeconomic variations contributes to observed trends as do patterns of change from climate models, although data contamination by regional socioeconomic variations is not assessed to be a major issue for observational records (Section 2.4.1.3).

Several studies which have aimed to separate forced surface temperature variations from those associated with internal variability have identified the North Atlantic as a dominant centre of multi-decadal internal variability, and in particular modes of variability related to the Atlantic Multidecadal Oscillation (AMO; Section 14.2.5.2). The AMO index is defined as an area average of North Atlantic SSTs, and it has an apparent period of around 70 years, which is long compared to the length of observational record making it difficult to deduce robust conclusions about the contribution of AMO from only 2 cycles. Nevertheless, several studies claim a role for internal variability associated with the AMO in driving enhanced warming in the past three decades, while attributing long-term warming to forced variations either by analysing timeseries of global temperatures, forcings, and indices of the AMO (Folland et al., 2012; Rohde et al., 2012) or by analysing both spatial and temporal patterns of temperature (DelSole et al., 2011; Swanson et al., 2009; Wu et al., 2011). Studies based on global mean timeseries could risk falsely attributing variability to the AMO when forcings, for example associated with aerosols, could also cause similar-looking variability. In contrast, studies using space-time patterns seek to distinguish the spatial structure of temperature anomalies associated with the AMO from those associated with forced variability. Unforced climate simulations indicate that internal multi-decadal variability in the Atlantic is characterized by surface anomalies of the same sign from equator to high latitudes, with maximum amplitudes in subpolar regions (DelSole et al., 2011; Delworth and Mann, 2000; Knight et al., 2005; Latif et al., 2004) while the net response to anthropogenic and natural forcing over the twentieth century is characterized by warming nearly everywhere on the globe, but with minimum warming or even cooling in the subpolar regions of the North Atlantic (Figure 10.2; DelSole et al., 2011; Ting et al., 2009).

While such studies point to a contribution of the AMO to global temperature variability it has also been shown that tropospheric aerosols can explain much of the decadal variability in the Atlantic interhemispheric temperature gradient (Chiang et al., 2012) which could be a confounding influence in the attribution to AMO discussed above. The AMO on the other hand is largely due to internal variability, notwithstanding some studies implicating tropospheric aerosols in driving decadal variations in tropical Atlantic SST (Evan et al., 2011), and temperature variations in eastern North America (Leibensperger et al., 2012) and a study claiming that tropospheric aerosols are a prime driver of twentieth-century North Atlantic climate variability (Booth et al., 2012a) although this model has been shown to be an outlier in this respect (Chiang et al., 2012; Zhang et al., 2012).

To summarise, recent studies using spatial features of observed temperature variations to separate AMO variability from externally-forced changes find that detection of external influence on global temperatures is not compromised by accounting for AMO-congruent variability (high confidence). There remains some uncertainty about how much decadal variability of global temperatures that is attributed to AMO in some studies is actually related to variability in forcing, notably from aerosols. There is agreement among studies that the contribution of the AMO to global warming since 1950 is very small (considerably less than 0.1°C, e.g., see Figure 10.5) and given that observed warming since 1950 is very large compared to climate model estimates of internal variability (Section 10.3.1.1.2), which are assessed to be adequate at global scale (Section 9.5.3.1), we conclude that it is *virtually certain* that warming since 1950 cannot be explained without external forcing.

Based on a range of detection and attribution analyses using multiple solar irradiance reconstructions and models, Hegerl et al. (2007b) concluded that it is very likely that greenhouse gases caused more global warming than solar irradiance variations over the 1950–1999 period. Detection and attribution analyses applied to the CMIP5 simulations (Figure 10.4b) indicate less than 0.1 K temperature change attributable to combined solar and volcanic forcing over the 1951–2010 period. Based on a regression of paleo temperatures onto the response to solar forcing simulated by an energy balance model, Scafetta and West (2007) find that up to 50% of the warming since 1900 may be solar-induced, but Benestad and Schmidt (2009) show this conclusion is not robust, being based on disregarding forcings other than solar in the preindustrial period, and assuming a high and precisely-known value for climate sensitivity. Despite claims

that more than half the warming since 1970 can be ascribed to solar variability (Loehle and Scafetta (2011)) , a conclusion based on an incorrect assumption of no anthropogenic influence before 1950 and a 60 year solar cycle influence on global temperature (see also Mazzarella and Scafetta, 2012), several studies show that solar variations cannot explain warming over the past 25 years, since solar irradiance has declined over this period (Lockwood and Fröhlich, 2007, 2008; Lockwood, 2008(Lockwood, 2012)). Lean and Rind (2008) conclude that solar forcing explains only 10% of the warming over the past 100 years, while contributing a small cooling over the past 25 years. Overall, we conclude that it is *extremely unlikely* that the contribution from solar forcing to the warming since 1950 was larger than that from greenhouse gases.

Overall, given that greenhouse gases *very likely* caused more than the observed warming of 0.6°C since the 1950s, with other anthropogenic forcings contributing much of the counter-acting cooling, and the effects of natural forcings and natural internal variability being small, we conclude that it is *extremely likely* that human activities have caused most of (at least 50%) the observed increases in global average temperatures since the 1950s.

The early 20th century warming

The instrumental surface air temperature (SAT) record shows a pronounced warming during the first half of the 20th century (Figure 10.1). The AR4 concluded that 'the early 20th century warming is very likely in part due to external forcing (Hegerl et al., 2007a), and that it is 'likely' that anthropogenic forcing contributed to this warming. Results since then have been consistent with that assessment. Shiogama et al. (2006) find an approximately equal contribution from solar and volcanic forcing to observed warming to 1949, and a quite small unexplained residual. In contrast, the residual warming found in a study of Northern Hemispheric records was substantial (Hegerl et al., 2007a; Hegerl et al., 2007b), pointing at a contribution by internal variability, consistent with other publications (Delworth and Knutson, 2000). Crook and Forster (2011) find that the observed 1918–1940 warming was significantly greater than that simulated by most of the CMIP3 models. Applying a Bayesian decision analysis, Min and Hense (2006) find strong evidence for either a natural or combined natural and anthropogenic signal in global mean temperature in the 1900–1949 period. Correction of residual biases in sea surface temperature observations leads to a higher estimate of 1950s temperatures, but does not substantially change the warming between 1900 and 1940 (Morice et al., 2012). A distinguishing feature of the early 20th century warming is its pattern (Bronnimann, 2009) which shows the most pronounced warming in the Arctic during the cold season, followed by North America during the warm season, the North Atlantic Ocean and the tropics. In contrast, there was no unusual warming in Australia and much of Asia (see Figure 10.2). Such a pronounced pattern points at a possible role for circulation change as a contributing factor to the regional anomalies contributing to this warming. Some studies suggested the warming is a response to a quasi-periodic oscillation in the overturning circulation of the North Atlantic ocean or some other governing aspect of the climate system (Knight et al., 2006; Polyakov et al., 2005; Schlesinger and Ramankutty, 1994), or a large but random expression of internal variability (Bengtsson et al., 2006; Wood and Overland, 2010). Knight et al. (2009) diagnose a shift from the negative to the positive phase of the AMO from 1910 to 1940, a mode of circulation that is estimated to contribute approximately 0.1°C, trough to peak, to global temperatures (Knight et al., 2005). However, recent research suggests that much of the variability in North Atlantic SST (Booth et al., 2012b; Mann and Emanuel, 2006a)or in the Atlantic inter-hemispheric sea surface temperature gradient (Chiang et al., 2012) may be forced by tropospheric and stratospheric aerosol changes. In conclusion, the early 20th century warming is *very likely* in part due to external forcing. It remains difficult to quantify the contribution to this warming from internal variability, natural forcing and anthropogenic forcing, due to forcing and response uncertainties and incomplete observational coverage.

The evolution of global temperature since 1998

Global mean surface temperatures have not increased strongly since 1998, a period over which the multi-model mean simulated temperature increased in response to steadily increasing greenhouse gas concentrations and constant or declining aerosol forcing (Figure 10.1; Figure 8.5; Figure 8.19). A key question, therefore, is whether the recent apparent slowdown in the rate of observed global warming is consistent with internal variability superposed on a steady anthropogenic warming trend (for example, as represented by the spread of model trends over the same time), or whether it has been driven by changes in radiative forcing. It is found that global temperature trends since 1998 are consistent with internal variability overlying the forced trends seen in climate model projections (Easterling and Wehner, 2009; Mitchell et al., 2012b); see also Figure 1.1, where differences between the observed and multimodl response of comparable

duration occurred earlier. Liebmann et al. (2010) conclude that observed HadCRUT3 global mean temperature trends of 2–10 years ending in 2009 are not unusual in the context of the record since 1850. After removal of ENSO influence, Knight et al. (2009) concluded that observed global mean temperature changes over a range of periods to 2008 are within the 90% range of simulated temperature changes in HadCM3. Over the period 1999–2008, ENSO contributed a warming influence, so the lack of warming seen in the global mean temperature over this period cannot be attributed to ENSO (Fyfe et al., 2011; Knight et al., 2009). Meehl et al. (2011) report that 21st century scenario simulations show decades with negative near surface temperature trends, even while the top of atmosphere radiative balance shows a net input of about 1 W m^{-2}, due to enhanced heat uptake below 300m associated largely with the negative phase of the Inter-decadal Pacific Oscillation (Meehl et al., 2012). Trenberth et al. (2009) argue that the observed heat uptake in the upper ocean is inconsistent with top of atmosphere radiation measurements showing a similar radiative imbalance, though Loeb et al. (2012) argue that upper ocean warming and top of atmosphere radiation are in fact consistent when observational uncertainty is fully accounted for.

Several studies have discussed possible forced contributions to the less rapid warming over the past decade. If some combination of ENSO, volcanic and solar influences are removed from the observational record, the residual exhibits progressive warming over the past decade (Folland et al., 2011; Foster and Rahmstorf, 2011; Kaufmann et al., 2011; Lean and Rind, 2008; Lockwood, 2008; Schonwiese et al., 2010) (Figure 10.5). Kaufmann et al. (2011) also argue that the muted warming is in part explained by an increase in tropospheric aerosol forcing over this period.

[INSERT FIGURE 10.5 HERE]

Figure 10.5: Top: the variations of the observed global mean air surface temperature anomaly from HadRCUT3 (grey line) and the best multivariate fits using the method of Lean (blue line) Lockwood (red line), Folland (green line) and Kaufmann (orange line). Below: the contributions to the fit from a) ENSO, b) volcanoes, c) solar contribution, d) anthropogenic contribution and e) other factors (AMO for Folland and a 17.5 year cycle, SAO, and AO from Lean). From Lockwood (2008), Lean and Rind (2009), Folland et al. (2011) and Kaufmann et al. (2011).

Solomon et al. (2010) show, based on satellite measurements, that stratospheric water vapour declined abruptly by about 10% after 2000 for unknown reasons. Based on radiative forcing calculations and a simple climate model they estimate that this change in stratospheric water vapour reduced the 2000–2009 temperature trend by 0.04 K per decade, though the net effect of this and the other forcings was still a strongly positive trend. Stratospheric aerosol concentration has increased by 4–7% since 2000 (Hofmann et al., 2009; Solomon et al., 2012; Vernier et al., 2011) (Figure 8.15), probably due to several small volcanic eruptions (Solomon et al., 2012; Vernier et al., 2011). Based on a simulation with the Bern EMIC, Solomon et al. (2012) calculate that this additional aerosol, not accounted for in the forcing datasets used in many climate models, would cause approximately a 0.07 K cooling between 1998 and 2010. In a simulation with an aerosol model driven by reanalysis winds, Korhonen et al. (2010) find that an increase in sea salt aerosol over the high latitude Southern Ocean, driven by an increase and poleward shift in the mid-latitude jet, led through its indirect effect to a summertime negative radiative forcing between 50°S and 65°S comparable to the positive radiative forcing due to CO_2 increases, though this effect has not been reproduced in other models.

In summary, while the trend in global mean temperature since 1998 is not significantly different from zero, it is also consistent with internal variability superposed on the anthropogenic greenhouse gas induced warming trends projected by climate models *(high confidence)*. Several candidate mechanisms have been proposed for forcing the variability that has been observed since 1998, but due to the short length of the period, it is not possible to confidently attribute observed temperature changes to one or more in particular.

10.3.1.1.4 Attribution of regional surface temperature change

Anthropogenic influence on climate has been robustly detected on the global scale, but for many applications an estimate of the anthropogenic contribution to recent temperature trends are useful on a limited region. However, detection and attribution of climate change at continental and smaller scales is more difficult than on the global scale for several reasons (Hegerl et al., 2007b; Stott et al., 2010). Firstly, the relative contribution of internal variability compared to the forced response to observed changes tends to be larger on smaller scales, since spatial differences in internal variations are averaged out in large-scale means. Secondly, since the patterns of response to climate forcings tend to be large-scale, there is less spatial information to help distinguish between the responses to different forcings when attention is restricted to a

sub-global area. Thirdly, forcings omitted in some global climate model simulations may be important on regional scales, such as land-use change or black carbon aerosol. Lastly, simulated internal variability and responses to forcings may be less reliable on smaller scales than on the global scale, although grid cell variability is not generally underestimated in models (Karoly and Wu, 2005b; Wu and Karoly, 2007).

Based on several studies, Hegerl et al. (2007b) conclude that *it is likely that there has been a substantial anthropogenic contribution to surface temperature increases in every continent except Antarctica since the middle of the 20th century*. Figure 10.6 shows comparisons of observed continental scale temperatures (Morice et al., 2011) with CMIP5 simluations including both anthropogenic and natural forcings (red lines) and including just natural forcings (blue lines). Observed temperatrures are within the range of simulations with anthropogenic forcings for all regions and outside the range of simulations with only natural forcings for all simulations except Antarctica (Jones et al., 2012). An attribution analysis on Antarctic land temperatures over the period 1950–1999 detects separate natural and anthropogenic responses of consistent magnitude in simulations and observations (Gillett et al., 2008a). Averaging over all observed locations, Antarctica has warmed over the 1950–2008 period (Gillett et al., 2008c; Jones et al., 2012), even though some individual locations have cooled, particularly in summer and autumn, and over the shorter 1960–1999 period (Thompson and Solomon, 2002; Turner et al., 2005). When temperature changes associated with changes in the Southern Annular Mode are removed by regression, both observations and model simulations indicate warming at all observed locations except the South Pole over the 1950–1999 period (Gillett et al., 2008c). Thus anthropogenic influence on climate has now been detected on all seven continents. However the evidence for human influence on warming over Antarctica is much weaker than for the other six continental regions. There is no clear separation of CMIP5 ensembles with and without anthropogenic forcings (Figure 10.6), there is only one formal attribution study for this region, and there is greater observational uncertainty than the other regions, with very few data before 1950, and sparse coverage that is mainly limited to the coast and the Antarctic peninsula. As a result of the observational uncertainties, there is *low confidence* in Antarctic region land surface air temperatures changes (Chapter 2) and we conclude that there is *low confidence* in attribution of Antarctic region land surface air temperatures.

[INSERT FIGURE 10.6 HERE]

Figure 10.6: Global, land, ocean and continental annual mean temperatures for CMIP3 and CMIP5 historical (red) and historicalNat (blue) simulations (multi-model means shown as thick lines, and 5-95% ranges shown as thin light lines) and for HadCRUT4 (black) for six continental sized regions formed from combining the sub-continental scale regions defned by Seneviratne et al. (2012). Temperatures shown with respect to 1880–1919 apart for Antarctica where temperatures are shown with respect to 1950–2010. From Jones et al. (2012).

Since the publication of the AR4 several other studies have applied attribution analyses to continental and sub-continental scale regions. Min and Hense (2007) apply a Bayesian decision analysis to continental-scale temperatures using the CMIP3 multi-model ensemble and conclude that forcing combinations including greenhouse gas increases provide the best explanation of 20th century observed changes in temperature on every inhabited continent except Europe, where the observational evidence is not decisive in their analysis. Jones et al. (2008) detect anthropogenic influence on summer temperatures, in an optimal detection analysis on the temperature responses to anthropogenic and natural forcings, over all Northern Hemisphere continents and in many subcontinental Northern Hemisphere land regions. Christidis et al. (2010) use a multi-model ensemble constrained by global-scale observed temperature changes to estimate the changes in probability of occurrence of warming or cooling trends over the 1950–1997 period over various sub-continental scale regions. They conclude that the probability of occurrence of warming trends has been at least doubled by anthropogenic forcing over all such regions except Central North America. Nonetheless, the estimated distribution of warming trends over the Central North America region was approximately centred on the observed trend, so no inconsistency between simulated and observed trends was identified here.

Several recent studies have applied attribution analyses to specific sub-continental regions. Anthropogenic influence has been found in winter minimum temperature over the Western USA (Bonfils et al., 2008; Pierce et al., 2009), a conclusion that is found to be robust to weighting models according to various aspects of their climatology (Pierce et al., 2009), in temperature trends over New Zealand (Dean and Stott, 2009) after circulation-related variability is removed as in Gillett et al. (2000) and in temperature trends over France, using a first order autoregressive model of internal variability (Ribes et al., 2010). Anthropogenic increases in greenhouse gases are found to be the main driver of the 20th-century SST increases in both Atlantic and Pacific tropical cyclogenesis regions (Gillett et al., 2008b; Santer and et al, 2006). Over both regions, the

response to anthropogenic forcings is detected when the response to natural forcings is also included in the analysis (Gillett et al., 2008b).

Gillett et al. (2008c) detect anthropogenic influence on near-surface Arctic temperatures over land, with a consistent magnitude in simulations and observations. Wang et al. (2007) also find that observed Arctic warming is inconsistent with simulated internal variability. Both studies ascribe Arctic warmth in the 1930s and 1940s largely to internal variability. Shindell and Faluvegi (2009) infer a large contribution to both mid-century Arctic cooling and late century warming from aerosol forcing changes, with greenhouse gases the dominant driver of long-term warming, though they infer aerosol forcing changes from temperature changes using an inverse approach which may lead to some changes associated with internal variability being attributed to aerosol forcing. We therefore conclude that despite the uncertainties introduced by limited observational coverage, high internal variability, modelling uncertainties (Crook et al., 2011) and poorly-understood local forcings, such as the effect of black carbon on snow, there is sufficiently strong evidence to conclude that it is likely that there has been an anthropogenic contribution to warming in Arctic land surface temperatures over the past 50 years.

Some attribution analyses have considered temperature trends at climate model grid box scale. At these spatial scales robust attribution is very difficult to obtain, since climate model often lack the processes needed to simulate regional details realistically, regionally important forcings may be missing in some models and observational uncertainties are very large for some regions of the world at grid box scale (Hegerl et al., 2007b; Stott et al., 2010). Nevertheless an attribution analysis has been carried out on Central England temperature, a record which has been corrected for the influence of urbanisation and which, extending back to 1659, is sufficiently long to demonstrate that the representation of muiti-decadal variability in the single grid box in the model used, HadCM3 is adequate for detection (Karoly and Stott, 2006). The observed trend in Central England Temperature is inconsistent with either internal variability or the simulated response to natural forcings, but is consistent with the simulated response when anthropogenic forcings are included (Karoly and Stott, 2006).

Analyses of grid box scales globally shows that observed 20th century grid cell trends from HadCRUT2v (Jones et al., 2001) are inconsistent with simulated internal variability at the 10% confidence level in around 80% of grid cells even using HadCM2 which was found to overestimate variability in 5-year mean temperatures at most latitudes (Karoly and Wu, 2005b). 60% of grid cells are found to exhibit significant warming trends, a much larger number than expected by chance (Karoly and Wu, 2005b; Wu and Karoly, 2007). and similar results apply when circulation-related variability is first regressed out (Wu and Karoly, 2007). However, as discussed in the AR4, when a global field significance test is applied, this becomes a global attribution study; since not all grid cells exhibit significant warming trends the overall interpretation of the results in terms of attribution at individual locations remains problematic. The global picture is illustrated in Figure 10.2 (third panel left column) which shows that in the great majority of grid cells with sufficient observational coverage (91%), observed trends over the 1901–2010 period are inconsistent with a combination of simulated internal variability and the response to natural forcings.

In summary, it is *likely* that anthropogenic forcing has made a substantial contribution to warming of the inhabited continents since 1950. There is *low confidence* that anthropogenic forcing has contributed to warming in Antarctica. Detection and attribution of climate change at continental and smaller scales is more difficult than at the global scale due to the greater contribution of internal variability, greater difficulties of distinguishing between different causal factors, and greater errors in climate models' representation of regional details.

10.3.1.2 Atmosphere

This section presents an assessment of the causes of global and regional temperature changes in the free atmosphere. In AR4, Hegerl et al. (2007b) concluded that 'the observed pattern of tropospheric warming and stratospheric cooling is very likely due to the influence of anthropogenic forcing, particularly greenhouse gases and stratospheric ozone depletion.' Since AR4 insight has been gained into regional aspects of free tropospheric trends and the causes of observed changes in stratospheric temperature.

Atmospheric temperature trends through the depth of the atmosphere, offer the possibility of separating the effects of multiple climate forcings, since climate model simulations indicate that each external forcing produces a different characteristic vertical and zonal pattern of temperature response (Hansen et al., 2005b; Hegerl et al., 2007b; Penner et al., 2007; Yoshimori and Broccoli, 2008). Greenhouse gas forcing is expected to warm the troposphere and cool the stratosphere. Stratospheric ozone depletion cools the stratosphere with the cooling being most pronounced in the polar regions. Tropospheric ozone increase, on the other hand, causes tropospheric warming. Reflective aerosols like sulphate cool the troposphere while absorbing aerosols like black carbon have a warming effect. Free atmosphere temperatures are also affected by natural forcings: Solar irradiance increases cause a general warming of the atmosphere and volcanic aerosol ejected into the stratosphere causes tropospheric cooling and stratospheric warming (Hegerl et al., 2007b).

10.3.1.2.1 Tropospheric temperature change

Chapter 2 concludes that it is *virtually certain* that globally the troposphere has warmed since the mid-twentieth century with only medium to low confidence in the rate and vertical structure of these changes. Evidence is robust that during the satellite era CMIP3 and CMIP5 models warm faster than observations specifically in the tropics (Fu et al., 2011; McKitrick et al., 2010; Santer et al., 2012) (see also Chapter 9). The likely causes for this inconsistency between observed and simulated free troposphere warming are not understood and include factors like errors in observations, specific manifestation of natural variability in observed coupled atmosphere-ocean system, forcing errors included in the historical simulations, and model response errors (Santer et al., 2012) (Chapter 9).

Utilizing a subset of CMIP5 experiments, (Lott et al., 2012) detect influences of both human induced greenhouse gas increase and other anthropogenic forcings (e.g., ozone and aerosols) in the spatio–temporal changes in tropospheric temperatures from 1961to 2010 estimated from radiosonde observations providing there are enough data to estimate internal variability. Figure 10.7 (right panel) illustrates that near globally (where there is sufficient observational coverage to make a meaningful comparison: 60°S–60°N), a subsample of six CMIP5 models forced with both anthropogenic and natural climate drivers exhibit trends that are consistent with radiosonde records in the troposphere up to about 300 hPa, albeit with a tendency for these six models to warm more than the observations (Figure 10.7, right panel, red). Similar results are seen in the Southern Hemisphere extratropical (Figure 10.7, first panel), tropical (Figure 10.7, second panel) and Northern Hemisphere extratropical bands (Figure 10.7, third panel). The observed warming of tropospheric temperatures can *very likely* not be explained by natural forcings alone (green profiles). The ensembles with both anthropogenic and natural forcings (red) and with greenhouse gas forcings only (blue) are not clearly separated suggesting that there could be some cancelation of the effects of increases in reflecting aerosols, which cool the troposphere, and absorbing aerosol (Penner et al., 2007) and tropospheric ozone, which warm the troposphere. The latter is more important in the Northern Hemisphere extratropics than in other parts of the globe (Chapter 8), although the subset of CMIP5 model ensembles shown in Figure 10.7 do not show more overlap of the relevant ensembles in the Northern Hemisphere extratropics than the other latitude bands shown in Figure 10.7. Note also that sulphur dioxide emissions peaked in the 1970s (Smith et al., 2011) and have subsequently declined, further muting the effects of sulphate aerosols on temperature trends over this 1961–2010 period. Above 300 hPa the three reanalysis products exhibit a larger spread as a result of larger uncertainties in the observational record (Thorne et al., 2011a). In this region of the upper troposphere simulated CMIP5 trends tend to be more positive than observed trends (Figure 10.7). Further, an assessment of causes of observed trends in the upper troposphere is less confident than an assessment of overall atmospheric temperature changes because of observational uncertainties and potential remaining systematic biases in observational datasets in this region (Haimberger et al., 2011; Thorne et al., 2011a).

[INSERT FIGURE 10.7 HERE]

Figure 10.7: Observed and simulated zonal mean temperatures trends from 1961 to 2010 for CMIP5 simulations containing both anthropogenic and natural forcings (red), natural forcings only (green) and greenhouse gas forcing only (blue) where the 5 to 95 percentile ranges of the ensembles are shown. Three radiosonde observations are shown (thick black line: HadAT2, thin black line: RAOBCORE 1.5, dark grey band : RICH-obs 1.5 ensemble and light grey: RICH-τ 1.5 ensemble. After (Lott et al., 2012).

The analysis of the signal-to-noise ratio (S/N) of the data record which for meteorological data tends to decrease with increasing record length is one approach to identify a climate change signal in a time series. For near global lower troposphere temperature and a confidence level of 95% Santer et al. (2011) determined that a climate change signal becomes detectable after 17 years of data. Santer et al. (2012) estimates the

geographic pattern of response to combine anthropogenic and natural external forcing using CMIP5 models and determine a signal to noise ratio for the 1979–2011 period of 3 to 6 with a confidence level of at least 99%. Even when all information on global-mean temperature changes is removed, the spatial fingerprint of change is found to be detectable in over 50% of all tests carried out by Santer et al. (2012).

AR4 concluded that increasing greenhouse gases are the main cause for warming of the troposphere. This result is supported by a subsample of CMIP5 models which also suggest that the warming effect of well mixed greenhouse gases is partly offset by the combined effects reflecting aerosols and other forcings. Our understanding has been increased regarding the time scale of detectability of global scale troposphere temperature. Taken together with increased understanding of the uncertainties in observational records of tropospheric temperatures (including residual systematic biases; Chapter 2) the assessment remains as it was for AR4 that it is *likely* that anthropogenic forcing has led to a detectable warming of tropospheric temperatures since 1961.

10.3.1.2.2 Stratospheric temperature change

Lower stratospheric temperatures did not evolve uniformly over the period since 1958 when the stratosphere has been observed. A long-term global cooling trend is interrupted by three two-year warming episodes following large volcanic eruptions (Chapter 2). Furthermore, during the satellite period the cooling evolved mainly in two steps occurring in the aftermath of the El Chichón eruption in 1982 and the Pinatubo eruption of 1991 with each cooling transition being followed by a period of relatively steady temperatures (Randel et al., 2009; Seidel et al., 2011)..

Since AR4, progress has been made in the capability of simulating the specific observed evolution of global mean lower stratospheric temperature change. One the one hand, this has been achieved by utilizing models with an improved representation of stratospheric processes (Chemistry Climate Models, subset of CMIP5 models) (Chapter 9). It is found that in these models which have a model lid above the stratopause (so-called high-top models), variability of lower stratosphere climate in general is well simulated (Butchart et al., 2011; Charlton-Perez et al., 2012; Gillett et al., 2011b) while in so called low-top models (including models participating in CMIP3) it is generally underestimated (Charlton-Perez et al., 2012; Cordero and Forster, 2006). On the other hand CMIP5 models consistently include the change of stratospheric ozone (Eyring et al., 2012) while only about half of the models participating in CMIP3 include stratospheric ozone changes. A comparison of a low-top and high-top version of the HadGEM2 model has shown detectable differences in modelled temperature changes, particularly in the lower tropical stratosphere, with the high-top version's simulation of temperature trends in the tropical troposphere in better agreement with radiosondes and reanalyses over 1981–2010 (Mitchell et al., 2012a)

CMIP5 models forced with changes in well mixed greenhouse gases and stratospheric ozone as well as with changes in solar irradiance and volcanic aerosol forcings simulate the evolution of observed global mean lower stratospheric temperatures over the satellite era although they tend to underestimate the long-term cooling trend. Compared with radiosonde data the cooling trend is also underestimated in a subset of CMIP5 simulations over the period 1961-2010 (Figure 10.7) and in CMIP3 models over the 1958 to 1999 period. Potential causes for biases in lower stratosphere temperature trends are forcing errors related to prescribed stratospheric aerosol loadings and stratospheric ozone changes affecting the tropical lower stratosphere (Free and Lanzante, 2009; Santer et al., 2012; Solomon et al., 2012) (see also Chapter 9).

Observational records of stratospheric temperatures are relatively short and estimates of detectability of climate change signals strongly rely on model studies. Over the satellite period (1979–2011) and utilizing three observational datasets and 14 CMIP5 models, Santer et al. (2012) detect a human caused climate influence in lower stratospheric temperatures with a signal to noise ratio of 21 to 29 depending on the observational data set. Using the GFDL CM2.1 model which simulates well stratospheric temperature trends after 1960, (Schwarzkopf and Ramaswamy, 2008) determine that a significant signal of external influence on the atmosphere in the global mean lower to middle stratosphere emerges by the early 20th century with the simulate cooling over this period resulting largely from carbon dioxide.

Since AR4 attribution studies have improved our knowledge about the specific role of anthropogenic and natural forcings on observed lower stratospheric temperature change. (Gillett et al., 2011b) use the suite of chemistry climate model simulations carried out as part of the Chemistry climate Model Validation

(CCMVal) activity phase 2 for an attribution study of observed changes in stratospheric zonal mean temperatures. They partition 1979–2005 MSU lower stratospheric temperature trends into ODS induced and greenhouse gas induced changes and find that both ODSs and natural forcing contributed to the observed stratospheric cooling in the lower stratosphere with the impact of ODS dominating. The influence of greenhouse gases on stratospheric temperature could not be detected independently of ODSs.

The step-like cooling of the lower stratosphere can only be explained by combined effect of changes in both anthropogenic and natural factors (Figure10.8) (Eyring et al., 2006; Ramaswamy et al., 2006). While the anthropogenic factors (ozone depletion and increases in well-mixed greenhouse gases) cause the overall cooling, the natural factors (solar irradiance variations and volcanic aerosols) modulate the evolution of the cooling (Figure 10.8) (Dall'Amico et al., 2010; Ramaswamy et al., 2006) with temporal variability of global mean ozone contributing to the step-like temperature evolution (Thompson and Solomon, 2009).

INSERT FIGURE 10.8 HERE]

Figure 10.8: Time series (1979–2010) of observed (black) and simulated global mean (82.5°S–82.5°N) MSU lower stratosphere temperature anomalies in a subset of six CMIP5 simulations (Simulations with both anthropogenic and natural forcings (red: Allforc), simulations with increases in well mixed greenhouse gases (blue: Wmghg), simulations with natural forcings (green: Nat) . Anomalies are calculated relative to 1996–2010. Adapted from Ramaswamy et al. (2006).

Models disagree with observations for seasonally-varying changes in the strength of the Brewer-Dobson circulation in the lower stratosphere (Ray et al., 2010) which has been linked to zonal and seasonal patterns of changes in lower stratospheric temperatures (Forster, 2011; Free, 2011; Fu et al., 2010; Lin et al., 2010b; Thompson and Solomon, 2009). One robust feature is the observed cooling in spring over the Antarctic, which is simulated in response to stratospheric ozone depletion in climate models (Young et al., 2012), although this has not been the subject of a formal detection and attribution study.

Since AR4 progress has been made in simulating the response of global mean lower stratosphere temperatures to natural and anthropogenic forcings by improving the representation of climate forcings and utilizing models that include more explicitly stratospheric processes. Evidence is robust that a combination of natural and anthropogenic forcings caused the specific observed temporal evolution of lower stratospheric temperatures characterized by a step-like cooling in the aftermath of volcanic eruptions especially in the satellite period. The long-term cooling trend is caused by a combination of increases in well mixed greenhouse gases and ozone depletion resulting from the increase in ODS, with ozone depletion dominant in the lower stratosphere. Volcanic aerosols modulate the evolution of the cooling causing two-year warming periods. New detection and attribution studies of lower stratospheric temperature changes made since AR4 support an assessment that it is *very likely* that anthropogenic forcing, dominated by ozone depleting substances, has led to a detectable cooling of stratospheric temperatures since 1961.

10.3.1.2.3 Overall atmospheric temperature change

When temperature trends from the troposphere and stratosphere are analysed together, detection and attribution studies using CMIP5 models show robust detections of the effects of greenhouse gases and other anthropogenic forcings on the distinctive fingerprint of troposheric warming and stratospheric cooling seen since 1961 in radiosonde data (Lott et al., 2012; Mitchell et al., 2012a). Combining the evidence from free atmosphere changes from both troposphere and stratosphere shows an increased confidence in the attribution of free atmosphere temperature changes compared to AR4 due to improved understanding of stratospheric temperature changes. It is therefore concluded that it is very likely anthropogenic forcing, particularly greenhouse gases and stratospheric ozone depletion, has led to a detectable observed pattern of tropospheric warming and stratospheric cooling since 1961.

10.3.2 Water Cycle

Detection and attribution studies of anthropogenic change in hydrologic variables are challenged by the length and quality of observed data sets, the large natural variability across a wide range of time and space scales exhibited by many hydrologic variables, and the challenges of simulating these variables in dynamical models. AR4 cautiously stated that anthropogenic influence has contributed to an increase in total atmospheric water vapour, that no detection of global precipitation change was indicated, and that observed

changes in the latitudinal distribution of precipitation, and increased incidence of drought, were suggestive of a possible human influence.

Many of the published studies cited in AR4, and some of the studies cited in this section, use less formal detection and attribution criteria than are often used for assessments of temperature change, due to difficulties defining large-scale fingerprint patterns of hydrologic change in models and isolating those fingerprints in data. For example, correlations between observed hydrologic changes and the patterns of change in models forced by increasing greenhouse gases can provide suggestive evidence toward attribution of change, as implied by the AR4 summary assessments quoted above.

Since the publication of AR4, in situ hydrologic data sets have been reanalyzed with more stringent quality control. Satellite-derived data records of worldwide water vapour and precipitation variations have lengthened. Recent detection/attribution studies have been carried out with newer models that potentially offer better simulations of natural variability. Reviews of detection and attribution of trends in various components of the water cycle have been published by Stott et al. (2010) and Trenberth (2011b).

10.3.2.1 Changes in Atmospheric Water Vapour

In situ surface humidity measurements have been reprocessed since AR4 to create new gridded analyses for climatic research, as discussed in Chapter 2. The HadCRUH Surface Humidity dataset (Willett et al., 2008) indicates significant increases in surface specific humidity between 1973 and 2003 over the globe, the tropics, and the Northern Hemisphere, with consistently larger trends in the tropics and in the Northern Hemisphere during summer, and negative or nonsignificant trends in relative humidity. These results are consistent with the hypothesis that the distribution of relative humidity should remain roughly constant under climate change (see Section 2.3). Simulations of the response to positive radiative forcing robustly generate an increase in atmospheric humidity, such that the positive feedback associated with water vapour amplifies the effect of the prescribed forcing (Chapter 9). This consistency is the basis for studies that attribute the observed specific humidity trends in recent decades to anthropogenic forcing that warms the surface (Willett et al., 2007). A recent cessation of the upward trend in specific humidity that was robustly observed over multiple continental areas in HadCRUH and is also found in the ERA-interim reanalysis was found to be temporally correlated with a levelling off of global ocean temperatures following the 1997–1998 El Niño event, and therefore tentatively explained the change in humidity trend as being controlled by ocean temperatures. (Simmons et al. (2010)

The anthropogenic water vapour fingerprint simulated by an ensemble of 22 climate models has been identified in lower tropospheric moisture content estimates derived from SSM/I data covering the period 1988–2006 (Santer et al., 2007). Santer et al. (2009) find that detection of an anthropogenic response in column water vapour is insensitive to the set of models used. They rank models based on their ability to simulate the observed mean total column water vapour, and its annual cycle and variability associated with ENSO. They report no appreciable differences between the fingerprints or detection results derived from the best or worst performing models.

Recent decreases in stratospheric water vapor, of magnitude sufficient to slightly, but measurably alter the greenhouse effect, have been described (Randel et al. (2006); Rosenlof and Reid (2008); Solomon et al. (2010). However uncertainties in the stratospheric water vapour data (Lanzante, 2009), combined with the difficulties in modeling upper atmospheric water vapor (Pierce et al., 2006b), still preclude definitive detection and attribution of water vapour change in the radiatively sensitive regions of the upper troposphere and stratosphere.

In summary, an anthropogenic contribution to increases in atmospheric moisture content at Earth's surface is found with medium confidence. Evidence of a recent shift in the apparent long-term surface atmospheric moistening trend over land needs to be better understood and simulated as a prerequisite to increased confidence in attribution studies. Length and quality of observational humidity data sets, especially above the surface, continue to limit detection and attribution.

10.3.2.2 Changes in Precipitation

Detection and attribution of regional precipitation changes has focused on continental areas using in situ data because poor observational coverage over oceans is limited to a few island stations (Arkin et al., 2010; Liu et al., 2012; Noake et al., 2012), although model-data comparisons over continents also illustrate large observational uncertainties (Balani Sarojini et al., 2012; Noake et al., 2011; Polson et al., 2012). Available satellite datasets that could supplement oceanic studies are short and not considered to be sufficiently reliable for this purpose (Chapter 2). Continuing uncertainties in climate model simulations of precipitation make quantitative model/data comparisons difficult (e.g., Stephens et al., 2010), which also limits confidence in detection and attribution. Although CMIP5 model simulations indicate that clear global and regional scale changes are expected to have already happened over land and oceans, sparse observational coverage of precipitation causes this fingerprint of change to be much more indistinct in observational records, making attribution more difficult (Balani Sarojini et al., 2012). Considering just land regions with sufficient observations, the largest signal of differences between models with and without anthropogenic forcings is in the high latitudes of the northern hemisphere, where increases in precipitation have been observed (Figure 10.9) that is reasonably robust to observational dataset used (Min et al., 2008a; Noake et al., 2011; Polson et al., 2012).

[INSERT FIGURE 10.9 HERE]

Figure 10.9: Global and zonal changes in annual mean precipitation (mm/day) over areas of land where there are observations, expressed relative to the baseline period of 1961-90, simulated by CMIP5 models forced with both anthropogenic and natural forcings (red lines) and natural forcings only (blue lines) for the global mean and for four latitude bands. Multi-model means are shown in thick solid lines and observations are in black solid line. A 5-year running mean is applied to both simulations and observations. Green stars show statistically significant changes at 5% level (p value <0.05) between the ensemble of runs with both anthropogenic and natural forcings (red lines) and the ensemble of runs with just natural forcings (blue lines) using a two-sample two-tailed t-test for the last 30 years of the time series. From (Balani Sarojini et al., 2012).

Attribution of zonally averaged precipitation trends has been carried out using different observational products and ensembles of forced simulations from both the CMIP3 and CMIP5 archives, for annual-averaged (Zhang et al., 2007c; Min et al., 2008b), and season-specific (Noake et al., 2012; Polson et al., 2012) results (Figure 10.10). Zhang et al. (2007b) detect the fingerpring of anthropogenic changes in zonal precipitation both over the period 1925–1999 and 1950–1999 and separate it from the influence of natural forcing. The fingerprint for external forcing is also detected over boreal spring in all datasets considered, and for boreal winter in all but one dataset (Noake et al., 2012), over the period 1951–1999 and to 2005. The fingerprint features increasing high latitude precipitation, and decreasing precipitation trends in parts of the tropics that are robustly observed in all datasets considered (Figure 10.10). Detection and attribution of precipitation change is less convincing for the JJA and SON seasons (results vary with different observation data sets; Noake et al., 2012; Polson et al., 2012). While Zhang et al. (2007b) detect anthropogenic changes even if a separate fingerprint for natural forcings is considered Polson et al. (2012) find that this results is sensitive to the dataset used and that the fingerprint can only be separated robustly for the dataset most closely constrained by station data (Figure 10.10). The analysis also finds that model simulated precipitation variability is smaller than observed variability in the tropics (Polson et al., 2012; Zhang et al., 2007b) which is addressed by increasing the estimate of variance from models.

Another detection and attribution study focused on precipitation in the Northern hemisphere high latitudes and found a detectable human influence (Min et al., 2008a). Both the study of Min et al. (2008b) and Zhang et al. (2007b) find that the obsesrved changes are significantly larger than the model simulated changes. However Noake et al. (2011, 2012) and Polson et al. (2012) find that the difference between models and observations decreases if changes are expressed in percent of climatological precipitation and that the observed and simulated changes are largely consistent between CMIP5 models and observations given data uncertainty. Apart from high latitude precipitation, regional scale attribution of precipitation change is still problematic although regional climate models have yielded simulations consistent with observed wintertime changes for northern Europe (Bhend and von Storch, 2008).

[INSERT FIGURE 10.10 HERE]

Figure 10.10: Detection and attribution results for precipitation trends in the second half of the 20th century (1951–2005), adapted from Noake et al. (2012), Polson et al. (2012), and for Northern high latitude precipitation (1950–1999) from Min et al. (2008b) and Northern hemisphere land extreme precipitation (1951–1999) from Min et al. (2011). TOP LEFT: Scaling factors for precipitation changes. Crosses show the best-guess scaling factor for the multi-model mean,

thick lines are the 5–95% uncertainty range for the raw variance added as noise, and thin lines are the 5–95% uncertainty range for double the variance. In each panel the black bars indicate estimated response to all forcings, red bars to natural forcing and blue bars to anthropogenic-only forcing. Panel labelled "Global land-Annual" shows scaling factors for both single fingerprint and two fingerprint results. Panel labelled "Global land-Seasonal" shows scaling factors resulting from single-fingerprint analyses for zonally and seasonally averaged precipitation, using four different datasets to estimate observed trends. Detectable results are found at the 5% significant level for the three datasets depicted by black bars. Panel labelled "Arctic" shows scaling factors for spatial pattern of Arctic precipitation trends. Panel labelled "Extreme" shows scaling factors for changes of a global-wide intense precipitation index. TOP RIGHT: Thick solid colored lines show observed trends [% per decade] in annual average precipitation relative to climatological means from four observational datasets, as a function of latitude for land points only. The best guess scaled multimodel mean ensemble is shown as a black solid line. Corresponding results from ensembles of 20 different climate models are shown as dashed and thin solid lines. Model results are derived from land points only, masked to match the spatial and temporal coverage of the GPCC dataset (denoted 'G' in the seasonal scaling factor panel). Grey area represents the individual simulations' 5–95% range; vertical shaded bands show where 75% of models yield positive and negative trends, respectively. BOTTOM LEFT, RIGHT: Thick solid colored lines show observed trends [% per decade] relative to climatological means from four observational datasets for JJA (left) and DJF (right) seasons, compared to the range of model simulations (grey shading) with the best guess scaled multimodel mean shown as a black solid line. Blue and orange vertical shaded bands indicate latitude ranges where all observational datasets and the multimodel mean indicate trends with the same sign (positive blue, negative orange).

Recent multi-year precipitation deficits in several continental regions in subtropical latitudes have been investigated in more detail since AR4. The Mediterranean region has experienced an overall drying trend and more frequent drought conditions over the 20th century (Mariotti, 2010; Hoerling et al., 2011). Australia was afflicted with the most severe and prolonged drought in the instrumental record from 1995 through 2010 (Ummenhofer et al., 2009) which has since abated. Southwestern North America has undergone severe drought conditions over much of the early 21st century (MacDonald, 2010). Each of these regions lies within the subtropical belts wherein model simulations project long-term drying in the winter season as climate warms, although definitive attribution of individual extreme episodes remains elusive.

In summary, there is medium confidence that human influence has contributed to large scale changes in precipitation patterns over land. The expected anthropogenic fingerprints of change in zonal mean precipitation—reductions in low latitudes and increases in northern hemisphere mid to high latitudes—have been detected in annual and some seasonal data. Observational uncertainties including limited global coverage, large natural variability, and challenges in precipitation modeling limit confidence in assessment of climatic changes in precipitation.

10.3.2.3 Changes in Surface Hydrologic Variables

This subsection summarizes recent research on detection and attribution of long-term changes in continental surface hydrologic variables, including soil moisture, evapotranspiration and streamflow. Cryospheric aspects of surface hydrology are discussed in Section 10.5; extremes in surface hydrology (such as drought) and precipitation are covered in Section 10.6.1. The variables discussed here are subject to large modeling uncertainties (Chapter 9) and observational challenges (Chapter 2), which in combination place severe limits on climate change detection and attribution. Detection and attribution of change in these variables were not addressed in AR4. Most studies since AR4 have focused on a few regions with high quality observations and a strong climate change signal.

Direct observational records of soil moisture and surface fluxes tend to be sparse and/or short and recent assessments do not include definitive attribution of change (Jung et al., 2010). Assimilated land surface data sets and new satellite observations (Chapter 2) are promising tools, but assessment of past and future climate change of these variables (Hoekema and Sridhar, 2011) is still generally carried out on derived quantities such as the Palmer Drought Severity Index, as discussed more fully in Section 10.6.1. Recent observations (Jung et al., 2010) show regional trends toward drier soils associated with increased temperature. An optimal detection analysis of reconstructed evapotranspiration detects the effects of anthropongic forcings on evapotranspiration, with the CNRM-CM5 model simulating changes consistent with those estimated to have occurred (Douville et al., 2012).

Streamflow observations can extend across multiple decades, but flows are subject to large non-climatic human influence such as diversions and land use change that must be accounted for in order to assess

climatic change. Trends toward earlier timing of snowmelt-driven streamflows in the western US since 1950 have been demonstrated to be different from natural variability (Hidalgo et al., 2009). Similarly, internal variability associated with naturally varying predictors such as the PDO could not account for recent declines in a statistical assessment of northern Rocky Mountain streamflow (St Jacques et al., 2010). Statistical analyses of streamflows demonstrate regionally varying changes consistent with increasing temperature, in Scandinavia (Wilson et al., 2010), Europe (Stahl et al., 2010), the United States (Krakauer and Fung, 2008); Wang and Hejazi (2011). Observed increases in Arctic river discharge, which could be a good integrator for monitoring changes in precipitation in high latitudes, are found to be explainable only if model simulations include anthropogenic forcings.

Barnett et al. (2008) analysed changes in the surface hydrology of the western United States, considering snow pack (measured as snow water equivalent), the timing of runoff into major rivers in the region, and average January to March daily minimum temperature over the region, the two hydrological variables they stdied being closely related to temperature. Observed changes were compared with the output of a regional hydrologic model forced by the PCM and MIROC climate models. They derived a fingerprint of anthropogenic changes from the two climate models and found that the observations, when projected onto the fingerprint of anthropogenic changes, show a positive signal strength consistent with the model simulations which falls outside the range expected from internal variability as estimated from 1,600 years of downscaled climate model data. They conclude that there is a detectable and attributable anthropogenic signature on the hydrology of this region.

In summary there is medium confidence that human influence has affected stream flow and evapotranspiration. Detection and attribution studies have only been applied to limited regions and using a few models. Observational uncertainties are large and in the case of evapotranspiration depend on reconstructions using land surface models.

10.3.3 Atmospheric Circulation and Patterns of Variability

The atmospheric circulation is driven by the uneven heating of the Earth's surface by solar radiation. The circulation transports heat from warm to cold regions and thereby acts to reduce temperature contrasts. Thus, changes in circulation and in patterns of variability are of critical importance for the climate system influencing regional climate and regional climate variability. Any such changes are important for local climate change since they could act to reinforce or counteract the effects of external forcings on climate in a particular region. Observed changes in atmospheric circulation and patterns of variability are reviewed in Section 2.6. While there are new and improved datasets now available, changes in patterns of variability remain difficult to detect.

Since AR4 progress has been made in understanding the causes of changes in circulation related climate phenomena and modes of variability like tropical circulation, NAM and SAM. For other climate phenomena, like ENSO, IOD, PDO, and monsoons, there are large observational and modelling uncertainties (see Chapters 2 and 14), and confidence is low that changes in these phenomena, if observed, can be attributed to human-induced influence.

10.3.3.1 Tropical Circulation

Various indicators of the width of the tropical belt determined based on independent data sets suggest that the tropical belt as a whole has widened since 1979, however the magnitude of this change is very uncertain (Davis and Rosenlof, 2012; Fu and Lin, 2011; Fu et al., 2006; Hu and Fu, 2007; Hu et al., 2011; Hudson et al., 2006; Lu et al., 2009; Seidel and Randel, 2007; Seidel et al., 2008; Wilcox et al., 2012).

CMIP5 simulations suggest that changes in anthropogenic forcings could contribute to the observed widening of the Hadley circulation (Hu et al., 2012). The poleward expansion of the Hadley circulation as determined from reanalysis (from 0.9° to 1.9° in latitude per decade) is considerably greater than determined from CMIP5 simulations (about 0.2° per decade). It is not clear why models systematically underestimate forced poleward expansion of the Hadley circulation and what is the contribution of natural variability to the observed magnitude of change.

There is robust evidence that Antarctic ozone depletion is a major factor in causing poleward expansion of the southern Hadley cell during austral summer (Figure 10.11) (Polvani et al., 2010; Son et al., 2009; Son et al., 2008; Son et al., 2010) . In reanalysis data a detectable signal of ozone forcing is separable from other external forcing including greenhouse gases when utilizing both CMIP5 and CMIP3 simulations combined (Min and Son, 2012). An analysis of CMIP3 simulations suggest that black carbon aerosols and tropospheric ozone were the main drivers of the observed poleward expansion of the northern Hadley cell in boreal summer (Allen et al., 2012). CMIP3 simulations for the 21st century show that global greenhouse warming will lead to widening of the Hadley circulation (Lu et al., 2007), and that projected ozone recovery in the 21st century would offset the widening of the southern Hadley cell caused by greenhouse warming (Son et al., 2009; Son et al., 2008; Son et al., 2010). CMIP5 simulations for the 21st century demonstrate that the widening of the Hadley circulation increases with external radiative forcing (Hu et al., 2012). Global greenhouse warming causes increase in static stability, such that the onset of baroclinicity is shifted poleward, leading to poleward expansion of the Hadley circulation (Frierson, 2006; Frierson et al., 2007; Hu and Fu, 2007; Lu et al., 2007) Tropical SST warming may also contribute to widening of the Hadley circulation. AGCM simulations forced by observed time-varying SST yield widening by about 1° in latitude over 1979–2002 (Hu et al., 2011).

[INSERT FIGURE 10.11 HERE]

Figure 10.11: December-February mean change of southern border of Hadley. Unit is degree in latitude per decade. Reanalysis datasets are marked with different colors. Trends are all calculated over the period of 1979–2005, except for ERA40 over 1979–2001 and ERA-interim over 1989–2005. According to CMIP5, historicalNAT, historicalGHG, and historical denote historical simulations with natural forcing, observed increasing GHG forcing, and all forcings, respectively. Adapted from Hu et al. (2012).

In summary, there are multiple lines of evidence that the Hadley cell and the tropical belt as a whole has widened since at least 1979; however the magnitude of the widening is very uncertain. Based on modelling studies there is medium confidence that stratospheric ozone depletion has contributed to the observed poleward shift of the southern Hadley cell border during austral summer. The contributions of increase in greenhouse gases. natural forcings and internal climate variability to the observed poleward expansion of the Hadley circulation remain very uncertain.

10.3.3.2 NAM/NAO

Since the publication of the AR4 the North Atlantic Oscillation has tended to be in a negative phase. This means that the positive trend in the NAO discussed in the AR4 has considerably weakened when evaluated up to 2011 (see also Chapter 2). Similar results apply to the closely-related Northern Annular Mode, though its upward trend over the past 60 years is marginally significant in the 20th Century Reanalysis (Compo et al., 2011) but not in HadSLP2r (Allan and Ansell, 2006) (Figure 10.12). An analysis of CMIP5 models show that they simulate positive trends in NAM over this period, albeit not as large as those observed, and still within the range of natural internal variability (Figure 10.12).

[INSERT FIGURE 10.12 HERE]

Figure 10.12: Simulated and observed 1951–2011 trends in the Northern Annular Mode (NAM) index (a) and Southern Annular Mode (SAM) index (b) by season. The NAM is a Li and Wang (Li and Wang, 2003) index based on the difference between zonal mean SLP at 35°N and 65°N. and the, and the SAM index is a difference between mean SLP at stations located at close to 40°S and stations located close to 65°S (Marshall, 2003). Both indices are defined without normalisation, so that the magnitudes of simulated and observed trends can be compared. Black lines show observed trends from the HadSLP2r dataset (Allan and Ansell, 2006) (solid), the 20th Century Reanalysis (Compo et al., 2011) (dotted) and the Marshall (2003) SAM index (dashed). While the synthetic Marshall indices have data present from 1951, the Marshall (2003) index itself begins in 1957. Grey bars show approximate 5th-95th percentile ranges of control trends, and coloured bars show 5–95% significance ranges for ensemble mean trends in response to greenhouse gas (red), aerosols (green), ozone (light blue) and natural (dark blue) forcings, based on CMIP5 individual forcing simulations. Taken from Gillett and Fyfe (2012).

Other work (Woollings, 2008) demonstrate while the Northern Annular Mode is largely barotropic in structure, the simulated response to anthropogenic forcing has a strong baroclinic component, with an opposite geopotential height trends in the mid-troposphere compared to the surface in many models. Thus while the circulation response to anthropogenic forcing may project onto the NAM, it is not entirely captured by the NAM index.

Consistent with previous findings (Hegerl et al., 2007b), Gillett and Fyfe (2012) find that greenhouse gases tend to drive a positive NAM response in the CMIP5 models. Recent modelling work also indicates that ozone changes drive a small positive NAM response in spring (Gillett and Fyfe, 2012; Morgenstern et al., 2010).

10.3.3.3 SAM

The Southern Annular Mode (SAM) index has remained mainly positive since the publication of the AR4, although it has not been as strongly positive as in the late 1990s. Nonetheless, an index of the SAM shows a significant positive trend in most seasons and datasets over the 1951–2011 period (Figure 10.11). Recent modelling studies confirm earlier findings that the increase in greenhouse gas concentrations tends to lead to a strengthening and poleward shift of the Southern Hemisphere midlatitude jet (Gillett and Fyfe, 2012; Karpechko et al., 2008; Sigmond et al., 2011; Son et al., 2008; Son et al., 2010; Staten et al., 2011) which projects onto the positive phase of the Southern Annular Mode. Stratospheric ozone depletion also induces a strengthening and poleward shift of the midlatitude jet, with the largest response in austral summer (Gillett and Fyfe, 2012; Karpechko et al., 2008; McLandress et al., 2011; Polvani et al., 2011; Sigmond et al., 2011; Son et al., 2008; Son et al., 2010). Sigmond et al. (2011) find approximately equal contributions to simulated annual mean SAM trends from greenhouse gases and stratospheric ozone depletion up to the present. Fogt et al. (2009) demonstrate that observed SAM trends over the period 1957–2005 are positive in all seasons, but only statistically significant in DJF and MAM, based on simulated internal variability. Roscoe and Haigh (2007) apply a regression-based approach and find that stratospheric ozone changes are the primary driver of observed trends in the SAM. Observed trends are also consistent with CMIP3 simulations including stratospheric ozone changes in all seasons, though in MAM observed trends are roughly twice as large as those simulated (Miller et al., 2006). Broadly consistent results are found when comparing observed trends and CMIP5 simulations (Figure 10.11), with a station-based SAM index showing a significant positive trend in MAM, JJA and DJF, compared to simulated internal variability over the 1951–2010 period. Fogt et al. (2009) find that the largest forced response has likely occurred in DJF, the season in which stratospheric ozone depletion has been the dominant contributor to the observed trends.

Taking these findings together, it is *likely* that the positive trend in the SAM seen in Austral summer since 1951 is due in part to stratospheric ozone depletion.

10.3.3.4 Change in Global Sea Level Pressure Patterns

A number of studies have applied formal detection and attribution studies to global fields of atmospheric sea level pressure (SLP) finding detection of human influence on global patterns of SLP (Gillett and Stott, 2009; Gillett et al., 2005; Gillett et al., 2003). Analysing the contributions of different forcings to observed changes in SLP, Gillett and Fyfe (2012) find detectable influences separately of greenhouse gas, aerosols and ozone changes, each of which have distinct zonal, meridional and seasonal structures in patterns of SLP, strengthening evidence for a human influence on SLP, including to annular mode trends. Based on the robustness of the evidence from multiple models we conclude that it is *likely* that human influence has altered sea level pressure patterns globally since 1951.

10.4 Changes in Ocean Properties

The objective of this section is to assess oceanic changes including in ocean heat content, ocean salinity and freshwater fluxes, sea level, and oxygen. The attribution of ocean acidification to rising carbon dioxide concentrations is discussed in Section 3.8.2 (Box 3.2 and Table 10.1)

10.4.1 Ocean Temperature and Heat Content

The oceans are key part of the earth's energy balance. Observational studies continue to demonstrate that the ocean heat content is increasing in the upper layers of the ocean during the second half of the 20th century and early 21st century (Section 3.2; Bindoff et al., 2007), and that this increase is consistent with a net positive radiative imbalance in the climate system. Significantly, this heat content increase is an order of magnitude larger than the increase in energy content of any other component of the Earth's ocean-

atmosphere-cryosphere system (e.g., Boxes 3.1 and 13.1; Bindoff et al., 2007; Church et al., 2011; Hansen et al., 2011).

Despite the evidence for anthropogenic warming of the ocean, the level of confidence in the conclusions of the AR4 report – that the warming of the upper several hundred meters of the ocean during the second half of the 20th century was "likely" to be due to anthropogenic forcing – reflected the level of uncertainties at that time. The major uncertainty was an apparently large decadal variability in the observational estimates not simulated by climate models (Hegerl et al., 2007b; Solomon et al., 2007, in their Table 9.4), raising concerns about the capacity of climate models to simulate observed variability as well as the presence of non-climate related biases in the observations of ocean heat content change (AchutaRao et al., 2006; Gregory et al., 2004).

After the IPCC AR4 report in 2007, time-and depth-dependent systematic errors in bathythermographs temperatures were discovered (Gouretski and Koltermann, 2007; and Section 3.2). Bathythermograph data account for a large fraction of the historical temperature observations and are therefore a source of bias in ocean heat content studies. Bias corrections were then developed and applied to observations. With the newer bias-corrected estimates (Domingues et al., 2008; Ishii and Kimoto, 2009; Levitus et al., 2009; Wijffels et al., 2008), it became obvious that the large decadal variability in earlier estimates of global upper-ocean heat content was an observational artifact (Section 3.2).

A comparison (Domingues et al., 2008) between estimates of global ocean heat content in the upper 700 m, based on bias-corrected ocean temperature data and two sets of CMIP3 models found that simulations forced with the most complete set of natural and anthropogenic forcings agreed more closely with observations, both in terms of the decadal variability and multi-decadal trend (Figure 10.13a). For the simulations with the most complete set of forcings, the multi-model ensemble mean trend was only 10% smaller than observed for 1961–1999. Model simulations that included only anthropogenic forcing (i.e., no solar or volcanic forcing) significantly overestimate the multi-decadal trend and underestimate decadal variability. This overestimate of the trend is partially caused by the ocean's response to volcanic eruptions, which results in rapid cooling followed by decadal or longer time variations during the recovery phase. Although it has been suggested (Gregory, 2010) that the cooling trend from successive volcanic events is an artifact because models were not spun up with volcanic forcing, this discrepancy is not expected to be as significant in the upper-ocean as in the deeper layers where longer term adjustments take place (Gregory et al., 2012). Thus for the upper ocean, the more frequent eruptions during the second half of the 20th century have caused a multi-decadal cooling that partially offsets the anthropogenic warming and contributes to the apparent variability (AchutaRao et al., 2007; Church et al., 2005; Delworth et al., 2005; Domingues et al., 2008; Fyfe, 2006; Gleckler et al., 2006; Gregory et al., 2006; Palmer et al., 2009; Stenchikov et al., 2009).

Gleckler et al. (2012) examined the detection and attribution of upper-ocean warming in the context of uncertainties in the underlying observational data sets, models and methods. Using three bias-corrected observational estimates of upper-ocean temperature changes (Domingues et al., 2008; Ishii and Kimoto, 2009; Levitus et al., 2009) and models from the CMIP3 multi-model archive, they found that multi-decadal trends in the observations were best understood by including contributions from both natural and anthropogenic forcings. The anthropogenic fingerprint in observed upper-ocean warming, driven by global mean and basin-scale pattern changes, was also detected. The strength of this signal (estimated from successively longer trend periods of ocean heat content starting from 1970) crossed the 5% and 1% significance threshold in 1980 and progressively becomes more strongly detected for longer trends (Figure 10.13b), for all ocean heat content time series. While the models do underestimate decadal variability, they would have to underestimate variability by a factor of two (not by 25–28% as the CMIP3 models did) in order to throw the anthropogenic fingerprint into question. This result is robust to a number of observational, model and methodological or structural uncertainties.

In an analysis of upper-ocean (0–700 m) temperature changes for 1955-2004, using bias-corrected observations and 12 global climate models from the recent CMIP5 experiments, (Pierce et al., 2012) build on previous detection and attribution studies of ocean temperature (Barnett et al., 2001; Barnett et al., 2005; Pierce et al., 2006a). They find that observed temperature changes are inconsistent with the effects of natural climate variability (signal strengths are separated from zero with $p < 0.05$) – either internal to the climate system alone or externally forced by solar fluctuations and volcanic eruptions. However, the observed

changes are consistent with those expected from anthropogenically induced changes in greenhouse gases and aerosols.

With greater consistency and agreement across observational data sets and simulations of the climate system with natural and anthropogenic forcings, the major uncertainties at the time of AR4 have now largely been resolved. Anthropogenic attribution of warming from recent formal detection and attribution studies (Gleckler et al., 2012; Pierce et al., 2012) have made use of bias-corrected observations and have systematically explored methodological uncertainties, yielding more confidence in the results. The very high levels of confidence and the increased understanding of the contributions from both natural and anthropogenic sources across the many studies mean that it is extremely certain (that is greater than 95% probability) that the increase in global ocean heat content observed in the upper 700 m in the latter half of the 20th century can be attributed to anthropogenic forcing.

While there is very high confidence in understanding the causes of global heat content increases, attribution of regional heat content changes are less certain. Earlier regional studies have used a fixed depth approach and only considered basin-scale averages (Barnett et al., 2005). At regional scales, however, changes in advection of ocean heat are important and need to be isolated from changes due to air-sea heat fluxes (Grist et al., 2010; Palmer et al., 2009). Their fixed isotherm (rather than fixed depth) approach to optimal detection analysis, in addition to being largely insensitive to observational biases, is designed to separate the ocean's response to air-sea flux changes from advective changes. Air-sea fluxes are the primary mechanism by which the oceans are expected to respond to externally forced anthropogenic and natural volcanic influences. The finer temporal resolution of the analysis allowed to attribute distinct short-lived cooling episodes to major volcanic eruptions while, at multi-decadal time scales, a more spatially uniform near-surface (~ upper 200 m) warming pattern was detected in all ocean basins and attributed to anthropogenic causes at the 95% confidence level. Considering that individual ocean basins are affected by different observational and modelling uncertainties and that internal variability is larger at smaller scales, simultaneous detection of significant anthropogenic forcing in each ocean basin (except in high latitudes where the isotherm approach has limitations due to outcropping of isotherms at the ocean surface) provides more compelling evidence of human influence at regional scales of the near-surface ocean warming observed during the latter half of the 20th century.

[INSERT FIGURE 10.13 HERE]

Figure 10.13: A) Comparison of observed global ocean heat content for the upper 700 m with simulations from six CMIP3 models that included anthropogenic and natural (solar and volcanic) forcings. The timing of volcanic eruptions and associated aerosol loadings are shown at base of panel (Domingues et al., 2008), B) Signal-to-noise (S/N) ratio (plotted as a function of increasing trend length L) of basin-scale changes in volume averaged temperature of newer, XBT-corrected data (solid red, orange and blue lines), older, uncorrected data (dashed red and orange lines); the average of the three corrected observational sets (AveObs; dashed purple line); and V and NoV models (black and grey solid lines respectively). The 1% and 5% significance thresholds are shown (as horizontal grey lines) and assume a Gaussian distribution of noise trends in the V-models control-run pseudo-principal components. The detection time is defined as the year at which S/N exceeds and remains above a stipulated significance threshold (Gleckler et al., 2012).

10.4.2 Ocean Salinity and Freshwater Fluxes

There is increasing recognition of the importance of ocean salinity as an essential climate variable (Doherty et al., 2009), particularly for understanding the hydrological cycle. In the IPCC Fourth Assessment Report observed ocean salinity change in the oceans indicated that there was a systematic pattern of increased salinity in the shallow subtropics and a tendency to freshening of waters that originate in the polar regions (Bindoff et al., 2007; Hegerl et al., 2007b) broadly consistent with an acceleration of the hydrological cycle (Figure 10.14a, upper and lower panels). New atlases and revisions of the earlier work based on the increasing number of the ARGO profile data, and historical data have extended the observational salinity data sets allowing the examination of the long term changes at the surface and interior of the ocean (Section 3.3) and broadly supports precipitation changes over land (see Section 10.3.2.2 and Chapter 2).

Patterns of subsurface salinity changes largely follow an enhancement of the existing mean pattern within the ocean. For example, the inter-basin contrast between the Atlantic (salty) and Pacific Oceans (fresh) has intensified over the observed record (Boyer et al., 2005; Durack and Wijffels, 2010; Hosoda et al., 2009; Roemmich and Gilson, 2009; von Schuckmann et al., 2009). In the Southern Ocean, many studies show a

coherent freshening of Antarctic Intermediate Water that is subducted at about 50°S (Bindoff and McDougall, 2000; Boyer et al., 2005; Curry et al., 2003; Durack and Wijffels, 2010; Helm et al., 2010; Hosoda et al., 2009; Johnson and Orsi, 1997; Roemmich and Gilson, 2009; Wong et al., 1999b). These new analyses also show a clear increase in salinity of the high-salinity subtropical waters, and a freshening of the high latitude waters (e.g., Figure 10.14a).

Observed surface salinity changes also suggest an amplification in the global water cycle has occurred and agrees with other regional studies (Cravatte et al., 2009; Curry et al., 2003; Wong et al., 1999a) , and other global analyses of surface, and subsurface salinity change (Boyer et al., 2005; Durack and Wijffels, 2010; Hosoda et al., 2009; Roemmich and Gilson, 2009) (see Figures 3.4a and 10.14b "ocean obs" point, correlation 0.7). The fifty year trends in surface salinity show that there is a strong positive correlation between the mean climate of the surface salinity and its temporal changes from 1950 to 2000. This correlation between the climate and the trends in surface salinity implies that fresh surface waters get fresher and salty waters get saltier (Durack et al., 2012; and Section 3.3). Such patterns of surface salinity change are also found in AOGCM simulations both for the 20th century and projected future changes into the 21st century (Figure 10.14b). The pattern of temporal change in observations from CMIP3 simulations is particularly strong for those projections using SRES emission scenarios which have pattern correlations greater than 0.6 (Figure 10.14b). For the period 1950–2000 the observations of surface salinity amplification, (as a function of global temperature increase per degree surface warming), is 16 ± 10%, and is twice the simulated surface salinity change in CMIP3 models. When the water flux amplification (that is precipitation minus evaporation) is examined in CMIP3 models, they show an amplification of the oceanic hydrological cycle to be about 8 ± 5%, and is consistent with the response that is expected from the Clausius-Clapeyron equation. The implication is that the CMIP3 ocean models mix surface salinity (and heat) too strongly into the ocean and stratify at a slower rate than is observed (Durack et al., 2012).

While there are now many established observed long term trends of salinity change at the ocean surface and within the interior ocean at regional and global scales (Section 3.3), there are relatively few formal detection and attribution studies of these changes due to anthropogenic forcing. Analysis at the regional scale of the observed recent surface salinity increases in the North Atlantic (20°N to 50°N) show an emerging signal that could be attributed to anthropogenic forcings but is not significant compared with internal variability (Stott et al., 2008b; Terray et al., 2011) and Figure 10.14c). On a larger spatial scale, the equatorial band from 30°S–50°N surface salinity patterns have detected significant changes at the 5–95% confidence level compared with internal variability and have been formally attributable to anthropogenic forcing (Terray et al., 2011), The strongest detected signals are in the tropics (TRO, 30°S–30°N) and the Western Pacific. The east-west contrast between the Pacific and Atlantic oceans is also enhanced with significant contributions from anthropogenic forcing. On a global scale surface and subsurface salinity changes (1955–2004) that cannot be explained by natural variability (probability is <0.05) over the upper 250 m of the water column (Pierce et al., 2012). However, the observed salinity changes match the model distribution of forced changes (greenhouse gases and tropospheric aerosols), with the observations typically falling between the 25th and 75th percentile of the model distribution at all depth levels for salinity (and temperature). Natural external variability taken from the historicalNat simulations does not match the observations at all thus excluding the hypothesis that observed trends are can be explained by just solar or volcanic variations.

The results from surface salinity trends and changes are consistent with the results from studies of precipitation over the tropical ocean from the shorter satellite record (Allan and Soden, 2008; Wentz et al., 2007). However, the surface salinity changes differ in amplitude with the much lower estimates of long-term precipitation changes obtained from continental land stations (Wentz et al., 2007; Zhang et al., 2007c) and this result remains unresolved. However, these surface salinity results are consistent with our understanding of the thermodynamic response of the atmosphere to warming (Held and Soden, 2006; Stephens and Hu, 2010) and the amplification of the oceanic water cycle. These expert studies and the detection and attribution studies for the tropical oceans (Terray et al., 2011) and global pattern of ocean salinity change (Pierce et al., 2012), when combined with our understanding of the physics of the water cycle and estimates of internal climate variability shows a a detectable signal that has a significant contribution from anthropogenic forcing. It is therefore likely that some of the observed changes in surface salinity in the 20th and early 21st century are attributable to anthropogenic forcing.

[INSERT FIGURE 10.14 HERE]

Figure 10.14: Ocean salinity change and hydrologic cycle. (A) Ocean salinity change observed in the interior of the ocean (A, lower panel) and comparison with 10 CMIP3 model projections of precipitation minus evaporation for the same period as the observed changes (1970 to 1990's) (A, top panel). (B) The amplification of the current surface salinity pattern over a 50 year period as a function of global temperature change. Ocean surface salinity pattern amplification has an 8% increase for the 1950 to 2000 period, and a correlation with surface salinity climatology of 0.7 (see text, and Section 3.3). Also on this panel coupled CMIP3 AOGCM with all forcings emission scenarios and from 20th and 21st century simulations. A total of 93 simulations have been used. The colours filling the simulation symbols indicate the correlation between the surface salinity change and the surface salinity climatology. Dark red is a correlation of 0.8 and dark blue is 0.0. (C) Regional detection and attribution in the equatorial Pacific and Atlantic Oceans for 1970 to 2002. Scaling factors for all forcings (anthropogenic) fingerprint are show (see Box 10.1) with their 5–95% uncertainty range, estimated using the total least square approach. Full domain (FDO, 30°S–50°N), Tropics (TRO, 30°S–30°N), Pacific (PAC, 30°S–30°N), west Pacific (WPAC, 120°E–160°W), east Pacific (EPAC, 160°W–80°W), Atlantic (ATL, 30°S–50°N), subtropical north Atlantic (NATL, 20°N–40°N) and equatorial Atlantic (EATL, 20°S–20°N) factors are shown. Black filled dots indicate when the residual consistency test passes with a truncation of 16 whereas empty circles indicate a needed higher truncation to pass the test. (A, B and C) are from (Helm et al., 2010), (Durack et al., 2012) and (Terray et al., 2011), respectively.

10.4.3 Sea Level

At the time of the AR4, the historical sea level rise budget had not been closed (within uncertainties), and there were few studies quantifying the contribution of anthropogenic forcing to the observed sea level rise and glacier melting. Relying on expert assessment, the AR4 had concluded based on modelling and ocean heat content studies that ocean warming and glacier mass loss had very likely contributed to sea level rise during the latter half of the 20th century. The AR4 had observed that climate models which included anthropogenic and natural forcings simulated the observed thermal expansion since 1961 reasonably well, and that it is very unlikely that the warming during the past half century is due only to known natural causes (Hegerl et al., 2007b).

Since then, corrections applied to instrumental errors in ocean temperature measurements have significantly improved estimates of upper-ocean heat content (see Sections 3.2 and 10.4.1), and therefore ocean thermal expansion . Along with other developments, this has enabled closure of the global sea level rise budget for recent decades (Section 13.3.6). Global energy budget calculations (Box 3.1 and Box 13.1) indicate that ocean warming accounts for over 90% of the earth's energy increase between 1971 and 2010. The budget calculations show that the two major contributions to the rate of sea level rise have been thermal expansion and glacier melting. Climate model simulations with historical forcings capture these contributions to a fair degree. The agreement between observed and modelled thermosteric sea level changes is found to be forcing dependent (Domingues et al., 2008). Inclusion of both anthropogenic (greenhouse gases and aerosols) and natural (solar and volcanic) forcings is required to simulate the multi-decadal trend in thermosteric sea level rise during the second half of the 20th century, and variability resulting from explosive volcanic eruptions (Palmer et al., 2009).

The strong physical relationship between thermosteric sea level and ocean heat content (through the equation of state for seawater) means that, we can draw the same conclusions for the global thermosteric height rise as for upper-ocean heat content (Section 10.4.1). That is, it is extremely certain that the increases in global mean thermosteric sea level observed during the second half of the 20th century has a substantial contribution from anthropogenic forcing.

On ocean basin scales, detection and attribution studies do show the emergence of detectable signals in the thermosteric component of sea level that can be largely attributed to human influence (Barnett et al., 2005; Pierce et al., 2012; and Figure 10.20) . Regional changes in sea level at the sub-ocean basin scales and finer exhibit more complex variations associated with natural (dynamical) modes of climate variability (Section 13.6). In some regions, sea level trends have been observed to differ significantly from global mean trends. These have been related to thermosteric changes in some areas and in others to changing wind fields and resulting changes in the ocean circulation (Han et al., 2010; Merrifield and Maltrud, 2011; Timmermann et al., 2010). The regional variability on decadal and longer time-scales can be quite large (and not well quantified in currently available observations) compared to secular changes in the winds that influence sea level. Detection of human influences on sea level at the regional scale (that is smaller than sub-ocean basin scales) is currently limited by the relatively small anthropogenic contributions (compared to natural variability) and the need for more sophisticated approaches than currently available.

10.4.4 Oxygen

Oxygen is an important physical and biological tracer in the ocean (Section 3.8.3), as well as an important element of the earth's carbon cycle (Section 6.4.6). Despite the relatively few observational studies of oxygen change in the oceans that are generally limited to a few individual basins and cruise sections (Aoki et al., 2005; Bindoff and McDougall, 2000; Emerson et al., 2004; Keeling and Garcia, 2002; Mecking et al., 2006; Nakanowatari et al., 2007; Ono et al., 2001) they all show pattern of change consistent with the known ocean circulation and surface ventilation. Global analyses of oxygen data from the 1960's to 1990's for change confirm these earlier results and extends the spatial coverage from local to global scales (Helm et al., 2011). The strongest decreases in oxygen occur in the mid-latitudes of both hemispheres, near regions where there is strong water renewal and exchange between the ocean interior and surface waters. Approximately 15% of the global decrease can be explained by a warmer mixed-layer reducing the capacity of water to store oxygen. The remainder of this global decrease is consistent with the patterns of change simulated by low resolution earth system models or ocean models including coupled bio-geochemical cycles (Deutsch et al., 2005; Matear and Hirst, 2003; Matear et al., 2000; Plattner et al., 2002). In all of these simulations the decrease in oxygen in the upper ocean results from decreased exchange of surface waters with the ocean interior caused largely by increased ocean stratification. The observed decrease $-0.55 \pm 0.13 \times 10^{14}$ mol yr^{-1} (Helm et al., 2011) is the same magnitude as the decrease estimated from rising oxygen concentrations in the atmosphere (Manning and Keeling, 2006). One detection and attribution study that used two Earth System Models concluded that observed changes for the Atlantic Ocean are "indistinguishable from natural internal variability" and the global zonal mean changes the external forcing (all forcings including greenhouse gases) has a detectable influence at the 90% confidence level. The chief sources of uncertainty are the paucity of oxygen observations, particularly in time, the precise role of the biological pump and changes in ocean productivity, and model biases particularly near the oxygen minimum zone in tropical waters (Keeling et al., 2010; Stramma et al., 2010; Brandt et al., 2010). These results and the surface temperatures (Section 10.3.2), increased ocean heat content (Section 10.4.1) and observed increased in ocean stratification (Section 3.2.2), and oxygen changes (this Section) have all been attributed human influence. When these lines of evidence are taken together with the physical understanding from simulations of oxygen change forced by warmer surface water or increasing greenhouse gases suggest it is about as likely as not that the observed oxygen decreases can be attributed to human influences.

10.5 Cryosphere

This section considers changes in sea ice, ice sheets and ice shelves, glaciers, snow cover and permafrost.

10.5.1 Sea Ice

10.5.1.1 Arctic and Antarctic Sea Ice

The Arctic cryosphere shows large visible changes over the last decade as noted in Chapter 4 and many of the shifts are indicators of major regional and global feedback processes (Kattsov et al., 2010). Of principal importance is “Arctic Amplification” (see Box 5.1) where surface temperatures in the Arctic are increasing faster than elsewhere in the world.

The rate of decline of Arctic sea ice thickness and September sea ice extent has increased considerably in the first decade of the 21st century (Alekseev et al., 2009; Comiso, 2012; Comiso and Nishio, 2008a, 2008b; Deser and Teng, 2008; Maslanik et al., 2007; Nghiem et al., 2007; Polyakov et al., 2012). There was a rapid reduction in September 2007 to 37% less extent relative to the 1979–2000 climatology (Figure 4.11, in Section 4.2.2). While at the time it was unclear whether the record minimum in 2007 was an extreme outlier or not, every year since then (2008–2011) has a lower September extent than the years before 2007, with 2011 being second lowest compared with 2007. All recent years have ice extents that fall below two standard deviations of the long term sea ice record and below the long term trend line. In addition the amount of old, thick multi-year sea ice in the Arctic has also decreased by 50% from 2005 through 2012 (Giles et al., 2008; Kwok and Untersteiner, 2011; Kwok et al., 2009) and Figures 4.13 and 4.14. Sea ice has become more mobile (Gascard and al, 2008). We now have five years of data which show sea ice conditions are now substantially different to that observed prior to 2007.

Confidence in detection of change comes in part from the consistency of multiple lines of evidence. In the last five years evidence has continued to accumulate from a range of observational studies that systematic changes are occurring in the Arctic. Persistent trends in many Arctic variables, including sea ice extent, the timing of spring snow melt, increased shrubbiness in tundra regions, changes in permafrost, increased area coverage of forest fires, increased ocean temperatures, changes in ecosystems, as well as Arctic-wide increases in air temperatures, can no longer be associated solely with the dominant climate variability patterns such as the Arctic Oscillation or Pacific North American pattern (Brown and Robinson, 2011; Nagato and Tanaka, 2012; Overland, 2009; Quadrelli and Wallace, 2004; Vorosmarty et al., 2008; Wassmann et al., 2011). Duarte et al. (2012) completed a meta-analysis calling for recognition of abrupt climate change in the Arctic.

The increase in the magnitude of recent Arctic temperature and decrease in sea ice changes are hypothesized to be due to coupled Arctic amplification mechanisms (Miller et al., 2010; Serreze and Francis, 2006). These feedbacks in the Arctic climate system suggest that the Arctic is sensitive to external forcing. Historically, changes were damped by the rapid formation of sea ice in autumn causing a negative feedback and rapid seasonal cooling. But recently, the increased mobility and loss of multi-year sea ice, combined with enhanced heat storage in the sea-ice free regions of the Arctic Ocean form a connected set of processes with positive feedbacks increasing Arctic temperatures and decreasing sea ice extent (Gascard and al, 2008; Serreze et al., 2009; Stroeve et al., 2012; Stroeve et al., 2011). In addition to the well known *ice albedo* feedback where decreased sea ice cover decreases the amount of *insolation* reflected from the surface, there is a late summer/early autumn positive *ice insulation* feedback due to additional ocean heat storage in areas previously covered by sea ice (Jackson et al., 2010). Arctic amplification is also a consequence of poleward heat transport in the atmosphere and ocean (Doscher et al., 2010; Graversen and Wang, 2009; Langen and Alexeev, 2007).

It appears that recent Arctic changes are in response to a combination of gradual global warming, warm anomalies in internal climate variability, and impacts from multiple feedbacks. For example, when the 2007 sea ice minimum occurred, Arctic temperatures had been rising and sea ice extent had been decreasing over the previous two decades (Screen and Simmonds, 2010; Stroeve et al., 2008). Nevertheless, it took an unusually persistent southerly wind pattern over the summer months to initiate the loss event in 2007 (Wang et al., 2009a; Zhang et al., 2008b). Similar wind patterns in previous years did not initiate major reductions in sea ice extent because the sea ice was too thick to respond (Overland et al., 2008). Increased oceanic heat transport by the Barents Sea inflow in the first decade of the 21st century may also play a role in determining sea ice anomalies in the Atlantic Arctic (Dickson et al., 2000; Semenov, 2008). It is likely that these Arctic amplification mechanisms are currently affecting regional Arctic climate, given the reduction of late summer sea ice extent over the last decade in the Barents Sea, the Arctic Ocean north of Siberia, and especially the Chukchi and Beaufort Seas, in addition to the loss of old thick sea ice, and record air temperatures in autumn observed at adjacent coastal stations. But it also suggests that the timing of such sea ice loss events in the future will be difficult to project. This conclusion is also supported by the range of results for ensemble members of sea ice model projections. The combination of internal variability of climate and the contribution of emissions by humans of greenhouse gases are likely responsible for the recent decreases in sea ice (Kay et al., 2011c; Kinnard et al., 2011; Notz and Marotzke, 2012; Overland et al., 2011 [in press]).

Turning to model based attribution studies, (Min et al., 2008c) compared the seasonal evolution of Arctic sea ice extent from observations with those simulated by multiple GCMs for 1953–2006. Comparing changes in both the amplitude and shape of the annual cycle of the sea ice extent reduces the likelihood of spurious detection due to coincidental agreement between the response to anthropogenic forcing and other factors, such as slow internal variability. They found that human influence on the sea ice extent changes can be robustly detected since the early 1990s. The detection result is also robust if the effect of the Northern Annular Mode on observed sea ice change is removed. The anthropogenic signal is also detectable for individual months from May to December, suggesting that human influence, strongest in late summer, now also extends into colder seasons. Kay et al. (2011c) and Jahn et al. (2011, Submitted) used the climate model (CCSM4) to investigate the influence of anthropogenic forcing on late 20th century and early 21st century Arctic sea ice extent trends. On all timescales examined (2–50+ years), the most extreme negative trends observed in the late 20th century cannot be explained by modeled internal variability alone. Comparing trends from the CCSM4 ensemble to observed trends suggests that internal variability could account for

approximately half of the observed 1979–2005 September Arctic sea ice extent loss. Detection of anthropogenic forcing is also shown by comparing September sea ice extent as projected by seven models from the set of CMIP5 models under 4.5 and 8.5RCP emission scenarios to control runs without anthropogenic forcing (Figure 10.15a; Wang and Overland, 2009). Sea ice extents in six of seven models' ensemble members are below the level of their control runs by 2015. The seventh model has large decadal variability (HadGEMS2ES). The same conclusion is reached in Chapter 12 by comparing future sea ice losses under anthropogenic forcing to a commitment scenario. Models also suggest that a continued loss of sea ice requires continued increase in anthropogenic forcing and rising temperatures (Armour et al., 2011; Mahlstein and Knutti, 2011, Submitted; Maslowski et al., 2012; Sedlacek et al., 2011, accepted; Tietsche et al., 2011; Zhang et al., 2010; Zhang, 2010). There does not seem to be evidence for a tipping point; a tipping point would imply that once sea ice extent or volume fell below a certain threshold amount that loss would continue due to internal sea ice processes. Comparing sea ice extent projections with the range of sea ice extent from CMIP5 control runs clearly shows that it is likely that an increased presence of external anthropogenic forcing results in a continued decline of summer sea ice extent, but with considerable inter-annual and decadal variability.

[INSERT FIGURE 10.15 HERE]

Figure 10.15: a) Northern Hemisphere September sea ice extent (>15% ice concentration) simulated by the seven CMIP5 models that matched the mean minimum and seasonality with less than 20% error compared with observations. The thin grey lines are based on pre-industrial control simulations (piControl). The coloured lines are historical runs (1950–2005) together with forced simulations (blue for RCP4.5, green for RCP6.0, and magenta for RCP8.5 emissions scenarios for the period 2006–2015). The thick black line is base on Hadley sea ice analysis (HadleyISST_ice). Panels A-G are models: CCSM4, HadGEM2CC, HadGEM2ES, MIROC−ESM, MIROC−ESMC, MPI−ESM−lr, and ACCESS1. **b)** Similar to a) but for the Southern Hemisphere. Panels A-F are models: CanESM2, MIROC-ESM, MIROC-ESMC, MRI-CGCM3, NorESM1 and BCC-CSM1. For Antarctic sea ice we show results for two models that passed the same selection criteria as for the Northern Hemisphere and the next four models with lowest error scores. Note that the presented models are different for the Northern and Southern Hemisphere based on the selection criteria.

The observed decrease in Arctic sea ice extent tends to exceed the reductions simulated by the climate models available for the IPCC AR4 (Boe et al., 2009; Holland et al., 2010; Stroeve et al., 2007; Vavrus et al., 2011, Submitted; Wang and Overland, 2009). For AR5 the multi-model ensemble mean for CMIP5 is near the observations for 1980-2000, but as in CMIP3 the model spread is relatively large (Massonnet et al., 2012; Stroeve et al., 2012; Stroeve et al., 2007; Wang and Overland, 2012); see also Chapters 11 and 12. This difference between CMIP3 and CMIP5 simulations may relate in part to an underestimate of sea ice drift in climate models (Rampal et al., 2011) and different computation of the sea ice mass balance (Boe et al., 2010; Zhang, 2010). It should be noted that this is a comparison of the single observed climate trajectory with a limited number of climate model projections with relatively few ensemble members to span the range of possible future conditions.

A question as recently as five years ago was whether the recent Arctic warming and sea-ice loss was unique in the instrumental record and whether the observed trend would continue (Serreze et al., 2007). Arctic temperature anomalies in the 1930s were apparently as large as those in the 1990s. The warming of the early 1990s was associated with a persistently positive Arctic Oscillation, which at the time was considered as either a natural variation or global warming (Feldstein, 2002; Overland and Wang, 2005; Overland et al., 2008; Palmer, 1999; Serreze et al., 2000). There is still considerable discussion of the proximate causes of the warm temperature anomalies that occurred in the Arctic in the1920s and 1930s (Ahlmann, 1948; Hegerl et al., 2007a; Hegerl et al., 2007b; Veryard, 1963). The early 20th century warm period, while reflected in the hemispheric average air temperature record (Brohan et al., 2006), did not appear consistently in the mid-latitudes nor on the Pacific side of the Arctic (Johannessen et al., 2004; Wood and Overland, 2010). Polyakov et al. (2003) argued that the Arctic air temperature records reflected a natural cycle of about 50–80 years. However, multiple authors (Bengtsson et al., 2004; Bronnimann et al., 2012; Grant et al., 2009; Wood and Overland, 2010) instead link the 1930s temperatures to internal variability in the North Atlantic atmospheric and ocean circulation as a single episode that was potentially sustained by ocean and sea ice processes in the Arctic and mid-latitude Atlantic. For example in the 1930s, loss of sea ice in the Atlantic sector was not matched by loss of sea ice north of Alaska. The Arctic wide temperature increases in the last decade contrasts with the regional increases in the early 20th century, suggesting that it is unlikely that recent increases are due to the same primary climate process as the early 20th century.

In the case of the Arctic we have high confidence in observations, models' results (comparing with and without anthropogenic forcing), and understanding of dominant physical processes; taking these three factors together it is *very likely* that anthropogenic forcing is a major contributor to the observed decreases in Arctic sea ice.

Whereas sea ice extent in the Arctic has decreased, sea ice extent in the Antarctic has increased slightly since the 1970s. Sea ice extent across the Southern Hemisphere over the year as a whole increased 1% per decade from 1978–2006 with the largest increase in the Ross Sea during the autumn, while sea ice extent has decreased in the Amundsen-Bellingshausen Sea (Comiso and Nishio, 2008b; Turner et al., 2009) (see also Section 4.2.3). However, the observed trend in Antarctic sea ice extent may not be significant compared to simulated internal variability (Turner et al., 2009), or indeed inconsistent with CMIP3 simulations including historical forcings (Hegerl et al., 2007b). Based on Figure 10.15b and (Meehl et al., 2007b), the trend of Antarctic sea ice loss in simulations due to changes in forcing is weak (relative to the Arctic) and the internal variability is high, and thus the time necessary for detection is longer than in the Arctic.

Nonetheless, several recent studies have investigated the possible causes of Antarctic sea ice trends. Inter-annual anomalies in the Southern Annular Mode are positively correlated with Antarctic sea ice extent, though the correlation is not statistically significant (Lefebvre and Goosse, 2008). This has led some investigators to propose that the observed sea ice extent increase has been driven by an increase in the SAM index (Goosse et al., 2009), which itself has likely been driven by greenhouse gas increases and stratospheric ozone depletion (Section 10.3.3.3). Turner et al. (2009) noted that autumn sea ice extent in the Ross Sea is negatively correlated with geopotential height over the Amundsen-Bellingshausen Sea, and that a decrease in geopotential height over this region is simulated in response to stratospheric ozone depletion, leading them to suggest that the observed increase in sea ice extent in the Ross Sea Sector may be a result of stratospheric ozone depletion (WMO, 2010). (Liu and Curry, 2010) note the potential role of precipitation changes to explain sea ice trends for the past three decades. One study of the response of sea ice to stratospheric ozone depletion using a coupled AOGCM suggests a decrease rather than an increase in Antarctic sea ice extent (Sigmond and Fyfe, 2010). An alternative explanation for the lack of melting of Antarctic sea ice is that sub-surface ocean warming, and enhanced freshwater input possibly in part from ice shelf melting, have made the high latitude southern ocean fresher (see Section 3.3) and more stratified, decreasing the upward heat flux and driving more sea ice formation (Goosse et al., 2009; Zhang, 2007). The competing processes causing the trends and variability in Antarctic sea-ice and its surrounding waters is complex and the literature appears contradictory. We therefore have low confidence in the scientific understanding of the observed increase in Antarctic sea ice extent. However the trends are small in both observations and CMIP5 simulations and within the bounds of internal variability.

10.5.2 Ice Sheets, Ice Shelves, and Glaciers

10.5.2.1 Greenland and Antarctic Ice Sheet

The Greenland and Antarctic Ice Sheets are important to regional and global climate because along with other cryospheric elements such as sea ice and permafrost they may cause a polar amplification of surface temperatures, fresh water flux to the ocean, and represent potentially irreversible changes to the state of the earth (HANSEN and LEBEDEFF, 1987). These two ice sheets are important contributors to sea-level rise representing 2/3 of the contributions from all ice covered regions (Jacob et al., 2012; Pritchard et al., 2012) (see Sections 4.4 and 13.4.2). Observations of surface mass balance (increased ablation versus increased snowfall) are dealt with in Section 4.4.3. and the state of ice sheet models are discussed in Sections 13.3 and 13.5. The assessment of attribution of human influences on warming over Antarctica is in Section 10.3.

Attribution of change is difficult as ice sheet and glacier changes are local and ice sheet processes are not generally well represented in climate models, precluding formal studies. However, Greenland observational records show large recent changes. Section 13.3 concludes that regional models for Greenland can reproduce the surface mass balance loss trend quite well if they are forced with the observed meteorological record but not with forcings from Global Climate Model. Regional model simulations (Fettweis et al., 2012) show that Greenland surface melt increases non-linearly with rising temperatures due to the positive feedback between surface albedo and melt.

There have been exceptional changes in Greenland since 2007 marked by record-setting high air temperatures, ice loss by melting, and marine-terminating glacier area loss (Hanna et al., 2012; Mernild et al., 2012) (Section 4.4. 4). Along Greenland's west coast temperatures in 2010 and 2011were the warmest since record keeping began in 1873 resulting in the highest observed melt rates since 1958 (Fettweis et al., 2011a). The annual rate of area loss in marine-terminating glaciers was 3.4 times that of the previous 8 years, when regular observations became available. The last decade (2001–2010) was not only the warmest since 1890, but also had the highest number of warm extremes, defined as occurrences that fall outside the 10% and 90% range of climatological values. The number of extreme values in 2001–2010 was 50% higher than the second most extreme decade of the 1940s. Record surface melts during 2007–2012 summers are linked to persistent atmospheric circulation that favored warm air advection over Greenland. These persistent events have changed in frequency since the beginning of the 2000s (Fettweis et al., 2011b; L'Heureux et al., 2010). Hanna et al. (2012) show a weak relation of Greenland temperatures and ice sheet runoff with the AMO; they are more strongly correlated with a Greenland atmospheric blocking index. Overland et al. (2012) and Francis and Vavrus (2012) suggest that the increased frequency of the Greenland blocking pattern is related to broader scale Arctic changes. Mass loss and melt is Glacier (Holland et al., 2008; Walker et al., 2009).

Hanna et al. (2008) attribute increased Greenland runoff and melt since 1990 to global warming; southern Greenland coastal and Northern Hemisphere summer temperatures were uncorrelated between the 1960s and early 1990s but were significantly positively correlated thereafter. This relationship was modulated by the North Atlantic Oscillation, whose summer index was significantly negatively correlated with southern Greenland summer temperatures until the early 1990s but not thereafter. The most important piece of information is that Greenland ice sheets show recent major melting episodes in response to record temperatures relative to the entire 20th century associated with persistent shifts in early summer atmospheric circulation, and these have become more pronounced since 2007. While many Greenland records are relatively short (two decades), we have confidence that regional modelling and observations tell a consistent story of the response of Greenland temperatures and ice sheet runoff to shifts in regional atmospheric circulation associated with larger scale flow patterns and global temperature increases. It is likely that anthropogenic forcing and internal variability are both contributors to recent observed changes on the Greenland ice sheet.

Estimates of ice mass in Antarctic since 2000 show that the greatest losses are at the edges (see Section 4.4). An analysis of observations underneath a floating ice shelf off West Antarctica leads to the conclusion that ocean warming and more transport of heat by ocean circulation are largely responsible for increasing melt rates (Jacobs et al., 2011; Joughin and Alley, 2011; Pritchard et al., 2012; Mankoff et al., 2012). While there is evidence that the ice sheet mass loss is a growing fraction of the total contribution to sea level, the underlying cause for the increased melt from the warming oceans depends on whether or not anthropogenic forcing is a contributor of ocean warming in the Southern Ocean (Section 3.2), and changing wind patterns. Section 10.4.1 concludes that it is extremely certain that the anthropogenic forcing is a significant contributor to warming of the ocean, and Section 10.3.3 concludes that there is low confidence in the anthropogenic contribution to the increased westerlies in the Southern Ocean.

Antarctica has regionally dependent decadal variability in surface temperature with variations in these trends depending on the strength of the Southern Annular Mode climate pattern and the impacts of ozone depletion in the stratosphere (Steig et al., 2009; Thompson and Solomon, 2002; Turner and Overland, 2009). Recent warming in continental west Antarctica has been linked to sea surface temperature changes in the tropical Pacific (Ding et al., 2011). Simulations using atmospheric general circulation models with observed surface boundary conditions over the last 50 years suggest contributions from rising greenhouse gases with the sign of ozone contributions being less certain (see Section 10.5.1). As with Antarctic sea ice, changes in Antarctic ice sheets have complex causes (Section 4.4.3). The observational record of Antarctic mass loss is short and the internal variability of the ice sheet is poorly understood. These factors combined with incomplete models in Antarctic ice sheet mass loss result in low confidence in scientific understanding and attribution of the mass balance of Antarctica to human influence is premature.

10.5.2.2 Glaciers

Historically, there is reliable evidence that large-scale internal climate variability governs interannual to decadal variability in glacier mass (Hodge et al., 1998; Huss et al., 2010; Nesje et al., 2000; Vuille et al.,

2008) and, along with glacier dynamics, impacts glacier length as well (Chinn et al., 2005). On longer time periods, there is now evidence of recent ice loss (See Section 4.3.3) due to increased ambient temperatures and associated regional moisture changes. However, few studies evaluate the direct attribution of the current observed mass loss to anthropogenic forcing, due to the difficulty associated with contrasting scales between glaciers and the large-scale atmospheric circulation (Molg and Kaser, 2011). Reichert et al. (2002b) show for two sample sites at mid and high latitude that internal climate variability over multiple millennia as represented in a GCM would not result in such short glacier lengths as observed in the 20th century. For a sample site at low latitude using multi-step attribution, Mölg et al, (2009) (and references therein) found a close relation between glacier mass loss and the atmosphere-ocean circulation in the Indian Ocean since the late 19th century. A second, larger group of studies makes use of century-scale glacier records (mostly glacier length but mass balance as well) to extract evidence for external drivers. These include local and regional changes in precipitation and air temperature, and related parameters (such as degree day factors) estimated from the observed change in glaciers. In general these studies show that the glacier changes reveal unique departures in most recent decades, and that inferred climatic drivers in the 20th century and particularly in most recent decades, exceed the internal variability of the earlier records (Huss and Bauder, 2009; Huss et al., 2010; Oerlemans, 2005; Yamaguchi et al., 2008). These results underline the contrast to former centuries where observed glacier fluctuations can be explained by internal climate variability (Reichert et al., 2002a; Roe and O'Neal, 2009). Anthropogenic land cover change is an unresolved forcing, but a first assessment suggests that it does not confound the impacts of recent temperature and precipitation changes (Mölg et al., 2011). The robustness of the estimates of observed mass loss (Section 4.3), the certainty we have for estimates of natural variations and internal variability from long term glacier records, and our understanding of glacier response to climatic drivers provides high confidence in the evidence, and it is likely that the substantial mass loss of glaciers is due to human influence.

10.5.3 Snow Cover and Permafrost

Observations of changes in snow are described in Section 4.5. Annual snow cover extent over the Northern Hemisphere, computed from satellite and *in situ* measurements, decreased during the period 1922–2012, with large decreases in summer and spring and a small increase in winter (Brown and Robinson, 2011) (see Section 4.5). Averaged March and April NH SCE was around 8% lower (7 Million km^2) over the period 1970–2010 than over the period 1922–1970. Major negative anomalies North American snow cover are seen in May and June for 2010–2012, relative to the previous 40 year record. This seasonality in snow cover trend is also consistent with those obtained from *in-situ* measurement (Kitaev and Kislov, 2008; Kitaev et al., 2007) over the Northern Eurasia. Other measures of snow have generally shown decreases: for example, the duration of the snow season averaged over NH shortened by 5.3 days per decade since winter 1972–1973 (Choi et al., 2010). In situ measurements of snow depth and snow water equivalent (SWE) generally show decreases especially at warm locations (mean winter temperature > –5°C) and generally show increases at extremely cold locations (Brown and Mote, 2009) (Section 4.5)

CMIP3 model biases in snow cover were largest near the Tibetan Plateau (Brown and Mote, 2009) and at higher latitudes these biases contributed to hemispheric albedo biases (Roesch, 2006). For CMIP5 models, hemispheric biases in SCE range from –12 to +8 million sq km (–34% to +22%) (Rupp et al., 2012a).

Formal detection and attribution studies have indicated anthropogenic influence on NH SCE (Rupp et al., 2012a) and western US SWE (Pierce et al., 2008). Pierce et al. (2008) detected anthropogenic influence in the ratio of 1 April SWE over October-March precipitation over the period 1950–1999. These reductions could not be explained by natural internal climate variability alone nor by changes in solar and volcanic forcing. In their analysis of NH SCE using 13 CMIP5 simulations over the 1922–2005 period, Rupp et al. (2012a) showed that all forcings could explain the observed long term decreases in snow extent, and that volcanic and solar variations (from four CMIP5 simulations) were inconsistent with observations. We conclude with medium confidence in the observational and modelling evidence that the decrease in northern hemisphere snow extent is likely to be caused by all forcings and has an anthropogenic contribution (see Table 10.1).

Wide spread permafrost degradation and warming appear to be in part a response to atmospheric warming. The warming trend of permafrost temperature increase from 0.22°C per decade to 0.34°C per decade in Russia during 1966–2005 reflects a similar magnitude of warming trend in surface air temperature (Pavlov

and Malkova, 2010). In Qinghai-Tibet Plateau, altitudinal permafrost boundary has moved up slope by 25 m in the north during last decades and by 50 to 80 m in the south (Cheng and Wu, 2007). Surface temperature and snow amount from CMIP3 model output were used as input parameters for a permafrost model in Pavlov et al. (2007). It was shown that the multi-model ensemble mean trend of seasonal soil freezing and thawing depths in northern Eurasia are consistent with observations.

Changes in snow cover also play a critical role in permafrost retreat (Osterkamp, 2005; Zhang et al., 2005). Trends towards earlier snowfall in autumn and thicker snow cover during winter have resulted in a stronger snow insulation effect, and as a result a much warmer permafrost temperature than air temperature in the Arctic. The lengthening of the thawing season and increases in summer air temperature have resulted in changes in active layer thickness. Near-isothermal conditions of warm permafrost are often observed in mountain permafrost regions and in these areas, permafrost temperatures have shown little on no change (see Section 4.7). There is a lack of detection and attribution studies for permafrost (see Table 10.1).

10.6 Extremes

Since many of the impacts of climate changes may manifest themselves through weather and climate extremes, there is increasing interest in quantifying the role of human and other external influences on those extremes. The IPCC SREX assessed causes of changes in different types of extremes inncluding temperature and precipitation, phenomena that influence the occurrence of extremes (e.g., storms, tropical cyclones), and impacts on the natural physical environment such as drought (Seneviratne et al., 2012). This section assesses current understanding of causes of changes in weather and climate extremes, using the AR4 as starting point. Any changes or modifications to the IPCC SREX assessment are highlighted.

10.6.1 Attribution of Changes in Frequency/Occurrence and Intensity of Extremes

This sub-section assesses attribution of changes in the characteristics of extremes including frequency and intensity of extremes. Many of the extremes discussed in this sub-section are moderate events. Attribution of specific extreme events, which are also very rare in general, is assessed in the next sub-section.

10.6.1.1 Temperature Extremes

The AR4 concluded that “surface temperature extremes have likely been affected by anthropogenic forcing”. Many indicators of climate extremes and variability showed changes consistent with warming including a widespread reduction in number of frost days in mid-latitude regions, and evidence that in many regions warm extremes had become warmer, and cold extremes had become less cold. We next assess new studies made since AR4.

Relatively rare seasonal mean temperatures (expected to be exceeded one year in ten) have seen a rapid increase in frequency for many regions worldwide (Jones et al., 2008; Stott et al., 2011)and this increase in frequencies has been attributed to human influence (Christidis et al., 2012b; Christidis et al., 2011b; Stott et al., 2011)

Considering daily extremes, both qualitative and quantitative comparison between observed and modelled values of the number of days exceeding the 90th percentile of daily maximum and daily minimum temperatures (referred to TX90 and TN90, see also Section 2.7) and the number of days with daily maximum and daily minimum temperatures below the 10th percentile (referred to TX10 and TN10, see also Section 2.7) suggests human influence. Trends in temperature extreme indices computed using observations and simulations of the 20th century with nine GCMs that include both anthropogenic and natural forcings are found to be consistent over Australia (Alexander and Arblaster, 2009) and the USA (Meehl et al., 2007a). Both observations and model simulations show a decrease in the number of frost days, and an increase in the growing season length, the heatwave intensity, and TN90 in the second half of the 20th century. Two of the models (PCM and CCSM3) with simulations that include only anthropogenic or only natural forcings indicate that the observed changes are simulated with anthropogenic forcings, but not with natural forcings (even though there are some differences in the details of the forcings). Morak et al. (2011a) found that over many sub-continental regions, the number of warm nights (TN90) show detectable changes over the second half of the 20th century that are consistent with the expected changes due to greenhouse gas increases

(Figure 10.16). They also found changes consistent with anthropogenic greenhouse gas increases when the data were analysed over the globe as a whole. As much of the long-term change in TN90 can be predicted based on the interannual correlation of TN90 with mean temperature, (Morak et al., 2011a) conclude that the detectable changes are probably in part due to greenhouse gas increases. (Morak et al., 2012)have extended this analysis to TN10, TX10, and TN90, using fingerprints from HadGEM and find detectable changes on global scales and in many regions (Figure 10.16).

Human influence has also been detected in two different measures of the intensity of extreme daily temperatures in a year. (Zwiers et al., 2011) compared annual maximum daily maximum and minimum temperatures (TXx, TNx) and annual minimum daily maximum and minimum temperatures (TXn, TNn) from observations and from simulations with anthropogenic forcing or anthropogenic and natural external forcings from seven GCMs. They fit probability distributions to the observed extreme temperatures with location parameters as linear functions of signals obtained from the model simulation, and found that both anthropogenic influence and combined influence of anthropogenic and natural forcing can be detected in all four extreme temperature variables at the global scale over the land, and also regionally over many large land areas (Figure 10.16). In a complmentary study, (Christidis et al., 2011a) used an optimal fingerprint method to compare observed and modelled time-varying location parameters of extreme temperature distribution (Brown et al., 2008). They detect the effects of anthropogenic forcing on extremely warm daily temperatures in a single fingerprint analysis, and are able to separate the effects of natural from anthropogenic forcings in a two fingerprint analysis. Both studies find that the model appeared to underestimate the change for cold extremes and overestimates it for warm extremes (Christidis et al., 2011a; Zwiers et al., 2011).

[INSERT FIGURE 10.16 HERE]

Figure 10.16: Detection results for changes in intensity and frequency of extreme events. Left side of each panel show scaling factors and their 90% confidence intervals for intensity of annual extreme temperatures in response to external forcings for the period 1951–2000. TNn and TXn represent annual minimum daily minimum and maximum temperatures, respectively, while TNx and TXx represent annual maximum daily minimum and maximum temperatures (updated from (Zwiers et al., 2011), fingerprints are based on simulations of CanESM2 with both anthropogenic and natural forcings). Right hand sides of each panel show scaling factors and their 90% confidence intervals for changes in thefrequency of temperature extremes for winter (October-March for Northern Hemisphere and April-September for Southern Hemisphere), and summer half years. TN10, TX10 are respectively the frequency for daily minimum and daily maximum temperatures falling below their 10th percentiles for the base period 1961–1990. TN90 and TX90 are the frequency of the occurrence of daily minimum and daily maximum temperatures above their respective 90th percentiles calculated for the 1961–1990 base period (Morak et al., 2012), fingerprints are based on simulations of HadGEM1 with both anthropogenic and natural forcings). Detection is claimed at the 10% significance level if the 90% confidence interval of a scaling factor is above zero line.

Human influence on annual extremes of daily temperatures may also be detected separately from natural forcing at the global scale (Christidis et al., 2011a; Min et al., 2012) and at continental and sub-continental scales (Min et al., 2012). Additionally, Wen et al. (2012) showed that over China and for TNn, TNx, TXn, and TXx, anthropogenic influence may be separately detected from natural forcing, although natural forcing cannot be detected, and that the influence of greenhouse gases may be separately detected from other anthropogenic forcings. Christidis et al. (2012a) found that on a quasi-global scale, the cooling effect due to the decrease in tree cover and increase in grass cover since pre-industrial times is detectable in the observed change of warm extremes.

These new studies show that there is stronger evidence for human influence on changes in extreme temperatures than at the time of the AR4 and SREX assessments. Since AR4, there is new evidence for detection of human influence on extremely warm daytime temperature and there is new evidence that influence of anthropogenic forcing may be separately detected from natural forcing at global and and in some continental and sub-continental scale regions. These new results suggest more clearly the role of anthropogenic forcing on temperature extremes which calls for adjustment to the AR4 and SREX assessments. We assess that it is *very likely* human influence has contributed to the observed changes in temperature extremes since the mid-20th century.

10.6.1.2 Precipitation Extremes

The observed changes in heavy precipitation appear to be consistent with the expected response to anthropogenic forcing as a result of an enhanced moisture content in the atmosphere but a direct cause-and-effect relationship between changes in external forcing and extreme precipitation had not been established at the time of the AR4. As a result, the AR4 concluded that it is *more likely than not* that anthropogenic influence had contributed to a global trend towards increases in the frequency of heavy precipitation events over the second half of the 20th century (Hegerl et al., 2007b).

New studies since the AR4 have strengthened the expectation of increase in extreme precipitation. Anthropogenic influence has been detected on various aspects of the global hydrological cycle (Stott et al., 2010; see also Section 10.3.2), which is directly relevant to extreme precipitation changes. An anthropogenic influence on increasing atmospheric moisture content has been detected (see Section 10.3.2). A higher moisture content in the atmosphere would be expected to lead to stronger extreme precipitation. Assuming that the distribution of relative humidity changes little under climate change, the Clausius-Clapeyron relation implies more moisture in the atmosphere, which in turn would mean stronger extreme precipitation, all other things being equal. This is seen in GCM projections of extreme precipitation under global warming. CMIP3 and CMIP5 simulations project an increase in the globally averaged 20-year return values of annual maximum 24-hour precipitation amounts of about 6–7% with each Kelvin of global warming, with the bulk of models simulating values in the range of 4–10% K^{-1} (Kharin et al., 2007; Kharin et al., 2012). Consistent with that, an observational analysis shows that winter season maximum daily precipitation in North America has statistically significant positive correlations with atmospheric moisture (Wang and Zhang, 2008). Analysis of observed annual maximum 1-day precipitation over global land areas indicates a significant increase in extreme percipitation on average globally, with a median increase about 7% per degree global average surface temperature increase (Westra et al., 2012). Other factors such as changes in atmospheric circulation, in the moist-adiabate temperature rapes rate,or in the upward velocity may modify the rate of extreme precipitation change in relation to tempertaure change (Chen et al., 2011; Chou et al., 2009; Chou et al., 2012; Emori and Brown, 2005; Hardwick Jones et al., 2010; O'Gorman and Schneider, 2009a, 2009b; Pall et al., 2007; Sugiyama et al., 2010). Extreme precipitation may decrease in areas where the availability of atmospheric moisture decreases (Hardwick Jones et al., 2010; Utsumi et al., 2011).

Despite a robust expectation of increased precipitation (Balani Sarojini et al., 2012) and precipitation extremes, there is only a modest body of literature that provides direct evidence that natural or anthropogenic forcing has affected global mean precipitation (see Section 10.3.2 and Figure 10.10). As precipitation is bounded by zero, a larger mean precipitation would in general lead to larger range in the precipitation distribution and thus larger variance if the probability of precipitation remains similar. It follows that the detection of human influence on the mean climatological distribution of precipitation would imply that there should also have been an influence on precipitation variability, and thus extremes. Regarding direct evidence for changes in extreme precipitation, a perfect model analysis with an ensemble of GCM simulations shows that anthropogenic influence should be detectable in precipitation extremes in the second half of the 20th century at global and hemispheric scales, and at continental scale as well but less robustly (Min et al., 2008b), see also (Hegerl et al., 2004). A formal detection and attribution study comparing observed and multi-model simulated annual maximum 1-day and 5-day precipitation amounts suggests that anthropogenic influence on extreme precipitation is detectable on hemispheric scales (Min et al., 2011). However the detection was less robust if using the fingerprint for combined anthropogenic and natural influences compared to that for anthropogenic influences only, possibly due to weak signal to noise ratio. Also, models still have difficulties in simulating extreme daily precipitation directly comparable with those observed at the station level, which has been addressed to some extent by (Min et al., 2011) by using a transform to an index that is more robust to spatial scales. Detection of anthropogenic influence on smaller spatial scales is more difficult due to increased level of noise and uncertainties and confounding factors on local scales. Fowler and Wilby (2010) suggested that there may only be 50% chance of detecting anthropogenic influence on UK extreme precipitation in winter by now, and a very small likelihood to detect it in other seasons.

Given the evidence of anthropogenic influence on various aspects of the global hydrological cycle that implies that extreme precipitation would be expected to have increased, some limited direct evidence of anthropogenic influence on extreme precipitation, and difficulties in simulating extreme precipitation by climate models, we assess, consistent with IPCC SREX (Seneviratne et al., 2012) that there is medium confidence that anthropogenic forcing has contributed to intensification of extreme precipitation at the global

scale since the mid-20th century. The use of new uncertainty guidance in SREX and AR5 makes direct comparison of this statement and the equivalent made in AR4 difficult as noted by (Seneviratne et al., 2012)

10.6.1.3 Drought

The AR4 (Hegerl et al., 2007b) concluded that it is *more likely than not* that anthropogenic influence has contributed to the increase in the droughts observed in the second half of the 20th century. This assessment was based on multiple lines of evidence including a detection study which identified an anthropogenic fingerprint in a global PDSI (Palmer Drought Severity Index) data set with high significance (Burke et al., 2006). The IPCC SREX (Seneviratne et al., 2012) assessed that there is *medium confidence* that anthropogenic influence has contributed to some changes in the drought patterns observed in the second half of the 20th century based on its attributed impact on precipitation and temperature changes.

Drought is a complex phenomenon that is affected by precipitation predominately, as well as by other climate variables including temperature, wind speed, solar radiation. It is also affected by non-atmospheric conditions such as antecedent soil moisture and land surface conditions. Droughts have been monitored by various indices as there is a lack of direct observations of drought related variables such as soil moisture. Trends in two important drought-related climate variables, namely precipitation and temperature, are consistent with expected responses to anthropogenic forcing (see also Sections 10.6.1.1 and 10.6.1.2) over the globe. However, there is large uncertainty in the detection of changes in drought and its attribution to causes globally. The evidence for changes in soil moisture indices and drought indices over the period since 1950 globally is conflicting (Dai, 2011; Sheffield and Wood, 2008), possibly due to, including different time periods and different forcing fields as well as due to uncertainties due to land surface models (Pitman and et al., 2009; Seneviratne et al., 2010). Over regional scales, land-atmosphere feedbacks and land use and land cover changes play significant role (see also Deo et al., 2009). It is also very difficult to distinguish low-frequency, decade-scale precipitation deficits in particular regions from long-term climate change. Recent long-term droughts in western North America (Cayan et al., 2010; Seager et al., 2010) have been assessed in terms of attribution studies but these droughts, pronounced as they are, cannot definitively be shown to be so severe as to lie outside the very large envelope of natural precipitation variability in this region, particularly that suggested by palaeoclimatic evidence (see Chapter 5). Low-frequency tropical ocean temperature anomalies in all ocean basins appear to force circulation changes that promote regional drought (Dai, 2011; Hoerling and Kumar, 2003; 2010; Seager et al., 2005). Uniform increases in SST are not particularly effective in this regard (Hoerling et al., 2011; Schubert et al., 2009). Therefore, the reliable separation of natural variability and forced climate change will require simulations that accurately reproduce changes in large-scale SST gradients at all time scales.

An assessment of the observational evidence indicates that the AR4 conclusions regarding global increasing trends in hydrological droughts since the 1970s are no longer supported. There is not enough evidence to support medium or high confidence of increasing trends as a result of observational uncertainties and conflicting geographical trends (Section 2.6.2.2). Combined with difficulties described above in distringuishing decadal scale variability in drought from long-term climate change we conclude there is low confidence in attributing changes in drought over global land since the mid-20th century to human influence.

10.6.1.4 Extra-Tropical Cyclones

The AR4 concluded that an anthropogenic influence on extratropical cyclones was not formally detected, owing to large internal variability and problems due to changes in observing systems. While there is evidence that there has been a poleward shift in the storm tracks (see Section 2.6.4) various causal factors have been cited including oceanic heating (Butler et al., 2010) and there is futher discussion of the effects of forcings on circulation in Section 10.3.3. Increases in midlatitude SST gradients generally lead to stronger storm tracks that are shifted poleward and increases in subtropical SST gradients may lead to storm tracks shift towards the equator (Brayshaw et al., 2008; Graff and LaCasce, 2012; Kodama and Iwasaki, 2009; Semmler et al., 2008). However, changes in storm-track intensity is much more complicated, as they are sensitive to the competing effects of changes in temperature gradients and static stability at different levels and are thus not linked to global temperatures in a simple way (O'Gorman, 2011). The average global cyclone activity is expected to change little under moderate greenhouse gas forcing (Bengtsson and Hodges,

2009; O'Gorman and Schneider, 2008) although in one study, human influence has been detected in geostrophic wind energy and ocean wave heights derived from sea level pressure data (Wang et al., 2009b).

10.6.1.5 Tropical Cyclones

The AR4 concluded that "anthropogenic factors more likely than not have contributed to an increase in tropical cyclone intensity" (Hegerl et al., 2007b). Evidence that supports this assessment was the strong correlation between the Power Dissipation Index (PDI, an index of the destructiveness of tropical cyclones) and tropical Atlantic sea surface temperatures (SSTs) (Elsner, 2006; Emanuel, 2005) and the association between Atlantic warming and the increase in global temperatures (Mann and Emanuel, 2006b; Trenberth and Shea, 2006). Observations seem to suggest an increase globally in the intensities of the strongest tropical cyclones (Elsner et al., 2008) but it is difficult to attribute such changes to particular causes (Knutson et al., 2010). The US CCSP (Kunkel et al., 2008) discussed human contributions to recent hurricane activity based on a two-step attribution approach. They concluded that it is very likely that human induced increase in greenhouse gases has contributed to the increase in SSTs in the hurricane formation regions and that over the past 50 years there has been a strong statistical connection between tropical Atlantic SSTs and Atlantic hurricane activity as measured by the PDI. Knutson et al. (2010), assessed that "…it remains uncertain whether past changes in tropical cyclone activity have exceeded the variability expected from natural causes. Seneviratne et al. (2012) concurred with this finding.

Studies that directly attribute tropical cyclone activity changes to anthropogenic greenhouse gases emission are lacking. Among many factors that may affect tropical cyclone activity, tropical SSTs have increased and this increase has been attributed at least in part to anthropogenic forcing (Gillett et al., 2008a; Karoly and Wu, 2005a; Knutson et al., 2006; Santer and et al, 2006). However, there are diverse views on the connection between tropical cyclone activity and SST (see Box 14.3 for details). Strong correlation between the PDI and tropical Atlantic SSTs (Elsner, 2006; Emanuel, 2005) would suggest an anthropogenic influence on tropical cyclone activity. However, recent studies also suggest that regional potential intensity is correlated with the difference between regional SSTs and spatially averaged SSTs in the tropics (Ramsay and Sobel, 2011; Vecchi and Soden, 2007; Xie et al., 2010) and projections are uncertain on whether the relative SST will increase over the 21st century under greenhouse gas forcing (Vecchi et al., 2008; Villarini and Vecchi, 2012a; Villarini and Vecchi, 2012b; Xie et al., 2010). Analyses of CMIP5 simulations suggest that while PDI over the North Atlantic is projected to increase towards late 21st century no detectable change in PDI should be present in the 20th century (Villarini and Vecchi, 2012b). On the other hand, (Emanuel et al., 2012) point out that while GCM hindcasts indeed predict little change over the 20th century, downscaling using reanalysis (as opposed to climate model) driving are in much better accord with observations and do indicate a late 20th century increase.

Studies suggest that the reduction in the aerosol forcing (both anthropogenic and natural) over the Atlantic since the 1970s may have contributed to the increase in tropical cyclone activity in the region (see Box 14.3 for details), and similarly that aerosols may have acted to reduce tropical cyclone activity in the Atlantic in earlier years when aerosol forcing was increasing (Villarini and Vecchi, 2012b). However, there are different views on the relative contribution of aerosols and decadal natural variability of the climate system to the observed changes in Atlantic tropical cyclone activity among these studies. Some studies indicate that aerosol changes have been the main driver (Booth et al., 2012a; Chang et al., 2011; Evan et al., 2009; Mann and Emanuel, 2006b; Villarini and Vecchi, 2012a; Villarini and Vecchi, 2012b). Some studies infer the influence of natural variability to be larger than that from aerosols (Villarini and Vecchi, 2012a; Villarini and Vecchi, 2012b; Zhang and Delworth, 2009; Zhang et al., 2007a). Other studies suggest that both aerosol changes and internal variability are important (Villarini and Vecchi, 2012a; Villarini and Vecchi, 2012b).

Globally, there is *low confidence* in any long term increases in tropical cyclone activity (Section 2.6.3) and *low confidence* in attributing global changes to any particular cause. In the North Atlantic region there is *medium confidence* that a reduction in aerosol forcing over the North Atlantic has contributed at least in part to the observed increase in tropical cyclone activity since the 1970s. There remains substantial disagreement on the relative importance of internal variability, greenhouse gas forcing, and aerosols for this observed trend. It remains uncertain whether past changes in tropical cyclone activity are outside the range of natural internal variability.

10.6.2 Attribution of Observed Weather and Climate Events

Since many of the impacts of climate change are likely to manifest themselves through extreme weather, there is increasing interest in quantifying the role of human and other external influences on climate in specific weather events. This presents particular challenges for both science and the communication of results (Allen, 2011a; Curry, 2011b; Hulme et al., 2011; Trenberth, 2011a). It has so far been attempted for a relatively small number of specific events although Petersen et al. (2012) attempt, for the first time, a coordinated assessment of the impact of external climate drivers on high-impact weather events of 2011. In this assessment, we use selected studies to illustrate issues in event attribution: see Stott et al. (2012) for a more exhaustive review.

Three distinct ways have emerged of framing the question of how an external climate driver like increased greenhouse gas levels may have contributed to an observed weather event. First, the "attributable risk" approach considers the event as a whole, and asks how the external driver may have increased the probability of occurrence an event of comparable magnitude (Allen, 2003; Christidis et al., 2011b; Pall et al., 2011; Stone et al., 2009; Stone and Allen, 2005b; Stott et al., 2004b). Second, the "attributable magnitude" approach considers how different external factors contributed to the event or, more specifically, how the external driver may have increased the magnitude of an event of comparable occurrence-probability (Perlwitz et al., 2009; Dole et al., 2011). Third, the "absolute risk" approach asks how likely, in absolute terms, a comparable event would have been in the absence of the driver in question (Hansen et al., 2012).

Quantifying the absolute risk or probability of an extreme weather event in the absence of human influence on climate is particularly challenging. Many of the most extreme events occur because a self-reinforcing process that only occurs under extreme conditions amplifies an initial anomaly (Fischer et al., 2007; Seneviratne et al., 2006; Seneviratne et al., 2012). Hence the probability of occurrence of such events cannot be estimated simply by extrapolating from the distribution of less extreme events that are sampled in the historical record. Proxy records of pre-industrial climate generally do not resolve high-frequency weather, and in any case natural multi-century climate variations mean that the frequency of occurrence of an event over the pre-industrial millennium cannot be equated with its probability of occurrence in the absence of human influence today. Quantifying absolute probabilities with climate models is also difficult because of known biases in their simulation of extreme events. Hence, with only a couple of exceptions (Hansen et al., 2012; Schär et al., 2004), studies have focussed on how risks have changed or how different factors have contributed to an observed event, rather than asking what the absolute risk of that event might have been in the absence of human influence on climate.

Even without considering absolute probabilities, there remain considerable uncertainties in quantifying changes in probabilities, and the way in which the event-attribution question is framed can substantially affect apparent conclusions (Otto et al., 2012). If an event occurs in the tail of the distribution, then a small shift in the distribution as a whole can result in a large increase in the probability of an event of that magnitude: hence it is possible for the same event to be both "mostly natural" in terms of attributable magnitude (if the shift in the distribution due to human influence is small relative to the size of the natural fluctuation that was the primary cause) and "mostly anthropogenic" in term of attributable risk (if human influence has increased its probability of occurrence by more than a factor of two). These issues are discussed further using the example of the 2010 Russian heat-wave below.

The majority of studies have focussed on quantifying attributable risk. Note that risk is a function of both hazard and vulnerability (Hulme et al., 2011), but any assessment of change in risk depends on an assumption of "all other things being equal", including natural drivers of climate change and vulnerability. Given this assumption, the change in hazard is proportional to the change in risk, so we will follow the published literature and continue to refer to Fraction Attributable Risk, defined as FAR=1-P0/P1, P0 being the probability of an event occurring in the absence of human influence on climate, and P1 the corresponding probability in a world in which human influence is included. FAR does not require knowledge of absolute values of P0 and P1, only their ratio.

For individual events with return-times greater than the time-scale over which the signal of human influence is emerging (30–50 years, meaning P0 and P1 less than 2–3% in any given year), it is impossible to observe a change in occurrence-frequency directly, so attribution is necessarily a multi-step procedure. Either a trend

in occurrence-frequency of more frequent events is attributed to human influence and a statistical extrapolation model then used to assess the implications for P0 and P1; or an attributable trend is identified in some other variable, such as surface temperature, and a physically-based weather model is used to assess the implications. Neither approach is free of assumptions: no weather model is perfect, but statistical extrapolation may also be misleading for reasons given above.

Pall et al. (2011) provide an example of multi-step assessment of attributable risk using a physically-based model, applied to the floods that occurred in the UK in the autumn of 2000, the wettest autumn to have occurred in England and Wales since records began. To assess the contribution of the anthropogenic increase in greenhouse gases to the risk of these floods, a several thousand member ensemble of atmospheric models with realistic atmospheric composition, sea surface temperature and sea ice boundary conditions imposed was compared with a second ensemble with composition and surface temperatures modified to simulate conditions that would have occurred had there been no anthropogenic increase in greenhouse gases since 1900. Simulated daily precipitation from these two ensembles was fed into an empirical rainfall-runoff model and daily England and Wales runoff used as a proxy for flood risk. Results (Figure 10.17 Panel a) show that . including the influence of anthropogenic greenhouse warming increases flood risk at the threshold relevant to autumn 2000 by around a factor of two in the majority of cases, but with a broad range of uncertainty: in 10% of cases the increase in risk is less than 20%.

[INSERT FIGURE 10.17 HERE]

Figure 10.17: Return times for precipitation-induced floods aggregated over England and Wales for (a) conditions corresponding to October to December 2000 with boundary conditions as observed (blue) and under a range of simulations of the conditions that would have obtained in the absence of anthropogenic greenhouse warming over the 20th century – colours correspond to different AOGCMs used to define the greenhouse signal, black horizontal line to the threshold exceeded in autumn 2000 – from Pall et al. (2011); (b) corresponding to January to March 2001 with boundary conditions as observed (blue) and under a range of simulations of the condition that would have obtained in the absence of anthropogenic greenhouse warming over the 20th century (green; adapted from Kay et al., (2011b)); (c) return periods of temperature-geopotential height conditions in the model for the 1960s (green) and the 2000s (blue). The vertical black arrow shows the anomaly of the Russian heatwave 2010 (black horizontal line) compared to the July mean temperatures of the 1960s (dashed line). The vertical red arrow gives the increase in temperature for the event whereas the horizontal red arrow shows the change in the return period.

Kay et al. (2011a), analysing the same ensembles but using a more sophisticated hydrological model found a reduction in the risk of snow-melt-induced flooding in the spring season (Figure 10.17, Panel b) which, aggregated over the entire year, largely compensated for the increased risk of precipitation-induced flooding in autumn. This illustrates an important general point: even if a particular flood event may have been made more likely by human influence on climate, there is no certainty that all kinds of flood events in that location have been made more likely.

Rahmstorf and Connou (2011) provide an example of an empirical approach to the estimation of attributable risk applied to the 2010 Russian heat-wave. They fit a non-linear trend to central Russian temperatures and show that the warming that has occurred in this region since the 1960s has increased the risk of a heat-wave of the magnitude observed in 2010 by around a factor of 5, corresponding to an FAR of 0.8. They do not address what has caused the trend since 1960, although they note that other studies have attributed most of the large-scale warming over this period to the anthropogenic increase in greenhouse gas concentrations.

Dole et al. (2011) take a different approach to the 2010 Russian heat-wave, focussing on attributable magnitude, analysing contributions from various external factors, and conclude that this event was “mainly natural in origin”. First, observations show no evidence of a trend in occurrence-frequency of hot summers in central Russia, and despite the warming that has occurred since the 1960s, mean summer temperatures in that region actually displaying a (statistically insignificant) cooling trend over the century as a whole, in contrast to the case for central and southern European summer temperatures (Fischer and Schär 2010; Stott et al., 2004a). Members of the CMIP3 multi-model ensemble likewise show no evidence of a trend towards warming summers in central Russia. Second, Dole et al. (2011) note that the 2010 Russian event was associated with a strong blocking atmospheric flow anomaly, and even the complete 2010 boundary conditions are insufficient to increase the probability of a prolonged blocking event in this region, in contrast again to the situation in Europe in 2003 (Feudale and Shukla, 2010).

Otto et al. (2012) argue that it is possible to reconcile the results of Rahmstorf and Coumou (2011) with those of Dole et al. (2011) by relating the attributable risk and attributable magnitude approaches to framing the event attribution question. This is illustrated in Figure 10.17, Panel c, which shows return-times of July temperatures in Central Russia in a large ensemble of atmospheric model simulations for the 1960s (in green) and 2000s (in blue). The threshold exceeded in 2010 is shown by the solid horizontal line which is almost 6°C above 1960s mean July temperatures, shown by the dashed line. The difference between the green and blue lines could be characterised as a 1.5°C increase in the magnitude of a 30-year event (the vertical red arrow, which is substantially smaller than the size of the anomaly itself, supporting the assertion that the event was "mainly natural" in terms of attributable magnitude. Alternatively, it could be characterised as a three-fold increase in the risk of the 2010 threshold being exceeded, supporting the assertion that risk of the event occurring was mainly attributable to the external trend, consistent with Rahmstorf and Coumou (2011). Rupp et al. (2012c) and Hoerling et al. (2012) reach similar conclusions about the 2011 Texas heat-wave, both noting the importance of La Niña conditions in the Pacific, with anthropogenic warming making a relatively small contribution to the magnitude of the event, but a more substantial contribution to the risk of temperatures exceeding a high threshold.

Since much of the magnitude of these events is attributable to atmospheric flow anomalies, any evidence of a causal link between rising greenhouse gases and the occurrence or persistence of flow anomalies such as blocking would have a very substantial impact on attribution claims (Perlwitz et al., 2009). Pall et al. (2011) argue that, although flow anomalies played a substantial role in the autumn 2000 floods in the UK, thermodynamic mechanisms were primarily responsible for the increase in risk between their ensembles. Regardless of whether the statistics of flow regimes themselves have changed, observed temperatures in recent years in Europe are distinctly warmer than would be expected for analogous atmospheric flow regimes in the past (Cattiaux et al., 2009, 2011; Cattiaux et al., 2010).

In summary, increasing numbers of studies are finding that events associated with extremely warm temperatures are occurring whose probability of occurrence has increased substantially due to the large-scale warming since the mid-20th century (Otto et al., 2012; Rahmstorf and Coumou, 2011; Rupp et al., 2012b; Stott et al., 2004a). Since most of this warming is very likely due to the increase in atmospheric greenhouse gas concentrations, it is possible to attribute, via a multi-step procedure, some of the increase in probability of these events to human influence on climate. Such an increase in probability is consistent with the implications of single-step attribution studies looking at the overall implications of increasing mean temperatures for the probabilities of exceeding temperature thresholds in some regions (Christidis et al., 2012b; Christidis et al., 2011b). We conclude that it is likely that human influence has substantially increased the probability of some observed heatwaves, Attributable risks found for extreme precipitation events are generally smaller and more uncertain. The science of event attribution is still confined to case studies, often using a single model, and typically focussing on high-impact events for which the issue of human influence has already arisen. Conclusions are hence specific to the events that have been considered so far.

Anthropogenic warming remains a relatively small contributor to the overall magnitude of any individual short-term event because its magnitude is small relative to natural random weather variability on short time-scales. Because of this random variability, weather events continue to occur that have been made less likely by human influence on climate, such as extreme winter cold events (Christidis and Stott, 2012; Massey et al., 2012), or whose probability of occurrence has not been significantly affected either way (van Oldenborgh et al., 2012).

Quantifying how different external factors contribute to current risks, and how risks are changing, is much easier than quantifying absolute risk. Biases in climate models, uncertainty in the probability distribution of the most extreme events and the ambiguity of paleoclimatic records for short-term events mean that it is not yet possible to quantify the absolute probability of occurrence of any observed weather event in a hypothetical pristine climate. At present, therefore, the evidence does not support the claim that we are observing weather events that would, individually, have been extremely unlikely in the absence of human-induced climate change, although observed trends in the concurrence of large numbers of events (see section 10.6.1) may be more easily attributable to external factors.

10.7 Multi Century to Millennia Perspective

Evaluating the causes of climate change before the late 20th century is an important test for understanding the role of internal and forced natural climate variability for the recent past. This section draws on assessment of reconstructions of climate change over the past millennium and their uncertainty in Chapter 5 (Sections 5.3.5; 5.5 for regional records), and on comparisons of models and data over the pre-instrumental period in Chapter 9. The section here focuses on the evidence for the contribution by radiatively forced climate change to reconstructions and early instrumental records. In addition, the residual variability that is not explained by forcing from palaeoclimatic records provides a useful comparison to estimates of climate model internal variability, beginning to address the model-dependence of estimates of internal variability that is an important uncertainty in detection and attribution results.

10.7.1 Relevance of and Challenges in Detection and Attribution Studies Prior to the 20th Century

The inputs for detection and attribution studies for periods covered by indirect, or proxy, data only are affected by more uncertainty than those from the instrumental period . Uncertainties in proxy-based reconstructions are discussed in Chapter 5 and relate to the sparse data coverage, particularly further back in time, and uncertainty in the link between proxy data and, for example, temperature. Most reconstructions are available for the Northern Hemisphere (Section 5.3), which is why this section focuses mostly on Northern Hemispheric variability.

Records of past radiative influences on climate are also uncertain (Section 5.2, see Schmidt et al., 2011). For the last millennium changes in solar, volcanic, greenhouse gas forcing, and land use change, along with a small orbital forcing are potentially important external drivers of climate change. Estimates of solar forcing (Figure 5.1a) are uncertain in their amplitude, and suffer from uncertainty in the relationship of sunspot numbers and cosmogenic isotopes to solar radiative forcing (Beer et al., 2009). Variations of solar insolation, particularly in the UV band are generally not accounted for in model simulations unless they sufficiently resolve the stratosphere (Gray et al., 2010). Estimates of past volcanism from ice core records from both Northern and Southern Hemispheres are reasonably well established in their timing, but the magnitude of the radiative forcing of individual eruptions is uncertain (Figure 5.1a). It is possible that large eruptions had a moderated climate effect due to faster fallout associated with larger particle size (Timmreck et al., 2009), increased amounts of injected water vapour (Joshi and Jones, 2009), and it has been speculated that tree-ring proxy records may not fully record the temperature response to very large eruptions (e.g., Mann et al., 2012, but see Secion 5.3.5.2). A further uncertainty is associated with reconstructed changes in land use (Pongratz et al., 2009; Kaplan et al., 2009). Greenhouse gas forcing shows subtle variations over the Last Millennium, including a small drop from the late 16th through 18th century (Chapter 5).

When interpreting uncertain reconstructions of past climate change with the help of climate models driven with uncertain estimates of past forcing, it helps that the uncertainties in reconstructions and forcing are independent from each other. Thus, uncertainties in forcing and reconstructions combined should lead to less, rather than more similarity between fingerprints of forced climate change and reconstructions, making it improbable that response to external drivers is spuriously detected. However, this is only the case if there are enough degrees of freedom in the fingerprint of climate change and data to avoid spurious correlation due to data uncertainties (Legras et al., 2010). Results are more reliable if all relevant forcings and their uncertainties are considered to avoid fictitious correlations between external forcings.

10.7.2 Causes of Change in Large-Scale Temperature over the Past Millennium

Despite the uncertainties in reconstructions of past Northern Hemisphere mean temperatures, there are well-defined robust climatic periods in the last Millennium (Chapter 5, see also Figure 10.18), which are generally well simulated by climate model of the last millennium (Chapter 9, Chapter 5).

10.7.2.1 Role of External Forcing in the Last Millennium

The AR4 concluded that 'A substantial fraction of the reconstructed Northern Hemisphere inter-decadal temperature variability of the seven centuries prior to 1950 is *very likely* attributable to natural external forcing'. The literature since the AR4, and the availability of more simulations of the last millennium with more complete forcing (see Schmidt et al., 2012), including solar, volcanic and greenhouse gas influences, and generally also land use change and orbital forcing) and more sophisticated models strengthen these conclusions. Results from

new modelling studies (e.g., Jungclaus et al., 2010; Fern´andez-Donado et al., 2012) support prior findings (Hegerl et al., 2007a; Tett et al., 2007; Yoshimori and Broccoli, 2008; Yoshimori et al., 2006) that external forcing significantly contributed to Northern Hemispheric temperature evolution over the last millennium (see Figures 5.9). An analysis based on PMIP3 and CMIP5 model simulations from 850 to 1950 finds that the fingerprint of external forcing is significantly detectable in all reconstructions considered (Schurer et al., 2012, see Figure 10.18). The authors find a smaller response to forcing than simulated, but this discrepancy is consistent with uncertainties in forcing or proxy response to it, particularly associated with volcanism. The level of agreement between fingerprints from multiple models in response to forcing and reconstructions decreases over time, but this may be partly due to weaker forcing and larger forcing uncertainty early in the millennium. (Fern´andez-Donado et al., 2012) also find significant correlations between most reconstructions and total external forcing of a similar range as those in pre-PMIP3 model simulations. Results suggest that external drivers contributed to the warm conditions in the 10th to 12th century, but cannot fully explain them in some of the reconstructions (Figure 10.18).

Data assimilation studies also support the result that external forcing, together with internal climate variability, provides a consistent explanation of climate change over the last millennium. Goosse et al. (Goosse et al., 2012a) (Goosse et al., 2010) (Goosse et al., 2012b) select, from a very large ensemble with an EMIC, the individual simulations that are closest to the spatial reconstructions of temperature between 30°N and 60°N by Mann et al. (2009). The method also varies the external forcing within uncertainties, determining a combined realization of the forced response and internal variability that best matches the data. Results (Figure 10.18) show that the results generally reproduce the target reconstruction generally well, possibly with the exception of very early in the millennium.

[INSERT FIGURE 10.18 HERE]

Figure 10.18: The top panel compares the mean annual Northern hemisphere surface air temperature from a multi-model ensemble to several NH temperature reconstructions, CH-blend from Hegerl et al. (2007a) in purple, which is a reconstruction of 30°N–90°N land only, Mann et al. (2009), plotted for the region 30°N–90°N land and sea (green) and D'Arrigo et al. (2006) in red, which is a reconstruction of 20°N–90°N land only. All results are shown with respect to the reference period 850–1950 (or for a shorter period depending on the maximum range of the reconstruction). The multi-model mean for the relevant region is scaled to fit each reconstruction in turn, using a total least squares (TLS) method (see e.g., Allen and Stott, 2003), with a 5–95% error range in scaling shown in orange with light orange shading. The best fit scaling values for each reconstruction are given in the insert as well as the scaling range for sixth other reconstructions (M8 – (Mann et al., 2008; Mann et al., 2009); AW – (Ammann and Wahl, 2007); Mo - (Moberg et al., 2005); Ju - (Juckes et al., 2007); CH – (Hegerl et al., 2007a); CL – (Christiansen and Ljungqvist, 2011) and inverse regressed onto the instrumental record CS; DA – (D'Arrigo et al., 2006); (Frank et al., 2007; Frank et al., 2010). An asterisk next to the reconstruction name indicates that the residuals (over the more robustly reconstructed period 1401–1950) are inconsistent with the internal variability generated by the control simulations of every climate model investigated (for details see Schurer et al., 2012) Also included on this plot are the NH temperature anomalies calculated in Goosse et al. (2012b) using a data-assimilation technique constrained by the Mann et al. (2009) temperature reconstruction using data from 30°N–90°N. This is plotted in blue, for the region 30°N–90°N land and sea, with the error range shown in light blue shading. The second panel is similar to the top panel, but showing the European region. The TLS scaling factors are calculated only for the period 1500–1950 for two reconstructions: (Luterbacher et al., 2004) for the region 35°N–60°N,-25°E–40°E, land only in red and labelled Lu in the insert and (Mann et al., 2009) averaged over the region 25°N–65°N, 0°–60°E, land and sea, in green and labelled M9 in the insert. The dotted coloured lines show the corresponding instrumental data. Also shown is the simulation from Goosse et al. (2012a) with data-assimilation constrained by the Mann et al. (2009) reconstruction. This is plotted in blue for the region 25°N–65°N, 0°–60°E, land and sea, with the error range shown in light blue shading.

10.7.2.2 Role of Individual Forcings

Much research shows that volcanic forcing plays an important role in explaining past cool episodes, for example, in the late 17th and early 19th century, and that this forcing is key to reproducing the reconstructed temperature evolution (see Chapter 5, Hegerl et al., 2007b; Jungclaus et al., 2010; Miller et al., 2012). Recent research shows that long-term cold conditions in high latitudes began close in time to a large volcanic eruption, which a model simulation explains by high latitude feedbacks (Miller et al., 2012). Schurer et al. (2012) detect the response to natural forcing, and attribute this largely to volcanic forcing. They also detect the fingerprint for the climate response to greenhouse gas variations between 1400 and 1900 in most reconstructions considered.

Even the multi-century perspective makes it difficult to distinguish century-scale variations in solar forcing from other forcings, due to the few degrees of freedom constraining this forcing. Hegerl et al. (2003) and Hegerl et al. (2007a) found solar forcing detectable in some cases. Simulations with higher than best guess solar forcing may reproduce the warm period around 1000 more closely, but the peak warming occurs around 1000 in reconstructions while solar forcing and with it model simulations peak about a century later (Jungclaus et al., 2010; Figure 5.9a,e, see also Figure 10.18). Even if solar forcing were on the high end of estimates for the last millennium, it would not be able to explain the recent warming according both to model simulations (Ammann et al., 2007; Feulner, 2011; Tett et al., 2007), and to detection and attribution approaches that scale the temporal fingerprint of solar forcing to best match the data (see Hegerl et al., 2007b; Schurer et al., 2012; Figure 10.18) . Recent research also suggests a role for orbital forcing (Kaufman et al., 2009), based on a comparison of the correspondence between long term Arctic cooling in models and data though the last millennium up to about 1750.

10.7.2.3 Causes or Contributors to Change in Specific Periods

Radiative forcing in the Little Ice Age (LIA, a period of relatively cold conditions, see chapter 5 and Glossary) includes a drop in solar forcing (with uncertain amplitude), and a slight reduction in greenhouse gas concentrations in the atmosphere (Chapter 5). The late 17th and early 19th century was also characterised by substantial pulses of volcanism, including the powerful eruption of Mount Tambora in 1815. Modelling studies reproduce cooling in reconstructions if forced with a combination of solar, volcanic, and greenhouse gas forcing (Ammann et al., 2007; Jungclaus et al., 2010; Tett et al., 2007). Large restimates of solar forcing lead to too large a cooling in some simulations (Ammann et al., 2007; Feulner, 2011), with better agreement if using intermediate-to-small solar forcing (Ammann et al., 2007), particularly if the reduction in greenhouse gas concentrations is included. Both model simulations (Jungclaus et al., 2010) and results from a detection and attribution study (Hegerl et al., 2007a; Schurer et al., 2012) suggest that the small drop in CO_2 during the LIA may have contributed to the cool conditions during the 16th and 17th century. In contrast, Palastanga et al. (2011) use data assimilation techniques to demonstrate that neither a slowdown of the thermohaline circulation nor a persistently negative NAO alone can explain the reconstructed temperature pattern over Europe during parts of the Little Ice Age (periods 1675–1715 and 1790–1820). (Miller et al., 2012) find that abrupt summer cooling recorded by glacier expansion and changes in sea ice was close in time to major volcanic eruptions, including in the 15th century. Model simulations suggest that summer cooling, maintained by anomalies in ocean heat transport may have contributed to sustained cooling. .

Temperatures during the Medieval Climate Anomaly (see Glossary) were substantially warmer than in the LIA, particularly in the 10th and 11th century, though the amplitude of the temperature difference is very uncertain (Figure 5.9.e,f; see also Figure 10.20). Solar forcing estimates in this period are uncertain, although results suggest an overall slightly elevated solar forcing (Figure 5.1), however, the timing of positive solar forcing anomalies is substantially later than that of the peak warmth in many reconstructions. In contrast to the LIA, the reconstructed elevated temperatures do not coincide with a CO_2 change in that period (Frank et al., 2007). The magnitude and even the sign of Land Use change forcing at the time is highly uncertain. Detection and attribution analyses of the entire millennium suggest that external forcing contributed to warm conditions in the 11th and 12th century (see Figure 10.18), but not around the turn of the millennium. Data assimilation methods (Goosse et al., 2012a; Goosse et al., 2012b) suggest that long-term changes in the atmospheric circulation may be able to explain some of the remaining difference between models and data (Figure 10.18). The technique, however, does not allow to determine if those circulation changes are purely related to the internal variability of the climate or to a response of the system to some forcing not well represented in the relatively simple climate model used in those experiments.

In conclusion, external forcing very likely contributed to the cold conditions during the LIA, while the role of external forcing in the MCA is less clear.

10.7.3 Changes of Past Regional Temperature

Several reconstructions of European regional temperature variability are available (Section 5.5). Bengtsson et al. (2006) concluded that preindustrial European climate captured in the Luterbacher et al. (2004) reconstruction of European seasonal temperature is ‘fundamentally a consequence of internal fluctuations of the climate system’ since short-term variability in an OAGCM control simulation closely resemble those in

this reconstruction. However, Hegerl et al. (2011a) analyzed 5-year averaged European seasonal temperatures, using a fingerprint for the response to forcing based on three climate model simulations, and find a detectable response to external forcing in summer temperatures in the period prior to 1900, and throughout the record for winter and spring, with the fingerprint of the forced response showing coherent time evolution between models and reconstructed temperatures over the entire analysed period (compare to annual results in Figure 10.18, using a larger multi-model ensemble) This suggests that the cold winter conditions in the late 17th and early 19th century and the warming in between were at least partly externally driven.

Data assimilation results focusing on the European sector again shows that the explanation of forced response combined with internal variability is self-consistent (Goosse et al., 2012a), Figure 10.18). While the simulations that are only forced and also those that include data assimilated both closely follow the reconstructions from 1400 onwards, the assimilated induces the simulations to more closely reproduce the warmth of the MCA than the forced only simulations do.

The response to individual forcings is difficult to distinguish from each other in noisier regional reconstructions. An epoch analysis of years immediately following volcanic eruptions shows that European summers following volcanic eruptions are significantly colder than average years, while winters show a noisy, but detectible response of warming in Northern Europe and cooling in Southern Europe (Hegerl et al., 2011a). There is also evidence for a decrease in SSTs following volcanic forcing in tropical reconstructions (D'Arrigo et al., 2009).

Model simulations are able to reproduce some of the variations exhibited by regional temperature reconstructions also in other regions (discussed in Section 5.5), but in some instances they lie outside even the broad uncertainty ranges (Figure 5.12). Determining whether these differences arise from model deficiencies would require quantitative comparisons that also consider internal variability (which makes a significant contribution at these regional scales), as is done in detection and attribution studies. However, few detection analyses for forced variability in regional temperatures are available at present that explicitly consider the influences of internal variability and all relevant forcings. There are some studies considering, for example, solar forcing (Zhang et al., 2008a). For example, Esper et al. (2012) suggest evidence for a role of orbital forcing in long-term Arctic records.

In conclusion, there is medium evidence for an influence by external forcing on European temperatures from 1500 onwards.

10.7.4 Estimates of Unforced Internal Climate Variability

The interdecadal and longer-term variability in large-scale temperatures in climate model simulations with and without past external forcing is quite different (Jungclaus et al., 2010; Tett et al., 2007), consistent with the finding that a large fraction of temperature variance in the last millennium has been externally driven. The residual variability in past climate that is not explained by changes in radiative forcing provides an estimate of internal variability of the climate system that is not directly derived from climate model simulations, but the residual variability in some reconstructions is somewhat larger than control simulation variability if the comparison is extended to the full period since 850 CE (Hegerl et al., 2007a). However, in all cases considered by (Schurer et al., 2012), the most recent 50-year trend from instrumental data is far outside the range of any 50-year trend in residuals from reconstructions of the past millennium.

10.7.5 Summary: Lessons from the Past

Detection and attribution studies show that external forcing contributed to past climate variability and change. Results suggest that particularly volcanic forcing and CO_2 forcing are important to explain past changes in Northern Hemispheric temperatures. Results from data assimilation runs confirms that internal variability combined with forcing provides a consistent explanation of the last millennium and suggest that changes in circulation may have further contributed to climate anomalies. The role of external forcing extends to regional records, for example, European seasonal temperatures. In summary, the evidence across a range of studies support and strengthen the conclusion that external forcing very likely contributed to Northern Hemispheric temperature change over the past seven centuries. There is medium evidence that

external forcing contributed to Northern Hemispheric temperature variability since 850 CE, and that it contributed to European temperatures of the last few centuries.

10.8 Implications for Climate System Properties and Projections

Detection and Attribution results also provide estimates of the magnitude of the climate system response to external forcing and can be used to predict future changes. The value and strength of the constraint on future changes depends on how relevant observable climate changes are for the predicted response, and on the signal-to-noise ratios of the change considered. Transient climate response (TCR) is a measure of the magnitude of transient warming while the system is not in equilibrium, and is particularly relevant for near-term temperature changes while emissions continue increasing or peak (e.g., Frame et al., 2006; Section 10.8.1; Annex 1; Glossary; see Chapter 12). TCR is more tightly constrained by the observations of transient warming than equilibrium sensitivity (see, for example, Baker and Roe, 2009; Frame et al., 2005; Forest et al., 2008). The Equilibrium Climate Sensitivity (ECS; Section 10.8.4) is an important climate system property and diagnostic of climate system feedbacks. It is used in determining the CO_2 concentration levels that are needed to keep equilibrium climate below particular temperature thresholds (see, e.g., Solomon et al., 2009). This use of ECS to determine the radiative forcing consistent with a particular temperature change requires further assumptions about the efficacy of different forcings (Box 12.1). Constraints on estimates of long-term climate change and equilibrium climate change from recent warming hinge on the rate at which the ocean has taken up heat (Section 3.2), and by the extent to which recent warming has been reduced by cooling from aerosol forcing. Therefore, attempts to estimate climate sensitivity (transient or equilibrium) often also estimate the total aerosol forcing and the rate of ocean heat uptake (Section 10.8.3). The AR4 had for the first time a detailed discussion on estimating these quantities relevant for projections, and included an appendix with the relevant estimation methods. Here, we build on the assessment from AR4, repeating information and discussion only where necessary to provide context.

10.8.1 Transient Climate Response

The AR4 discussed for the first time estimates of the transient climate response. TCR was originally defined as the warming at the time of CO_2 doubling (i.e., after 70 years) in a 1% yr^{-1} increasing CO_2 experiment (see (Hegerl et al., 2007b), but like ECS, it can also be thought of as a generic property of the climate system that determines the transient response to any gradual increase in radiative forcing taking place over a similar timescale (Frame et al., 2006; Held et al., 2010). Frame et al. (2006) introduce a 'normalised TCR', defined as the rate of warming in degrees per year divided by the fractional rate of CO_2 increase per year over, to avoid the apparent scenario-dependence of the original definition of TCR. If, however, we adopt a more generic interpretation of TCR, there is no need for any new notation, since their normalised TCR is simply this generic TCR divided by 0.7. Likewise, Held et al. (2010) used the simple two-box model of Gregory (2000) to show that deep ocean heat exchange affects the surface temperature response as if it were an enhanced radiative damping: hence the difficulty of placing an upper bound on climate sensitivity from observed surface warming alone (Forest et al., 2002; Frame et al., 2005). Heating of the deep ocean introduces a slow, or 'recalcitrant', component of the response which could not be reversed for many decades even if it were possible to return radiative forcing to pre-industrial values. They show that the fast component of the response, which they refer to as the 'Transient Climate Sensitivity' but could equally be thought of as this generic TCR, is approximately independent of the actual percent-per-year rate of CO_2 increase. Hence we will use TCR as well as ECS to describe generic emergent properties of a climate model or the climate system itself rather than the outcome of a specific scenario.

Since TCR focuses on the short term response, constraining TCR with observations is a key step in narrowing estimates of future global temperature change in the relatively short term (Lorenz et al., 2012) and under scenarios where forcing continues to increase or peak (Frame et al., 2006). After stabilisation, the ECS eventually becomes the relevant climate system property. Based on observational constraints alone, the AR4 concluded that TCR is very likely to be larger than 1°C and very unlikely to be greater than 3.5°C (Hegerl et al., 2007b). This supported the overall assessment that the transient climate response is very unlikely greater than 3°C and very likely greater than 1°C (Meehl et al., 2007a). Since the AR4 report, new estimates of the TCR are now available.

Recently observed climate change provides opportunities to estimate the TCR (Allen et al., 2000). Scaling factors derived from fingerprint detection and attribution (see Section 10.2) express how model responses to greenhouse gases and aerosols need to be scaled to match the observations over the historical period. These scaled responses may be used to provide probabilistic projections of the future response to these forcings (Allen et al., 2000; Kettleborough et al., 2007; Meehl et al., 2007b; Stott and Kettleborough, 2002; Stott and Forest, 2007; Stott et al., 2008a; Stott et al., 2006). Allen et al. (2000), Frame et al. (2006) and Kettleborough et al. (2007) demonstrate a near linear relationship for a wide range of parameters between 20th century warming, TCR and warming by the mid-21st century in Energy Balance Models, thus justifying this approach to estimating future responses from observationally-constrained projections. Projections based on scaling factors from detection and attribution studies (Stott et al., 2006) were used in the AR4 (Meehl et al., 2007b) for estimating probabilistic ranges of future changes of global temperature and TCR. Stott et al. (2008a) demonstrated that optimal detection analysis of 20th century temperature changes (using HadCM3) are able to exclude the very high and low temperature responses to aerosol forcing. Consequently, projected 21st century warming may be more closely constrained than if the full range of aerosol forcings is used (Andreae et al., 2005). Stott and Forest (2007) demonstrate that projections obtained from such an approach are similar to those obtained by constraining energy balance model (EBM) parameters from observations. Stott et al. (2011), using HadGEM2-ES, and Gillett et al. (2011a), using CanESM2, both show that the inclusion of observations between 2000 and 2010 in such an analysis substantially reduces the uncertainties in projected warming in the 21st century, and tends to constrain the maximum projected warming to below that projected using data to 2000 only. Such an improvement is consistent with prior expectations of how additional data will narrow uncertainties (Stott and Kettleborough, 2002).

TCR estimates have been derived using a variety of methods. Knutti and Tomassini (2008) derive a probability density function shifted slightly towards lower values with a 5–95% percent range of 1.1–2.3 K. Using a single model and observations from 1851 to 2010 Gillett et al. (2011a) derive a 5–95% range of 1.3–1.8 K and using a single model, but multiple sets of observations and analysis periods ending in 2010 and beginning in 1910 or earlier, Stott et al. (2011) derive 5–95% ranges that were generally between 1 K and 3 K. Both Stott et al. (2011) and Gillett et al. (2011a) find that the inclusion of data between 2000 and 2010 helps to constrain the upper bound of TCR. Gillett et al. (2011a) find that the inclusion of data prior to 1900 also helps to constrain TCR, though Stott et al. (2011) do not find such sensitivity, perhaps due to relatively low internal variability on timescales longer than 100 years in the model used by Gillett et al. (2011a).Three estimates of TCR estimated in this way are shown in Figure 10.19. Using greenhouse gas scaling factors calculated from the HadGEM2, CNRM and CanESM2 models and from the weighted multi-model mean shown in Figure 10.4. (Libardoni and Forest, 2011) show that the TCR along with other climate system parameters (see below) can be estimated from a range of 20th century surface temperature atmospheric and ocean temperatures datasets. They estimate a 5–95% range of TCR of 0.9 to 2.4 K. Several of the estimates of TCR that were cited by Hegerl et al. (2007b) used 20th century radiative forcing due to well-mixed greenhouse gases and these studies may have under-estimated the efficacies of non-CO_2 gases relative to the more recent estimates in Forster et al. (2007). Since the observationally constrained estimates of TCR are based on the ratio between past attributable warming and past forcing, this could account for a high bias in some of the inputs used for the AR4 TCR estimate.

Held et al. (2010) show that their two-box model, distinguishing the fast and recalcitrant responses, fits both historical simulations and instantaneous doubled CO_2 simulations of the GFDL coupled model CM2.1. In the instantaneous simulations the fast response has a relaxation time of 3–5 years, and where the historical simulation is almost completely described by this fast component of warming. Padilla et al. (2011) use this simple model to derive an observationally-constrained estimate of the TCR of 1.3–2.6 K, similar to other recent estimates. TCR is necessarily lower than ECS. Hence the lower bound on TCR is closely linked to the lower bound on ECS, minus the uncertain contribution from ocean heat uptake, while the upper bound on TCR is primarily determined by observed warming and uncertainty in forcing.

A recent study based an estimate of TCR on the response to the 11-year solar cycle as estimated from observations and reanalysis data, using discriminant analysis and find a relatively high estimate >2.5 to 3.6 K (Camp and Tung, 2007). However, this estimate may be affected by different mechanisms by which solar forcing across wavelengths affects climate, and despite attempts to avoid aliasing the response to other forcings in the 20th century, the estimate may be influenced by it and by internal climate variability – see discussion in (North and Stevens, 1998).

Based on this evidence, including the new 21st century observations that were not yet available to AR4, we conclude that TCR is very likely to be larger than 1°C and very unlikely to be greater than 3°C on the basis of observational constraints. This range for TCR is smaller than given at the time of AR4, due to the stronger observational constraints and the wider range of studies now available.

10.8.2 Constraints on Long Term Climate Change and the Equilibrium Climate Sensitivity

The equilibrium climate sensitivity (ECS) is defined as the warming in response to a sustained doubling of carbon dioxide in the atmosphere relative to preindustrial levels (see AR4). The ECS cannot be directly deduced from transient warming attributable to greenhouse gases, or from TCR, since the role of ocean heat uptake has to be taken into account (see (Forest et al., 2000; Frame et al., 2005; Hegerl et al., 2007b). Estimating the ECS generally relies on the same paradigm of a comparison of observed change with results from a physically based climate model, given uncertainty in the model, data, radiative forcing, and internal variability.

The equilibrium to which the ECS refers to is generally assumed to be an equilibrium involving the ocean-atmosphere system, which does not include earth system feedbacks such as long-term melting of ice sheets and ice caps, dust forcing, or vegetation changes (see Chapter 5, Chapter 12, Section 12.5.3; Hansen et al., 2005a). Estimates of climate sensitivity can be based on estimating, with uncertainties, past warming per unit forcing change, and then adapting this sensitivity parameter by multiplying it with the forcing associated with CO_2 doubling (which is itself uncertain, see Chapter 9). However, simple energy balance calculations introduce substantial uncertainties: for example, they might assume a single response timescale rather than the multiple response timescales that are observed, and cannot account for nonlinearities in the climate system that may lead to changes in feedbacks for different forcings (see Chapter 9). Alternative approaches are estimates that use climate model ensembles with varying parameters that evaluate the ECS of individual models and then infer the probability density function (pdf) for the ECS from the model-data agreement or by using optimization methods (Tanaka et al., 2009). As discussed in the AR4, such estimates are inherently based on Bayesian statistics and therefore, even if it is not explicitly stated, involve using prior information or prior beliefs. This prior information shapes the sampling distribution of the models and since the constraints by data on transient warming is fairly weak, results are sensitive to the prior constraints or assumptions (Aldrin et al., 2012; Sanso and Forest, 2009) . Constraints on the upper tail of ECS are particularly weak if the assumed prior distribution levels off for high sensitivities, as is the case for uniform priors (e.g., Frame et al., 2006). Uniform priors have been criticised (e.g., Annan and Hargreaves, 2011), but this point applies to any prior: if the data do not distinguish between a high and very-high value for ECS, their relative probability must be determined by the prior. Results will also be sensitive to the extent to which uncertainties in forcing, models and observations are taken into account. Analyses that make a more complete effort to estimate all uncertainties affecting the model-data comparison lead to more trustworthy results, but appear to heave larger uncertainties than methods that apply more assumptions (Knutti and Hegerl, 2008; Tanaka et al., 2009).

The detection and attribution chapter in AR4 (Hegerl et al., 2007b) concluded that 'Estimates based on observational constraints indicate that it is *very likely* that the equilibrium climate sensitivity is larger than 1.5°C with a most likely value between 2°C and 3°C' supporting the overall assessment here that the 'likely' range of ECS is 2°C–4.5°C,'(Meehl et al., 2007b).

10.8.2.1 Estimates from Recent Surface Temperature Change

A range of new estimates of ECS are shown in Figure 10.19. As discussed in AR4, analyses based on global scale data find that within data uncertainties, a strong aerosol forcing or a large ocean heat uptake might have masked a strong greenhouse warming (see, e.g., Stern, 2006; Forest et al., 2002; Frame et al., 2006; Hannart et al., 2009; Roe and Baker, 2007; Urban and Keller, 2009). This is consistent with the finding that a set of models with a large range of ECS and aerosol forcing could be consistent with the observed warming (Kiehl, 2007). Consequently, such analyses find that constraints on aerosol forcing are essential to provide tighter constraints on future warming (Schwartz et al., 2010; Tanaka et al., 2009). Huber and Knutti (2012) and Aldrin et al. (2012) analyze the observed record from 1850 for surface temperature, and ocean heat content since the middle of the 20th century. Aldrin et al. (2012) find a narrower range than Huber and Knutti

(2012), possibly in part due to the use of hemispheric rather than global mean data. However, Aldrin et al. (2012) do not properly account for climate variability (Figure 10.19) and find that wider ranges are consistent with the observations if cloud lifetime effects due to aerosols are significant. Olson et al. (2012) use similar global scale constraints and arrive at a range of 1.8°C to 4.9°C using a uniform prior. An approach based on regressing forcing histories used in 20th century simulations on observed surface temperatures (Schwartz, 2012), accounting for ocean heat uptake, finds a sampling range of ECS of 1.1°C to 6.1°C for a doubling of CO_2.

Estimates of ECS and TCR that make use of both spatial and temporal information, or separate the greenhouse gas attributable warming using fingerprint methods can yield tighter estimates (e.g., Forest et al., 2008; Frame et al., 2005; Libardoni and Forest, 2011). The resulting greenhouse gas attributable warming tends to be reasonably robust to uncertainties in aerosol forcing (see Section 10.3.1.1.3). Forest et al. (2008) have updated their earlier study using a newer version of the MIT model and 5 different surface temperature datasets (Libardoni and Forest, 2011). The overarching 5–95% range of effective climate sensitivity widens from 2–5 K from (Forest et al., 2008) to 1.2–5.3 K when all five datasets are used, and constraints on effective ocean diffusivity become very weak. Uncertainties would likely further increase if estimates of forcing uncertainty, say due to natural forcings, are also included (Forest et al., 2006). Lewis (2012) re-analyzed the data used in Forest et al. (2006) using an objective Bayesian method and find that use of a non-uniform prior lowers the upper limit of ECS. However, this author also presents two very different results based on differently processed versions of the data used in Forest et al. (2006), one of them unpublished, suggesting this may arise from a data-processing error. Hence neither the latter results nor Lewis (2012) are shown here until these differences are resolved. Libardoni and Forest (2011) and Forest et al. (2008) used new model simulations and hence do not depend on the Forests et al. (2006) dataset.

In summary, recent work on instrumental temperature change explores data and forcing uncertainty more completely than available at the time of AR4, and benefits from a longer instrumental record but cannot provide a robusts upper limit on ECS alone.

10.8.2.2 Estimates Based on Top-of the Atmosphere (TOA) Radiative Balance

With the satellite era, measurements are now long enough to allow direct estimates of variations in the energy budget of the planet (see Box 13.1). Using a simple energy balance relationship between net energy flow towards the Earth, net forcing and a climate feedback parameter and the satellite measurements (Murphy et al., 2009) made direct estimates of the climate feedback parameter as the regression coefficient of radiative response against global mean temperature. The feedback parameter in turn is inversely proportional to the ECS (see e.g., Forster and Gregory, 2006). Spencer and Braswell (2008) suggest that such an analysis method of the feedback parameter biases estimates of sensitivity to high values, but Murphy and Forster (2010) show that this is largely an artefact of unrealistic assumptions and parameter values, (see also, Gregory and Forster, 2008). Also, the trend in shortwave outgoing radiation and with it net radiation budget is affected by uncertainties in measurements, (Harries and Belotti, 2010). Lindzen and Choi (2009) used data from the radiative budget and simple energy balance models over the tropics to investigate if the feedbacks shown in climate models are realistic and claim that climate models overestimate the outgoing shortwave radiation compared to ERBE data, leading to an overall mis-estimation of the radiative budget. However, the use of a limited sample of periods and the use of a domain limited to low latitudes makes the result unreliable (Murphy and Forster, 2010). Lindzen and Choi (2011) address some of these criticism (Chung et al., 2010; Lindzen and Choi, 2009; Trenberth et al., 2010). However, key assumptions like the use of lagged correlation to determine the whether TOA or SST causes the fluctuations in the energy balance are questioned by (Dessler, 2011), as the lag-lead relationship found in (Lindzen and Choi, 2011) is replicated by AMIP simulations where SST cannot respond; confirming that observed temperature variations on short timescales are a combination of radiatively forced and internal variations Murphy et al. (2009) also question if estimates of the feedback parameter are suitable to estimate the ECS, since multiple timescales are involved in feedbacks that contribute to climate sensitivity (Knutti and Hegerl, 2008; see also Dessler, 2010). Lin et al. (2010a) use data over the 20th century combined with an estimate of present TOA imbalance based on modelling (Hansen et al., 2005a) to estimate the energy budget of the planet and give a best estimate of ECS of 3.1K, but do not attempt to estimate a distribution that accounts fully for uncertainties. In conclusion, some recent estimates of high feedback/low sensitivities based on aspects of the observed radiation budget are not robust to measurement and method uncertainties, which are substantial. Consequently present TOA

radiation budgets appear consistent with other estimates of climate sensitivity. These estimates often hinge on assumptions and are affected by uncertainties, and hence are unable to constrain further these climate sensitivity estimates.

10.8.2.3 Estimates Based on Response to Natural Forcing or Internal Variability

Some analyses used in AR4 were based on the well observed forcing and responses to major volcanic eruptions during the 20th century. The constraint is fairly weak since the peak response to short-term volcanic forcing depends nonlinearly on ECS (Boer et al., 2007; Wigley et al., 2005). Recently, Bender at al. (2010) re-evaluated the constraint and found a close relationship in 9 out of 10 AR4 models between the shortwave TOA imbalance, the simulated response to the eruption of Mount Pinatubo and the ECS. Applying the constraint from observations suggests a range of ECS of 1.7–4.1 K. This range for ECS is subject to observational uncertainty, uncertainty due to internal climate variability, and is derived from a limited sample of models. Tung et al. (2008) estimated a lower limit on ECS based on the estimated TCR in response to solar cycle, but the estimate is affected by uncertainties in their relationship between ECS and TCR, uncertainty in the distribution of solar forcing across the spectrum, as well as possible changes in circulation. Schwartz (2007) tried to relate the ECS to the strength of natural variability using the fluctuation dissipation theorem but studies suggest that the observations are too short to support a well constrained and reliable estimate and yielded an underestimate of sensitivity (Kirk-Davidoff, 2009); and that assuming single timescales is too simplistic for the climate system (Foster et al., 2008; Knutti et al., 2008). Thus, credible estimates of ECS from the response to natural and internal variability do not disagree with other estimates, but at present, cannot provide more reliable estimates of ECS.

10.8.2.4 Paleoclimatic Evidence

Palaeoclimatic evidence is promising for estimating ECS (Edwards et al., 2007). This section reports on probabilistic estimates of ECS derived from paleoclimatic data by drawing on Chapter 5 information on forcing and temperature changes. For periods of past climate, which were close to radiative balance or when climate was changing slowly, for example, the Last Glacial Maximum (LGM), radiative imbalance and with it ocean heat uptake is not important. However, for the LGM the uncertainty in the radiative forcing due to ice sheets, dust, and CO_2 decreases leads to large forcing uncertainty (see Chapter 5.3.3). The possibility of small forcing having led to the reconstructed change lengthens the tail in the estimates of ECS. Koehler et al. (2010) used an estimate of LGM cooling along with its uncertainties together with estimates of LGM radiative forcing and its uncertainty to derive an overall estimate of climate sensitivity. This method accounts for the effect of changes in feedbacks for this very different climatic state using published estimates of changes in feedback factors (see Section 5.3.3; Hargreaves et al., 2007; Otto-Bliesner et al., 2009). The authors find a best estimate of 2.4°C and a 5–95% range of ECS from 1.4°C–5.2°C, with sensitivities beyond 6°C difficult to reconcile with the data. In contrast, Chylek and Lohmann (2008b) estimate the ECS to be 1.3°C to 2.3°C based on data for the transition from the LGM to the Holocene, but consider only a a small number of datapoints and neglect uncertainties, thus underestimating the range of sensitivities consistent with data (Chylek and Lohmann, 2008a; Ganopolski and Schneider von Deimling, 2008; Hargreaves and Annan, 2009).

At the time of the AR4, several studies were assessed in which parameters in climate models had been perturbed systematically in order to estimate ECS, and further studies have been published since, some making use of expanded data for LGM climate change (see Chapter 5; Schmittner et al., 2011). Sometimes substantial differences between estimates based on similar data reflect not only differences in assumptions on forcing and use of data, but also structural model uncertainties, for example in how feedbacks change between different climatic states (e.g., Hargreaves et al., 2007; Schneider von Deimling et al., 2006, see also Otto-Bliesner et al., 2009; Holden et al., 2010) analyzed which versions of the EMIC Genie are consistent with LGM tropical SSTs and find a 90% range of 2.0–5.0 K, again emphasizing the role of structural model uncertainty. Recently, new data synthesis products have become available for assessment with climate model simulations of the LGM (Otto-Bliesner et al., 2009), which together with further data cover much more of the LGM ocean and land areas, although there are still substantial gaps (see Chapter 5). An analysis of the recent SST and land temperature reconstructions for the LGM shows that land only data support a 90% range of 2.2–4.6 K, while the SSTs yield a much tighter constraint of 1.3°C–2.7°C (Schmittner et al., 2011).

However, the true uncertainties are likely larger given the possibility of systematic biases in data, structural model uncertainty, and forcing uncertainties.

Estimates of ECS from other, more distant paleoclimate periods (e.g., Royer, 2008; Royer et al., 2007; Lunt et al., 2010; Pagani et al., 2009), are difficult to directly compare, as the response on very long timescales is determined by the Earth System Sensitivity, which includes very slow feedbacks by ice sheets and vegetation (see Sections 5.3.3, 12.5.3). Recently, PALEOSENS (2012) re-analysed the relationship between radiative forcing and temperature response from paleoclimatic studies, considering earth system feedbacks as forcings in order to derive a Charney-type ECS, and find that resulting estimates are reasonably consistent over the past 65 million years. They estimate a 95% range of 1.1°C to 7.0°C (assuming a radiative forcing of 3.7 W m^{-2} to CO_2 doubling), largely based on the past 800,000 years. However, uncertainties in the deep past are substantially larger, due to substantial differences in the earth system compared to today as well as uncertainties in processes, records and their dating (see Section 5.3.1). In conclusion, estimates of ECS have continued to emerge from palaeoclimatic periods that support upper limits on ECS at 6°C or lower, but uncertainties are substantial.

10.8.2.5 Combining Evidence and Overall Assessment

Most studies find a lower 5% limit for ECS between 1°C and 2°C (see Figure 10.19). The combined evidence thus indicates that the net feedbacks to radiative forcing are significantly positive and emphasizes that greenhouse warming will not be small. Presently, there is no credible individual line of evidence which yields very high or very low climate sensitivity as best estimate. Some recent studies suggest a low climate sensitivity (Chylek et al., 2007; Lindzen and Choi, 2009; Schwartz et al., 2007). However, these are based on problematic assumptions, for example, about the climate's response time, the cause of climate fluctuations, or serious neglect of uncertainty in forcing, observations, and internal variability (as discussed in Foster et al., 2008; Knutti et al., 2008; Lin et al., 2010b; Murphy and Forster, 2010). In some cases the estimates of the ECS have been refuted by testing the method of estimation with a climate model of known sensitivity (e.g., Kirk-Davidoff, 2009).

The difficulty in constraining the upper tail of ECS (illustrated in Figure 10.19) is due to a variety of reasons. Since the ECS is proportional to the inverse of feedbacks, long tails originate from normal uncertainty distributions of feedbacks which cannot be easily reduced by estimating feedbacks individually (Roe and Baker, 2007), although the linearity assumption may lead to an overly pessimistic assumption of the ability to constrain ECS (Zaliapin and Ghil, 2010). Several estimates have modes that are smaller than those from the overall estimate. However, low estimates of modes can arise due to forcing error (e.g., see Hegerl et al., 2006) and sampling uncertainty.

Several authors (Annan and Hargreaves, 2006, 2010; Hegerl et al., 2006) have proposed combining estimates of climate sensitivity from different lines of evidence. This formalizes that if independent data point at similar values for ECS, the evidence strengthens, and the uncertainties reduce. However, if several climate properties are estimated simultaneously that are not independent, such as ECS and ocean heat uptake, this needs to be accounted for in combinations of evidence. Also, neglected uncertainties will become increasingly important as other uncertainties are reduced. All this may lead to overly confident assessments (Annan and Hargreaves, 2011; Henriksson et al., 2010), a reason why results combining multiple lines of evidence are still treated with caution.

In conclusion, estimates based on observational constraints continue to indicate that it is very likely that the equilibrium climate sensitivity is larger than 1.5°C. New evidence continues to support from observations the overall assessment (Chapter 12, Box 12.2) that the equilibrium climate sensitivity is likely in the range from 2°C–4.5°C. Uncertainties are better understood than at the time of AR4, and some new lines of evidence have emerged. An expert assessment of multiple lines of observational evidence supports the overall conclusion (Chapter 12) that an ECS greater than about 6°C–7°C is very unlikely. Earth system feedbacks can lead to different, probably larger, warming than indicated by ECS on very long timescales.

[INSERT FIGURE 10.19 HERE]

Figure 10.19: Top: Distributions of the transient climate response (TCR, top) and the equilibrium climate sensitivity (bottom). PDFs and ranges (5–95%) for the transient climate response estimated by different studies (see text). The grey

shaded range marks the very likely range of 1°C–3°C for TCR as assessed in this section. Bottom: Estimates of equilibrium climate sensitivity from observed / reconstructed changes in climate compared to overall assessed likely range (grey). The figure compares some selected old estimates used in AR4 (no labels) with new estimates available since (labelled). Distributions are shown where available, together with 5–95% ranges. Ranges that have been queried in the literature or have problematic assumptions are labelled by arrows at the border. Estimates are based on top-of the atmosphere radiative balance (top row), instrumental changes including surface temperature (2nd row); changes from palaeoclimatic data (3rd row), and studies using nonuniform priors or combining evidence (for details of studies, see text; fourth row). The boxes on the right hand side indicate limitations and strengths of each line of evidence given in a separate panel, for example, if a period has a similar climatic base state, if feedbacks are similar to those operating under CO_2 doubling, if the observed change is close to equlibrium, if, between all lines of evidence plotted, uncertainty is accounted for relatively completely, and summarizes the level of scientific understanding of this line of evidence overall. Green marks indicate an overall line of evidence that is well understood, has small uncertainty, or many studies and overall high confidence. Yellow indicates medium and red low confidence (i.e., poorly understood, very few studies, poor agreement, unknown limitations). After Knutti and Hegerl (2008). The data shown is as follows. Satellite period: (orange) (Lin et al., 2010a) (cyan) (Lindzen and Choi, 2011) (yellow) (Forster and Gregory, 2006), using a uniform prior on feedbacks and (red) using a uniform prior on ECS; 20th Century: (pink) (Aldrin et al., 2012), using different assumptions and priors,, (dark green) (Libardoni and Forest, 2011), based on 5 observational datasets, (cyan) Olson et al., (2012), (dark blue) (Schwartz, 2012), (green) Knutti et al, 2002; (yellow) Gregory et al., 2002; (orange) Frame et al., 2005; (red) (Bender et al., 2010) Palaeoclimate: (red) (Chylek and Lohmann, 2008b), (orange) (Holden et al., 2010) (yellow) (Koehler et al., 2010) (cyan) (Paleosens Members (E.J. Rohling and R.S.W. van de Wal, 2012) (green solid) Schmittner et al, 2011, land-and-ocean; (green dashed) (Schmittner et al., 2011),land-only; and dash dotted, ocean-only; (purple dashed) Annan LGM, 2005. Combination of evidence: (yellow) (Libardoni and Forest, 2011) using different datasets, cyan (Olsen et al.,) compared to (red) (Annan and Hargreaves, 2006) and orange, Hegerl et al., 2006.

10.8.3 Consequences for Aerosol Forcing and Ocean Heat Uptake

Some estimates of ECS also yield estimates of aerosol forcing that are consistent with observational records, which we briefly mention here for cross reference for Chapter 7. Murphy et al. (2009) use correlations between surface temperature and outgoing shortwave and longwave flux over the satellite period to estimate how much of the total recent forcing has been reduced by aerosol total reflection, which they estimate as -1.1 ± 0.4 W m^{-2} from 1970 to 2000 (1 standard deviation), while Libardoni and Forest (2011), see also Forest et al. (2008), based on the 20th century, find somewhat lower estimates, namely a 90% bound of –0.83 to –0.19 W m^{-2} for the 1980s.

Forest and Reynolds (2008) find that the effective diffusivity K_v in many of the CMIP3 models lies above the median value based on observational constraints, resulting in a positive bias in their ocean heat uptake. However, this finding was found to be very sensitive to datasets used for surface temperature (Libardoni and Forest, 2011) and ocean heat content (Sokolov et al., 2010). Thus, estimates of effective vertical diffusivity raise questions about the way models transport heat into the ocean, but results are inconclusive. Recent analysis of CMIP3 and CMIP5 models combined also suggests that the heat uptake efficiency by the models may be too high (see also Sections 9.4.2, 10.4.1, 10.4.3, 13.4.1), leading to a tendency to bias ocean warming high and surface warming low (Kuhlbrodt and Gregory, 2012). However this tendency seems to make only a small contribution to the model spread in TCR.

10.8.4 Earth System Properties

A number of papers have found the global warming response to carbon dioxide emissions to be determined primarily by total cumulative emissions of CO2, irrespective of the timing of those emissions over a broad range of scenarios (Allen et al., 2009; Matthews et al., 2009; Zickfeld et al., 2009; Chapter 6, Section 6.5.1.2), although Bowerman et al. (2011) find that, when scenarios with persistent "emission floors" are included, the strongest predictor of peak warming is cumulative emissions to 2200. Moreover, the ratio of global warming to cumulative carbon emissions, known variously as the Absolute Global Temperature Change Potential (defined for an infinitesimal pulse emission; AGTP) (Shine et al., 2005), the Cumulative Warming Commitment (defined based on peak warming in response to a finite injection; CWC) (Allen et al., 2009) or the Carbon Climate Response (CCR) (Matthews et al., 2009), is scenario independent and approximately constant in time.

The ratio of CO_2-induced warming realised by a given year to cumulative carbon emissions to that year, known as the Transient Response to Cumulative Emissions (TRCE, see Chapter 12), depends on properties of the physical climate system and the carbon cycle. It may be estimated from observations by dividing warming to date attributable to CO_2 by historical cumulative carbon emissions, which gives a 5–95% range of 1.0°C to 2.1°C TtC^{-1} (Matthews et al., 2009) or 1.4°C to 2.5°C TtC^{-1} (Allen et al., 2009), the higher range reflecting a higher estimate of CO_2-attributable warming to 2000 in the latter study. The peak warming induced by a given total cumulative carbon emission (Peak Response to Cumulative Emissions, PRCE) is less well constrained, since warming may continue even after a complete cessation of CO_2 emissions, particularly for high-response models or scenarios. Using a combination of observations and models to constrain temperature and carbon cycle parameters in a simple ESM, Allen et al. (2009), obtain a PRCE of 5–95% confidence interval of 1.3°C to 3.9°C TtC^{-1}. They also report that Meinshausen et al. (2009) obtain a 5–95% range in PRCE of 1.1°C to 2.7°C TtC^{-1} using a Bayesian approach with a different EMIC, with climate parameters constrained by observed warming and carbon cycle parameters constrained by the C4MIP simulations. Gillett et al. (2012b) update the analysis of Matthews et al. (2009) and obtain an observationally-constrained estimate of TRCE of 0.8°C–2.1°C TtC^{-1}.

The ratio of warming to cumulative emissions, the Transient Climate Response to Cumulative Emissions is estimated to be very likely between 0.8°C TtC^{-1} and 3ºC TtC^{-1} based on observational constraints.

10.9 Synthesis

The evidence accumulated from widespread anthropogenic changes detected in aspects of the climate system, and documented in the preceding sections, including near surface temperature (Section 10.3.1.1), free atmosphere temperature (Section 10.3.1.2), atmospheric moisture content (Section 10.3.2.1), precipitation over land (Section 10.3.2.2), ocean heat content (Section 10.4.1), ocean salinity (Section 10.4.2), and Arctic sea ice (10.5.1) as well as aspects of climate extremes (Section 10.6) and during the last millennia (Section 10.7). These results strengthen the conclusion that human influence has played the dominant role in observed warming over the past several decades. However, the approach so far has been to examine each aspect of the climate system – the atmosphere and surface, oceans, cryosphere, and some extremes – separately. In this section we look across the whole climate system to assess to what extent a consistent picture emerges across sub-systems and across climate variables.

10.9.1 Remaining Challenges

One of the remaining challenges is the explicit use of multi-variable approaches to a more comprehensive level across the climate system. There have been relatively few applications of multi-variable detection and attribution studies in the literature. A combined analysis of near-surface temperature from weather stations and free atmosphere temperatures from radiosondes detected an anthropogenic influence on the joint changes in temperatures near the surface and aloft (Jones et al., 2003). In a Bayesian application of detection and attribution (Schnur and Hasselmann, 2005) combined surface temperature, diurnal temperature range and precipitation into a single analysis and showed strong net evidence for detection of anthropogenic forcings despite low likelihood ratios for diurnal temperature range and precipitation on their own. Barnett et al.(2008) applied a multi-variable approach in analysing changes in the hydrology of the Western United States (see also Section 10.3.2.3).

The potential for a multi-variable analysis to have greater power to discriminate between forced changes and internal variability was also demonstrated by (Stott and Jones, 2009) and Pierce et al. (2012). In the former case, they showed that a multi-variable fingerprint consisting of the responses of global mean temperature and sub-tropical Atlantic salinity has a higher signal to noise than the fingerprints of each variable separately. They found reduced detection times as a result of low correlations between the two variables in the control simulation although the detection result depends on the ability of the models to represent the co-variability of the variables concerned. Multi-variable attribution studies potentially provide a stronger test of climate models than single variable attribution studies although there can be sensitivity to weighting of different components of the multi-variable fingerprint. In an analysis of ocean variables, Pierce et al. (2012) found that the joint analysis of temperature and salinity changes yielded a stronger signal on the climate than "either salinity or temperature alone". Further insights can be gained from considering a synthesis of evidence across the climate system. This is the subject of the next subsection.

10.9.2 Whole Climate System

To build robust interpretations of the observed climate changes in terms of the causes we rely on an analysis of a suite of detection and attribution studies across all of the common elements of the of the climate system (Figure 10.20). The instrumental records associated with each element of the climate system are generally independent, and consequently joint interpretations across observations from the main components of the climate system increases the confidence to higher levels than from any single study or component of the climate system. Similarly, using models of the climate system, and requiring that they replicate the response of the different forcings (within internal variability) across a wider suite of climate indicators also builds confidence in the capacity of CMIP3 and CMIP5 models to simulate the earth's climate.

The coherence of observed changes with simulations of anthropogenic and natural forcing in the physical system is remarkable (Figure 10.20), particularly for temperature related variables. Surface temperature and ocean heat content show emerging anthropogenic and natural signals in both records, and a clear separation from the alternative hypothesis of just natural variations (Figure 10.20, Global panels). These signals do not just appear in the global means, but also appear on regional scales at continental and ocean basin scales in these variables. Sea-ice emerges strongly for the Arctic and in the case of Antarctica remains within the range of internal variability.

[INSERT FIGURE 10.20 HERE]

Figure 10.20: Detection and attribution signals in some elements of the climate system. Brown panels are land surface temperature time series, green panels are precipitation time series, blue panels are ocean heat content time series, and white panels are sea-ice time series. On each panel is observations (shown in black or black and shades of grey as in ocean heat content). Blue shading is the model time series for natural forcing simulations and red shading is the natural and anthropogenic forcings. The dark blue and dark red lines are the ensemble means from simulations. For surface temperature the 5 to 95% interval is plotted and is based on the Jones et al. (2012) (and Figure 10.1). The observed surface temperature is from HadCRUT4. For precipitation data the mean and one standard deviation shading of the simulations is plotted. Observed precipitation is from Zhang et al. (2007c). For Ocean Heat Content the mean and one standard deviation shading is plotted for an ensemble of CMIP5 models. Three observed records of OHC are shown. The sea ice extents simulations and observations are the same as in Figure 10.15. More details are in the Supplementary Material (Appendix 10.A).

Table 10.1 illustrates a larger suite of detection and attribution results than in Figure 10.20 across even more elements of the climate system that cover both the instrumental record and paleo-reconstructions on a range of time scales ranging from extreme precipitation events to millennium timescales.

The surface of the earth, the upper oceans (ocean heat content and thermal expansion), the troposphere, and the temperature gradient between the troposphere and stratosphere all have detectable anthropogenic forced signals that exceed internal variability of the climate system across a range of likelihoods from likely to extremely likely. Indeed to successfully describe the observed global trends in these three components since the1960 and 1970's contributions from both anthropogenic forcing and natural forcings are required (i.e., volcanic eruptions and solar) (results 1,2,3,4 and 9,10, and 5,7 in Table 10.1). This is consistent with anthropogenic forcing warming the surface of the earth, troposphere and oceans, with the three large eruptions since the 1960's having cooled these components, and these two causes give much of the observed response (see also Figures 10.1, 10.4, 10.5, 10.6 and 10.15). This is important because both sources of forcing are required to understand underlying causes of warming of the earth system. The many studies that support this attribution to anthropogenic forcing of the climate range in confidence level from very likely for the troposphere to extremely likely for warming at the surface and the long term trends in ocean heat content.

Water in the free atmosphere is expected to increase, and at local scales expected to increase as a consequence of warming at 7% K^{-1} by Clausius-Claperyon equation. Atmospheric circulation controls global distribution of rain and evaporation. Simulations show that greenhouse gases increase moisture transport and amplify these global patterns or rain and evaporation, although some aspects of this rainfall pattern is affected by tropospheric aerosols. The patterns of rain and evaporation are quite distinct from the patterns of warming. The observations show that water is increasing in the free atmosphere (result 16, medium confidence, Table 10.1) evidence, that precipitation is increasing in wet areas and reducing in dry areas (result 14,15, medium confidence) in the Northern Hemisphere, and the global patterns of ocean salinity at

the surface (and at depth) also confirms this tendency since 1960, (result 11, likely, Table 10.1) for the wet regions becoming wetter and the dry regions becoming dryer. These results together give a global coverage of the earth's surface and confirm (with varying confidence and likelihoods) that there is an anthropogenic cause to the acceleration of the water cycle.

Warming of the atmosphere and the oceans can affect the cryosphere, and in the case of snow and sea-ice lead to positive feedbacks that amplify the warming response in the atmosphere and oceans. Retreat of mountain glaciers has been observed with an anthropogenic influence detected (result 17, likely, Table 10.1), Greenland ice sheet has melted at the edges and accumulating snow at the higher elevations consistent with greenhouse gas warming. Greenland ice sheet's surface mass balance was negative (result 18, likely, Table 10.1). Our level of scientific understanding is too low to provide a satisfactory quantifiable explanation of the observed mass loss of Antarctic (result 19, Table 10.1). Sea ice in the Arctic is decreasing rapidly and the changes now exceeds the internal variability (result 20, likely, Table 10.1) while Antarctic sea ice extent is growing but within the envelope internal variability of climate models (result 21, medium confidence, Table 10.1). The warming is likely to be reducing the amount of snow cover and permafrost (result 22, Table 10.1).

The warming is also affecting temperature on continental scales, with human influences detected in mean temperature on all inhabited continents (result 28, likely, Table 10.1), while because of observational uncertainties there is low confidence in attribution of Antarctica warming. On millennium time scales anthropogenic forcing and volcanic eruptions are detected in Europe in some seasons (29, medium confidence, Table 10.1). By contrast it is likely that human influence on extremes in temperature has been detected at some sub-continental scales (result 30, likely, Table 10.1) and also on probability of heat waves has risen (result 31, likely, Table 10.1).

An analysis of these results (from Table 10.1) shows that the greatest confidence and strongest likelihood levels come from atmospheric measurements of temperature (Section 10.3.1), from ocean heat content (Section 10.4.1) and from surface ocean acidification, (Section 10.4). Our weakest knowledge of the anthropogenic drivers is around moisture and precipitation where there is only medium confidence (Section 10.3.2) and some aspects of circulation change (Section 10.3.3).

[START FAQ 10.1 HERE]

FAQ 10.1: Climate is Always Changing. How do We Determine the Most Likely Causes of the Observed Changes?

The most likely causes of observed climate change are identified by predictable 'fingerprint' of climate change in the spatial and temporal patterns of observed changes. These fingerprints are derived from computer model simulations of the different patterns of climate change caused by climate forcings, such as greenhouse gas increases, or changes in solar brightness. By comparing the simulated fingerprint patterns with observed climate changes,we can determine whether observed changes are best explained by those fingerprint patterns, or by natural variability, which occurs without any forcing.

The fingerprint of human-caused greenhouse gas increases is clearly apparent in the pattern of observed 20th century climate change. The observed change cannot be otherwise explained by the fingerprints of natural forcings or natural variability. Attribution studies therefore support the conclusion that "it is extremely likely that human activities have caused most of (at least 50%) the observed increase in global average temperatures since the 1950s."

The Earth's climate is always changing, and that can occur for many reasons. To determine the most likely causes of observed changes, we must first detect whether an observed change in climate is different from other fluctuations which occur without any forcing at all. Climate variability without forcing—called internal variability—is the consequence of processes within the atmosphere and ocean. Large scale oceanic fluctuations, such as those connected to the El Niño-Southern Oscillation (ENSO) cycle in the Pacific Ocean, are the dominant sources of internal climate variability on decadal to centennial time scales.

Climate change can also result from natural forcings external to the climate system, such as volcanic eruptions, or changes in the brightness of the sun. Forcings such as these are responsible for the huge

changes in climate that are clearly present in the geological record. Possible human-caused forcings include greenhouse gas emissions or atmospheric particulate pollution. Attribution studies attempt to determine the most likely causes of a detected change in observed climate.

Formal climate change attribution studies are carried out using controlled experiments with climate models. The model-simulated responses to specific climate forcings are often called the fingerprints of those forcings. The fingerprint patterns are used to determine the most likely causes of observed change.

FAQ 10.1, Figure 1 illustrates a fingerprint assessment of global temperature change at the surface and in the upper atmosphere during the late 20th century. The observed change in the latter half of the 20th century , shown by the black time series in the left panels, is larger than expected from just internal variability. Simulations driven only by natural forcings fail to reproduce late 20th century global warming at the surface (upper left) with a spatial pattern of change (upper right) completely different from the observed pattern of change (middle right). Simulations including both natural and human-caused forcings provide a much better representation of the time rate of change (lower left) and spatial pattern (lower right) of observed surface temperature change.

Both panels on the left show that computer models correctly reproduce the naturally-forced surface cooling observed for a year or two after major volcanic eruptions in 1982 and 1992. The small inset time series in the left panels show temperature change in the upper atmosphere (the stratosphere). If solar forcing were the primary cause of the observed temperature changes, then we would also expect both the surface and the stratosphere to warm during the late 20th century. Instead, the stratosphere shows a cooling trend since 1981. In addition the surface cools and the stratosphere warms for a year or two following volcanic eruptions, as expected. Natural forcing simulations capture the short-lived temperature changes following eruptions. However only the natural+human caused forcing simulations correctly simulate the long-term stratospheric cooling trend (which is principally due to human-caused ozone depletion).

Overall, FAQ 10.1, Figure 1 shows that the pattern of observed temperature change is significantly different than the pattern of response to natural forcings alone. The simulated response to all forcings, including human-caused forcings, provides a good match to the observed changes at the surface and in the stratosphere. We cannot correctly simulate recent observed climate change without including the response to human-caused forcings, including greenhouse gases, stratospheric ozone, and aerosols. Natural causes of change are still at work in the climate system, but recent trends in temperature are largely attributable to human-caused forcing.

[INSERT FAQ 10.1, FIGURE 1 HERE]

FAQ 10.1, Figure 1: Left: Time series of global and annual-average surface temperature change from 1860 to 2010. The top panel shows results from two ensemble of climate models driven with just natural forcings, shown as blue and yellow lines. The lower panel shows simulations by the same models, but driven with both natural forcing and human-induced changes in greenhouse gases and aerosols. The black lines in each panel show different estimates of global and annual-averaged observed temperature change. Small inset panels show global stratospheric temperature time series from 1981–2010. Observations are shown as black lines; green lines in the upper inset panel show simulations driven by natural forcing only, and orange lines in the lower inset panel show simulations driven by natural+human forcings. Vertical dashed lines denote major volcanic eruptions in 1982 and 1992. Right: Spatial patterns of local surface temperature trends from 1951–2010. The upper panel shows the pattern of trends from a large ensemble of simulations driven with just natural forcings. The bottom panel shows trends from a corresponding ensemble driven with natural+human forcings. The middle panel shows the pattern of observed trends during this period.

[END FAQ 10.1 HERE]

[START FAQ 10.2 HERE]

FAQ 10.2: When will Human Influences on Climate be Obvious on Local Scales?

Human-caused warming is already becoming obvious on land in tropical regions, especially during the warm part of the year. Warming should become obvious in middle latitudes—during summer at first—within the next several decades. The trend is expected to emerge more slowly there, especially during winter, because natural climate variability increases with distance from the equator and during the cold season.

Temperature trends already detected in many regions have been attributed to human influence. Temperature-sensitive climate variables, such as Arctic sea ice, also show detectable trends attributable to human influence.

Warming trends caused by global change are generally less obvious at local scales than in the global temperature average. This is because most of the variability of local climate is averaged away in the global mean. Global averaging makes a long-term trend caused by widespread changes in greenhouse gases more apparent. Multi-decadal warming trends detected in many regions are considered to be outside the range of trends one might expect from natural internal variability of the climate system. But a detected trend will only become obvious when the local mean climate emerges from the "noise" of year-to-year variability. How quickly this happens depends on both the rate of the warming trend and the amount of local variability.

In some tropical regions, the warming trend has already emerged from local variability (FAQ 10.2, Figure 1). This happens more quickly in the tropics because there is less variability there than in other parts of the globe. Projected warming may not emerge in middle latitudes until the mid-21st century—even though warming trends there are larger—because local temperature variability is substantially greater there than in the tropics. On a seasonal basis, local temperature variability tends to be smaller in summer than in winter. Warming therefore tends to emerge first in summer, even in regions where the warming trend is larger in winter, such as in central Eurasia in FAQ 10.2, Figure 1.

Variables other than temperature also show different rates of long-term change compared to natural variability. For example, Arctic sea ice extent is declining very rapidly, and already shows a human influence. On the other hand, local precipitation trends are very hard to detect because at most locations the variability in precipitation is quite large. The probability of record-setting warm summer temperatures has increased throughout much of the Northern Hemisphere. High temperatures presently considered extreme are projected to become closer to the norm over the coming decades. The probabilities of other extreme events, including some cold spells, have lessened.

In the present climate, individual extreme weather events cannot be unambiguously ascribed to climate change, since such events could have happened in an unchanged climate. However the odds of such events could have changed significantly at a particular location—"loading the weather dice", as it were. Human-induced increases in greenhouse gases may have contributed substantially to the probability of some heatwaves. Similarly, climate model studies suggest that increased greenhouse gases have contributed to the observed intensification of heavy precipitation events found over parts of the Northern Hemisphere. However, the probability of many other extreme weather events may not have changed substantially. Therefore, it is incorrect to ascribe every new weather record to climate change.

The precise date of future emergence of projected warming trends also depends on local climate variability, which can temporarily increase or decrease temperatures. Furthermore, the projected local temperature curves shown in FAQ 10.2, Figure 1 are based on multiple climate model simulations forced by the same assumed future emissions scenario. A different rate of atmospheric greenhouse gas accumulation would cause a different warming trend, so the spread of model warming projections (the coloured shading in FAQ 10.2, Figure 1) would be wider if the figure included a spread of greenhouse gas emissions scenarios. The increase required for summer temperature change to emerge from 20th century local variability (regardless of the rate of change) is depicted on the central map in FAQ 10.2, Figure 1.

A full answer to the question of when human influence on local climate will be obvious depends on the strength of evidence one considers sufficient to render something "obvious". The most convincing scientific evidence for the effect of climate change on local scales comes from analysing the global picture, and from the wealth of evidence from across the climate system linking many observed changes to human influence.

[INSERT FIGURE FAQ 10.2, FIGURE 1 HERE]

FAQ 10.2, Figure 1: Time series of projected temperature change shown at four representative locations for summer (red) and winter (blue). Each time series is surrounded by an envelope of projected changes (pink for summer, blue for winter) yielded by 24 different model simulations, emerging from a gray envelope of natural local variability simulated by the models using early 20th century conditions. The warming signal emerges first in the tropics during summer. The central map shows the global temperature increase (°C) needed for a temperatures in summer at individual locations to emerge from the envelope of early 20th century variability. All calculations are based on CMIP5 global climate model

simulations forced by the RCP8.5 emissions scenario. Envelopes of projected change and natural variability are defined as ±2 standard deviations. Adapted and updated from Mahlstein et al. (2011).

[END FAQ 10.2 HERE]

References

AchutaRao, K. M., B. D. Santer, P. J. Gleckler, K. E. Taylor, D. W. Pierce, T. P. Barnett, and T. M. L. Wigley, 2006: Variability of ocean heat uptake: Reconciling observations and models. *Journal of Geophysical Research*, **111**, C05019.

AchutaRao, K. M., et al., 2007: Simulated and observed variability in ocean temperature and heat content. *Proceedings of the National Academy of Sciences*, **104**, 10768-10773.

Ahlmann, H. W., 1948: The present climatic fluctuation. Geographical Journal, 165-195.

Aldrin, M., M. Holden, P. Guttorp, R. Skeie, G. Myhre, and T. Berntsen, 2012: Bayesian estimation of climate sensitivity based on a simple climate model fitted to observations of hemispheric temperatures and global ocean heat content. *Environmetrics*, **23**, 253-271.

Alekseev, G., A. Danilov, V. Kattsov, S. Kuz'mina, and N. Ivanov, 2009: Changes in the climate and sea ice of the Northern Hemisphere in the 20th and 21st centuries from data of observations and modeling. *Izvestiya Atmospheric and Oceanic Physics*. doi:DOI 10.1134/S0001433809060012, 675-686.

Alexander, L. V., and J. M. Arblaster, 2009: Assessing trends in observed and modelled climate extremes over Australia in relation to future projections. *International Journal of Climatology*, **29**, 417-435.

Allan, R., and T. Ansell, 2006: A new globally complete monthly historical gridded mean sea level pressure dataset (HadSLP2): 1850-2004. *Journal of Climate*, **19**, 5816-5842.

Allan, R., and B. Soden, 2008: Atmospheric warming and the amplification of precipitation extremes. *Science*. doi:DOI 10.1126/science.1160787, 1481-1484.

Allen, M., 2011a: In defense of the traditional null hypothesis: remarks on the Trenberth and Curry WIREs opinion articles. *Wiley Interdisciplinary Reviews: Climate Change*, **2**, 931-934.

——, 2011b: In defense of the traditional null hypothesis: remarks on the Trenberth and Curry WIREs opinion articles.

Allen, M., and S. Tett, 1999: Checking for model consistency in optimal fingerprinting. *Climate Dynamics*. 419-434.

Allen, M., and P. Stott, 2003: Estimating signal amplitudes in optimal fingerprinting, part I: theory. *Climate Dynamics*. doi:DOI 10.1007/s00382-003-0313-9, 477-491.

Allen, M., P. Stott, J. Mitchell, R. Schnur, and T. Delworth, 2000: Quantifying the uncertainty in forecasts of anthropogenic climate change. *Nature*. 617-620.

Allen, M., D. Frame, C. Huntingford, C. Jones, J. Lowe, M. Meinshausen, and N. Meinshausen, 2009: Warming caused by cumulative carbon emissions towards the trillionth tonne. *Nature*, **458**, 1163-1166.

Allen, M. R., 2003: Liability for climate change. 891-892.

Allen, R. J., S. C. Sherwood, J. R. Norris, and C. S. Zender, 2012: Recent Northern Hemisphere tropical expansion primarily driven by black carbon and tropospheric ozone. *Nature*, **485**, 350-U393.

Ammann, C. M., and E. R. Wahl, 2007: The importance of the geophysical context in statistical evaluations of climate reconstruction procedures. *Clim. Change*, **85**.

Ammann, C. M., F. Joos, D. S. Schimel, B. L. Otto-Bliesner, and R. A. Tomas, 2007: Solar influence on climate during the past millennium: Results from transient simulations with the NCAR Climate System Model. *Proceedings of the National Academy of Sciences of the United States of America*, **104**, 3713-3718.

Andreae, M., C. Jones, and P. Cox, 2005: Strong present-day aerosol cooling implies a hot future. *Nature*. doi:DOI 10.1038/nature03671, 1187-1190.

Annan, J., and J. Hargreaves, 2006: Using multiple observationally-based constraints to estimate climate sensitivity. *Geophys. Res. Lett.* doi:ARTN L06704, DOI 10.1029/2005GL025259, -.

——, 2010: Reliability of the CMIP3 ensemble. *Geophys. Res. Lett.* doi:ARTN L02703, DOI 10.1029/2009GL041994, -.

——, 2011: Reply to Henriksson et al.'s comment on "Using multiple observationally-based constraints to estimate climate sensitivity" by Annan and Hargreaves (2010). *Clim. Past.*, **7**, 587-589.

Aoki, S., N. Bindoff, and J. Church, 2005: Interdecadal water mass changes in the Southern Ocean between 30 degrees E and 160 degrees E. *Geophys. Res. Lett.* doi:ARTN L07607, DOI 10.1029/2004GL022220, -.

Arkin, P. A., T. M. Smith, M. R. P. Sapiano, and J. Janowiak, 2010: The observed sensitivity of the global hydrological cycle to changes in surface temperature. *Environmental Research Letters*, **5**.

Armour, K., I. Eisenman, E. Blanchard-Wrigglesworth, K. McCusker, and C. Bitz, 2011: The reversibility of sea ice loss in a state-of-the-art climate model. *Geophys. Res. Lett.*, **38**, -.

Baker, M., and G. Roe, 2009: The Shape of Things to Come: Why Is Climate Change So Predictable? *Journal of Climate*, **22**, 4574-4589.

Balani Sarojini, B., P. Stott, E. Black, and D. Polson, 2012: Fingerprints of changes in annual and seasonal precipitation from CMIP5 models over land and ocean. *To be submitted.*

Barnett, T., D. Pierce, and R. Schnur, 2001: Detection of anthropogenic climate change in the world's oceans. *Science*, **292**, 270-274.

Barnett, T., D. Pierce, K. Achutarao, P. Gleckler, B. Santer, J. Gregory, and W. Washington, 2005: Penetration of Human-Induced Warming into the World's Oceans. *Science*, **309**, 284-287.

Barnett, T. P., et al., 2008: Human-induced changes in the hydrology of the western United States. *Science*, **319**, 1080-1083.

Beer, J., J. Abreu, and F. Steinhilber, 2009: Sun and planets from a climate point of view. *Universal Heliophysical Processes*. doi:DOI 10.1017/S1743921309029056, 29-43.
Bender, F., A. Ekman, and H. Rodhe, 2010: Response to the eruption of Mount Pinatubo in relation to climate sensitivity in the CMIP3 models. *Climate Dynamics*. doi:DOI 10.1007/s00382-010-0777-3, 875-886.
Benestad, R. E., and G. A. Schmidt, 2009: Solar trends and global warming. *Journal of Geophysical Research-Atmospheres*, **114**.
Bengtsson, L., and K. I. Hodges, 2009: On the evaluation of temperature trends in the tropical troposphere. *Clim. Dyn.*
Bengtsson, L., V. Semenov, and O. Johannessen, 2004: The early twentieth-century warming in the Arctic - A possible mechanism. *Journal of Climate*. 4045-4057.
Bengtsson, L., K. I. Hodges, E. Roeckner, and R. Brokopf, 2006: On the natural variability of the pre-industrial European climate. *Clim Dyn*, **27**, 17.
Bhend, J., and H. von Storch, 2008: Consistency of observed winter precipitation trends in northern Europe with regional climate change projections. *Climate Dynamics*, **31**, 17-28.
Bindoff, N., and T. McDougall, 2000: Decadal changes along an Indian ocean section at 32 degrees S and their interpretation. *Journal of Physical Oceanography*. 1207-1222.
Bindoff, N. L., et al., 2007: Observations: Oceanic Climate Change and Sea Level. *Climate Change 2007: The Physical Science Basis. Contribution of Working Group I to the Fourth Assessment Report of the Intergovernmental Panel on Climate Change*, Cambridge University Press.
Boe, J., A. Hall, and X. Qu, 2009: September sea-ice cover in the Arctic Ocean projected to vanish by 2100. *Nature Geoscience*. doi:DOI 10.1038/NGEO467, 341-343.
Boe, J., A. Hall, and X. Qu, 2010: Sources of spread in simulations of Arctic sea ice loss over the twenty-first century. *Climate Change*, **99**, 637-645.
Boer, G., M. Stowasser, and K. Hamilton, 2007: Inferring climate sensitivity from volcanic events. *Climate Dynamics*. doi:DOI 10.1007/s00382-006-0193-x, 481-502.
Boer, G. J., 2011: The ratio of land to ocean temperature change under global warming *Climate Dynamics*. doi:10.1007/s00382-011-1112-3.
Bonfils, C., P. B. Duffy, B. D. Santer, T. M. L. Wigley, D. B. Lobell, T. J. Phillips, and C. Doutriaux, 2008: Identification of external influences on temperatures in California. *Clim. Change*, **87**, S43-S55.
Booth, B. B. B., N. J. Dunstone, P. R. Halloran, T. Andrews, and N. Bellouin, 2012a: Aerosols implicated as a prime driver of twentieth-century North Atlantic climate variability. *Nature*, **484**, 228-232.
Booth, B. B. B., N. J. Dunstone, P. R. Halloran, T. Andrews, and N. Bellouin, 2012b: Aerosols implicated as a prime driver of twentieth-century North Atlantic climate variability. *Nature*, **484**, 228-U110.
Bowerman, N., D. Frame, C. Huntingford, J. Lowe, and M. Allen, 2011: Cumulative carbon emissions, emissions floors and short-term rates of warming: implications for policy. *Philosophical Transactions of the Royal Society a-Mathematical Physical and Engineering Sciences*, **369**, 45-66.
Boyer, T., S. Levitus, J. Antonov, R. Locarnini, and H. Garcia, 2005: Linear trends in salinity for the World Ocean, 1955-1998. *Geophys. Res. Lett.* doi:ARTN L01604, DOI 10.1029/2004GL021791, -.
Brayshaw, D. J., B. Hoskins, and M. Blackburn, 2008: he Storm-Track Response to Idealized SST Perturbations in an Aquaplanet GCM. *Journal of Atmospheric Sciences*, **65**, 2842–2860.
Brohan, P., J. J. Kennedy, I. Harris, S. F. B. Tett, and P. D. Jones, 2006: Uncertainty estimates in regional and global observed temperature changes: A new data set from 1850. *Journal of Geophysical Research-Atmospheres*, **111**.
Bronnimann, S., 2009: Early twentieth-century warming. *Nature Geoscience*. doi:DOI 10.1038/ngeo670, 735-736.
Bronnimann, S., et al., 2012: A multi-data set comparison of the vertical structure of temperature variability and change over the Arctic during the past 100 year. *Clim. Dyn.*, **DOI 10.1007/s00382-012-1291-6.**
Brown, P. T., and E. C. Cordero, 2012: Past unforced surface temperature variability and its implication on contemporary climate change. *Nature Climate Change*.
Brown, R., and P. Mote, 2009: The Response of Northern Hemisphere Snow Cover to a Changing Climate. *Journal of Climate*. doi:DOI 10.1175/2008JCLI2665.1, 2124-2145.
Brown, R. D., and D. A. Robinson, 2011: Northern Hemisphere spring snow cover variability and change over 1922-2010 including an assessment of uncertainty. *The Cryosphere*, **5**, 219-229.
Brown, S. J., J. Caesar, and C. A. T. Ferro, 2008: Global changes in extreme daily temperature since 1950. *Journal of Geophysical Research-Atmospheres*, **113**.
Burke, E. J., S. J. Brown, and N. Christidis, 2006: Modeling the recent evolution of global drought and projections for the twenty-first century with the Hadley Centre climate model. *Journal of Hydrometeorology*, **7(5)**, 1113-1125.
Butchart, N., et al., 2011: Multimodel climate and variability of the stratosphere. *Journal of Geophysical Research-Atmospheres*, **116**.
Butler, A. H., D. W. Thompson, and R. Heikes, 2010: The steady-state atmospheric circulation resions to 1021 climate change-like thermal forcings in a simple general circulation model. *Journal of Climate*, **23**, 23.
Camp, C., and K. Tung, 2007: Surface warming by the solar cycle as revealed by the composite mean difference projection. *Geophys. Res. Lett.*, **34**, -.
Cattiaux, J., R. Vautard, and P. Yiou, 2009: Origins of the extremely warm European fall of 2006. *Geophys. Res. Lett.*, **36**.

——, 2011: North-Atlantic SST amplified recent wintertime European land temperature extremes and trends. *Climate Dynamics*, **36**, 2113-2128.
Cattiaux, J., R. Vautard, C. Cassou, P. Yiou, V. Masson-Delmotte, and F. Codron, 2010: Winter 2010 in Europe: A cold extreme in a warming climate. *Geophys. Res. Lett.* doi:ARTN L20704, 10.1029/2010GL044613, -.
Cayan, D. R., T. Das, D. W. Pierce, T. P. Barnett, M. Tyree, and A. Gershunov, 2010: Future dryness in the southwest US and the hydrology of the early 21st century drought. *Proceedings of the National Academy of Sciences*, **107**, 21271-21276.
Chang, C., J. Chiang, M. Wehner, A. Friedman, and R. Ruedy, 2011: Sulfate Aerosol Control of Tropical Atlantic Climate over the Twentieth Century. Journal of Climate, 24(10): 2540-
2555. *Journal of Climate*, **24**, 2540-2555.
Charlton-Perez, A. J., et al., 2012: Mean climate and variability of the stratosphere in CMIP5 models. *J. Geophys. Res.*, submitted.
Chen, G., Y. Ming, N. D. Singer, and J. Lu, 2011: Testing the Clausius‐Clapeyron constraint on the aerosol‐induced changes in mean and extreme precipitation. *Geophys. Res. Lett.*, **38**.
Cheng, G., and T. Wu, 2007: Responses of permafrost to climate change and their environmental significance, Qinghai-Tibet Plateau. *Journal of Geophysical Research*, **112**.
Chiang, J. C. H., C. Y. Chang, and M. F. Wehner, 2012: Long-term trends of the Atlantic Interhemispheric SST Gradient in the CMIP5 Historical Simulations. *J. Climate*.
Chinn, T., S. Winkler, M. Salinger, and N. Haakensen, 2005: Srecent glacier advances in Norway and New Zealand: A comparison of their glaciological and meteorological causes. *Geografiska Annaler Series a-Physical Geography*. 141-157.
Choi, G., D. Robinson, and S. Kang, 2010: Changing Northern Hemisphere Snow Seasons. *Journal of Climate*. doi:DOI 10.1175/2010JCLI3644.1, 5305-5310.
Chou, C., J. D. Neelin, C. C.A., and J.-Y. Tu, 2009: Evaluating the "rich-get-richer" mechanism in tropical precipitation change under global warming. *Journal of Climate*, **22**, 1981-2005.
Chou, C., C.-A. Chen, P.-H. Tan, and K. T. Chen, 2012: Mechanisms for global warming impacts on precipitation frequency and intensity. *Journal of Climate*, **25**, 3291-3306.
Christiansen, B., and F. C. Ljungqvist, 2011: Reconstruction of the Extratropical NH Mean Temperature over the Last Millennium with a Method that Preserves Low-Frequency Variability. *Journal of Climate*, **24**.
Christidis, N., and P. Stott, 2012: LENGTHENED ODDS OF THE COLD UK WINTER OF 2010/11 ATTRIBUTABLE TO HUMAN INFLUENCE. 1060-1062.
Christidis, N., P. A. Stott, and S. J. Brown, 2011a: The role of human activity in the recent warming of extremely warm daytime temperatures.
Christidis, N., P. A. Stott, G. C. Hegerl, and R. A. Betts, 2012a: The role of land use change in the recent warming of daily extreme temperatures. *Geophys. Res. Lett.*, **submitted**.
Christidis, N., P. A. Stott, F. W. Zwiers, H. Shiogama, and T. Nozawa, 2010: Probabilistic estimates of recent changes in temperature: a multi-scale attribution analysis. *Climate Dynamics*, **34**, 1139-1156.
Christidis, N., P. A. Stott, F. W. Zwiers, H. Shiogama, and T. Nozawa, 2012b: The contribution of anthropogenic forcings to regional changes in tempertaure during the last decade. *Climate Dynamics*. doi:10.1007/s00382-011-1184-0.
Christidis, N., P. A. Stott, G. S. Jones, H. Shiogama, T. Nozawa, and J. Luterbacher, 2011b: Human activity and anomalously warm seasons in Europe. *International Journal of Climatology*. doi:10.1002/joc.2262.
Chung, E., B. Soden, and B. Sohn, 2010: Revisiting the determination of climate sensitivity from relationships between surface temperature and radiative fluxes. *Geophys. Res. Lett.* doi:ARTN L10703, 10.1029/2010GL043051, -.
Church, J., N. White, and J. Arblaster, 2005: Significant decadal-scale impact of volcanic eruptions on sea level and ocean heat content. *Nature*, **438**, 74-77.
Church, J., et al., 2011: Revisiting the Earth's sea-level and energy budgets from 1961 to 2008. *Geophys. Res. Lett.*, **38**, -.
Chylek, P., and U. Lohmann, 2008a: Reply to comment by Andrey Ganopolski and Thomas Schneider von Deimling on "Aerosol radiative forcing and climate sensitivity deduced from the Last Glacial Maximum to Holocene transition". *Geophys. Res. Lett.* doi:ARTN L23704, 10.1029/2008GL034308, -.
——, 2008b: Aerosol radiative forcing and climate sensitivity deduced from the last glacial maximum to Holocene transition. *Geophys. Res. Lett.* doi:ARTN L04804, 10.1029/2007GL032759, -.
Chylek, P., U. Lohmann, M. Dubey, M. Mishchenko, R. Kahn, and A. Ohmura, 2007: Limits on climate sensitivity derived from recent satellite and surface observations. *Journal of Geophysical Research-Atmospheres*, **112**.
Comiso, J., 2012: Large decadal decline in Arctic multiyear ice cover. *J. Climate*, **25**, 1176-1193.
Comiso, J., and F. Nishio, 2008a: Trends in the sea ice cover using enhanced and compatible AMSR-E, SSM/I, and SMMR data. *Journal of Geophysical Research-Oceans*, **113**, -.
——, 2008b: Trends in the sea ice cover using enhanced and compatible AMSR-E, SSM/I, and SMMR data. *Journal of Geophysical Research-Oceans*. doi:ARTN C02S07, 10.1029/2007JC004257, -.
Compo, G., et al., 2011: The Twentieth Century Reanalysis Project. *Quarterly Journal of the Royal Meteorological Society*, **137**, 1-28.

Cordero, E. C., and P. M. D. Forster, 2006: Stratospheric variability and trends in models used for the IPCC AR4. *Atmospheric Chemistry and Physics*, **6**, 5369-5380.
Cravatte, S., T. Delcroix, D. Zhang, M. McPhaden, and J. Leloup, 2009: Observed freshening and warming of the western Pacific Warm Pool. *Climate Dynamics*. doi:DOI 10.1007/s00382-009-0526-7, 565-589.
Crook, J., and P. Forster, 2011: A balance between radiative forcing and climate feedback in the modeled 20th century temperature response. *Journal of Geophysical Research-Atmospheres*, **116**.
Crook, J., P. Forster, and N. Stuber, 2011: Spatial Patterns of Modeled Climate Feedback and Contributions to Temperature Response and Polar Amplification. *Journal of Climate*, **24**, 3575-3592.
Crowley, T. J., G. Zielinski, B. Vinther, R. Udisti, K. Kreutzs, J. Cole-Dai, and E. Castellano, 2008: Volcanism and the Little Ice Age. *PAGES news*, **16**, 22-23.
Curry, J., 2011a: Nullifying the climate null hypothesis.
——, 2011b: Nullifying the climate null hypothesis. *Wiley Interdisciplinary Reviews: Climate Change*, **2**, 919-924.
Curry, J. A., and P. J. Webster, 2011: **Climate Science and the Uncertainty Monster**. ***Bulletin of the American Meteorological Society***. doi:10.1175/2011BAMS3139.1, in press.
Curry, R., B. Dickson, and I. Yashayaev, 2003: A change in the freshwater balance of the Atlantic Ocean over the past four decades. *Nature*. doi:DOI 10.1038/nature02206, 826-829.
D'Arrigo, R., R. Wilson, and G. Jacoby, 2006: On the long-term context for late twentieth century warming. *Journal of Geophysical Research-Atmospheres*, **111**.
D'Arrigo, R., R. Wilson, and A. Tudhope, 2009: The impact of volcanic forcing on tropical temperatures during the past four centuries. *Nature Geoscience*, **2**, 51-56.
Dai, A., 2011: Drought under global warming: a review. *Wiley Interdisciplinary Reviews: Climate Change*, **2**, 21.
Dall'Amico, M., L. J. Gray, K. H. Rosenlof, A. A. Scaife, K. P. Shine, and P. A. Stott, 2010: Stratospheric temperature trends: impact of ozone variability and the QBO. *Climate Dynamics*, **34**, 381-398.
Davis, S. M., and K. H. Rosenlof, 2012: A Multidiagnostic Intercomparison of Tropical-Width Time Series Using Reanalyses and Satellite Observations. *Journal of Climate*, **25**, 1061-1078.
Dean, S. M., and P. A. Stott, 2009: The Effect of Local Circulation Variability on the Detection and Attribution of New Zealand Temperature Trends. *Journal of Climate*, **22**, 6217-6229.
Dee, D.P., et al., 2011: The ERA-Interim reanalysis: configuration and performance of the data assimilation system. Quarterly Journal of the Royal Meteorological Society, 137, 553–597. doi: 10.1002/qj.828
DelSole, T., M. K. Tippett, and J. Shukla, 2011: A significant component of unforced multidecadal variability in the recent acceleration of global warming. Journal of Climate, 24, 18.
Delworth, T., and M. Mann, 2000: Observed and simulated multidecadal variability in the Northern Hemisphere. *Climate Dynamics*, **16**, 661-676.
Delworth, T., V. Ramaswamy, and G. Stenchikov, 2005: The impact of aerosols on simulated ocean temperature and heat content in the 20th century. *Geophys. Res. Lett.*, **32**, L24709.
Delworth, T. L., and T. R. Knutson, 2000: Simulation of Early 20th Century Global Warming. *Science*, **287**, 5.
Deo, R. C., J. I. Syktus, C. A. McAlpine, P. J. Lawrence, H. A. McGowan, and S. R. Phinn, 2009: Impact of historical land cover change on daily indices of climate extremes including droughts in eastern <country-region>Australia</country-region>. *Geophys. Res. Lett.*, **36(L08705)**.
Deser, C., and H. Teng, 2008: Evolution of Arctic sea ice concentration trends and the role of atmospheric circulation forcing, 1979-2007. *Geophys. Res. Lett.* doi:ARTN L02504, 10.1029/2007GL032023, -.
Dessler, A., 2010: A Determination of the Cloud Feedback from Climate Variations over the Past Decade. *Science*, **330**, 1523-1527.
——, 2011: Cloud variations and the Earth's energy budget. *Geophys. Res. Lett.*, **38**.
Deutsch, C., S. Emerson, and L. Thompson, 2005: Fingerprints of climate change in North Pacific oxygen (vol 32, art no L16604, 2005). *Geophys. Res. Lett.* doi:ARTN L17610, 10.1029/2005GL024471, -.
Dickson, R., et al., 2000: The Arctic Ocean response to the North Atlantic oscillation. *Journal of Climate*. 2671-2696.
Ding, Q., E. Steig, D. Battisti, and M. Kuttel, 2011: Winter warming in West Antarctica caused by central tropical Pacific warming. *Nature Geoscience*, **4**, 398-403.
Doherty, S., et al., 2009: LESSONS LEARNED FROM IPCC AR4 Scientific Developments Needed To Understand, Predict, And Respond To Climate Change. *Bulletin of the American Meteorological Society*. doi:DOI 10.1175/2008BAMS2643.1, 497-+.
Dole, R., et al., 2011: Was there a basis for anticipating the 2010 Russian heat wave? *Geophys. Res. Lett.*, **38**.
Domingues, C., J. Church, N. White, P. Gleckler, S. Wijffels, P. Barker, and J. Dunn, 2008: Improved estimates of upper-ocean warming and multi-decadal sea-level rise. *Nature*, **453**, 1090-1093.
Doscher, R., K. Wyser, H. Meier, M. Qian, and R. Redler, 2010: Quantifying Arctic contributions to climate predictability in a regional coupled ocean-ice-atmosphere model. *Climate Dynamics*. doi:DOI 10.1007/s00382-009-0567-y, 1157-1176.
Douglass, D., E. Blackman, and R. Knox, 2004: Temperature response of Earth to the annual solar irradiance cycle (vol 323, pg 315, 2004). *Physics Letters a*. doi:DOI 10.1016/j.physleta.2004.03.029, 175-176.
Douville, H., A. Ribes, B. Decharme, R. Alkama, and J. Sheffield, 2012: Anthropogenic influence on multidecadal changes in reconstructed global evapotranspiration. *Nature Climate Change*. doi:10.1038/nclimate1632.

Drost, F., and D. Karoly, 2012: Evaluating global climate responses to different forcings using simple indices. *Geophys. Res. Lett.*

Drost, F., D. Karoly, and K. Braganza, 2011: Communicating global climate change using simple indices: an update *Climate Dynamics*. doi:10.1007/s00382-011-1227-6.

Duarte, C. M., T. M. Lenton, P. Wadhams, and P. Wassmann, 2012: Abrupt climate change in the Arctic. *Nature Climate Change*, **2**, 60-62.

Durack, P., and S. Wijffels, 2010: Fifty-Year Trends in Global Ocean Salinities and Their Relationship to Broad-Scale Warming. *Journal of Climate*. doi:DOI 10.1175/2010JCLI3377.1, 4342-4362.

Durack, P., S. Wijffels, and R. Matear, 2012: Ocean Salinities Reveal Strong Global Water Cycle Intensification During 1950 to 2000. *Science*, **336**, 455-458.

Easterling, D. R., and M. F. Wehner, 2009: Is the climate warming or cooling? *Geophys. Res. Lett.*, **36**.

Edwards, T., M. Crucifix, and S. Harrison, 2007: Using the past to constrain the future: how the palaeorecord can improve estimates of global warming. *Progress in Physical Geography*. doi:DOI 10.1177/0309133307083295, 481-500.

Elsner, J. B., 2006: Evidence in support of the climate change–Atlantic hurricane hypothesis. *Geophys. Res. Lett.*

Elsner, J. B., J. P. Kossin, and T. H. Jagger, 2008: The increasing intensity of the strongest tropical cyclones. *Nature*, **455(7209)**.

Emanuel, K., 2005: Increasing destructiveness of tropical cyclones over the past 30 years. *Nature*, **436**, 686-688.

Emanuel, K., S. Solomon, D. Folini, S. Davis, and C. Cagnazzo, 2012: Influence of tropical tropopause layer cooling on Atlantic hurricane activity. *Journal of Climate*.

Emerson, S., Y. Watanabe, T. Ono, and S. Mecking, 2004: Temporal trends in apparent oxygen utilization in the upper pycnocline of the North Pacific: 1980-2000. *Journal of Oceanography*. 139-147.

Emori, S., and S. J. Brown, 2005: Dynamic and thermodynamic changes in mean and extreme precipitation under changed climate. *Geophys. Res. Lett.*, **32(L17706)**.

Esper, J., et al., 2012: Orbital forcing of tree-ring data. *Nature Climate Change*, **advance online publication**.

Evan, A., G. Foltz, D. Zhang, and D. Vimont, 2011: Influence of African dust on ocean-atmosphere variability in the tropical Atlantic. *Nature Geoscience*, **4**, 762-765.

Evan, A. T., D. J. Vimont, A. K. Heidinger, J. P. Kossin, and R. Bennartz, 2009: The Role of Aerosols in the Evolution of Tropical North Atlantic Ocean Temperature Anomalies. *Science*, **324**, 778-781.

Eyring, V., and Co-authors, 2012: Long-term changes in tropospheric and stratospheric ozone and associated climate impacts in CMIP5 simulations. *J. Geophys. Res.*, submitted.

Eyring, V., et al., 2006: Assessment of temperature, trace species, and ozone in chemistry-climate model simulations of the recent past. *Journal of Geophysical Research-Atmospheres*, **111**.

Feldstein, S., 2002: The recent trend and variance increase of the annular mode. *Journal of Climate*. 88-94.

Fern´andez-Donado, L., et al., 2012: Temperature response to external forcing in simulations and reconstructions of the last millennium. *Climate of the Past Discussions*, **submitted**.

Fettweis, X., et al., 2012: Estimating Greenland ice sheet surface mass balance contribution to future sea level rise using the regional atmospheric climate model MAR. *The Cryosphere*. submitted.

Fettweis, X., G. Mabille, M. Erpicum, S. Nicolay, and M. Van den Broeke, 2011a: The 1958-2009 Greenland ice sheet surface melt and the mid-tropospheric atmospheric circulation. *Climate Dynamics*. doi:DOI 10.1007/s00382-010-0772-8, 139-159.

——, 2011b: The 1958-2009 Greenland ice sheet surface melt and the mid-tropospheric atmospheric circulation. *Climate Dynamics*, **36**, 139-159.

Feudale, L., and J. Shukla, 2010: Influence of sea surface temperature on the European heat wave of 2003 summer. Part I: an observational study. *Clim. Dyn.* doi:DOI 10.1007/s00382-010-0788-0.

Feulner, G., 2011: Are the most recent estimates for Maunder Minimum solar irradiance in agreement with temperature reconstructions? *Geophys. Res. Lett.*, **38**.

Fischer, E. M., and C. Schär 2010: Consistent geographical patterns of changes in high-impact European heatwaves. *Nature Geoscience*, **3**, 398-403.

Fischer, E. M., S. I. Seneviratne, P. L. Vidale, D. Luthi, and C. Schar, 2007: Soil moisture - Atmosphere interactions during the 2003 European summer heat wave. *Journal of Climate*, **20**, 5081-5099.

Fogt, R., J. Perlwitz, A. Monaghan, D. Bromwich, J. Jones, and G. Marshall, 2009: Historical SAM Variability. Part II: Twentieth-Century Variability and Trends from Reconstructions, Observations, and the IPCC AR4 Models. *Journal of Climate*. doi:DOI 10.1175/2009JCLI2786.1, 5346-5365.

Folland, C. K., O. Boucher, J. Knight, D. E. Parker, S. P. A., and J.-P. Vernier, 2012: The Atlantic Multidecadal Oscillation, other natural and anthropogenic forcing factors and global mean surface temperature, 1891-2010. *J. Geohys. Res. Atmos.*

Folland, C. K., et al., 2011: High predictive skill of global surface temperature a year ahead. *Met Office Hadley Centre Climate Programme (MOHCCP) 2010-2012*, Met Office Hadley Centre, 21.

Forest, C., and R. Reynolds, 2008: Climate change - Hot questions of temperature bias. *Nature*. doi:DOI 10.1038/453601a, 601-602.

Forest, C., P. Stone, and A. Sokolov, 2006: Estimated PDFs of climate system properties including natural and anthropogenic forcings. *Geophys. Res. Lett.* doi:ARTN L01705, 10.1029/2005GL023977, -.

——, 2008: Constraining climate model parameters from observed 20th century changes. *Tellus Series a-Dynamic Meteorology and Oceanography*. doi:DOI 10.1111/j.1600-0870.2008.00346.x, 911-920.
Forest, C., M. Allen, P. Stone, and A. Sokolov, 2000: Constraining uncertainties in climate models using climate change detection techniques. *Geophys. Res. Lett.*, 569-572.
Forest, C., P. Stone, A. Sokolov, M. Allen, and M. Webster, 2002: Quantifying uncertainties in climate system properties with the use of recent climate observations. *Science*. 113-117.
Forster, P., and K. Taylor, 2006: Climate forcings and climate sensitivities diagnosed from coupled climate model integrations. *Journal of Climate*, **19**, 6181-6194.
Forster, P., and J. Gregory, 2006: The climate sensitivity and its components diagnosed from Earth Radiation Budget data. *Journal of Climate*. 39-52.
Forster, P., et al., 2007: Changes in Atmospheric Constituents and in Radiative Forcing. *Climate Change 2007: The Physical Science Basis. Contribution of Working Group I to the Fourth Assessment Report of the Intergovernmental Panel on Climate Change*, Cambridge University Press.
Forster, P. M., T. Andrews, P. Good, J. M. Gregory, L. S. Jackson, and M. Zelinka, 2012: Evaluating adjusted forcing and model spread for historical and future scenarios in the CMIP5 generation of climate models. *J. Geophys. Res. (Atmos)*.
Forster, P. M., et al., 2011: Stratospheric changes and climate, Chapter 4 in *Scientific Assessment of Ozone Depletion: 2010. Global Ozone Research and Monitoring Project-Report No. 52 (in press)*, P. M. Forster, et al., Ed., World Meteorological Organization.
Foster, G., and S. Rahmstorf, 2011: Global temperature evolution 1979-2010. *Environmental Research Letters*, **6**.
Foster, G., J. Annan, G. Schmidt, and M. Mann, 2008: Comment on "Heat capacity, time constant, and sensitivity of Earth's climate system" by S. E. Schwartz. *Journal of Geophysical Research-Atmospheres*, **113**.
Fowler, H. J., and R. L. Wilby, 2010: Detecting changes in seasonal precipitation extremes using regional climate model projections: Implications for managing fluvial flood risk. *Water Resources Research*, **46(W0525)**.
Frame, D., D. Stone, P. Stott, and M. Allen, 2006: Alternatives to stabilization scenarios. *Geophys. Res. Lett.* doi:ARTN L14707, DOI 10.1029/2006GL025801, -.
Frame, D., B. Booth, J. Kettleborough, D. Stainforth, J. Gregory, M. Collins, and M. Allen, 2005: Constraining climate forecasts: The role of prior assumptions. *Geophys. Res. Lett.* doi:ARTN L09702, 10.1029/2004GL022241, -.
Francis, J. A., and S. J. Vavrus 2012: Evidence Linking Arctic Amplification to Extreme Weather in Mid-Latitudes. *Geophys. Res. Lett.*, **39**, L06801, doi:06810.01029/02012GL051000.
Frank, D., J. Esper, and E. R. Cook, 2007: Adjustment for proxy number and coherence in a large-scale temperature reconstruction. *Geophys. Res. Lett.*, **34**.
Frank, D. C., J. Esper, C. C. Raible, U. Buntgen, V. Trouet, B. Stocker, and F. Joos, 2010: Ensemble reconstruction constraints on the global carbon cycle sensitivity to climate, **463**, 6.
Franzke, C., 2010: Long-Range Dependence and Climate Noise Characteristics of Antarctic Temperature Data. *Journal of Climate*. doi:DOI 10.1175/2010JCLI3654.1, 6074-6081.
Free, M., 2011: The Seasonal Structure of Temperature Trends in the Tropical Lower Stratosphere. *Journal of Climate*, **24**, 859-866.
Free, M., and J. Lanzante, 2009: Effect of Volcanic Eruptions on the Vertical Temperature Profile in Radiosonde Data and Climate Models. *Journal of Climate*, **22**, 2925-2939.
Frierson, D. M. W., 2006: Robust increases in midlatitude static stability in simulations of global warming. *Geophys. Res. Lett.*, **33**.
Frierson, D. M. W., J. Lu, and G. Chen, 2007: Width of the Hadley cell in simple and comprehensive general circulation models. *Geophys. Res. Lett.*, **34**.
Fu, Q., and P. Lin, 2011: Poleward shift of subtropical jets inferred from satellite-observed lower stratospheric temperatures. *J. Climate*, **24**, 5597-5603.
Fu, Q., S. Solomon, and P. Lin, 2010: On the seasonal dependence of tropical lower-stratospheric temperature trends. *Atmospheric Chemistry and Physics*, **10**, 2643-2653.
Fu, Q., S. Manabe, and C. M. Johanson, 2011: On the warming in the tropical upper troposphere: Models versus observations. *Geophys. Res. Lett.*, **38**.
Fu, Q., C. M. Johanson, J. M. Wallace, and T. Reichler, 2006: Enhanced mid-latitude tropospheric warming in satellite measurements. *Science*, **312**, 1179-1179.
Fyfe, J., 2006: Southern Ocean warming due to human influence. *Geophys. Res. Lett.*, **33**, -.
Fyfe, J. C., N. P. Gillett, and D. W. J. Thompson, 2010: Comparing variability and trends in observed and modelled global-mean surface temperature. *Geophys. Res. Lett.*, **37**.
Fyfe, J. C., M. J. Merryfield, V. Kharin, G. J. Boer, W.-S. Lee, and K. v. Salzen, 2011: Skillful predictions of decadal trends in global mean surface temperatur. *Geophys. Res. Lett.*, **38**.
Ganopolski, A., and T. Schneider von Deimling, 2008: Comment on "Aerosol radiative forcing and climate sensitivity deduced from the Last Glacial Maximum to Holocene transition" by Petr Chylek and Ulrike Lohmann. *Geophys. Res. Lett.* doi:ARTN L23703, 10.1029/2008GL033888, -.
Gao, C., A. Robock, and C. Ammann, 2008: Volcanic forcing of climate over the past 1500 years: An improved ice core-based index for climate models. *Journal of Geophysical Research-Atmospheres*, **113**.
Gascard, J. C., and e. al, 2008: Exploring Arcitc transpolar drift during dramatic sea ice retreat. *EOS*, **89**, 3.

Giles, K., S. Laxon, and A. Ridout, 2008: Circumpolar thinning of Arctic sea ice following the 2007 record ice extent minimum. *Geophys. Res. Lett.* doi:ARTN L22502, 10.1029/2008GL035710, -.
Gillett, N., and P. Stott, 2009: Attribution of anthropogenic influence on seasonal sea level pressure. *Geophys. Res. Lett.* doi:ARTN L23709, 10.1029/2009GL041269, -.
Gillett, N., V. Arora, G. Flato, J. Scinocca, and K. von Salzen, 2012a: Improved constraints on 21st-century warming derived using 160 years of temperature observations. *Geophys. Res. Lett.*, **39**.
Gillett, N., et al., 2008a: Attribution of polar warming to human influence. *Nature Geoscience*, **1**, 750-754.
Gillett, N. P., and J. C. Fyfe, 2012: Attribution of observed sea level pressure trends to greenhouse gas, aerosol and ozone changes. *Nature Climate Change*.
Gillett, N. P., R. J. Allan, and T. J. Ansell, 2005: Detection of external influence on sea level pressure with a multi-model ensemble. *Geophys. Res. Lett.*, **32(L19714)**.
Gillett, N. P., P. A. Stott, and B. D. Santer, 2008b: Attribution of cyclogenesis region sea surface temperature change to anthropogenic influence. *Geophys. Res. Lett.*, **35**.
Gillett, N. P., G. C. Hegerl, M. R. Allen, and P. A. Stott, 2000: Implications of changes in the Northern Hemisphere circulation for the detection of anthropogenic climate change. *Geophys. Res. Lett.*, **27**, 993-996.
Gillett, N. P., F. W. Zwiers, A. J. Weaver, and P. A. Stott, 2003: Detection of human influence on sea-level pressure. *Nature*, **422**, 292-294.
Gillett, N. P., V. K. Arora, G. M. Flato, J. F. Scinocca, and K. von Salzen, 2011a: Improved constraints on 21st-century warming derived using 160 years of temperature observations. *Geophys. Res. Lett.*
Gillett, N. P., V. K. Arora, D. Matthews, P. A. Stott, and M. R. Allen, 2012b: Constraining the ratio of global warming to cumulative CO2 emissions using CMIP5 simulations. *J. Clim.*
Gillett, N. P., et al., 2008c: Attribution of polar warming to human influence. *Nature Geoscience*, **1**, 750-754.
Gillett, N. P., et al., 2011b: Attribution of observed changes in stratospheric ozone and temperature. *Atmos. Chem. Phys*, 599-609.
Gleckler, P. J., T. M. L. Wigley, B. D. Santer, J. M. Gregory, K. AchutaRao, and K. E. Taylor, 2006: Volcanoes and climate: Krakatoa's signature persists in the ocean. *Nature*, **439**, 675-675.
Gleckler, P. J., et al., 2012: Human-induced global ocean warming on multidecadal timescales. *Nature Clim. Change*, **2**, 524-529.
Goosse, H., W. Lefebvre, A. de Montety, E. Crespin, and A. Orsi, 2009: Consistent past half-century trends in the atmosphere, the sea ice and the ocean at high southern latitudes. *Climate Dynamics*. doi:DOI 10.1007/s00382-008-0500-9, 999-1016.
Goosse, H., J. Guiot, M. Mann, S. Dubinkina, and Y. Sallaz-Damaz, 2012a: The medieval climate anomaly in Europe: Comparison of the summer and annual mean signals in two reconstructions and in simulations with data assimilation. *Global and Planetary Change*, **84-85**, 35-47.
Goosse, H., E. Crespin, A. de Montety, M. Mann, H. Renssen, and A. Timmermann, 2010: Reconstructing surface temperature changes over the past 600 years using climate model simulations with data assimilation. *Journal of Geophysical Research-Atmospheres*. doi:ARTN D09108, 10.1029/2009JD012737, -.
Goosse, H., et al., 2012b: The role of forcing and internal dynamics in explaining the "Medieval Climate Anomaly". *Climate Dynamics*, **Doi: 10.1007/s00382-012-1297-0**.
Gouretski, V., and K. Koltermann, 2007: How much is the ocean really warming? *Geophys. Res. Lett.*, **34**, L01610.
Graff, L. S., and J. H. LaCasce, 2012: Changes in the extratropical storm tracks in response to changes in SST in an GCM. *Journal of Climate*. doi:10.1175/JCLI-D-11-00174.1.
Grant, A., S. Bronnimann, T. Ewen, T. Griesser, and A. Stickler, 2009: The early twentieth century warm period in the European Arctic. *Meteorologische Zeitschrift*, **18**, 425-432.
Graversen, R., and M. Wang, 2009: Polar amplification in a coupled climate model with locked albedo. *Climate Dynamics*. doi:DOI 10.1007/s00382-009-0535-6, 629-643.
Gray, L., et al., 2010: SOLAR INFLUENCES ON CLIMATE. *Reviews of Geophysics*, **48**, -.
Gregory, J., 2000: Vertical heat transports in the ocean and their effect an time-dependent climate change. *Climate Dynamics*. 501-515.
Gregory, J., J. Lowe, and S. Tett, 2006: Simulated global-mean sea level changes over the last half-millennium. *Journal of Climate*, **19**, 4576-4591.
Gregory, J. M., 2010: Long-term effect of volcanic forcing on ocean heat content. *Geophys. Res. Lett.*, **37**, L22701.
Gregory, J. M., and P. M. Forster, 2008: Transient climate response estimated from radiative forcing and observed temperature change. *Journal of Geophysical Research-Atmospheres*, **113**.
Gregory, J. M., H. T. Banks, P. A. Stott, J. A. Lowe, and M. D. Palmer, 2004: Simulated and observed decadal variability in ocean heat content. *Geophys. Res. Lett.*, **31**, L15312.
Gregory, J. M., et al., 2012: Twentieth-century global-mean sea-level rise: is the whole greater than the sum of the parts? *Journal of Climate*, **(Submitted)**.
Grist, J., et al., 2010: The roles of surface heat flux and ocean heat transport convergence in determining Atlantic Ocean temperature variability. *Ocean Dynamics*, **60**, 771-790.
Haimberger, L., C. Tavolato, and S. Sperka, 2011: On the persistence of a tropical tropospheric warming maximum during five decades of radiosonde observations. *submitted to Science*.
Han, W., et al., 2010: Patterns of Indian Ocean sea-level change in a warming climate. *Nature Geoscience*, **3**, 546-550.

Hanna, E., J. M. Jones, J. Cappelen, S. H. Mernild, L. Wood, K. Steffen, and Huybrechts P., 2012: The influence of North Atlantic atmospheric and oceanic forcing effects on 1900-2010 Greenland summer climate and ice melt/runoff. *International Journal of Climatology*. DOI: 10.1002/joc.3475.

Hanna, E., et al., 2008: Increased runoff from melt from the Greenland Ice Sheet: A response to global warming. *Journal of Climate*, **21**, 331-341.

Hannart, A., J. Dufresne, and P. Naveau, 2009: Why climate sensitivity may not be so unpredictable. *Geophys. Res. Lett.* doi:ARTN L16707, 10.1029/2009GL039640, -.

HANSEN, J., and S. LEBEDEFF, 1987: GLOBAL TRENDS OF MEASURED SURFACE AIR-TEMPERATURE. *Journal of Geophysical Research-Atmospheres*. 13345-13372.

Hansen, J., M. Sato, and R. Ruedy, 2012: Perception of climate change. **doi:10.1073/pnas.1205276109**.

Hansen, J., R. Ruedy, M. Sato, and K. Lo, 2010: GLOBAL SURFACE TEMPERATURE CHANGE. *Reviews of Geophysics*, **48**.

Hansen, J., M. Sato, P. Kharecha, and K. von Schuckmann, 2011: Earth's energy imbalance and implications. *Atmospheric Chemistry and Physics*, **11**, 13421-13449.

Hansen, J., et al., 2005a: Earth's energy imbalance: Confirmation and implications. *Science*. doi:DOI 10.1126/science.1110252, 1431-1435.

Hansen, J., et al., 2005b: Efficacy of climate forcings. *Journal of Geophysical Research-Atmospheres*, **110**.

Hardwick Jones, R., S. Westra, and A. Sharma, 2010: Observed relationships between extreme sub-daily precipitation, surface temperature, and relative humidity. *Geophys. Res. Lett.*, **37**.

Hargreaves, J., and J. Annan, 2009: Comment on 'Aerosol radiative forcing and climate sensitivity deduced from the Last Glacial Maximum to Holocene transition', by P. Chylek and U. Lohmann, Geophys. Res. Lett., 2008. *Clim. Past.*, **5**, 143-145.

Hargreaves, J., A. Abe-Ouchi, and J. Annan, 2007: Linking glacial and future climates through an ensemble of GCM simulations. *Clim. Past.*, 77-87.

Harries, J., and C. Belotti, 2010: On the Variability of the Global Net Radiative Energy Balance of the Nonequilibrium Earth. *Journal of Climate*. doi:DOI 10.1175/2009JCLI2797.1, 1277-1290.

HASSELMANN, K., 1976: STOCHASTIC CLIMATE MODELS .1. THEORY. *Tellus*, **28**, 473-485.

——, 1997: Multi-pattern fingerprint method for detection and attribution of climate change. *Climate Dynamics*. 601-611.

Hegerl, G., and F. Zwiers, 2011: Use of models in detection and attribution of climate change. *Wiley Interdisciplinary Reviews-Climate Change*, **2**, 570-591.

Hegerl, G., F. Zwiers, P. Stott, and V. Kharin, 2004: Detectability of anthropogenic changes in annual temperature and precipitation extremes. *Journal of Climate*. 3683-3700.

Hegerl, G., T. Crowley, W. Hyde, and D. Frame, 2006: Climate sensitivity constrained by temperature reconstructions over the past seven centuries. *Nature*. doi:DOI 10.1038/nature04679, 1029-1032.

Hegerl, G., T. Crowley, S. Baum, K. Kim, and W. Hyde, 2003: Detection of volcanic, solar and greenhouse gas signals in paleo-reconstructions of Northern Hemispheric temperature. *Geophys. Res. Lett.* doi:ARTN 1242, 10.1029/2002GL016635, -.

Hegerl, G., J. Luterbacher, F. Gonzalez-Rouco, S. F. B. Tett, T. Crowley, and E. Xoplaki, 2011a: Influence of human and natural forcing on European seasonal temperatures. *Nature Geoscience*, **published online 16 January 2011**, 5.

Hegerl, G., K. Hasselmann, U. Cubasch, J. Mitchell, E. Roeckner, R. Voss, and J. Waszkewitz, 1997: Multi-fingerprint detection and attribution analysis of greenhouse gas, greenhouse gas-plus-aerosol and solar forced climate change. *Climate Dynamics*. 613-634.

Hegerl, G., T. Crowley, M. Allen, W. Hyde, H. Pollack, J. Smerdon, and E. Zorita, 2007a: Detection of human influence on a new, validated 1500-year temperature reconstruction. *Journal of Climate*. doi:DOI 10.1175/JCLI4011.1, 650-666.

Hegerl, G. C., F. W. Zwiers, and C. Tebaldi, 2011b: Patterns of change: Whose fingerprint is seen in global warming? *Environmental Research Letters*.

Hegerl, G. C., P. Stott, S. Solomon, and F. W. Zwiers, 2011c: Comment on Climate Science and the Uncertainty Monster by J.A. Curry and P.J. Webster. *Bulletin of the American Meteorological Society*, **in press**.

Hegerl, G. C., et al., 2010: Good Practice Guidance Paper on Detection and Attribution Related to Anthropogenic Climate Change. IPCC Working Group I Technical Support Unit, University of Bern, Bern, Switzerland.

Hegerl, G. C., et al., 2007b: Understanding and Attributing Climate Change. *Climate Change 2007: The Physical Science Basis. Contribution of Working Group I to the Fourth Assessment Report of the Intergovernmental Panel on Climate Change*, Cambridge University Press.

Hegerl, G. C., et al., 2007b: Understanding and Attributing climate change, climate change 2007: The Physical Science Basis. Contribution of Working Group I to the Fourth Assessment Report of the Intergovernment Panel on Climate Change., Cambridge University Press, Cambridge, United Kingdom and New York, USA.

Held, I., M. Winton, K. Takahashi, T. Delworth, F. Zeng, and G. Vallis, 2010: Probing the Fast and Slow Components of Global Warming by Returning Abruptly to Preindustrial Forcing. *Journal of Climate*. doi:DOI 10.1175/2009JCLI3466.1, 2418-2427.

Held, I. M., and B. J. Soden, 2006: Robust responses of the hydrological cycle to global warming. *Journal of Climate*, **19**, 5686-5699.
Helm, K., N. Bindoff, and J. Church, 2010: Changes in the global hydrological-cycle inferred from ocean salinity. *Geophys. Res. Lett.* doi:ARTN L18701, 10.1029/2010GL044222, -.
Helm, K. P., N. L. Bindoff, and J. A. Church, 2011: Observed decreases in oxygen content of the global ocean. Geophysical research letters.
Henriksson, S., E. Arjas, M. Laine, J. Tamminen, and A. Laaksonen, 2010: Comment on 'Using multiple observationally-based constraints to estimate climate sensitivity' by J. D. Annan and J. C. Hargreaves, Geophys. Res. Lett., 2006. *Clim. Past.* doi:DOI 10.5194/cp-6-411-2010, 411-414.
Hidalgo, H. G., et al., 2009: Detection and Attribution of Streamflow Timing Changes to Climate Change in the Western United States. *Journal of Climate*, **22**, 3838-3855.
Hodge, S., D. Trabant, R. Krimmel, T. Heinrichs, R. March, and E. Josberger, 1998: Climate variations and changes in mass of three glaciers in western North America. *Journal of Climate*. 2161-2179.
Hoekema, D. J., and V. Sridhar, 2011: Relating climatic attributes and water resources allocation: A study using surface water supply and soil moisture indices in the Snake River basin, Idaho. *Water Resources Research*, **47**.
Hoerling, M., and A. Kumar, 2003: The perfect ocean for drought. *Science*, **299**, 691-694.
Hoerling, M., J. Eischeid, J. Perlwitz, X. Quan, T. Zhang, and P. Pegion, 2011: On the increased frequency of Mediterranean drought. *J. Climate*, **submitted**.
Hoerling, M., et al., 2012: **Anatomy of an Extreme Event**. submitted.
Hofmann, D., J. Barnes, M. O'Neill, M. Trudeau, and R. Neely, 2009: Increase in background stratospheric aerosol observed with lidar at Mauna Loa Observatory and Boulder, Colorado. *Geophys. Res. Lett.*, **36**.
Holden, P., N. Edwards, K. Oliver, T. Lenton, and R. Wilkinson, 2010: A probabilistic calibration of climate sensitivity and terrestrial carbon change in GENIE-1. *Climate Dynamics*, **35**, 785-806.
Holland, D., R. Thomas, B. De Young, M. Ribergaard, and B. Lyberth, 2008: Acceleration of Jakobshavn Isbrae triggered by warm subsurface ocean waters. *Nature Geoscience*. doi:DOI 10.1038/ngeo316, 659-664.
Holland, M., M. Serreze, and J. Stroeve, 2010: The sea ice mass budget of the Arctic and its future change as simulated by coupled climate models. *Climate Dynamics*. doi:DOI 10.1007/s00382-008-0493-4, 185-200.
Hosoda, S., T. Suga, N. Shikama, and K. Mizuno, 2009: Global Surface Layer Salinity Change Detected by Argo and Its Implication for Hydrological Cycle Intensification. *Journal of Oceanography*. 579-586.
Hu, Y., and Q. Fu, 2007: Observed poleward expansion of the Hadley circulation since 1979. *Atmospheric Chemistry and Physics*, **7**, 5229-5236.
Hu, Y., and L. Tao, 2012: Poleward expansion of the Hadley circulation in CMIP5. *Submitted to Adv. Atmos. Sci.*
Hu, Y., L. Tao, and J. Liu, 2012: Poleward expansion of the Hadley circulation in CMIP5 simulations. *Adv. Atmos. Sci.*, submitted.
Hu, Y. Y., C. Zhou, and J. P. Liu, 2011: Observational Evidence for Poleward Expansion of the Hadley Circulation. *Advances in Atmospheric Sciences*, **28**, 33-44.
Huber, M. B., and R. Knutti, 2012: Probabilistic climate projections with an intermediatecomplexity model.Part II: Application to observational datasets. *Submitted*.
Hudson, R. D., M. F. Andrade, M. B. Follette, and A. D. Frolov, 2006: The total ozone field separated into meteorological regimes - Part II: Northern Hemisphere mid-latitude total ozone trends. *Atmospheric Chemistry and Physics*, **6**, 5183-5191.
Hulme, M., S. J. O'Neill, and S. Dessai, 2011: Is Weather Event Attribution Necessary for Adaptation Funding? *Science*, **334**.
Huntingford, C., P. Stott, M. Allen, and F. Lambert, 2006: Incorporating model uncertainty into attribution of observed temperature change. *Geophys. Res. Lett.* doi:ARTN L05710, 10.1029/2005GL024831, -.
Hurtt, G. C., et al., 2009: Harmonization of Global Land-Use Scenarios for the Period 1500-2100 for IPCC-AR5. *Integrated Land Ecosystem-Atmosphere Processes Study (iLEAPS) Newsletter*, **7**, 6-8.
Huss, M., and A. Bauder, 2009: 20th-century climate change inferred from four long-term point observations of seasonal mass balance. *Annals of Glaciology*, **50**, 207-214.
Huss, M., R. Hock, A. Bauder, and M. Funk, 2010: 100-year mass changes in the Swiss Alps linked to the Atlantic Multidecadal Oscillation. *Geophys. Res. Lett.* doi:ARTN L10501, 10.1029/2010GL042616, -.
Huybers, P., 2010: Compensation between Model Feedbacks and Curtailment of Climate Sensitivity. *Journal of Climate*, **23**, 3009-3018.
Imbers, J., A. Lopez, C. Huntingford, and M. R. Allen, 2012: Testing the robustness of the anthropogenic climate change detection statements using different empirical models, **draft**.
Imbers, J., A. Lopez, C. Huntingford, and M. R. Allen, 2012a: Sensitivity of climate change detection and attribution to the characterisation of internal variability.
Ishii, M., and M. Kimoto, 2009: Reevaluation of historical ocean heat content variations with time-varying XBT and MBT depth bias corrections. *Journal of Oceanography*, **65**, 287-299.
Jackson, J., E. Carmack, F. McLaughlin, S. Allen, and R. Ingram, 2010: Identification, characterization, and change of the near-surface temperature maximum in the Canada Basin, 1993-2008. *Journal of Geophysical Research-Oceans*. doi:ARTN C05021, 10.1029/2009JC005265, -.

Jacob, T., J. Wahr, W. T. Pfeffer, and S. Swenson, 2012: Recent contributions of glaciers and ice caps to sea level rise. *Nature*, **482**, 514-518.
Jacobs, S., A. Jenkins, C. Giulivi, and P. Dutrieux, 2011: Stronger ocean circulation and increased melting under Pine Island Glacier ice shelf. *Nature Geoscience*, **4**, 519-523.
Jahn, A., et al., 2011 [Submitted]: Late 20th Century simulation of Arctic Sea-ice and ocean properties in the CCSM4. J. Climate.
Johannessen, O., et al., 2004: Arctic climate change: observed and modelled temperature and sea-ice variability (vol 56A, pg 328, 2004). *Tellus Series a-Dynamic Meteorology and Oceanography*. 559-560.
Johnson, G., and A. Orsi, 1997: Southwest Pacific Ocean water-mass changes between 1968/69 and 1990/91. *Journal of Climate*. 306-316.
Jones, G. S., and P. A. Stott, 2011: Sensitivity of the attribution of near surface temperature warming to the choice of observational dataset.
Jones, G. S., S. F. B. Tett, and P. A. Stott, 2003: Causes of atmospheric temperature change 1960–2000: A combined attribution analysis. *Geophys. Res. Lett.,*, **30**.
Jones, G. S., P. A. Stott, and N. Christidis, 2008: Human contribution to rapidly increasing frequency of very warm Northern Hemisphere summers. *Journal of Geophysical Research-Atmospheres*, **113**.
Jones, G. S., N. Christidis, and P. A. Stott, 2010: Detecting the influence of fossil fuel and bio-fuel black carbon aerosols on near surface temperature changes. *Atmos. Chem. Phys. Discuss.*, 20921-20974.
Jones, G. S., P. A. Stott, and N. Christidis, 2012: Attribution of observed historical near surface temperature variations to anthropogenic and natural causes using CMIP5 simulations.
Jones, P., et al., 2001: Adjusting for sampling density in grid box land and ocean surface temperature time series. *Journal of Geophysical Research-Atmospheres*, **106**, 3371-3380.
Joshi, M., and G. Jones, 2009: The climatic effects of the direct injection of water vapour into the stratosphere by large volcanic eruptions. *Atmospheric Chemistry and Physics*. 6109-6118.
Joughin, I., and R. Alley, 2011: Stability of the West Antarctic ice sheet in a warming world. *Nature Geoscience*, **4**, 506-513.
Juckes, M. N., et al., 2007: Millennial temperature reconstruction intercomparison and evaluation. *Clim. Past.*, **3**.
Jung, M., et al., 2010: Recent decline in the global land evapotranspiration trend due to limited moisture supply. *Nature*, **467**, 951-954.
Jungclaus, J., et al., 2010: Climate and carbon-cycle variability over the last millennium. *Clim. Past.* doi:DOI 10.5194/cp-6-723-2010, 723-737.
Kaplan, J., K. Krumhardt, and N. Zimmermann, 2009: The prehistoric and preindustrial deforestation of Europe. *Quaternary Science Reviews*, **28**, 3016-3034.
Karoly, D., and Q. Wu, 2005a: Detection of regional surface temperature trends. *Journal of Climate*. 4337-4343.
Karoly, D. J., and Q. G. Wu, 2005b: Detection of regional surface temperature trends. *Journal of Climate*, **18**, 4337-4343.
Karoly, D. J., and P. A. Stott, 2006: Anthropogenic warming of central England temperature. *Atmos. Sci. Let.*, 81-85.
Karpechko, A. Y., N. P. Gillett, G. J. Marshall, and A. A. Scaife, 2008: Stratospheric influence on circulation changes in the Southern Hemisphere troposphere in coupled climate models. *Geophys. Res. Lett.*, **35**.
Kattsov, V., et al., 2010: Arctic sea-ice change: a grand challenge of climate science. *Journal of Glaciology*, **56**, 1115-1121.
Kaufman, D., et al., 2009: Recent Warming Reverses Long-Term Arctic Cooling. *Science*, **325**, 1236-1239.
Kaufmann, R., and D. Stern, 1997: Evidence for human influence on climate from hemispheric temperature relations. *Nature*, **388**, 39-44.
Kaufmann, R. K., H. Kauppi, M. L. Mann, and J. H. Stock, 2011: Reconciling anthropogenic climate change with observed temperature 1998–2008. *Proceedings of the National Academy of Sciences of the United States of America*. doi:10.1073/pnas.1102467108.
Kay, A. L., S. M. Crooks, P. Pall, and D. A. Stone, 2011a: Attribution of Autumn 2000 flood risk in England to anthropogenic climate change. submitted.
Kay, A. L., S. M. Crooks, P. Pall, and D. A. Stone, 2011b: Attribution of Autumn/Winter 2000 flood risk in England to anthropogenic climate change: A catchment-based study. *Journal of Hydrology*, **406**, 97-112.
Kay, J., M. Holland, and A. Jahn, 2011c: Inter-annual to multi-decadal Arctic sea ice extent trends in a warming world. *Geophys. Res. Lett.*, **38**, -.
Keeling, R., and H. Garcia, 2002: The change in oceanic O-2 inventory associated with recent global warming. *Proceedings of the National Academy of Sciences of the United States of America*. doi:DOI 10.1073/pnas.122154899, 7848-7853.
Keeling, R., A. Kortzinger, and N. Gruber, 2010: Ocean Deoxygenation in a Warming World. *Annual Review of Marine Science*, **2**, 199-229.
Kettleborough, J., B. Booth, P. Stott, and M. Allen, 2007: Estimates of uncertainty in predictions of global mean surface temperature. *Journal of Climate*. doi:DOI 10.1175/JCLI4012.1, 843-855.
Kharin, V. V., F. W. Zwiers, X. Zhang, and G. C. Hegerl, 2007: Changes in temperature and precipitation extremes in the IPCC ensemble of global coupled model simulations. *Journal of Climate*, **20**, 1419-1444.

Kharin, V. V., F. W. Zwiers, X. Zhang, and M. Wehner, 2012: Changes in temperature and precipitation extremes in the CMIP5 ensemble. *Clim. Change*.
Kiehl, J. T., 2007: Twentieth century climate model response and climate sensitivity. *Geophys. Res. Lett.*, **34**, 4.
Kinnard, C., et al., 2011: Reconstructed changes in Arctic sea ice cover over the past 1450 years. *Nature*, **479**, 509-513.
Kirk-Davidoff, D., 2009: On the diagnosis of climate sensitivity using observations of fluctuations. *Atmospheric Chemistry and Physics*. 813-822.
Kitaev, L. M., and A. V. Kislov, 2008: Regional differences of snow accumulation - contemporary and future changes (on the example of Northern Europe and northern part of West Siberia). *Kriosfera Zemly (Earth Cryosphere)*, **12**, 98-104.
Kitaev, L. M., T. B. Titkova, and E. A. Cherenkova, 2007: Snow accumulation tendencies in Northern Eurasia , Vol.11, No.3, 71-77. *Kriosfera Zemly (Earth Cryosphere)*, **11**, 71-77.
Knight, J., et al., 2009: Do global temperature trends over the last decade falsify climate predictions? *In: State of the climate in 2008*, Bull. Amer. Meteor. Soc., S22-S23.
Knight, J. R., C. K. Folland, and A. A. Scaife, 2006: Climate impacts of the Atlantic Multidecadal Oscillation. *Geophys. Res. Lett.*, **33**.
Knight, J. R., R. J. Allan, C. K. Folland, M. Vellinga, and M. E. Mann, 2005: A signature of persistent natural thermohaline circulation cycles in observed climate. *Geophys. Res. Lett.*, **32**.
Knutson, T., et al., 2006: Assessment of twentieth-century regional surface temperature trends using the GFDL CM2 coupled models. *Journal of Climate*. 1624-1651.
Knutson, T. R., et al., 2010: Tropical cyclones and climate change. *Nature Geoscience*, **3**, 157-163.
Knutti, R., 2008: Why are climate models reproducing the observed global surface warming so well? *Geophys. Res. Lett.* doi:ARTN L18704, 10.1029/2008GL034932, -.
Knutti, R., and G. Hegerl, 2008: The equilibrium sensitivity of the Earth's temperature to radiation changes. *Nature Geoscience*. doi:DOI 10.1038/ngeo337, 735-743.
Knutti, R., and L. Tomassini, 2008: Constraints on the transient climate response from observed global temperature and ocean heat uptake. *Geophys. Res. Lett.* doi:ARTN L09701, 10.1029/2007GL032904, -.
Knutti, R., et al., 2008: A review of uncertainties in global temperature projections over the twenty-first century. *Journal of Climate*, **21**, 2651-2663.
Kodama, C., and T. Iwasaki, 2009: Influence of the SST Rise on Baroclinic Instability Wave Activity under an Aquaplanet Condition. *J. Atmos. Sci.*, **66**, 2272–2287.
Koehler, P., R. Bintanja, H. Fischer, F. Joos, R. Knutti, G. Lohmann, and V. Masson-Delmotte, 2010: What caused Earth's temperature variations during the last 800,000 years? Data-based evidence on radiative forcing and constraints on climate sensitivity. *Quaternary Science Reviews*. doi:DOI 10.1016/j.quascirev.2009.09.026, 129-145.
Korhonen, H., K. S. Carslaw, P. M. Forster, S. Mikkonen, N. D. Gordon, and H. Kokkola, 2010: Aerosol climate feedback due to decadal increases in Southern Hemisphere wind speeds. *Geophys. Res. Lett.*, **37**.
Krakauer, N. Y., and I. Fung, 2008: Mapping and attribution of change in streamflow in the coterminous United States. *Hydrology and Earth System Sciences*, **12**, 1111-1120.
Kuhlbrodt, T., and J. M. Gregory, 2012: Ocean heat uptake and its consequences for the magnitude of 1sea level rise and climate change. *Geophys. Res. Lett.*, **submitted**.
Kunkel, K. E., et al., 2008: Observed Changes in Weather and Climate Extremes. *Weather and Climate Extremes in a Changing Climate. Regions of Focus: North America, Hawaii, Caribbean, and U.S. Pacific Islands*, G. A. M. T. R. Karl, C. D. Miller, S. J. Hassol, A. M. Waple, and W. L. Murray, Ed., A Report by the U.S. Climate Change Science Program and the Subcommittee on Global Change Research.
Kwok, R., and N. Untersteiner, 2011: The thinning of Arctic sea ice. *Physics Today*, **64**, 36-41.
Kwok, R., G. Cunningham, M. Wensnahan, I. Rigor, H. Zwally, and D. Yi, 2009: Thinning and volume loss of the Arctic Ocean sea ice cover: 2003-2008. *Journal of Geophysical Research-Oceans*. doi:ARTN C07005, 10.1029/2009JC005312, -.
L'Heureux, M., A. Butler, B. Jha, A. Kumar, and W. Wang, 2010: Unusual extremes in the negative phase of the Arctic Oscillation during 2009. *Geophys. Res. Lett.* doi:ARTN L10704, 10.1029/2010GL043338, -.
Langen, P., and V. Alexeev, 2007: Polar amplification as a preferred response in an idealized aquaplanet GCM. *Climate Dynamics*. doi:DOI 10.1007/s00382-006-0221-x, 305-317.
Lanzante, J.R., 1996: Resistant, robust, and nonparametric techniques for the analysis of climate data: Theory and examples, including applications to historical radiosonde station data. *Int. J. Climatol.*, **16**, 1197-1226.
Lanzante, J. R., 2009: Comment on ‘‘Trends in the temperature and water vapor content of the tropical lower stratosphere: Sea surface connection’’ by Karen H. Rosenlof and George C. Reid. *Journal of Geophysical Research*, **114**.
Latif, M., et al., 2004: Reconstructing, monitoring, and predicting multidecadal-scale changes in the North Atlantic thermohaline circulation with sea surface temperature. *Journal of Climate*, **17**, 1605-1614.
Lean, J., 2006: Comment on "Estimated solar contribution to the global surface warming using the ACRIM TSI satellite composite" by N. Scafetta and B. J. West. *Geophys. Res. Lett.* doi:ARTN L15701, 10.1029/2005GL025342, -.
Lean, J., and D. Rind, 2008: How natural and anthropogenic influences alter global and regional surface temperatures: 1889 to 2006. *Geophys. Res. Lett.* doi:ARTN L18701, 10.1029/2008GL034864, -.

Lean, J. L., and D. H. Rind, 2009: How will Earth's surface temperature change in future decades? *Geophys. Res. Lett.*, **36**.
Ledoit, O., and M. Wolf, 2004: A well-conditioned estimator for large-dimensional covariance matrices. *Journal of Multivariate Analysis*. doi:DOI 10.1016/S0047-259X(03)00096-4, 365-411.
Lefebvre, W., and H. Goosse, 2008: An analysis of the atmospheric processes driving the large-scale winter sea ice variability in the Southern Ocean. *Journal of Geophysical Research-Oceans*, **113**, -.
Legras, B., O. Mestre, E. Bard, and P. Yiou, 2010: A critical look at solar-climate relationships from long temperature series. *Clim. Past.*, **6**, 745-758.
Leibensperger, E., et al., 2012: Climatic effects of 1950-2050 changes in US anthropogenic aerosols - Part 1: Aerosol trends and radiative forcing. *Atmospheric Chemistry and Physics*, **12**, 3333-3348.
Levitus, S., J. Antonov, T. Boyer, R. Locarnini, H. Garcia, and A. Mishonov, 2009: Global ocean heat content 1955-2008 in light of recently revealed instrumentation problems. *Geophys. Res. Lett.*, **36**, -.
Lewis, N., 2012: Improved methodology for applying optimal fingerprint techniques to estimate climate sensitivity. *Journal of Climate*.
Li, J., and J. Wang, 2003: A modified zonal index and its physical sense. *Geophys. Res. Lett.*, **30**.
Libardoni, A. G., and C. E. Forest, 2011: Sensitivity of distributions of climate system properties to the surface temperature dataset, **38** L22705.
Liebmann, B., R. M. Dole, C. Jones, I. Blade, and D. Allured, 2010: INFLUENCE OF CHOICE OF TIME PERIOD ON GLOBAL SURFACE TEMPERATURE TREND ESTIMATES. *Bulletin of the American Meteorological Society*, **91**, 1485-U1471.
Lin, B., et al., 2010a: Estimations of climate sensitivity based on top-of-atmosphere radiation imbalance. *Atmospheric Chemistry and Physics*, **10**, 1923-1930.
Lin, P., Q. A. Fu, S. Solomon, and J. M. Wallace, 2010b: Temperature Trend Patterns in Southern Hemisphere High Latitudes: Novel Indicators of Stratospheric Change (vol 22, pg 6325, 2009). *Journal of Climate*, **23**, 4263-4280.
Lindzen, R., and Y. Choi, 2009: On the determination of climate feedbacks from ERBE data. *Geophys. Res. Lett.* doi:ARTN L16705, 10.1029/2009GL039628, -.
——, 2011: On the observational determination of climate sensitivity and its implications. *Asia-Pacific Journal of Atmospheric Sciences*, **47**, 377-390.
Liu, C., R. P. Allan, and G. J. Huffman, 2012: Co-variation of temperature and precipitation in CMIP5 models and satellite observations. *Geophys. Res. Lett.*, **39**.
Liu, J., and J. Curry, 2010: Accelerated warming of the Southern Ocean and its impacts on the hydrological cycle and sea ice. *Proceedings of the National Academy of Sciences of the United States of America*, **107**, 14987-14992.
Lockwood, M., 2008: Recent changes in solar outputs and the global mean surface temperature. III. Analysis of contributions to global mean air surface temperature rise. *Proc. R. Soc. A-Math. Phys. Eng. Sci.*, **464**, 1387-1404.
——, 2012: Solar Influence on Global and Regional Climates. *Surveys in Geophysics*, **33**, 503-534.
Loeb, N., et al., 2012: Observed changes in top-of-the-atmosphere radiation and upper-ocean heating consistent within uncertainty. *Nature Geoscience*, **5**, 110-113.
Loehle, C., and N. Scaffetta, 2011: Climate change attribution using empirical decomposition of climatic data. *The Open Atmospheric Science Journal*, **5**, 74-86.
Lorenz, A., B. J. Todd, N. Bowerman, D. Frame, and M. R. Allen, 2012: Climate System Properties determining the Social Cost of Emissions. *Nature Climate Change*, **submitted**.
Lott, F. C., et al., 2012: Models versus Radiosondes in the Free Atmosphere: A New Detection And Attribution Analysis of Temperature. *J. Geophys. Res.*, submitted.
Lu, J., G. A. Vecchi, and T. Reichler, 2007: Expansion of the Hadley cell under global warming. *Geophys. Res. Lett.*, **34**.
Lu, J., C. Deser, and T. Reichler, 2009: Cause of the widening of the tropical belt since 1958. *Geophys. Res. Lett.*, **36**.
Lunt, D., A. Haywood, G. Schmidt, U. Salzmann, P. Valdes, and H. Dowsett, 2010: Earth system sensitivity inferred from Pliocene modelling and data. *Nature Geoscience*. doi:DOI 10.1038/NGEO706, 60-64.
Luterbacher, J., D. Dietrich, E. Xoplaki, M. Grosjean, and H. Wanner, 2004: European Seasonal and Annual Temperature Variability, Trend, and Extremes Since 1500. *Science*, **303**, 5.
MacDonald, G., 2010: Water, climate change, and sustainability in the southwest. *Proceedings of the National Academy of Science*, **107**, 21256-21262.
MacFarling Meure, C., et al., 2006: Law Dome CO(2), CH(4) and N(2)O ice core records extended to 2000 years BP. *Geophys. Res. Lett.*, **33**.
Mahlstein, I., and R. Knutti, 2011 [Submitted]: September Arctic sea ice predicted to disappear for 2oC global warming above present. Journal of Geophysical Research.
Mahlstein, I., R. Knutti, S. Solomon, and R. W. Portmann, 2011: Early onset of significant local warming in low latitude countries. *Environmental Research Letters*, **6**.
Mankoff K.D., Jacobs, S. S., Tulaczyk, S. M., and Stammerjohn, S. E., 2012: The role of Pine Island Glacier ice shelf basal channels in deep water upwelling, polynyas and ocean circulation in Pine Island Bay, Antarctica. *Annals of Glaciology*, **53**, 123-128
Mann, M., J. Fuentes, and S. Rutherford, 2012: Underestimation of volcanic cooling in tree-ring-based reconstructions of hemispheric temperatures. *Nature Geoscience*, **5**, 202-205.

Mann, M., Z. Zhang, M. Hughes, R. Bradley, S. Miller, S. Rutherford, and F. Ni, 2008: Proxy-based reconstructions of hemispheric and global surface temperature variations over the past two millennia. *Proceedings of the National Academy of Sciences of the United States of America*. doi:DOI 10.1073/pnas.0805721105, 13252-13257.

Mann, M., et al., 2009: Global Signatures and Dynamical Origins of the Little Ice Age and Medieval Climate Anomaly. *Science*. doi:DOI 10.1126/science.1177303, 1256-1260.

Mann, M. E., and K. A. Emanuel, 2006a: *Atlantic hurricane trends linked to climate change*. *Eos, Transactions American Geophysical Union*, **87**, 233-238.

Mann, M. E., and K. A. Emanuel, 2006b: Atlantic hurricane trends linked to climate change. *Eos Transactions*, **87(24)**, 233-241.

Manning, A., and R. Keeling, 2006: Global oceanic and land biotic carbon sinks from the Scripps atmospheric oxygen flask sampling network. *Tellus Series B-Chemical and Physical Meteorology*, **58**, 95-116.

Mariotti, A., 2010: Recent Changes in the Mediterranean Water Cycle: A Pathway toward Long-Term Regional Hydroclimatic Change? *Journal of Climate*, **23**, 1513-1525.

Marshall, G., 2003: Trends in the southern annular mode from observations and reanalyses. *Journal of Climate*, **16**, 4134-4143.

Maslanik, J., C. Fowler, J. Stroeve, S. Drobot, J. Zwally, D. Yi, and W. Emery, 2007: A younger, thinner Arctic ice cover: Increased potential for rapid, extensive sea-ice loss. *Geophys. Res. Lett.* doi:ARTN L24501, 10.1029/2007GL032043, -.

Maslowski, W., et al., 2012: The future of Arctic sea ice. *Annu. Rev. Earth Planet Sci.*, **40**, 625-654.

Massey, N., T. Anna, Rye C., F. E. L. Otto, S. Wilson, R. G. Jones, and M. R. Allen, 2012: HAVE THE ODDS OF WARM NOVEMBER TEMPERATURES AND OF COLD DECEMBER TEMPERATURES IN CENTRAL ENGLAND CHANGED? , *Bull. Amer. Meteor. Soc.*,.

Massonnet, T., et al., 2012: The trends in summer Arctic sea ice extent are nonlinearly related to the mean sea ice state in CMIP5 models. *The Crysopshere*, **In Review**.

Mastrandrea, M. D., et al., 2011: Guidance Note for Lead Authors of the IPCC Fifth Assessment Report on Consistent Treatment of Uncertainties. Intergovernmental Panel on Climate Change (IPCC).

Matear, R., and A. Hirst, 2003: Long-term changes in dissolved oxygen concentrations in the ocean caused by protracted global warming. *Global Biogeochemical Cycles*. doi:ARTN 1125, 10.1029/2002GB001997, -.

Matear, R. J., A. C. Hirst, and B. I. McNeil, 2000: Changes in dissolved oxygen in the Southern Ocean with climate change. *Geochemistry, Geophysics, Geosystems. An electronic journal of the Earth Sciences*, **1**, 12.

Matthews, H., N. Gillett, P. Stott, and K. Zickfeld, 2009: The proportionality of global warming to cumulative carbon emissions. *Nature*, **459**, 829-U823.

Mazzarella, A., and N. Scafetta, 2012: Evidences for a quasi 60-year North Atlantic Oscillation since 1700 and its meaning for global climate change. *Theoretical and Applied Climatology*, **107**, 599-609.

McKitrick, R., and L. Tole, 2012: Evaluating explanatory models of the spatial pattern of surface climate trends using model selection and Bayesian averaging methods. *Climate Dynamics*. doi:DOI 10.1007/s00382-012-1418-9.

McKitrick, R., S. McIntyre, and C. Herman, 2010: Panel and multivariate methods for tests of trend equivalence in climate data series. *Atmospheric Science Letters*, **11**, 270-277.

McLandress, C., T. Shepherd, J. Scinocca, D. Plummer, M. Sigmond, A. Jonsson, and M. Reader, 2011: Separating the Dynamical Effects of Climate Change and Ozone Depletion. Part II Southern Hemisphere Troposphere. *Journal of Climate*, **24**, 1850-1868.

Mecking, S., M. Warner, and J. Bullister, 2006: Temporal changes in pCFC-12 ages and AOU along two hydrographic sections in the eastern subtropical North Pacific. *Deep-Sea Research Part I-Oceanographic Research Papers*. doi:DOI 10.1016/j.dsr.2005.06.018, 169-187.

Meehl, G. A., J. M. Arblaster, and C. Tebaldi, 2007a: Contributions of natural and anthropogenic forcing to changes in temperature extremes over the U.S. *Geophys. Res. Lett.*, **34**.

Meehl, G. A., J. M. Arblaster, J. T. Fasullo, A. Hu, and K. E. Trenberth, 2011: Model-based evidence of deep-ocean heat uptake during surface-temperature hiatus periods 360-364.

Meehl, G. A., A. Hu, J. Arblaster, J. Fasullo, and K. E. Trenberth, 2012: Externally forced and internally generated 6 decadal climate variability associated with the Interdecadal Pacific Oscillation. *J. Climate*.

Meehl, G. A., et al., 2007b: Global Climate Projections. *Climate Change 2007: The Physical Science Basis. Contribution of Working Group I to the Fourth Assessment Report of the Intergovernmental Panel on Climate Change*, Cambridge University Press.

Meinshausen, M., et al., 2009: Greenhouse-gas emission targets for limiting global warming to 2 degrees C. *Nature*, **458**, 1158-U1196.

Mernild, S. H., E. Hanna, J. C. Yde, J. Cappelen, and M. J. K., *2012*: Extreme Greenland air temperatures in a warming climate,1890-2010, and impacts on Greenland ice sheet surface mass balance. *J. Geophys. Res.,*, **submitted**.

Merrifield, M., and M. Maltrud, 2011: Regional sea level trends due to a Pacific trade wind intensification. *Geophys. Res. Lett.*, **38**, L21605.

Miller, G., R. Alley, J. Brigham-Grette, J. Fitzpatrick, L. Polyak, M. Serreze, and J. White, 2010: Arctic amplification: can the past constrain the future? *Quaternary Science Reviews*. doi:DOI 10.1016/j.quascirev.2010.02.008, 1779-1790.

Miller, G., et al., 2012: Abrupt onset of the Little Ice Age triggered by volcanism and sustained by sea-ice/ocean feedbacks. *Geophys. Res. Lett.*, **39**.
Miller, R. L., G. A. Schmidt, and D. T. Shindell, 2006: Forced annular variations in the 20th century intergovernmental panel on climate change fourth assessment report models. *Journal of Geophysical Research-Atmospheres*, **111**.
Min, S.-K., and S.-W. Son, 2012: Multi-model attribution of the Southern Hemisphere Hadley cell widening: CMIP3 and CMIP5 models. *J. Geophys. Res.*, submitted.
Min, S.-K., X. Zhang, F. W. Zwiers, and G. C. Hegerl, 2011: **Human contribution to more intense precipitation extremes**. *Nature*, **470**, 378-381.
Min, S.-K., X. Zhang, F. Zwiers, H. Shiogama, Y.-S. Tung, and M. Wehner, 2012: Multi-model detection and attribution of extreme temperature changes. *Journal of Climate*.
Min, S., and A. Hense, 2006: A Bayesian assessment of climate change using multimodel ensembles. Part I: Global mean surface temperature. *Journal of Climate*, **19**, 3237-3256.
Min, S., X. Zhang, and F. Zwiers, 2008a: Human-induced arctic moistening. *Science*, **320**, 518-520.
——, 2008b: Human-induced arctic moistening. *Science*. doi:DOI 10.1126/science.1153468, 518-520.
Min, S., X. Zhang, F. Zwiers, and T. Agnew, 2008c: Human influence on Arctic sea ice detectable from early 1990s onwards. *Geophys. Res. Lett.* doi:ARTN L21701, 10.1029/2008GL035725, -.
Min, S. K., and A. Hense, 2007: A Bayesian assessment of climate change using multimodel ensembles. Part II: Regional and seasonal mean surface temperatures. *Journal of Climate*, **20**, 2769-2790.
Mitchell, D. M., P. A. Stott, L. J. Gray, F. C. Lott, N. Butchart, S. C. Hardiman, and S. M. Osprey, 2012a: The Impact of Stratospheric Resolution on the Detectability of Climate Change Signals in the Free Atmosphere.
Mitchell, J. F. B., P. A. Stott, G. S. Jones, and M. R. Allen, 2012b: Are climate predictions falsifiable ? *Geophys. Res. Lett.*
Moberg, A., D. Sonechkin, K. Holmgren, N. Datsenko, and W. Karlen, 2005: Highly variable Northern Hemisphere temperatures reconstructed from low- and high-resolution proxy data. *Nature*, **433**, 613-617.
Molg, T., and G. Kaser, 2011: Unifying large-scale atmospheric dynamics and glacier scale mass balance without the need for scale bridging. *Geophysical Research*, **13**.
Molg, T., N. Cullen, D. Hardy, M. Winkler, and G. Kaser, 2009: Quantifying Climate Change in the Tropical Midtroposphere over East Africa from Glacier Shrinkage on Kilimanjaro. *Journal of Climate*. doi:DOI 10.1175/2009JCLI2954.1, 4162-4181.
Mölg, T., M. Großhauser, A. Hemp, M. Hofer, and B. Marzeion, 2011: Is there additional forcing of mountain glacier loss through land cover change? *Nature*, **Submitted**.
Morak, S., G. C. Hegerl, and J. Kenyon, 2011a: Detectable regional changes in the number of warm nights. *Geophysical Research Letters*, **38**.
——, 2011b: Detectable regional changes in the number of warm nights. *(submitted)*.
Morak, S., G. C. Hegerl, and N. Christidis, 2012: Detectable changes in the frequency of temperature extremes. *Journal of Climate*.
Morgenstern, O., et al., 2010: Anthropogenic forcing of the Northern Annular Mode in CCMVal-2 models. *Journal of Geophysical Research-Atmospheres*, **115**.
Morice, C., J. Kennedy, N. Rayner, and P. Jones, 2012: Quantifying uncertainties in global and regional temperature change using an ensemble of observational estimates: The HadCRUT4 data set. *Journal of Geophysical Research-Atmospheres*, **117**.
Morice, C. P., J. J. Kennedy, N. A. Rayner, and P. D. Jones, 2011: Quantifying uncertainties in global and regional temperature change using an ensemble of observational estimates: the HadCRUT4 dataset. *Journal of Geophysical Research*. submitted.
Murphy, D., and P. Forster, 2010: On the Accuracy of Deriving Climate Feedback Parameters from Correlations between Surface Temperature and Outgoing Radiation. *Journal of Climate*. doi:DOI 10.1175/2010JCLI3657.1, 4983-4988.
Murphy, D., S. Solomon, R. Portmann, K. Rosenlof, P. Forster, and T. Wong, 2009: An observationally based energy balance for the Earth since 1950. *Journal of Geophysical Research-Atmospheres*. doi:ARTN D17107, 10.1029/2009JD012105, -.
Nagato, Y., and H. L. Tanaka, 2012: Global warming trend without the contribution from decadal variability of the Arctic oscillation. *Polar Science*, **6**, 15-22.
Nakanowatari, T., K. Ohshima, and M. Wakatsuchi, 2007: Warming and oxygen decrease of intermediate water in the northwestern North Pacific, originating from the Sea of Okhotsk, 1955-2004. *Geophys. Res. Lett.* doi:ARTN L04602, 10.1029/2006GL028243, -.
Nesje, A., O. Lie, and S. Dahl, 2000: Is the North Atlantic Oscillation reflected in Scandinavian glacier mass balance records? *Journal of Quaternary Science*. 587-601.
Nghiem, S., I. Rigor, D. Perovich, P. Clemente-Colon, J. Weatherly, and G. Neumann, 2007: Rapid reduction of Arctic perennial sea ice. *Geophys. Res. Lett.* doi:ARTN L19504, 10.1029/2007GL031138, -.
Noake, K., D. Polson, G. Hegerl, and X. Zhang, 2011: Changes in seasonal precipitation during the 20th Century. *Geophys. Res. Lett.*, **submitted for publication**.
——, 2012: Changes in seasonal land precipitation during the latter 20th Century. *Geophys. Res. Lett.*, **39**.

North, G., and M. Stevens, 1998: Detecting climate signals in the surface temperature record. *Journal of Climate*. 563-577.
Notz, D., and J. Marotzke, 2012: Observations reveal external driver for Arctic sea-ice retreat. *Geophys. Res. Lett.,*, **39**, L08502, doi:08510.01029/02012GL051094.
O'Gorman, P. A., and T. Schneider, 2008: Energy of Midlatitude Transient Eddies in Idealized Simulations of Changed Climates. *Journal of Climate*, **21(22)**, 5797-5806.
——, 2009a: The physical basis for increases in precipitation extremes in simulations of 21st-century climate change. *Proceedings of the National Academy of Sciences of the Unied States of America*, **106(35)**, 14773-14777.
——, 2009b: Scaling of Precipitation Extremes over a Wide Range of Climates Simulated with an Idealized GCM. *Journal of Climate*, **22(21)**, 5676-5685.
O'Gorman, P. A., 2011: Understanding the varied response of the extratropical storm tracks to climate change. *Proceedings of the National Academy of Sciences*. doi:10.1073/pnas.1011547107.
Oerlemans, J., 2005: Extracting a climate signal from 169 glacier records. *Science*, **308**, 675-677.
Olson, R., R. Sriver, M. Goes, N. Urban, H. Matthews, M. Haran, and K. Keller, 2012: A climate sensitivity estimate using Bayesian fusion of instrumental observations and an Earth System model. *Journal of Geophysical Research-Atmospheres*, **117**.
Ono, T., T. Midorikawa, Y. Watanabe, K. Tadokoro, and T. Saino, 2001: Temporal increases of phosphate and apparent oxygen utilization in the subsurface waters of western subarctic Pacific from 1968 to 1998. *Geophys. Res. Lett.*, 3285-3288.
Osterkamp, T. E., 2005: The recent warming of permafrost in Alaska. *Global and Planetary Change*, **49**, 187-202.
Otto-Bliesner, B., et al., 2009: A comparison of PMIP2 model simulations and the MARGO proxy reconstruction for tropical sea surface temperatures at last glacial maximum. *Climate Dynamics*. doi:DOI 10.1007/s00382-008-0509-0, 799-815.
Otto, F. E. L., N. Massey, G. J. van Oldenborgh, R. G. Jones, and M. R. Allen, 2012: Reconciling two approaches to attribution of the 2010 Russian heat wave. *Geophys. Res. Lett.*, **39**.
Overland, J., 2009: The case for global warming in the Arctic. *Influence of Climate Change on the Changing Arctic and Sub-Arctic Conditions*. 13-23.
Overland, J., and M. Wang, 2005: The Arctic climate paradox: The recent decrease of the Arctic Oscillation. *Geophys. Res. Lett.* doi:ARTN L06701, 10.1029/2004GL021752, -.
Overland, J., M. Wang, and S. Salo, 2008: The recent Arctic warm period. *Tellus Series a-Dynamic Meteorology and Oceanography*. doi:DOI 10.1111/j.1600-0870.2008.00327.x, 589-597.
Overland, J. E., K. R. Wood, and M. Wang, 2011 [in press]: Warm Arctic-Cold Continents: Impact of the newley open Arctic Sea., Polar Res.
Overland, J. E., J. A. Francis, E. Hanna, and Wang M., 2012: The Recent Shift in Early Summer Arctic Atmospheric Circulation. *Geophys Res. Lett.,*, **submitted**.
Padilla, L., G. Vallis, and C. Rowley, 2011: Probabilistic Estimates of Transient Climate Sensitivity Subject to Uncertainty in Forcing and Natural Variability. *Journal of Climate*, **24**, 5521-5537.
Pagani, M., K. Caldeira, R. Berner, and D. Beerling, 2009: The role of terrestrial plants in limiting atmospheric CO2 decline over the past 24 million years. *Nature*. doi:DOI 10.1038/nature08133, 85-U94.
Palastanga, V., G. van der Schrier, S. L. Weber, T. Kleinen, K. R. Briffa, and T. J. Osborn, 2011: Atmosphere and ocean dynamics: contributors to the Little Ice Age and Medieval Climate Anomaly. 973-987.
Paleosens Members (E.J. Rohling*, A. S., H.A. Dijkstra, P. Köhler,, and A. S. v. d. H. e. a. R.S.W. van de Wal, 2012: Making sense of palaeoclimate sensitivity. *Nature*, **in review**.
Pall, P., A. M. R., and D. A. Stone, 2007: Testing the Clausius-Clapeyron constraint on changes in extreme precipitation under CO_2 warming. *Climate Dynamics*, **28**, 353-361.
Pall, P., et al., 2011: Anthropogenic greenhouse gas contribution to <country-region>UK</country-region> autumn flood risk. *Nature*. doi:doi:10.1038/nature09762.
Palmer, M. D., S. A. Good, K. Haines, N. A. Rayner, and P. A. Stott, 2009: A new perspective on warming of the global oceans. *Geophys. Res. Lett.*, **36**, L20709.
Palmer, T., 1999: A nonlinear dynamical perspective on climate prediction. *Journal of Climate*. 575-591.
Pavlov, A. V., and V. G. Malkova, 2010: Dynamics of permafrost zone of Russia under changing climate conditions. *Izvestiya, Ser. Geogr.*, **5**, 44-51.
Pavlova, T. V., V. M. Kattsov, E. D. Nadyozhina, P. V. Sporyshev, and V. A. Govorkova, 2007: Terrestrial cryosphere evolution through the 20th and 21st centuries as simulated with the new generation of global climate models. *Kriosfera Zemli (Earth Cryosphere)*, **11**, 3-13 (in Russian).
Penner, J., M. Wang, A. Kumar, L. Rotstayn, and B. Santer, 2007: Effect of black carbon on mid-troposphere and surface temperature trends. *Human-Induced Climate Change: An Interdisciplinary Assessment*, M. Schlesinger, et al., Ed., 18-33.
Perlwitz, J., M. Hoerling, J. Eischeid, T. Xu, and A. Kumar, 2009: A strong bout of natural cooling in 2008. *Geophys. Res. Lett.*, **36**.
Petersen, T. C., P. A. Stott, and S. Herring, 2012: Explaining Extreme Events of 2011 from a Climate Perspective. *Bull. Amer. Meteor. Soc.*, **93**, 1041–1067.

Pierce, D., T. Barnett, K. AchutaRao, P. Gleckler, J. Gregory, and W. Washington, 2006a: Anthropogenic Warming of the Oceans: Observations and Model Results. *Journal of Climate*, **19**, 1873-1900.

Pierce, D. W., and e. al, 2008: Attribution of declining Western US Snowpack to Human effects. *American Meteorological Society*. doi:10.1175/2008JCLI2405.1, 20.

Pierce, D. W., T. P. Barnett, E. J. Fetzer, and P. J. Gleckler, 2006b: Three-dimensional tropospheric water vapor in coupled climate models compared with observations from the AIRS satellite system. *Geophys. Res. Lett.*, **33**.

Pierce, D. W., T. P. Barnett, B. D. Santer, and P. J. Gleckler, 2009: Selecting global climate models for regional climate change studies. *Proceedings of the National Academy of Sciences of the United States of America*, **106**, 8441-8446.

Pierce, D. W., P. J. Gleckler, T. P. Barnett, B. D. Santer, and P. Durack, 2012: The fingerprint of human-induced changes in the ocean's salinity and temperature fields. *Geophys. Res. Lett.,*, **(Submitted)**.

Pierce, D. W., et al., 2008: Attribution of Declining Western U.S. Snowpack to Human Effects. *Journal of Climate*, **21**, 6425-6444.

Pitman, A. J., and et al., 2009: Uncertainties in climate responses to past land cover change: first results from the LUCID intercomparison study. *Geophys. Res. Lett.*, **36(L14814)**.

Plattner, G. K., F. Joos, and T. F. Stocker, 2002: Revision of the global carbon budget due to changing air-sea oxygen fluxes. *Global Biogeochemical Cycles*, **16**, 12.

Polson, D., G. C. Hegerl, X. Zhang, and T. J. Osborn, 2012: Causes of robust seasonal land precipitation changes. *Journal of Climate*, **submitted for publication**.

Polvani, L. M., D. W. Waugh, G. J. P. Correa, and S.-W. Son, 2010: Stratospheric ozone depletion: the main driver of 20th Century atmospheric circulation changes in the Southern Hemisphere. *Journal of Climate*. doi:10.1175/2010jcli3772.1.

Polvani, L. M., D. W. Waugh, G. J. P. Correa, and S. W. Son, 2011: Stratospheric Ozone Depletion: The Main Driver of Twentieth-Century Atmospheric Circulation Changes in the Southern Hemisphere. *Journal of Climate*, **24**, 795-812.

Polyakov, I., J. Walsh, and R. Kwok, 2012: Recent Changes of Arctic Multiyear Sea Ice Coverage and the Likely Causes. *Bulletin of the American Meteorological Society*, **93**, 145-151.

Polyakov, I., U. Bhatt, H. Simmons, D. Walsh, J. Walsh, and X. Zhang, 2005: Multidecadal variability of North Atlantic temperature and salinity during the twentieth century. *Journal of Climate*. 4562-4581.

Polyakov, I., et al., 2003: Variability and trends of air temperature and pressure in the maritime Arctic, 1875-2000. *Journal of Climate*. 2067-2077.

Pongratz, J., C. Reick, T. Raddatz, and M. Claussen, 2008: A reconstruction of global agricultural areas and land cover for the last millennium. *Global Biogeochemical Cycles*, **22**.

Pongratz, J., C. Reick, T. Raddatz, and M. Claussen, 2009: Effects of anthropogenic land cover change on the carbon cycle of the last millennium. *Global Biogeochemical Cycles*. doi:ARTN GB4001, 10.1029/2009GB003488, -.

Pritchard, H. D., et al., 2012: Antarctic ice sheet loss driven by basal melting of ice shelves. *Nature*, **484**, 502-505.

Quadrelli, R., and J. Wallace, 2004: A simplified linear framework for interpreting patterns of Northern Hemisphere wintertime climate variability. *Journal of Climate*. 3728-3744.

Rahmstorf, S., and D. Coumou, 2011: Increase of extreme events in a warming world. *Proceedings of the National Academy of Sciences of the United States of America*, **108**, 17905-17909.

Ramaswamy, V., M. D. Schwarzkopf, W. J. Randel, B. D. Santer, B. J. Soden, and G. L. Stenchikov, 2006: Anthropogenic and natural influences in the evolution of lower stratospheric cooling. *Science*, **311**, 1138-1141.

Rampal, P., J. Weiss, C. Dubois, and J. Campin, 2011: IPCC climate models do not capture Arctic sea ice drift acceleration: Consequences in terms of projected sea ice thinning and decline. *Journal of Geophysical Research-Oceans*, **116**, -.

Ramsay, H. A., and A. H. Sobel, 2011: The effects of relative and absolute sea surface temperature on tropical cyclone potential intensity using a single column model. *Journal of Climate, (in press)*.

Randel, W. J., F. Wu, H. V˙mel, G. E. Nedoluha, and P. Forster, 2006: Decreases in stratospheric water vapor after 2001: Links to changes in the tropical tropopause and the Brewer-Dobson circulation. *J. Geophys. Res.*, **111**, D12312.

Randel, W. J., et al., 2009: An update of observed stratospheric temperature trends. *Journal of Geophysical Research-Atmospheres*, **114**, 21.

Ray, E., et al., 2010: Evidence for changes in stratospheric transport and mixing over the past three decades based on multiple data sets and tropical leaky pipe analysis. *Journal of Geophysical Research-Atmospheres*, **115**, -.

Reichert, B., L. Bengtsson, and J. Oerlemans, 2002a: Recent glacier retreat exceeds internal variability. *Journal of Climate*. 3069-3081.

——, 2002b: Recent glacier retreat exceeds internal variability. *Journal of Climate*, **15**, 3069-3081.

Ribes, A., and L. Terray, 2012: Regularised optimal fingerprint analysis for attribution. Part II: application to global near-surface temperature based on CMIP5 simulations.

Ribes, A., J. M. Azais, and S. Planton, 2009: Adaptation of the optimal fingerprint method for climate change detection using a well-conditioned covariance matrix estimate. *Climate Dynamics*, **33**, 707-722.

——, 2010: A method for regional climate change detection using smooth temporal patterns. *Climate Dynamics*, **35**, 391-406.

Ribes, A., S. Planton, and L. Terray, 2012: Regularised optimal fingerprint for attribution. Part I: method, properties and idealised analysis. *Clim Dyn*.
Roe, G., and M. Baker, 2007: Why is climate sensitivity so unpredictable? *Science*. doi:DOI 10.1126/science.1144735, 629-632.
Roe, G., and M. O'Neal, 2009: The response of glaciers to intrinsic climate variability: observations and models of late-Holocene variations in the Pacific Northwest. *Journal of Glaciology*. 839-854.
Roemmich, D., and J. Gilson, 2009: The 2004-2008 mean and annual cycle of temperature, salinity, and steric height in the global ocean from the Argo Program. *Progress in Oceanography*. doi:DOI 10.1016/j.pocean.2009.03.004, 81-100.
Roesch, A., 2006: Evaluation of surface albedo and snow cover in AR4 coupled climate models. *J. Geophys. Res.*, **111**, doi:10.1029/2005JD006473.
Rohde, R., et al., 2012: A New Estimate of the Average Earth Surface Land Temperature Spanning 1753 to 2011. *J. Geophys. Res.*
Roscoe, H. K., and J. D. Haigh, 2007: Influences of ozone depletion, the solar cycle and the QBO on the Southern Annular Mode. *Quarterly Journal of the Royal Meteorological Society*, **133**, 1855-1864.
Rosenlof, K. H., and G. C. Reid, 2008: Trends in the temperature and water vapor content of the tropical lower stratosphere: Sea surface connection. *Journal of Geophysical Research-Atmospheres*, **113**.
Royer, D., 2008: Linkages between CO2, climate, and evolution in deep time. *Proceedings of the National Academy of Sciences of the United States of America*. doi:DOI 10.1073/pnas.0710915105, 407-408.
Royer, D., R. Berner, and J. Park, 2007: Climate sensitivity constrained by CO2 concentrations over the past 420 million years. *Nature*. doi:DOI 10.1038/nature05699, 530-532.
Rupp, D. E., Mote P. W., N. L. Bindoff, P. A. Stott, and D. A. Robinson, 2012a: Detection and attribution of observed changes in Northern Hemisphere spring snow cover. *J. Climate*. submitted.
Rupp, D. E., P. W. Mote, N. Massey, J. R. Cameron, R. Jones, and M. R. Allen, 2012b: DID HUMAN INFLUENCE ON CLIMATE MAKE THE 2011 TEXAS DROUGHT MORE PROBABLE? , 1052-1054.
——, 2012c: DID HUMAN INFLUENCE ON CLIMATE MAKE THE 2011 TEXAS DROUGHT MORE PROBABLE? , 1052-1054.
Sanso, B., and C. Forest, 2009: Statistical calibration of climate system properties. *Journal of the Royal Statistical Society Series C-Applied Statistics*, **58**, 485-503.
Santer, B. D., et al., 2012: Identifying human influences on atmospheric temperature: are results robust to Uncertainties. *PNAS*. submitted.
Santer, B. D., and et al, 2006: Forced and unforced ocean temperature changes in Atlantic and Pacific tropical cyclogenesis regions. *Proceedings of the National Academy of Sciences*, **103(38)**, 13905-13910.
Santer, B. D., W. Bruggemann, U. Cubasch, K. Hasselmann, H. Hock, E. Maierreimer, and U. Mikolajewicz, 1994: SIGNAL-TO-NOISE ANALYSIS OF TIME-DEPENDENT GREENHOUSE WARMING EXPERIMENTS .1. PATTERN-ANALYSIS. *Climate Dynamics*, **9**, 267-285.
Santer, B. D., et al., 2009: Incorporating model quality information in climate change detection and attribution studies. *Proceedings of the National Academy of Sciences of the United States of America*, **106**, 14778-14783.
Santer, B. D., et al., 2007: Identification of human-induced changes in atmospheric moisture content. *Proceedings of the National Academy of Sciences of the United States of America*, **104**, 15248-15253.
Santer, B. D., et al., 2011: Separating signal and noise in atmospheric temperature changes: The importance of timescale. *Journal of Geophysical Research-Atmospheres*, **116**.
Scafetta, N., and B. West, 2007: Phenomenological reconstructions of the solar signature in the Northern Hemisphere surface temperature records since 1600. *Journal of Geophysical Research-Atmospheres*. doi:ARTN D24S03, 10.1029/2007JD008437, -.
Schär, C., P. L. Vidale, D. Lüthi, C. Frei, C. Häberl, M. A. Liniger, and C. Appenzeller, 2004: The role of increasing temperature variability in European summer heatwaves. *Nature*, **427**, 332-336.
SCHLESINGER, M., and N. RAMANKUTTY, 1994: AN OSCILLATION IN THE GLOBAL CLIMATE SYSTEM OF PERIOD 65-70 YEARS. *Nature*. 723-726.
Schmidt, G., et al., 2011: Climate forcing reconstructions for use in PMIP simulations of the last millennium (v1.0). *Geoscientific Model Development*, **4**, 33-45.
Schmidt, G., et al., 2012: Climate forcing reconstructions for use in PMIP simulations of the Last Millennium (v1.1). **5**, 185-191.
Schmittner, A., et al., 2011: Climate Sensitivity Estimated from Temperature Reconstructions of the Last Glacial Maximum. *Science*, **334**, 1385-1388.
Schneider, T., and I. Held, 2001: Discriminants of twentieth-century changes in earth surface temperatures. *Journal of Climate*. 249-254.
Schneider von Deimling, T., H. Held, A. Ganopolski, and S. Rahmstorf, 2006: Climate sensitivity estimated from ensemble simulations of glacial climate. *Climate Dynamics*. doi:DOI 10.1007/s00382-006-0126-8, 149-163.
Schnur, R., and K. Hasselmann, 2005: Optimal filtering for Bayesian detection and attribution of climate change. *Climate Dynamics*, **24**, 45-55.
Schonwiese, C., A. Walter, and S. Brinckmann, 2010: Statistical assessments of anthropogenic and natural global climate forcing. An update. *Meteorologische Zeitschrift*, **19**, 3-10.

Schubert, S., et al., 2009: A US CLIVAR Project to Assess and Compare the Responses of Global Climate Models to Drought-Related SST Forcing Patterns: Overview and Results. *Journal of Climate*, **22**, 5251-5272.
Schurer, A., G. Hegerl, M. Mann, S. F. B. Tett, and S. Phipps, 2012: Separating forced from chaotic climate variability over the last millennium. *Nature GeoScience* **submitted**.
Schwartz, S., 2007: Heat capacity, time constant, and sensitivity of Earth's climate system. *Journal of Geophysical Research-Atmospheres*. doi:ARTN D24S05, 10.1029/2007JD008746, -.
——, 2012: Determination of Earth's Transient and Equilibrium Climate Sensitivities from Observations Over the Twentieth Century: Strong Dependence on Assumed Forcing. *Surveys in Geophysics*, **33**, 745-777.
Schwartz, S., R. Charlson, R. Kahn, J. Ogren, and H. Rodhe, 2010: Why Hasn't Earth Warmed as Much as Expected? *Journal of Climate*. doi:DOI 10.1175/2009JCLI3461.1, 2453-2464.
Schwartz, S. E., R. J. Charlson, and H. Rodhe, 2007: Quantifying climate change — too rosy a picture? *Nature Reports Climate Change*, 23-24.
Schwarzkopf, M. D., and V. Ramaswamy, 2008: Evolution of stratospheric temperature in the 20th century. *Geophys. Res. Lett.*, **35**, 6.
Screen, J., and I. Simmonds, 2010: Increasing fall-winter energy loss from the Arctic Ocean and its role in Arctic temperature amplification. *Geophys. Res. Lett.* doi:ARTN L16707, 10.1029/2010GL044136, -.
Seager, R., N. Naik, and G. Vecchi, 2010: Thermodynamic and Dynamic Mechanisms for Large-Scale Changes in the Hydrological Cycle in Response to Global Warming. *Journal of Climate*. doi:DOI 10.1175/2010JCLI3655.1, 4651-4668.
Seager, R., Y. Kushnir, C. Herweijer, N. Naik, and J. Velez, 2005: Modeling of tropical forcing of persistent droughts and pluvials over western North America: 1856-2000. *Journal of Climate*, **18**, 4065-4088.
Sedlacek, J. R., O. Knutti, O. Martius, and U. Beyerle, 2011 [accepted- June 2011]: Impact of a reduced Arctic Sea-ice cover on ocean and atmospheric properties., Journal of Climate.
Sedlacek, K., and R. Knutti, 2012: Evidence for external forcing on 20th-century climate from combined ocean1 atmosphere warming patterns. *Geophys. Res. Lett.*
Seidel, D. J., and W. J. Randel, 2007: Recent widening of the tropical belt: Evidence from tropopause observations. *Journal of Geophysical Research-Atmospheres*, **112**.
Seidel, D. J., Q. Fu, W. J. Randel, and T. J. Reichler, 2008: Widening of the tropical belt in a changing climate. *Nature Geoscience*, **1**, 21-24.
Seidel, D. J., N. P. Gillett, J. R. Lanzante, K. P. Shine, and P. W. Thorne, 2011: Stratospheric temperature trends: Our evolving understanding. *Wiley Interdisciplinary Reviews: Climate Change*, **2**, 592-616.
Semenov, V., 2008: Influence of oceanic inflow to the Barents Sea on climate variability in the Arctic region. *Doklady Earth Sciences*. doi:DOI 10.1134/S1028334X08010200, 91-94.
Semmler, T., S. Varghese, R. McGrath, P. Nolan, S. L. Wang, P., and C. O'Dowd, 2008: Regional climate model simulations of NorthAtlantic cyclones: frequency and intensity changes. *Climate Research*, **36**.
Seneviratne, S. I., D. Luthi, M. Litschi, and C. Schar, 2006: Land-atmosphere coupling and climate change in Europe. *Nature*, **443**, 205-209.
Seneviratne, S. I., et al., 2010: Investigating soil moisture-climate interactions in a changing climate: A review. *Earth Science Reviews*, 125-161.
Seneviratne, S. I., et al., 2012: Chapter 3: Changes in climate extremes and their impacts on the natural physical environment. *IPCC-SREX (in preparation)*.
Serreze, M., and J. Francis, 2006: The arctic amplification debate. *Clim. Change*. doi:DOI 10.1007/s10584-005-9017-y, 241-264.
Serreze, M., M. Holland, and J. Stroeve, 2007: Perspectives on the Arctic's shrinking sea-ice cover. *Science*. doi:DOI 10.1126/science.1139426, 1533-1536.
Serreze, M., et al., 2000: Observational evidence of recent change in the northern high-latitude environment. *Clim. Change*. 159-207.
Serreze, M. C., A. P. Barrett, J. C. Stroeve, D. N. Kindig, and M. M. Holland, 2009: The emergence of surface-based Arctic amplification. *The Cryosphere*, **3**, 9.
Sheffield, J., and E. F. Wood, 2008: Global trends and variability in soil moisture and drought characteristics, 1950-2000, from observation-driven simulations of the terrestrial hydrologic cycle. *Journal of Climate*, **21**, 26.
Shindell, D., and G. Faluvegi, 2009: Climate response to regional radiative forcing during the twentieth century. *Nature Geoscience*, **2**, 294-300.
Shine, K., J. Fuglestvedt, K. Hailemariam, and N. Stuber, 2005: Alternatives to the global warming potential for comparing climate impacts of emissions of greenhouse gases. *Clim. Change*, **68**, 281-302.
Shiogama, H., T. Nagashima, T. Yokohata, S. Crooks, and T. Nozawa, 2006: Influence of volcanic activity and changes in solar irradiance on surface air temperatures in the early twentieth century. *Geophys. Res. Lett.* doi:ARTN L09702, 10.1029/2005GL025622, -.
Shiogama, H., D. A. Stone, T. Nagashima, T. Nozawa, and S. Emori, 2012: On the linear additivity of climate forcing-response relationships at global and continental scales. *International Journal of Climatology*, **Submitted**.
Sigmond, M., and J. Fyfe, 2010: Has the ozone hole contributed to increased Antarctic sea ice extent? *Geophys. Res. Lett.* doi:ARTN L18502, 10.1029/2010GL044301, -.

Sigmond, M., M. C. Reader, J. C. Fyfe, and N. P. Gillett, 2011: Drivers of past and future Southern Ocean change: Stratospheric ozone versus greenhouse gas impacts. *Geophys. Res. Lett.*, **38**.
Simmons, A. J., K. M. Willett, P. D. Jones, P. W. Thorne, and D. P. Dee, 2010: Low-frequency variations in surface atmospheric humidity, temperature, and precipitation: Inferences from reanalyses and monthly gridded observational data sets. *Journal of Geophysical Research-Atmospheres*, **115**.
Smirnov, D., and I. Mokhov, 2009: From Granger causality to long-term causality: Application to climatic data. *Physical Review E*. doi:ARTN 016208, 10.1103/PhysRevE.80.016208, -.
Smith, S., J. van Aardenne, Z. Klimont, R. Andres, A. Volke, and S. Arias, 2011: Anthropogenic sulfur dioxide emissions: 1850-2005. *Atmospheric Chemistry and Physics*, **11**, 1101-1116.
Sokolov, A., C. Forest, and P. Stone, 2010: Sensitivity of climate change projections to uncertainties in the estimates of observed changes in deep-ocean heat content. *Climate Dynamics*, **34**, 735-745.
Solomon, S., P. J. Young, and B. Hassler, 2012: Uncertainties in the evolution of stratospheric ozone and implications for recent temperature changes in the tropical lower stratosphere. *Geophys. Res. Lett.*, accepted.
Solomon, S., G. Plattner, R. Knutti, and P. Friedlingstein, 2009: Irreversible climate change due to carbon dioxide emissions. *Proceedings of the National Academy of Sciences of the United States of America*, **106**, 1704-1709.
Solomon, S., K. H. Rosenlof, R. W. Portmann, J. S. Daniel, S. M. Davis, T. J. Sanford, and G. K. Plattner, 2010: Contributions of Stratospheric Water Vapor to Decadal Changes in the Rate of Global Warming. *Science*, **327**, 1219-1223.
Solomon, S., et al., 2007: Technical Summary. *Climate Change 2007: The Physical Science Basis. Contribution of Working Group I to the Fourth Assessment Report of the Intergovernmental Panel on Climate Change*, Cambridge University Press.
Son, S. W., N. F. Tandon, L. M. Polvani, and D. W. Waugh, 2009: Ozone hole and Southern Hemisphere climate change. *Geophys. Res. Lett.*, **36**.
Son, S. W., et al., 2008: The impact of stratospheric ozone recovery on the Southern Hemisphere westerly jet. *Science*, **320**, 1486-1489.
Son, S. W., et al., 2010: Impact of stratospheric ozone on Southern Hemisphere circulation change: A multimodel assessment. *Journal of Geophysical Research-Atmospheres*, **115**.
Spencer, R., and W. Braswell, 2008: Potential Biases in Feedback Diagnosis from Observational Data: A Simple Model Demonstration. *Journal of Climate*, **21**, 5624-5628.
St Jacques, J. M., D. J. Sauchyn, and Y. Zhao, 2010: Northern Rocky Mountain streamflow records: Global warming trends, human impacts or natural variability? *Geophys. Res. Lett.*, **37**.
Stahl, K., et al., 2010: Streamflow trends in Europe: evidence from a dataset of near-natural catchments. *Hydrology and Earth System Sciences*, **14**, 2367-2382.
Staten, P. W., J. J. Rutz, T. Reichler, and J. Lu, 2011: Breaking down the tropospheric circulation response by forcing. *Clim. Dyn.*, DOI 10.1007/s00382-00011-01267-y.
Steig, E., D. Schneider, S. Rutherford, M. Mann, J. Comiso, and D. Shindell, 2009: Warming of the Antarctic ice-sheet surface since the 1957 International Geophysical Year (vol 457, pg 459, 2009). *Nature*. doi:DOI 10.1038/nature08286, 766-766.
Steinhilber, F., J. Beer, and C. Froehlich, 2009: Total solar irradiance during the Holocene. *Geophys. Res. Lett.*, **36**.
Stenchikov, G., T. Delworth, V. Ramaswamy, R. Stouffer, A. Wittenberg, and F. Zeng, 2009: Volcanic signals in oceans. *Journal of Geophysical Research-Atmospheres*, **114**, -.
Stephens, G., and Y. Hu, 2010: Are climate-related changes to the character of global-mean precipitation predictable? *Environmental Research Letters*, **5**, -.
Stephens, G. L., et al., 2010: Dreary state of precipitation in global models. *Journal of Geophysical Research-Atmospheres*, **115**.
Stern, D., 2006: An atmosphere-ocean time series model of global climate change. *Computational Statistics & Data Analysis*, **51**, 1330-1346.
Stone, D., and M. Allen, 2005a: Attribution of global surface warming without dynamical models. *Geophys. Res. Lett.* doi:ARTN L18711, 10.1029/2005GL023682, -.
Stone, D., M. Allen, P. Stott, P. Pall, S. Min, T. Nozawa, and S. Yukimoto, 2009: The Detection and Attribution of Human Influence on Climate. *Annual Review of Environment and Resources*. doi:DOI 10.1146/annurev.environ.040308.101032, 1-16.
Stone, D. A., and M. R. Allen, 2005b: The end-to-end attribution problem: From emissions to impacts. *Clim. Change*, **71**, 303-318.
Stott, P., and J. Kettleborough, 2002: Origins and estimates of uncertainty in predictions of twenty-first century temperature rise (vol 416, pg 723, 2002). *Nature*. 205-205.
Stott, P., and C. Forest, 2007: Ensemble climate predictions using climate models and observational constraints. *Philosophical Transactions of the Royal Society a-Mathematical Physical and Engineering Sciences*. doi:DOI 10.1098/rsta.2007.2075, 2029-2052.
Stott, P., D. Stone, and M. Allen, 2004a: Human contribution to the European heatwave of 2003. *Nature*. doi:DOI 10.1038/nature03089, 610-614.

Stott, P., C. Huntingford, C. Jones, and J. Kettleborough, 2008a: Observed climate change constrains the likelihood of extreme future global warming. *Tellus Series B-Chemical and Physical Meteorology*. doi:DOI 10.1111/j.1600-0889.2007.00329.x, 76-81.

Stott, P. A., and G. S. Jones, 2009: Variability of high latitude amplification of anthropogenic warming. *Geophys. Res. Lett.*, **36**, 6.

——, 2011: Observed 21st century temperatures further constrain decadal predictions of future warming. *Atmospheric Science Letters*.

Stott, P. A., D. A. Stone, and M. R. Allen, 2004b: Human contribution to the European heatwave of 2003. *Nature*, **432**, 610-614.

Stott, P. A., R. T. Sutton, and D. M. Smith, 2008b: Detection and attribution of Atlantic salinity changes. *Geophys. Res. Lett.*, **35**, 5.

Stott, P. A., G. S. Jones, N. Christidis, F. W. Zwiers, G. Hegerl, and H. Shiogama, 2011: Single-step attribution of increasing frequencies of very warm regional temperatures to human influence. *Atmospheric Science Letters*, **12**, 220-227.

Stott, P. A., J. F. B. Mitchell, M. R. Allen, T. L. Delworth, J. M. Gregory, G. A. Meehl, and B. D. Santer, 2006: Observational constraints on past attributable warming and predictions of future global warming. *Journal of Climate*, **19**, 3055-3069.

Stott, P. A., N. P. Gillett, G. C. Hegerl, D. J. Karoly, D. A. Stone, X. Zhang, and F. Zwiers, 2010: Detection and attribution of climate change: a regional perspective. *Wiley Interdisciplinary Reviews: Climate Change*, **1**, 192-211.

Stott, P. A., et al., 2012: Attribution of Weather and Climate-Related Events. J. Hurrell., Ed., revised.

Stramma, L., S. Schmidtko, L. Levin, and G. Johnson, 2010: Ocean oxygen minima expansions and their biological impacts. *Deep Sea Research Part I: Oceanographic Research Papers*, **57**, 587-595.

Stroeve, J., et al., 2012: Trends in Arctic Sea ice from CMIP3, Cmip5, and observations. *Geophys. Res. Lett.*, **in press**.

Stroeve, J., M. Holland, W. Meier, T. Scambos, and M. Serreze, 2007: Arctic sea ice decline: Faster than forecast. *Geophys. Res. Lett.* doi:ARTN L09501, 10.1029/2007GL029703, -.

Stroeve, J., et al., 2008: Arctic Sea ice extent plumments in 2007. EOS, Trans. Amer. Geophys. Union.

Stroeve, J. C., M. C. Serreze, M. M. Holland, J. E. Kay, W. Meier, and A. P. Barrett, 2011: The Arctic's rapidly shrinking sea ice cover: A research synthesis. Climate Change.

Sugiyama, M., H. Shiogama, and S. Emori, 2010: Precipitation extreme changes exceeding moisture content increases in MIROC and IPCC climate models. *Proceedings of the National Academy of Sciences of the <country-region>United States of America</country-region>*, **107(2)**, 571-575.

Swanson, K., G. Sugihara, and A. Tsonis, 2009: Long-term natural variability and 20th century climate change. *Proceedings of the National Academy of Sciences of the United States of America*, **106**, 16120-16123.

Tanaka, K., T. Raddatz, B. O'Neill, and C. Reick, 2009: Insufficient forcing uncertainty underestimates the risk of high climate sensitivity. *Geophys. Res. Lett.*, **36**, -.

Taylor, K.E. et al., 2011: An Overview of CMIP5 and the experiment design, *Bull Amer Meteor Soc*, doi:10.1175/BAMS-D-11-00094.1

Terray, L., L. Corre, S. Cravatte, T. Delcroix, G. Reverdin, and A. Ribes, 2011: Near-Surface Salinity as Nature's Rain Gauge to Detect Human Influence on the Tropical Water Cycle. *Journal of Climate*, **25**, 958-977.

Tett, S., et al., 2007: The impact of natural and anthropogenic forcings on climate and hydrology since 1550. *Climate Dynamics*. doi:DOI 10.1007/s00382-006-0165-1, 3-34.

Thompson, D., and S. Solomon, 2002: Interpretation of recent Southern Hemisphere climate change. *Science*. 895-899.

Thompson, D., J. Wallace, P. Jones, and J. Kennedy, 2009: Identifying Signatures of Natural Climate Variability in Time Series of Global-Mean Surface Temperature: Methodology and Insights. *Journal of Climate*. doi:DOI 10.1175/2009JCLI3089.1, 6120-6141.

Thompson, D. W. J., and S. Solomon, 2009: Understanding Recent Stratospheric Climate Change. *Journal of Climate*, **22**, 1934-1943.

Thorne, P.W., et al., 2005: Revisiting radiosonde upper air temperatures from 1958 to 2002. *J. Geophys. Res.*, **110**, D18105, doi:10.1029/2004JD005753.

Thorne, P. W., et al., 2011a: A quantification of uncertainties in historical tropical tropospheric temperature trends from radiosondes. *Journal of Geophysical Research-Atmospheres*, **116**, 19.

Thorne, P. W. et al., 2011b, Tropospheric temperature trends: History of an ongoing controversy. *WIRES: Climate Change*, **2**: 66-88.

Tietsche, S., D. Notz, J. Jungclaus, and J. Marotzke, 2011: Recovery mechanisms of Arctic summer sea ice. *Geophys. Res. Lett.*, **38**, -.

Timmermann, A., S. McGregor, and F. Jin, 2010: Wind Effects on Past and Future Regional Sea Level Trends in the Southern Indo-Pacific. *Journal of Climate*, **23**, 4429-4437.

Timmreck, C., S. Lorenz, T. Crowley, S. Kinne, T. Raddatz, M. Thomas, and J. Jungclaus, 2009: Limited temperature response to the very large AD 1258 volcanic eruption. *Geophys. Res. Lett.* doi:ARTN L21708, 10.1029/2009GL040083, -.

Ting, M., Y. Kushnir, R. Seager, and C. Li, 2009: Forced and Internal Twentieth-Century SST Trends in the North Atlantic. *Journal of Climate*. doi:DOI 10.1175/2008JCLI2561.1, 1469-1481.

Trenberth, K., 2011a: Attribution of climate variations and trends to human influences and natural variability. *Wiley Interdisciplinary Reviews: Climate Change*, **2**, 925-930.
——, 2011b: Attribution of climate variations and trends to human influences and natural variability.
Trenberth, K., J. Fasullo, and J. Kiehl, 2009: EARTH'S GLOBAL ENERGY BUDGET. *Bulletin of the American Meteorological Society*, **90**, 311-+.
Trenberth, K., J. Fasullo, C. O'Dell, and T. Wong, 2010: Relationships between tropical sea surface temperature and top-of-atmosphere radiation. *Geophys. Res. Lett.* doi:ARTN L03702, 10.1029/2009GL042314, -.
Trenberth, K. E., and D. J. Shea, 2006: Atlantic hurricanes and natural variability in 2005. *Geophys. Res. Lett.*, **33**.
Tung, K., J. Zhou, and C. Camp, 2008: Constraining model transient climate response using independent observations of solar-cycle forcing and response. *Geophys. Res. Lett.*, **35**, -.
Turner, J., and J. Overland, 2009: Contrasting climate change in the two polar regions. *Polar Research*. doi:DOI 10.1111/j.1751-8369.2009.00128.x, 146-164.
Turner, J., et al., 2005: Antarctic change during the last 50 years (vol 25, pg 279, 2005). *International Journal of Climatology*. doi:DOI 10.1002/joc.1212, 1147-1148.
Turner, J., et al., 2009: Non-annular atmospheric circulation change induced by stratospheric ozone depletion and its role in the recent increase of Antarctic sea ice extent. *Geophys. Res. Lett.* doi:ARTN L08502, 10.1029/2009GL037524, -.
Ummenhofer, C. C., et al., 2009: What causes southeast Australia's worst droughts? *Geophys. Res. Lett.*, **36**.
Uppala, S.M., et al., 2005: The ERA-40 re-analysis. *Quart J Roy Meteor Soc*, **131**, 2961-3012.
Urban, N., and K. Keller, 2009: Complementary observational constraints on climate sensitivity. *Geophys. Res. Lett.* doi:ARTN L04708, 10.1029/2008GL036457, -.
Utsumi, N., S. Seto, S. Kanae, E. E. Maeda, and T. Oki, 2011: Does higher surface temperature intensify extreme precipitation? *Geophys. Res. Lett.*, **38, L16708**.
van Oldenborgh, G. J., A. van Urk, and M. Allen, 2012: THE ABSENCE OF A ROLE OF CLIMATE CHANGE IN THE 2011 THAILAND FLOODS. 1047-1049.
Vavrus, S. J., M. M. Holland, A. Jahn, D. A. Bailey, and B. A. Blazey, 2011 [Submitted]: 21st Century Arctic climate change in CCSM4. J.Climate.
Vecchi, G. A., and B. J. Soden, 2007: Global Warming and the Weakening of the Tropical Circulation. *Journal of Climate*, **20**, 4316-4340.
Vecchi, G. A., K. L. Swanson, and B. J. Soden, 2008: Whither hurricane activity. *Science*, **322**.
Vernier, J., et al., 2011: Overshooting of clean tropospheric air in the tropical lower stratosphere as seen by the CALIPSO lidar. *Atmospheric Chemistry and Physics*, **11**, 9683-9696.
Veryard, H. G., 1963: A review of studies on climate fluctuations during the period of the meteorological. Changes of Climate: Proceedings of the Rome Symposium Organised by UNESCO and WMO, 3-15.
Vieira, L. E. A., S. K. Solanki, N. A. Krivova, and I. Usoskin, 2011: Evolution of the solar irradiance during the Holocene. *Astronomy & Astrophysics*, **531**.
Villarini, G., and G. A. Vecchi, 2012a: 21st Century Projections of North Atlantic Tropical Storms from CMIP5 Models. *Nature Climate Change*. doi:10:1038/NCLIMATE1530.
Villarini, G., and G. A. Vecchi, 2012b: Projected Increases in North Atlantic Tropical Cyclone Intensity from CMIP5 Models. *Journal of Climate*, **submitted**.
von Schuckmann, K., F. Gaillard, and P. Le Traon, 2009: Global hydrographic variability patterns during 2003-2008. *Journal of Geophysical Research-Oceans*. doi:ARTN C09007, 10.1029/2008JC005237, -.
Vorosmarty, C., L. Hinzman, and J. Pundsack, 2008: Introduction to special section on Changes in the Arctic Freshwater System: Identification, Attribution, and Impacts at Local and Global Scales. *Journal of Geophysical Research-Biogeosciences*. doi:ARTN G01S91, 10.1029/2007JG000615, -.
Vuille, M., G. Kaser, and I. Juen, 2008: Glacier mass balance variability in the Cordillera Blanca, Peru and its relationship with climate and the large-scale circulation. *Global and Planetary Change*. doi:DOI 10.1016/j.gloplacha.2007.11.003, 14-28.
Walker, R., T. Dupont, D. Holland, B. Parizek, and R. Alley, 2009: Initial effects of oceanic warming on a coupled ocean-ice shelf-ice stream system. *Earth and Planetary Science Letters*. doi:DOI 10.1016/j.epsl.2009.08.032, 483-487.
Wang, D. B., and M. Hejazi, 2011: Quantifying the relative contribution of the climate and direct human impacts on mean annual streamflow in the contiguous United States. *Water Resources Research*, **47**.
Wang, J., and X. Zhang, 2008: Downscaling and projection of winter extreme daily precipitation over North America. *Journal of Climate*, **21**, 923-937.
Wang, J., et al., 2009a: Is the Dipole Anomaly a major driver to record lows in Arctic summer sea ice extent? *Geophys. Res. Lett.*, **36**, -.
Wang, M., and J. Overland, 2009: A sea ice free summer Arctic within 30 years? *Geophys. Res. Lett.* doi:ARTN L07502, 10.1029/2009GL037820, -.
Wang, M., and J. E. Overland, 2012: Summer Arctic sea ice will be gone sooner or later – an update from CMIP5 models. *Geophys Res. Lett.*, **in press**.

Wang, M., J. Overland, V. Kattsov, J. Walsh, X. Zhang, and T. Pavlova, 2007: Intrinsic versus forced variation in coupled climate model simulations over the Arctic during the twentieth century. *Journal of Climate*. doi:DOI 10.1175/JCLI4043.1, 1093-1107.

Wang, X. L., V. R. Swail, F. W. Zwiers, X. Zhang, and Y. Feng, 2009b: Detection of external influence on trends of atmospheric storminess and northern oceans wave heights. *Climate Dynamics*, **32(2-3)**, 189-203.

Wang, Y. M., J. L. Lean, and N. R. Sheeley, 2005: Modeling the sun's magnetic field and irradiance since 1713. *Astrophysical Journal*, **625**, 522-538.

Wassmann, P., C. M. Duarte, S. Agusti, and M. K. Sejr, 2011: Footprints of climate change in the Arctic marine ecosystem. *Global Change Biology*, **17**, DOI: 10.1111/j.1365-2486.2010.02311.x.

Wen, Q. H., X. Zhang, Y. Xu, and B. Wang, 2012: Detecting human influence on extreme temperatures in China. *Geophys. Res. Lett.*

Wentz, F., L. Ricciardulli, K. Hilburn, and C. Mears, 2007: How much more rain will global warming bring? *Science*. doi:DOI 10.1126/science.1140746, 233-235.

Westra, S., L. V. Alexander, and F. W. Zwiers, 2012: Global increasing trends in annual maximum daily precipitation. *Journal of Climate*.

Wigley, T., C. Ammann, B. Santer, and K. Taylor, 2005: Comment on "Climate forcing by the volcanic eruption of Mount Pinatubo" by David H. Douglass and Robert S. Knox. *Geophys. Res. Lett.* doi:ARTN L20709, 10.1029/2005GL023312, -.

Wijffels, S., et al., 2008: Changing Expendable Bathythermograph Fall Rates and Their Impact on Estimates of Thermosteric Sea Level Rise. *Journal of Climate*, **21**, 5657-5672.

Wilcox, L. J., B. J. Hoskins, and K. P. Shine, 2012: A global blended tropopause based on ERA data. Part II: Trends and tropical broadening. *Quarterly Journal of the Royal Meteorological Society*, **138**, 576-584.

Willett, K. M., N. P. Gillett, P. D. Jones, and P. W. Thorne, 2007: Attribution of observed surface humidity changes to human influence. *Nature*, **449**, 710-U716.

Willett, K. M., P. D. Jones, N. P. Gillett, and P. W. Thorne, 2008: Recent Changes in Surface Humidity: Development of the HadCRUH Dataset. *Journal of Climate*, **21**, 5364-5383.

Wilson, D., H. Hisdal, and D. Lawrence, 2010: Has streamflow changed in the Nordic countries? - Recent trends and comparisons to hydrological projections. *Journal of Hydrology*, **394**, 334-346.

WMO, 2010: Scientific Assessment of Ozone Depletion: 2010. WMO.

Wong, A., N. Bindoff, and J. Church, 1999a: Large-scale freshening of intermediate waters in the Pacific and Indian oceans. *Nature*, **400**, 440-443.

——, 1999b: Large-scale freshening of intermediate waters in the Pacific and Indian oceans. *Nature*. 440-443.

Wood, K., and J. Overland, 2010: Early 20th century Arctic warming in retrospect. *International Journal of Climatology*. doi:DOI 10.1002/joc.1973, 1269-1279.

Woollings, T., 2008: Vertical structure of anthropogenic zonal-mean atmospheric circulation change. *Geophys. Res. Lett.*, **35**.

Wu, Q., and D. Karoly, 2007: Implications of changes in the atmospheric circulation on the detection of regional surface air temperature trends. *Geophys. Res. Lett.* doi:ARTN L08703, 10.1029/2006GL028502, -.

Wu, Z., N. Huang, J. Wallace, B. Smoliak, and X. Chen, 2011: On the time-varying trend in global-mean surface temperature. *Climate Dynamics*, **37**, 759-773.

Xie, S.-P., C. Deser, G. A. Vecchi, J. Ma, H. Teng, and A. T. Wittenberg, 2010: Global Warming Pattern Formation: Sea Surface Temperature and Rainfall. *Journal of Climate*, **23(4)**, 966-986.

Yamaguchi, S., R. Naruse, and T. Shiraiwa, 2008: Climate reconstruction since the Little Ice Age by modelling Koryto glacier, Kamchatka Peninsula, Russia. *Journal of Glaciology*, **54**, 125-130.

Yoshimori, M., and A. J. Broccoli, 2008: Equilibrium response of an atmosphere-mixed layer ocean model to different radiative forcing agents: Global and zonal mean response. *Journal of Climate*, **21**, 4399-4423.

Yoshimori, M., C. Raible, T. Stocker, and M. Renold, 2006: On the interpretation of low-latitude hydrological proxy records based on Maunder Minimum AOGCM simulations. *Climate Dynamics*. doi:DOI 10.1007/s00382-006-0144-6, 493-513.

Young, P. J., et al., 2012: Late twentieth century Southern Hemisphere stratospheric temperature trends in observations and CCMVal-2, CMIP3 and CMIP5 models. *J. Geophys. Res.*, submitted.

Zaliapin, I., and M. Ghil, 2010: Another look at climate sensitivity. *Nonlinear Processes in Geophysics*, **17**, 113-122.

Zhang, J., 2007: Increasing Antarctic sea ice under warming atmospheric and oceanic conditions. *Journal of Climate*, **20**, 2515-2529.

Zhang, J., M. Steele, and A. Schweiger, 2010: Arctic sea ice response to atmospheric forcings with varying levels of anthropogenic warming and climate variability. *Geophys. Res. Lett.*, **37**, -.

Zhang, P., et al., 2008a: A Test of Climate, Sun, and Culture Relationships from an 1810-Year Chinese Cave Record. *Science*, **322**.

Zhang, R., and T. Delworth, 2009: A new method for attributing climate variations over the Atlantic Hurricane Basin's main development region. *Geophys. Res. Lett.*, **36**, -.

Zhang, R., T. L. Delworth, and I. M. Held, 2007a: Can the Atlantic Ocean drive the observed multidecadal variability in Northern Hemisphere mean temperature? *Geophys. Res. Lett.*, **34**.

Zhang, R., et al., 2012: Have Aerosols Caused the Observed Atlantic Multidecadal Variability? *Submitted to Nature*.

Zhang, T., et al., 2005: Spatial and temporal variability of active layer thickness over the Russian Arctic drainage basin. *Journal of Geophysical Research*, **110**.

Zhang, X., 2010: Sensitivity of arctic summer sea ice coverage to global warming forcing: towards reducing uncertainty in arctic climate change projections. *Tellus Series a-Dynamic Meteorology and Oceanography*, **62**, 220-227.

Zhang, X., A. Sorteberg, J. Zhang, R. Gerdes, and J. Comiso, 2008b: Recent radical shifts of atmospheric circulations and rapid changes in Arctic climate system. *Geophys. Res. Lett.* doi:ARTN L22701, 10.1029/2008GL035607, -.

Zhang, X., et al., 2007b: Detection of human influence on twentieth-century precipitation trends. *Nature*. doi:DOI 10.1038/nature06025, 461-U464.

Zhang, X. B., et al., 2007c: Detection of human influence on twentieth-century precipitation trends. *Nature*, **448**, 461-U464.

Zickfeld, K., M. Eby, H. Matthews, and A. Weaver, 2009: Setting cumulative emissions targets to reduce the risk of dangerous climate change. *Proceedings of the National Academy of Sciences of the United States of America*, **106**, 16129-16134.

Zorita, E., T. Stocker, and H. von Storch, 2008: How unusual is the recent series of warm years? *Geophys. Res. Lett.* doi:ARTN L24706, 10.1029/2008GL036228, -.

Zwiers, F. W., X. Zhang, and Y. Feng, 2011: Anthropogenic influence on long return period daily temperature extremes at regional scales. *Journal of Climate*. doi:10.1175/2010JCLI3908.1.

Appendix 10.A: Notes and Technical Details on Figures Displayed in Chapter 10

Box 10.1, Figure 1

a) Observed global annual mean temperatures relative to 1880–1920 (coloured dots) compared with CMIP-5 ensemble-mean response to anthropogenic forcing (red),natural forcing (green) and best-fit linear combination (black dotted). Anthropogenic and natural simulations have been masked to correspond to observations following Jones et al. (2012) and noise-reduced with 5-point and 3-point running means respectively; b) Observed temperatures versus model-simulated anthropogenic and natural temperature changes, with best-fit plane, obtained by an unweighted least-squares fit through all 150 points, shown by coloured square. c) Gradient of best-fit plane in panel (b), or scaling on model-simulated responses required to fit observations (red diamond) with one- and two-dimensional uncertainty estimates (red ellipse and cross) derived by fitting a Gaussian distribution to projections of CMIP-5 control integrations onto anthropogenic and natural signals (black diamonds).

Figure 10.1, Figure 10.2, Figure 10.3

Process and data to create AR5 figures from observational and model near surface temperatures. The text in italics are highlighting other choices that could be made that may (or may not) influence interpretation of the figures.

Data
All of the data used was provided as monthly netcdf files, from the CMIP3, CMIP5 archives, Daithi Stone (providing data used in the AR4 figures that were not in the CMIP3 archive).

Creation of annual means
Annual mean spatial fields calculated from monthly fields, following calendar year (1/1/year to 31/12/year). For the observational datasets for a given grid point, the annual mean is calculated when at least 2/3rds of the months have data. From here on dates refer to these model years, e.g., 1901 to 2010 refers to the period 1/1/1901 to 31/12/2010.

Model anomalies
For all the model grid points the 30 year mean (1961–1990 or 1/1/1961–31/12/1990) is subtracted to allow anomalies to be calculated.

Regridding
All data are re-gridded onto the HadCRUT3 spatial grid (5° × 5°). As HadCRUT3 has usually the smallest overall coverage, i.e., no infilling into grid boxes with no observations, the dataset is usually used for limiting spatial coverage to available data, so we re-grid all the data to this dataset's grid. The re-gridding is done by area averaging any parts of the old grid that lie within the new grid to produce a new gridpoint value.

Masking
Where required, the data spatial/temporal coverage is limited to where the data exists in the equivalent year/gridpoint of HadCRUT3.

Global means
Global mean temperature anomalies calculated by area averaging all available points for each year

Reference period
For the specific given reference periods used in the figures (e.g., 1880-1909), the average of the global mean for the period is calculated, allowing any amount of missing data. The anomalies are then calculated with respect to the average of the reference period. Some of the model data start in 1890 and one model has a 1900 start. For the 1880-1909 reference period there is less data in these simulations to be used in the reference period mean.

Global mean against time plot

The period shown is arbitrary. Some models and only one observational dataset start in 1850. All model simulations are displayed even if they do not cover the whole period. With more observational data these figures will be updated to extend the end date.

Spatial trends

For each grid point a linear regression is applied to the available data to calculate the trend, requiring at least 50% of the years to be available AND no period longer than 10 years with missing data to calculate the trend. NB this will be re-examined,

[CHOICE:- do as is done in AR4 and only include trends where there are less than six consecutive years of missing data.]

Zonal trends

For each latitude (on HadCRUT3 grid), the average of the trend across the longitudes is calculated.

Model spread

For plots showing spread of models rather than individual model simulations, the ranges are estimated by ordering the data then choosing the central 90% (or the closest number greater than 90%) of the points and using the minimum and maximum value as limits.

Data

Table 10.A.1: Observational datasets.

Observational Data Set	Period Covered
NASA GISS	1880–2010
HadCRUT3	1850–2010
NOAA NCDC	1880–2010

Table 10.A.2: Model Data. Summary of data used. Historical data extended into 21st century either by using any available A1B SRES simulations (for CMIP3) and RCP4.5 (for CMIP5 - and RCP8.5 when RCP4.5 not available)

	Archive	Number of models used / that cover 1901–2010 period	Total number of members / that cover 1901–2010 period
historical	CMIP3	13 / 9	63 / 35
	CMIP5	13 / 12	78 / 59
historicalNat	CMIP3	7 / 0	30 / 0
	CMIP5	8 / 6	28 / 22
historicalGHG	CMIP3	NA	NA
	CMIP5	7 / 5	23 / 17

Figure 10.4

Estimated contributions from greenhouse gas (red), other anthropogenic (green) and natural (blue) components to observed global surface temperature changes a) from HadCRUT4 (Morice et al., 2011) showing 5–95% uncertainty limits on scaling factors estimated using eight climate models and a multi-model average (multi) and based on an analysis over the 1951–2010 period and b) The corresponding estimated contributions of forced changes to temperature trends over the 1951–2010 period (Jones et al., 2012). c) and d) As for a) and b) but estimated using seven climate models, a multi-model average (multi), and an estimate taking account of model uncertainty (eiv; (Huntingford et al., 2006)) based on an analysis over 1861–2010 period (Gillett et al., 2012b) e) and f) as for a) and b) but for the 1900–1999 period, for the HadCM3 model and for five different observational datasets; (HadCRUT2v, HadCRUT3v, GISTEMP, NCDC, JMA. (Jones and Stott, 2011).

Figure 10.5

This figure is reproduced exactly from Imbers et al. (2012) where it is described in detail. Estimates of contributions to global temperature changes taken from individual contributing papers.

Figure 10.6

Taken from Jones et al. (2012).

Figure 10.7

A number of new radiosonde datasets have been developed since the studies of a decade ago. Following the review by Thorne et al. (2011b) and having assessed which sets had coverage for the entire period, four datasets were chosen for analysis. The first of these is HadAT2 (Thorne et al., 2005). Of the observational data sets, this has the least spatial coverage, and thus is used as a common mask for all other data, both observations and models, to allow a like for like comparison.

The other three observational datasets are from the RICH/RAOBCORE family (Haimberger et al., 2012). The first of these sets used is RAOBCORE 1.5, which uses the ERA-40 (Uppala et al., 2005) and ERA-Interim reanalyses (Dee et al., 2011) to detect and adjust breakpoints. The other two are the ensembles of realizations known as RICH-obs 1.5 and RICH- τ 1.5. Both of these generate the ensemble by varying processing decisions (such as minimum number of data points or treatment of transitions), with breakpoint detection derived from RAOBCORE. However, they differ in the way they handle the adjustments. RICH-obs makes adjustments by directly comparing station time series, while RICH- τ compares the differences between the time series and the ERA-Interim background.

For the selection of model datasets, the decision was limited by the need for that model to have runs with natural forcings (NAT), as well as runs with only greenhouse gas forcings (GHG) and finally with all historical (i.e., anthropogenic and natural) forcings (ALL), between 1961 and 2010 available on the CMIP5 (Taylor et al., 2011) archive at the time the analysis was undertaken. This led to the models shown in Table 10.A.3 being used.

Table 10.A.3: CMIP5 models used for this study, and the number runs with each forcing.

		Members included		
Modeling Centre (or Group)	Model(s)	ALL	NAT	GHG
Commonwealth Scientific and Industrial Research Organization in collaboration with Queensland Climate Change Centre of Excellence	CSIRO-Mk3.6.0	10	5	5
NASA Goddard Institute for Space Studies	GISS-E2-R	5	5	5
	GISS-E2-H	5	5	5
Canadian Centre for Climate Modelling and Analysis	CanESM2	5	5	5
Met Office Hadley Centre	HadGEM2-ES	4	4	4
Beijing Climate Center, China Meteorological Administration	BCC-CSM1.1	3	1	1

All datasets were adjusted to a common temperature anomaly relative to the 1961–1990 climatology, re-gridded to the HadAT2 grid and masked before zonal averages were taken. The following set of pressure levels common to all datasets was used: 850, 700, 500, 300, 200, 150, 100, 50 and 30 hPa. The three latitude bands analyzed are a tropical zone (20ºS to 20ºN) and north and south extra-tropical zones (60ºS to 20ºS and 20ºN to 60ºN), along with the average over the whole studied area (i.e., 60ºS to 60ºN).

For both the models and observations, the trends at each pressure level were calculated using a median pair-wise algorithm (as this copes better with outliers than a conventional linear fit) [Lanzante *et al.* 1996]. These trends were plotted against pressure level, for all models and forcings within them. For each forcing ensemble of model runs, the shaded region shows the 5–95% range determined based on individual runs. Red represents all-forcings runs, green shows natural forcings and blue is greenhouse-gas-forced only. The thick black line is HadAT2, thin black line is RAOBCORE 1.5, while the dark grey band is the RICH-obs

1.5 ensemble range and light grey is the RICH-τ 1.5 ensemble range. Each band is displayed 25% translucent to better distinguish where forcings and observations overlap.

Figure 10.8

This figure shows time series of annual mean lower stratosphere temperatures from three satellite data sets and CMIP5 experiments. It uses the same CMIP5 model runs as Figure 10.7 and individual model runs are shown. Synthetic lower stratosphere temperatures were calculated using global MSU weighting functions for the lower stratosphere. The three observational data sets are used to address observational consistent: RSS Version 3.3, UAH version 5.4 and STAR version 2.0 (see Santer et al., 2012).

Synthetic MSU temperature time series from model data were calculated as follows:

1. Select area from 82.5°S–82.5°N of atmosphere temperature fields and time period and calculate area weighted averages;
2. Select time series from January 1979 to December 2010, calculate annual averages and anomalies relative to the period 1996–2010;
3. Select pressure levels (Pa): 100000, 92500, 85000, 70000, 60000, 50000, 40000, 30000, 25000, 20000, 15000, 10000, 7000, 5000, 3000, 2000, 1000;
4. Apply MSU lower stratosphere weighting function.

Figure 10.9

Taken from Balani Sarojini et al. (2012).

Figure 10.10

Figure based on Polson et al. (2012); Zhang et al. (2007); Min et al. (2008); and Min et al. (2001).

Left top panel: 'Global Land-Annual results from Polson et al. (2012) after Zhang et al. (2007); 'Global Land-Seasonal results from Polson et al. (2012); 'Arctic': Results from Min et al. (2008) and 'Extreme' Results from Min et al. (2011). Right top panel: After Zhang et al. (2007); but updated following Polson et al. (2012): changes expressed in percent climatology and CMIP5 models plotted. Bottom left and right panel: from Polson et al. (2012).

Figure 10.11

Adapted from Hu et al. (2012).

Figure 10.12

Taken from Gillett and Fyfe (2012).

Figure 10.13

Panel (A) is from Domingues et al. (2008) and (B) is from Gleckler et al. (2012).

Figure 10.14

A, B and C are from Helm et al. (2010), Durack et al. (2012), and Terray et al. (2011), respectively.

Figure 10.15

a) Northern Hemisphere September sea ice extent (>15% ice concentration) simulated by the seven CMIP5 models that matched the mean minimum and seasonality with less than 20% error compared with observations. The thin grey lines are based on pre-industrial control simulations (piControl). The coloured lines are historical runs (1950–2005) together with forced simulations (blue for RCP4.5, green for RCP6.0, and magenta for RCP8.5 emissions scenarios for the period 2006–2015). The thick black line is base on

Hadley sea ice analysis (HadleyISST_ice). Panels A-G are models: CCSM4, HadGEM2CC, HadGEM2ES, MIROC−ESM, MIROC−ESMC, MPI−ESM−lr, and ACCESS1. **b)** Similar to a) but for the Southern Hemisphere. Panels A-F are models: CanESM2, MIROC-ESM, MIROC-ESMC, MRI-CGCM3, NorESM1 and BCC-CSM1. For Antarctic sea ice we show results for two models that passed the same selection criteria as for the Northern Hemisphere and the next four models with lowest error scores. Note that the presented models are different for the Northern and Southern Hemisphere based on the selection criteria.

Figure 10.16

Detection results for changes in intensity and frequency of extreme events. Left side of each panel show scaling factors and their 90% confidence intervals for intensity of annual extreme temperatures in response to external forcings for the period 1951–2000. TNn and TXn represent annual minimum daily minimum and maximum temperatures, respectively, while TNx and TXx represent annual maximum daily minimum and maximum temperatures (updated from Zwiers et al., 2011), fingerprints are based on simulations of CanESM2 with both anthropogenic and natural forcings). Right hand sides of each panel show scaling factors and their 90% confidence intervals for changes in thefrequency of temperature extremes for winter (October-March for Northern Hemisphere and April-September for Southern Hemisphere), and summer half years. TN10, TX10 are respectively the frequency for daily minimum and daily maximum temperatures falling below their 10th percentiles for the base period 1961–1990. TN90 and TX90 are the frequency of the occurrence of daily minimum and daily maximum temperatures above their respective 90th percentiles calculated for the 1961–1990 base period (Morak et al., 2012), fingerprints are based on simulations of HadGEM1 with both anthropogenic and natural forcings). Detection is claimed at the 10% significance level if the 90% confidence interval of a scaling factor is above zero line.

Figure 10.17

Panel (a) is reproduced from Pall et al. (2011), supplementary information. Panel (b) is precisely the same plot using the flood diagnostics computed for the Don region in Spring 2001 by Kay et al. (2011b), and Panel (c) is reproduced from Otto et al, 2012.

Figure 10.18

All reconstructions used are the same as in Schurer et al. (2012). Except the Mann et al. (2009) reconstruction which in the top panel is for 30°N–9°0N land and sea and in the bottom panel is for 0°–60°E 25°N–65°N land and sea. And the Luterbacher et al. 2004 reconstruction in the bottom panel which is for the region 25°W–40°E 35°N–70°N land only.

All models used to construct the multi-model ensemble and the control simulations used for samples of internal variability are the same as in Schurer et al. (2012) (see Table 10.A.4). To calculate the multi-model mean each model set-up contributes equally i.e., the mean of the five MPI-COSMOS simulations counts as one model whereas the GISS-E2-R simulations are treated separately since they contain different forcings. The GISS-E2-R simulations included a significant initial model drift which was removed from the control simulation by fitting a second order polynomial to the control simulation.

Table 10.A.4: Details of the models used.

Model	Ens.	Resolution		Forcings			
	Members	Atmosphere	Ocean	Volc	Solar	GHG	Land-use
* CCSM4[16*]	1	288x192xL26	320x384xL60	GEA	VK/WLS	SJA	PEA/Hur
MPI-COSMOS[15]	5	96x48xL19	GR3.0xL40	CEA	JLT	Interactive	PEA
MPI-ESM-P	1	196x98xL47	256x220xL40	CEA	VK/WLS	SJA	PEA
HadCM3[17,18]	1	96x73xL19	288x144xL20	CEA	SBF/WLS	SJA	PEA
GISS-E2-R	1	144x90xL40	288x180xL32	CEA	VK/WLS	SJA	PEA/Hur
GISS-E2-R	1	144x90xL40	288x180xL32	GRA	VK/WLS	SJA	KK10/Hur
Bcc-csm1-1[19]	1	128x64xL40	360x232xL40	GRA	VK/WLS	SJA	X

Notes:

Further details can be found in the references for the model and the forcings used; the references are CEA – Crowley et al. (2008) [20], GRA – Gao et al., (2008) [21], VSK – Viera et al. (2011) [22], SBF – Steinhilber et al. (2009) [23] , WLS – Wang et al. (2005) [24], SJA – Schmidt et al. (2012) [11], PEA – Pongratz et al. (2008) [25], Hur- Hurtt et al. (2009) [12], KK10 – Kaplan et al. (2009) [26]. JLT – Jungclaus et al. (2010) [15] ,MM - MacFarling Meure et al. (2006) [27], . An X indicates that the forcing is not included. The models indicated by asterisks have been made available as part of the CMIP5 project.

The Goosse simulations are taken directly from the simulation described in Goosse et al. (2012a) and Goosse et al. (2012b), constrained by the Mann et al. (2009) reconstruction from 30°N–90°N. In the top panel the annual mean of the region 30°N–90°N land and sea is shown and in the bottom panel the annual mean of the region 0°–60°E, 25°N–65°N.

The instrumental data is taken from Morice et al. (2012).

All analysis is done on decadally smoothed time-series, using an 11-year box car filter. For display purposes all time-series have an additional 7-year box car smoothing.

Figure 10.19

PDFs and histograms taken from the literature and plotted based on input from authors of papers cited. Rest see caption.

Figure 10.20

Brown panels are land surface temperature time series, green panels are precipitation time series, blue panels are ocean heat content time series, and white panels are sea-ice time series.

Surface Temperature
For surface temperature the 5 to 95% interval is plotted and is based on the Jones et al. (2012) (and Figure 10.1). The observed surface temperature is from HadCRUT4.

Precipitation
For precipitation data the mean and one standard deviation shading of the simulations is plotted. Observed precipitation is from Zhang et al. (2007b).

All forcing runs used from the following models: 'bcc-csm1-1', 'CanESM2', 'CNRM-CM5', 'CSIRO-Mk3-6-0', 'GISS-E2-H', 'GISS-E2-R', 'HadGEM2ES', 'inmcm4_esm', 'IPSL-CM5A-LR', 'NorESM1-M'. Natural forcing runs used from the following models: 'bcc-csm1-1', 'CanESM2', 'CNRM-CM5', 'CSIRO-Mk3-6-0', 'HadGEM2-ES', 'NorESM1-M'

Ocean Heat Content (OHC)
For Ocean Heat Content the mean and one standard deviation shading is plotted for an ensemble of CMIP5 models. Three observed records of OHC are shown; Domingues et al., 2008; Levitus et al., 2009; and Ishii and Kimoto, 2009. The CMIP5 model curves are based on Pierce et al., (2012, submitted). Model OHC is calculated over the top 700 m (as in the observations) from volume average temperatures and using a constant volume for each basin.

Sea ice
The sea ice extents simulations and observations are the same as in Figure 10.15.

Tables

Table 10.1: Synthesis of detection and attribution results across the climate system. Note that we follow the guidance note for lead authors of the IPCC AR5 on consistent treatment of uncertainties (Mastrandrea et al., 2011). Where the confidence is medium or less there is no assessment of the quantified measure (i.e., likelihood) is given and the table cell is marked not applicable (N/A).

	1) Statement about variable or property: time, season	2) Confidence (Very high, High, medium or low, very low)	3) Quantified measure of uncertainty where the probability of the outcome can be quantified (Likelihood given generally only if high or very high confidence)	4) Data sources Observational evidence (Chapters 2-5); Models (9) (limited, medium, robust)	5) No and type of attribution studies (formal (single step); multiple step; qualitative)	6) Type, amount, quality, consistency of evidence (limited, medium, robust)	7) Degree of agreement of studies (low, medium, high)	8) Factors contributing to the assessment Including Physical understanding, observational uncertainty. Trace statements back to sections. Uncertainties and caveats.
	Global Scale Temperature Changes							
1	Most of the observed increase in global average temperatures since the mid-20th century is due to anthropogenic forcings.	High	Extremely likely	Four global surface temperature series. CMIP3 and CMIP5 models.	Many formal attribution studies, including optimal fingerprint time-space studies and time series based studies.	Robust evidence. Attribution of more than half of warming since 1950 to anthropogenic forcings seen in multiple independent analyses using different observational datasets and climate models.	High agreement. Studies agree in dominant role of anthropogenic forcing to observed warming that is larger than any other factor including internal variability.	The observed warming is well understood in terms of contributions of anthropogenic forcings such as greenhouse gases and tropospheric aerosols and natural forcings from volcanic eruptions. Solar forcing is the only other forcing that could explain long-term warming but pattern of warming is not consistent with observed pattern of change in time, vertical change and estimated to be small. AMO could be confounding influence but studies that find significant role for AMO show this does not project strongly onto 60 year trends.. (10.3.1.1 Fig 10.4)
2	Early 20th century warming is due in part to external forcing.	High	Very likely	Four global surface temperature series. CMIP3 and CMIP5 models; reconstructions of the last millennium (Section 10.7).	Some formal detection and attribution studies looking at early century warming and studies for the last few hundred years.	Attribution studies find detectable contributions from external forcings although they vary in contributions from different forcings.	High agreement across a number of studies. Agree in detecting external forcings.	Modelling studies show contribution from external forcings to early century warming. Pattern of warming and residual differenced between models and observations indicate role for circulation changes as contributor (10.3.1.1, Fig 10.1).
3	Warming since 1950 cannot be explained without external forcing.	High	Virtually certain	Estimates of internal variability from CMIP3 and CMIP5 models, observation based process models and from paleo data.	Many, including optimal fingerprint time-space studies and time-series based studiesand paleo data studies.	Robust evidence. Detection of greenhouse gas fingerprint robustly seen in independent analyses using	High	Based on all evidence above combined. Observed warming since 1950 is very large compared to climate model estimates of internal variability which are assessed to be adequate at global scale. The warming since 1950 is far outside the range of any similar length trend in residuals from

						different observational datasets and climate models of any complexity.		reconstructions of the past millennium. The spatial pattern of observed warming differ from those associated with internal variability. (9.5.3.1, 10.3.1.1, 10.7.5)
4	Global temperature changes since 1998 are consistent with internal variability super-posed on the anthropogenic greenhouse gas induced warming trend projected by climate models.	High	N/.A	Three observational datasets, and CMIP3 simulations.	Several studies compare observed trends with CMIP3 simulations and previously observed decadal trends.	Medium amount of evidence, and consistent findings.	All studies agree that there is no inconsistency between simulated and observed trends over this period.	Based on comparisons of simulated and observed trends. (10.3.1.1.3).
5	Anthropogenic forcing has led to a detectable warming of troposphere temperatures since 1961.	High	Likely	Multiple radiosonde datasets from 1958 and satellite datasets from 1979 to present.	Formal attribution studies on CMIP3 models (assessed in AR4) and three new studies on CMIP5 models.	Robust detection and attribution of anthropogenic influence on tropospheric warming which does not depend on including stratospheric cooling in the fingerprint pattern of response.	Studies agree in detecting an anthropogenic influence on tropospheric warming trends. No new studies yet reported post 2000.	Observational uncertainties in radiosonde are now much better sampled than at time of AR4. It is virtually certain that the troposphere has warmed since the mid-20th century but there is low confidence in te rate and vertical structure of those changes. Evidence is robust that during the satellite era CMIP3 and CMIP5 models warm faster than observations in the tropics. A climate change signal on tropospheric temperatures from both radiosondes and satellites is robustly detected. (2.4.5, 9.4.1.3.2, 10.3.1.2.1, Fig 10.7)
6	Anthropogenic forcing dominated by ozone deleting substances, has led to a detectable cooling of lower stratosphere temperatures since 1961.	High	Very Likely	Radiosonde data from 1958 and MSU satellite data from 1979 to present. CCMVal simulations, CMIP3 and CMIP5 simulations.	One formal optimal detection attribution study (using stratosphere resolving models) combined with many separate modelling studies and observational studies.	Physical understanding and model studies show very consistent understanding of observed evolution of stratospheric temperatures, consistent with formal detection and attribution results. Not many studies.	Studies agree in showing very strong cooling signal in stratosphere that can only be explained by anthropogenic forcings dominated by ozone depleting substances.	New generation of stratosphere resolving models appear to have adequate representation of lower stratospheric variability. Structure of stratospheric temperature trends and variability well represented by models. (10.3.1.2.2, Fig 10.8)
7	Anthropogenic forcing, particularly greenhouse gases and stratospheric ozone depletion has led to a detectable observed	High	Very likely	Radiosonde data from 1958 and satellite data from 1979 to present.	Several studies using CMIP3 models and 20th century data.	Physical reasoning and modelling supports robust expected fingerprint of anthropogenic influence which is	Fingerprint of anthropogenic influence is robustly detected in different measures of free atmosphere	Fingerprint of changes expected from physical understanding and as simulated by models is detected in observations. Understanding of stratospheric changes has improved since AR4. Understanding of observational uncertainty has improved although uncertainties remain

	tropospheric warming and stratospheric cooling since 1961.					robustly detected in observational records.	temperature changes including tropospheric warming, and a very clear identification of stratospheric cooling in models that include anthropogenic forcings.	particularly in the upper troposphere.(10.3.1.2.3, Figure 10.7)
8	Anthropogenic forcing has contributed to the observed changes in temperatures extremes over global land since the mid-20th century..	High	Very Likely	Indices for extreme temperatures including annual maximum and annual minimum daily temperatures, over the all land except parts of Africa and South America. CMIP3 and CMIP5 simulations, 1950–2005.	Several studies including fingerprint time-space studies.	Detection of anthropogenic influence robustly seen in independent analysis using different methods, different data sets. Les robust detection of other forcings.	Studies agree in robust detection of anthropogenic influence on extreme temperatures.	Expected from physical principles that changes in mean temperature should bring changes in extremes, confirmed by correlations/regressions. New evidence since AR4 for detection of human influence on extremely warm daytime temperatures and new evidence that influence of anthropogenic forcing can be separately detected from natural forcing. More limited observational data and greater observational uncertainties than for mean temperatures. (10.6.1.1)
	Oceans							
9	More than half of the rising ocean heat content in the upper 700m since the 1970's is caused by anthropogenic forcing and volcanic eruptions.	Very high confidence	Very likely	Section 3.2, and many global estimates from observations of increasing heat content in the upper 70m of the water column. High level of agreement on long term trends. All models of 20th century runs show global rises in heat content. Evidence is robust.	3-5 new attribution studies of role of anthropogenic and volcanic forcing of ocean's global heat content.	The evidence is very robust, and tested against known structural deficiencies in the observations, and in models.	High levels of agreement across attribution studies and observation and model comparison studies. Now tested against known structural deficiencies in the observations, and in models.	New understanding of the structural errors and their correction in the temperature data sets that are the basis of the observations. The errors reported in AR4 have largely been resolved. The observations and climate simulations have the same trend (including anthropogenic and volcanic forcings) and similar decadal variability. The detection is well above signal to noise levels required at 1 and 5% percent levels, even for observation data sets that include some of the structural uncertainties, in both models and observations. The new results show the conclusions to be very robust to these structural uncertainties in observations and 20th century simulations. No significant confounding factors for global heat content.
10	More than half of the rising themosteric sea level since the 1970's is caused by anthropogenic	Very high confidence	Very likely	Section 3.2 and Section 3.7, and many global estimates from observations of	3–5 new attribution studies of role of anthropogenic and volcanic forcing of ocean's thermal	The evidence is very robust, and tested against known structural deficiencies in the	High levels of agreement across attribution studies and observation and model comparison	Very high confidence, based on the number of studies, the updates to earlier results in AR4, and new understanding of the systematic errors in observational estimates of ocean thermal expansion (from ocean heat content, and the

	forcing and volcanic eruptions.			thermal expansion. High level of agreement on long term trends. All models of 20th century runs show global rises in steric sea level. Evidence is robust.	expansion (through ocean heat content change).	observations, and in models.	studies. Now tested against known structural deficiencies in the observations, and in models.	physical relationship between steric height and ocean heat content). (Section 10.4.3)
11	The observed ocean surface and sub-surface salinity changes since 1960's are due in part to a rising greenhouse gases.	High confidence	Likely	Oceans chapter (Section 3.3) and studies in this chapter.	4 new attribution and model and data comparison studies for all forcings.	Medium evidence. Observational evidence is very robust. CMIP3 OAGCM show patterns of salinity change consistent with observations, but number of formal attributions studies that test against changes with full characterisation of internal variability is only two papers.	Medium agreement based on two attribution studies, with incomplete characterisation of internal variability. High agreement for observations, and medium for models and attribution studies.	From Section 3.3 more than 40 studies of regional and global surface and subsurface salinity show patterns consistent with acceleration of hydrological water cycle. Based on understanding of the thermodynamics of the free atmosphere (Clausius Claperyon and atmospheres engery budget), the robust observational evidence from ocean salinity measurements, and OAGCM show same amplification consistent with physical understanding of free atmosphere. The likely confidence level based on incomplete understanding of the internal variability of the surface and sub-surface salinity fields from CMIP3 OAGCM. (Section 10.4.2)
12	Observed increase in surface ocean acidification since 1980's is mostly caused by rising atmospheric CO_2	Very high confidence	Extremely likely	Evidence from Section 3.8.2 and Box 3.2	Based on ocean chemistry, e xpert judgement, and many analyses of time series and other indirect measurements	Robust evidence from time series measurements. Measurements have a high degree of certainty (see Table 3.2) and instrumental record show virtually certain increase in ocean acidity	High agreement of the trends, measurement uncertainty across the oceanographic literature.	Very high confidence, based on the number of studies, the updates to earlier results in AR4, and the very well established physical understanding of gas exchange between atmosphere and ocean, ocean chemistry and the sources of excess carbon dioxide in the atmosphere. Alternative processes and hypothese can be excluded (Section 3.8.2 and Box 3.2)
13	Observed decrease in global oxygen content is inconsistent with internal variability.	Medium confidence	About as likely as not	Evidence from Section 3.5 and studies in Section 10.4.4.	Qualitative / expert judgement based on comparison of observed and expected changes in response to increasing CO_2.	Medium evidence. 1 specific global ocean studies, many studies of hydrographic sections and repeat station data, high agreement across studies. Decadal variability is not well understood in global	Medium agreement. One attribution studies, and only limited regional and large scale modelling and observation comparisons.	Physical understanding of ocean circulation and ventilation, and from the global carbon cycle, and from simulations of ocean oxygen concentrations from coupled bio-geochemical models with OACGM's. Main uncertainty is decadal variability which is not well understood in global and regional inventories of oxygen in the oceans (Section 10.4.4)

						inventories of oxygen in the oceans.		
	Water Cycle							
14	Global precipitation patterns have changed significantly due to anthropogenic forcings with increases at mid and high NH latitudes; increases in part of the tropics and reductions in the low latitudes.	Medium	N/A	Rain gauge observations over land, dominated by the Northern Hemisphere. Salinity changes in ocean.	Several land precipitation studies examining annual and seasonal, land precipitation, two salinity study inferring changes for precipitation minus evaporation.	Evidence is consistent in showing changes in global precipitation patterns. Attribution studies have not separated out signature of greenhouse gases from that of aerosols.	Good degree of agreement of studies. Seasonal attribution study points to robustly detected anthropogenic changes in boreal winter and spring.	Zonal precipitation changes expected to be more robust than spatial patterns (Held and Soden; Allen and Ingram) and good process understanding for their origin; large uncertainty in aerosol contribution. Some indications, model simulated changes smaller than observed. Global-land average long-term changes small at present time, whereas decadal variability over some land areas is large. Observations are very uncertain and poor coverage of precipitation expected to make fingerprint of changes much more indistinct. Salinity changes in the ocean confirm pattern expected and detected over land. (10.3.2.2, 10.4.2, Fig 10.10, 10.14)
15	Anthropogenic forcing has contributed to intensification of extreme precipitation at the global scale since the mid-20th century.	Medium confidence	N/A	Wettest 1-day and 5-day precipitation in a year, observations, CMIP3 simulations.	Only 1 study restricted to Northern hemisphere land where observations were available.	Limited, only one study. Not able to differentiate anthropogenic from natural forcings and found stronger detectability for models without natural forcings.	Only one formal attribution study but findings agree with physical expectations.	Evidence for anthropogenic influence on various aspects of the hydrological cycle that implies extreme precipitation would be expected to increase. Climate models have difficulties in simulating extreme precipitation. There are large observational uncertainties and poor global coverage. (10.6.1.2)
16	Anthropogenic contribution to global increase in atmospheric water content.	Medium confidence	N/A	Observations of atmospheric moisture content over ocean from satellite; observations of surface humidity from weather stations and radiosondes over land.	Several studies including optimal detection studies.	Detection of anthropogenic influence on atmospheric moisture content over oceans robust to choice of models.	Studies looking at different variables agree in detecting humidity changes.	Recent reductions in relative humidity over land and levelling off of specific humidity not fully understood. Length and quality of observational datasets limit detection and attribution and assimilated analyses not judged sufficiently reliable for detection and attribution (10.3.2.1).
	Hemispheric Scale Changes; Basin Scale Changes							
	Cryosphere							
17	Glaciers have diminished significantly due to human influence since the 1960's.	High confidence	Likely	Robust agreement across *in situ* and satellite derived estimates of surface mass balance (Section 4.2).	Two new studies and several recent studies since last assessment.	Robust evidence from different sources	High agreement limited number of across studies.	Documented evidence of surface mass loss (Section 4.3.3). Confounding factor is the poor characterisation of the internal variability of the surface mass balance (strong dependent on atmospheric variability). The surface mass loss was strongly driven by large atmospheric winds in

								2010 and 2011 and the relatively short record length. (Section 10.5.2.2)
18	Anthropogenic forcing contributes to declines in the surface mass balance of Greenland ice.	High confidence	Likely	Robust agreement across *in situ* and satellite derived estimates of surface mass balance (Section 4.2). Nested or downscaled model simulations show pattern of change consistent with warming.	Two new studies and several recent studies since last assessment.	Robust evidence from different sources.	High agreement limited number of across studies.	Documented evidence of surface mass loss (Section 4.4). Confounding factor is the poor characterisation of the internal variability of the surface mass balance (strong dependent on atmospheric variability). The surface mass loss was strongly driven by large atmospheric winds in 2010 and 2011 and the relatively short record length. (Section 10.5.2.1)
19	Antarctic ice sheet mass balance loss is caused by anthropogenic forcing.	Very low confidence based on low scientific understanding.	N/A	Observational evidence for Antarctic mass sheet loss is well established across a broad range of studies (Section 4.2).	No formal studies exist. The internal variability of ice sheet mass balance is not well characterised and there is increasing evidence that the ice sheet can respond on short time scales.	Processes for mass loss for Antarctica are not well understood. Regional warming and changed wind patterns (increased westerlies, increase in the SAM) could contribute to enhanced melt of Antarctica. Surface mass balance also has strong internal variability.	High agreement in observational studies. Low agreement in scientific understanding and consequently modelling studies only explore some aspects of Antarctic Ice sheet mass balance.	Low confidence, because of the current state of modelling of Antarctic ice sheet and their interaction with atmosphere and oceans. Attribution requires better models of ice sheets, ocean circulation and atmospheres, and better simulations of the role of the regional changes in winds and warming around Antarctica, and their attribution to anthropogenic forcing. (Section 4.4, Section 13.4 and Section 10.5.2.1)
20	Anthropogenic contribution is the cause of most of the Arctic sea ice retreat in recent decades.	High confidence, based on number of studies and size the sea ice reduction (and relative instrumental record).	Very Likely	Robust agreement across all observations. Section 4.1. , model control runs and last 5 yrs versus before 2007. Substantial retreat, larger than models, D&A studies using CMIP3 models.	Two detection and attributions studies, large number of model simulations and data comparisons for instrumental record.	Robust set of studies simulations of sea-ice and observed sea-ice extent.	High agreement between studies of sea ice simulations and observed sea-ice extent.	There are documented observations of ice extent loss, and also good evidence for a significant reduction in sea-ice volume; The understanding of the physics of arctic sea-ice is well understood and consistent with the observed warming in the region, and from simulations of arctic sea-ice extent to anthropogenic forcing. (Section 10.5.1)
21	Antarctic sea ice extent shows little change and is still consistent with anthropogenic and natural forcings on	Medium	N/A	The evidence of an increase in extent is robust, based on satellite measurements and ship based	No formal attribution studies, although there are Antarctic sea-ice and model comparisons.	The trends in sea ice extent are small relative to internal variability. The current increase is within the current	Medium evidence. Modelling studies have a low level of agreement on the physical processes from the observed	Small increases in sea-ice extent. Low scientific understanding of the changes in the Antarctic sea-ice with plausible evidence for contributions from ozone, GHG, atmosphere and ocean circulation, Southern Annular Mode and other source of internal variability. (Section 10.5.1)

	climate simulations (20th century and sea-ice projections).			measurements (Section 4.5.2).		internal variability of sea-ice.	increase. Observational evidence is robust.	
22	Snow cover and Permafrost reductions since 1970's have anthropogenic influence.	High confidence	likely	Observation shows decrease in snow cover which is consistent with CMIP3 simulations.	Two snow cover and two perma frost attribution studies and	Decrease in snow cover, wide spread permafrost degradation in the observations are consistent among many studies.	High	Expert judgement and attribution studies support the human influence on reduction in snow cover extent. (Section 10.5.3)
	Atmospheric Circulation and Patterns of Variability							
23	Human influence has altered sea level pressure patterns globally.	High	Likely	Two observational gridded datasets as well as reanalyses.	Four formal detection and attribution studies	Formal attribution study based on CMIP5 models finds detectable influences separately of greenhouse gases, aerosols and ozone changes, each of which have distinct zonal, meridional and seasonal structures in patterns of sea level pressure.	All studies show detectable anthropogenic influence on sea level pressure patterns.	Detectable anthropogenic influence on changes in sea level pressure patterns is found in several attribution studies including one study that identifies distinctive patterns from different forcings in observations. Observational uncertainties not fully sampled as results based largely on one gridded dataset. (10.3.3.4)
24	The positive trend in the SAM seen in Austral summer is due in part to stratospheric ozone depletion.	High	Likely	Measurements since 1957. Clear signal of SAM trend in DJF robust to observational uncertainty.	Many studies comparing consistency of observed and modelled trends, and consistency of observed trend with simulated internal variability.	Observed trends are consistent with CMIP3 and CMIP5 simulations including stratospheric ozone depletion.	Several studies show that the observed increase in the DJF SAM is inconsistent with simulated internal variability. High agreement of modelling studies that ozone depletion and GHG increases drive an increase in the DJF SAM index.	Consistent modelling result that the main aspect of the anthropogenically forced response is the impact of ozone depletion on the DJF SAM. Caveats: Shortness of the observational record, observational uncertainties, DJF SAM trend only marginally inconsistent with internal variability over the most recent 50 year period in some datasets. (10.3.3.3, Fig 10.12)
25	Stratospheric ozone depletion has contributed to the poleward shift of the Southern Hadley cell during Austral summer.	Medium	N/A	Multiple observational lines of evidence for widening but large spread in the magnitude. Reanalysis suggest a southward shift of	No formal attribution studies.	Consistent evidence for effects of stratospheric ozone depletion but not for other forcings.	Evidence from modelling studies is robust that stratospheric ozone drives a poleward shift of the southern Hadley Cell border during austral	The observed magnitude of the tropical belt widening is uncertain. The contribution of increases in greenhouse gases, natural forcings, and internal climate variability to the observed poleward expansion of the Hadley circulation remains veryuncertain. (10.3.3.1, Figure 10.11)

				southern Hadley cell border during DJF.			summer. The magnitude of the shift is very uncertain.	
26	Attribution of changes in tropical cyclone activity to human influence.	Low	N/A	Incomplete and short observational records.	Formal attribution studies on SSTs in tropics. However mechanisms linking anthropogenically induced SST increases and changes in tropical cyclone activity poorly understood.	Attribution assessments depend on multi-step attribution linking anthropogenic influence to large scale drivers and thence to tropical cyclone activity.	Low agreement lacking between studies, medium evidence.	Insufficient observational evidence of multi-decadal scale variability. Physical understanding lacking. There remains substantial disagreement on the relative importance of internal variability, greenhouse gas forcing, and aerosols. (10.6.1.5, Box 14.3)
	Millennium Timescale							
27	Detectable role of forcing in reconstructions of hemispheric scale temperature.	High confidence period post 1400 AD, medium confidence record prior to 1400 AD.	Reconstructed changes very unlikely due to internal variability alone over past 7 centuriesmedium confidence in results from 850 on	See Chapter 5 for reconstructions; simulationsfrom CMIP5/PMIP3 and earlier models, period: 1400 on and 1400-1950, much weaker results for entire millennium.	A small number of detection and attribution studies and further evidence from climate modelling studies and data assimilation.	Medium confidence from 850 on, robust agreement in data from Number of studies using a range of models (EBMs to ESMs). Conclusion robust that models are able to reproduce key features of last 7 centuries, medium confidence for entire millennium.	High agreement across studies, with robust evidence for past 7 centuries, medium evidence from 850 on	Large uncertainty in reconstructions particularly for the first half of the millennium ; but good agreement between reconstructed and simulated large scale features; detection of forced influence robust for a large range of reconstructions; Difficult to separate role of individual forcings; results prior to 1400 much more uncertain, partly due to larger data and forcing uncertainty.
	Continental to Regional Scale Changes							
28	Anthropogenic forcing has made a substantial contribution to warming of theinhabited continents.	High	Likely	Robust observational evidence except for Africa due to poor sampling.	New studies since AR4 detect anthropogenic warming on continental and sub-continental scales.	Robust detection of human influence on continental scales agrees with global attribution of widespread warming over land to human influence.	Studies agree in detecting human influence on continental scales.	Anthropogenic pattern of warming widespread across all inhabited continents. Lower signal to noise at continental scales than global scales. Separation of response to forcings more difficult at these scales. Models have greater errors in representation of regional details. (10.3.1.1,4, Box 11.2).
29	Human contribution to Antarctic temperature changes (separately due to different dynamics).	Low	N/A	Poor observational coverage of Antarctica with most observations around coast.	One optimal detection study, and some modelling studies.	Clear detection in one optimal detection study.	Only one study.	Some contribution to changes from SAM increase. Residual shows warming consistent with expectation. High data uncertainty (individual stations only), large uncertainty in level of internal variability (only 50 years; high feedback region). (10.3.1.1.4, 2.4.1.1)

30	Contribution by forcing to reconstructed European temperature variability over centuries.	Medium	N/A	European seasonal temperatures 1500 on.	One study and several modelling studies.	Clear detection in one study; robust volcanic signal in several studies (see also Chapter 5).	Only one study.	Robust volcanic response detected in Epoch analyses in several studies. Models reproduce low-frequency evolution if forced with all temperatures. Some uncertainty in overall level of variability, uncertainty in reconstruction particularly prior to late 17th century.
31	Human influence is detectable on temperatures, and frequency and intensity of temperature extremes for some sub-continental regions of the world.	High	Likely for mean temperatures in some sub-regions of North America, Europe, Asia and Australasia, more likely than not for temperature extremes in some regions.	Good observational coverage for some regions (e.g., Europe) and poor for others (e.g., Africa, Arctic). Coverage poorer for extremes.	A number of formal detection and attribution studies have analyzed temperatures on scales from Giorgi regions to climate model grid box scale.	Several formal detection and attribution studies for mean temperature, and one each for extreme temperature intensity and frequency.	Many studies agree in showing that an anthropogenic signal is apparent in many sub-continental scale regions. In some sub-continental-scale regions circulation changes have played a bigger role.	Larger role of internal variability at smaller scales relative to signal. In some regions observational coverage is poor. Local forcings and feedbacks as well as circulation changes matter, particularly for extremes, and may not be well simulated in all regions.
32	Human influence has substantially increased the probability of some observed heatwaves.	High	Likely	Good observational coverage for some regions and poor for others (thus biasing studies to regions where observational coverage is good) and multi model data including targeted experiments with models forced with prescribed sea surface temperatures.	Event multi-step attribution studies have been made of some events including Europe 2003 and Moscow 2010 backed up by single-step attribution studies looking at the overall implications of increasing mean temperatures for the probabilities of exceeding temperature thresholds in some regions.	To infer the probability of a heatwave, extrapolation has to be made from the scales on which most attribution studies have been carried out to the spatial and temporal scales of heatwaves.	Studies agree in finding robust evidence for overall increase in probability of extreme temperatures.	In some instances circulation changes could be more important than thermodynamic changes. Possible confounding influences include urban heat island effect. (10.6.2)

1
2

Chapter 10: Detection and Attribution of Climate Change: from Global to Regional

Coordinating Lead Authors: Nathaniel Bindoff (Australia), Peter Stott (UK)

Lead Authors: Krishna Mirle AchutaRao (India), Myles Allen (UK), Nathan Gillett (Canada), David Gutzler (USA), Kabumbwe Hansingo (Zambia), Gabriele Hegerl (UK), Yongyun Hu (China), Suman Jain (Zambia), Igor Mokhov (Russia), James Overland (USA), Judith Perlwitz (USA), Rachid Sebbari (Morocco), Xuebin Zhang (Canada)

Contributing Authors: Beena Balan Sarojini, Pascale Braconnot, Oliver Browne, Ping Chang, Nikolaos Christidis, Tim DelSole, Catia M. Domingues, Paul J. Durack, Alexey Eliseev, Kerry Emanuel, Chris Forest, Hugues Goosse, Jonathan Gregory, Isaac Held, Greg Holland, Jara Imbers Quintana, Gareth S. Jones, Johann Jungclaus, Georg Kaser, Tom Knutson, Reto Knutti, James Kossin, Mike Lockwood, Fraser Lott, Jian Lu, Irina Mahlstein, Damon Matthews, Seung-Ki Min, Daniel Mitchell, Thomas Moelg, Simone Morak, Friederike Otto, David Pierce, Debbie Polson, Andrew Schurer, Tim Osborn , Joeri Rogelj, Vladimir Semenov, Dmitry Smirnov, Peter Thorne, Muyin Wang, Rong Zhang

Review Editors: Judit Bartholy (Hungary), Robert Vautard (France), Tetsuzo Yasunari (Japan)

Date of Draft: 5 October 2012

Notes: TSU Compiled Version

Figures

a)

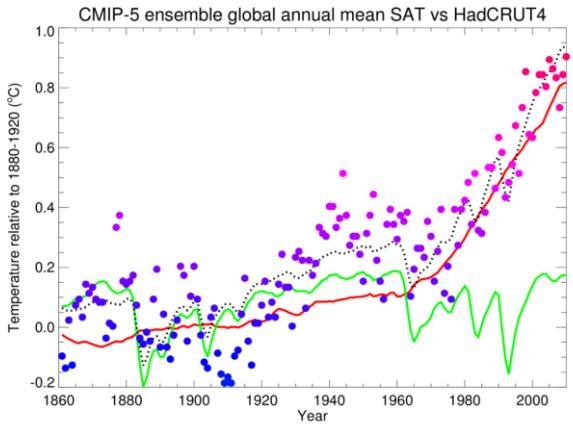

b)

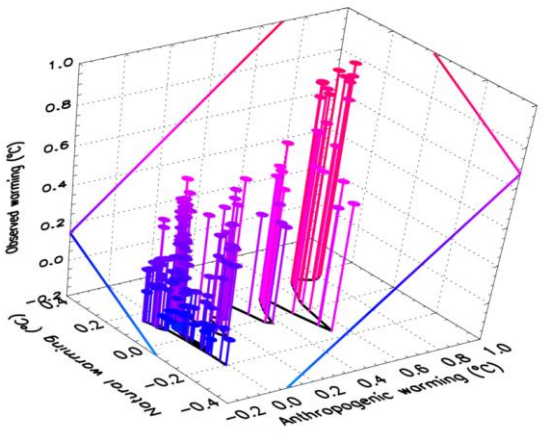

c)

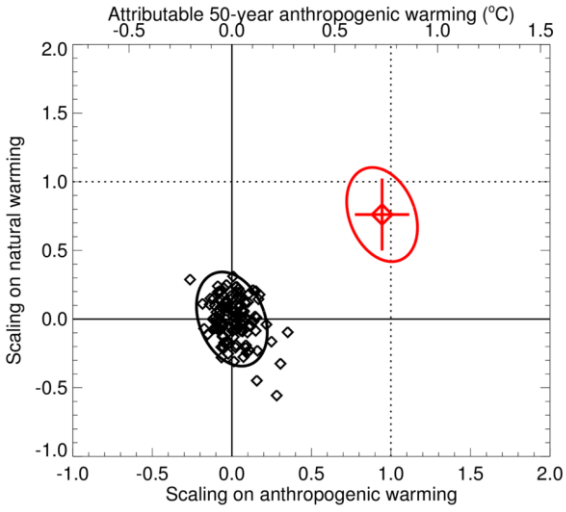

Box 10.1, Figure 1: Schematic of detection and attribution. a) Observed global annual mean temperatures relative to 1880–1920 (coloured dots) compared with CMIP-5 ensemble-mean response to anthropogenic forcing (red), natural forcing (green) and best-fit linear combination (black dotted); b) Observed temperatures versus model-simulated anthropogenic and

natural temperature changes, with best-fit plane shown by coloured square. c) Gradient of best-fit plane in panel (b), or scaling on model-simulated responses required to fit observations (red diamond) with uncertainty estimate (red ellipse and cross) based on CMIP-5 control integrations (black diamonds). Implied anthropogenic warming 1951–2010 indicated by the top axis. Anthropogenic and natural responses noise-reduced with 5-point and 3-point running means respectively.

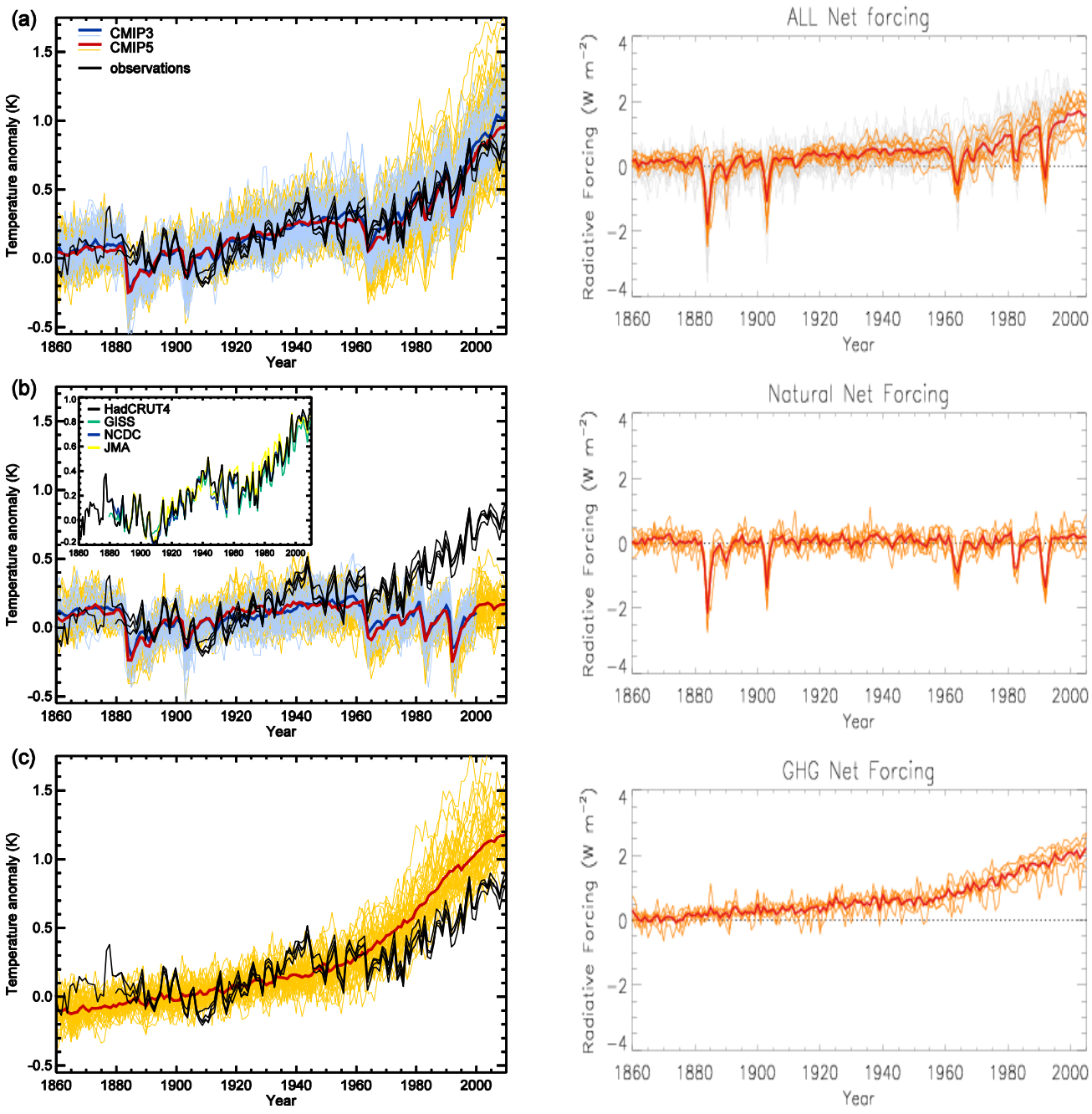

Figure 10.1: Left hand column: Four observational estimates of global mean temperature (black lines) from HadCRUT4, GISTEMP, and NOAA NCDC, JMA, compared to model simulations [both CMIP3 – thin blue lines and CMIP5 models – thin yellow lines] with greenhouse gas forcings only (bottom panel), natural forcings only (middle panel) and anthropogenic and natural forcings (upper panel). Thick red and blue lines are averages across all available CMIP3 and CMIP5 simulations respectively . Ensemble members are shown by thin yellow lines for CMIP5, thin blue lines for CMIP3 All simulated and observed data were masked using the HadCRUT4 coverage, and global average anomalies are shown with respect to 1880–1919, where all data are first calculated as anomalies relative to 1961–1990 in each grid box. Inset to middle panel shows the four observational datasets distinguished by different colours. Right hand column: Net forcings for CMIP3 and CMIP5 models estimated using the method of Forster and Taylor (2006). Ensemble members are shown by thin yellow lines for CMIP5, CMIP5 multi-model means are shown as thick red lines.

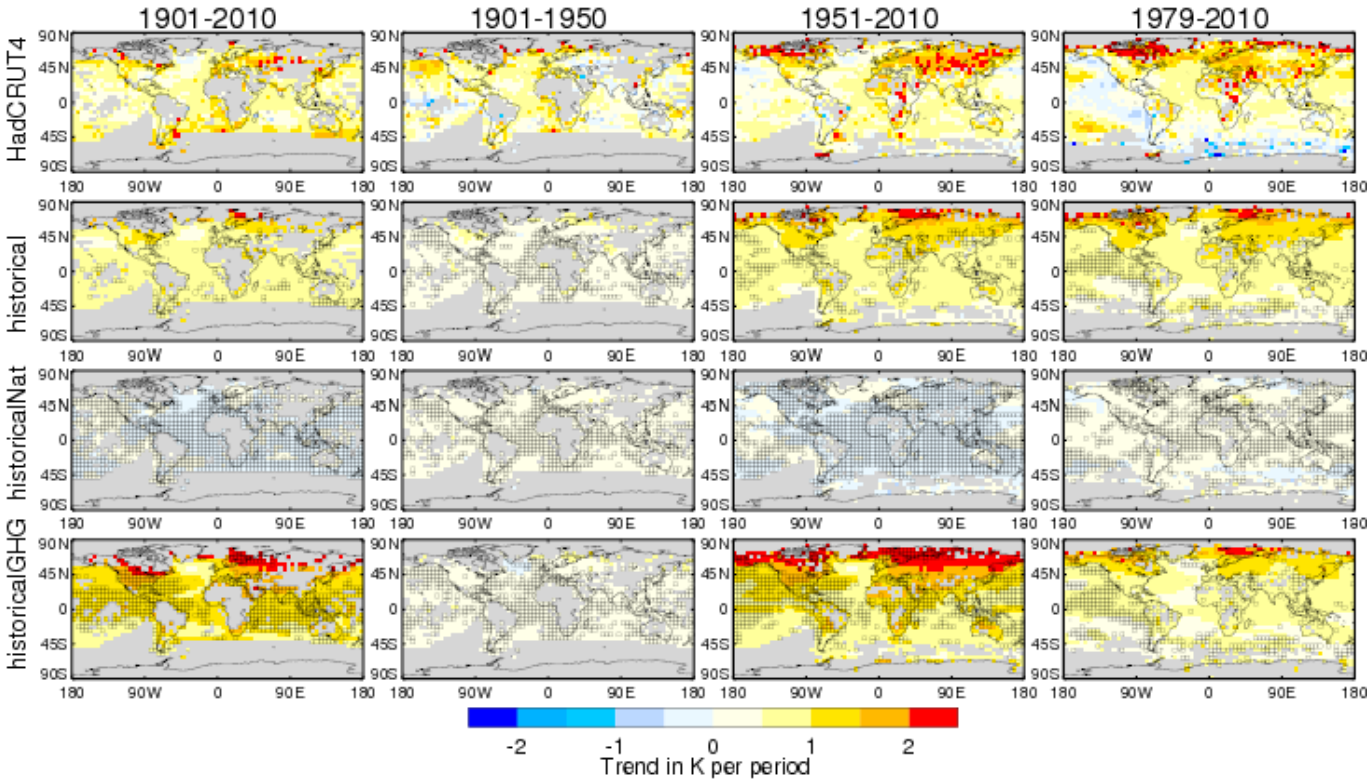

Figure 10.2: Trends in observed and simulated temperatures (K over the period shown) over the 1901–2010, 1901–1950, 1951–2010 and 1979–2010 periods (as labelled). Trends in observed temperatures for the HadCRUT4 dataset (first row), model simulations including anthropogenic and natural forcings (second row), model simulations including natural forcings only (third row) and model simulations including GHG forcings only (fourth row). Trends are shown only where observational data are available in the HadCRUT4 dataset. Boxes in the 2nd, 3rd and 4th rows show where the observed trend lies outside the 5th to 95th percentile range of simulated trends.

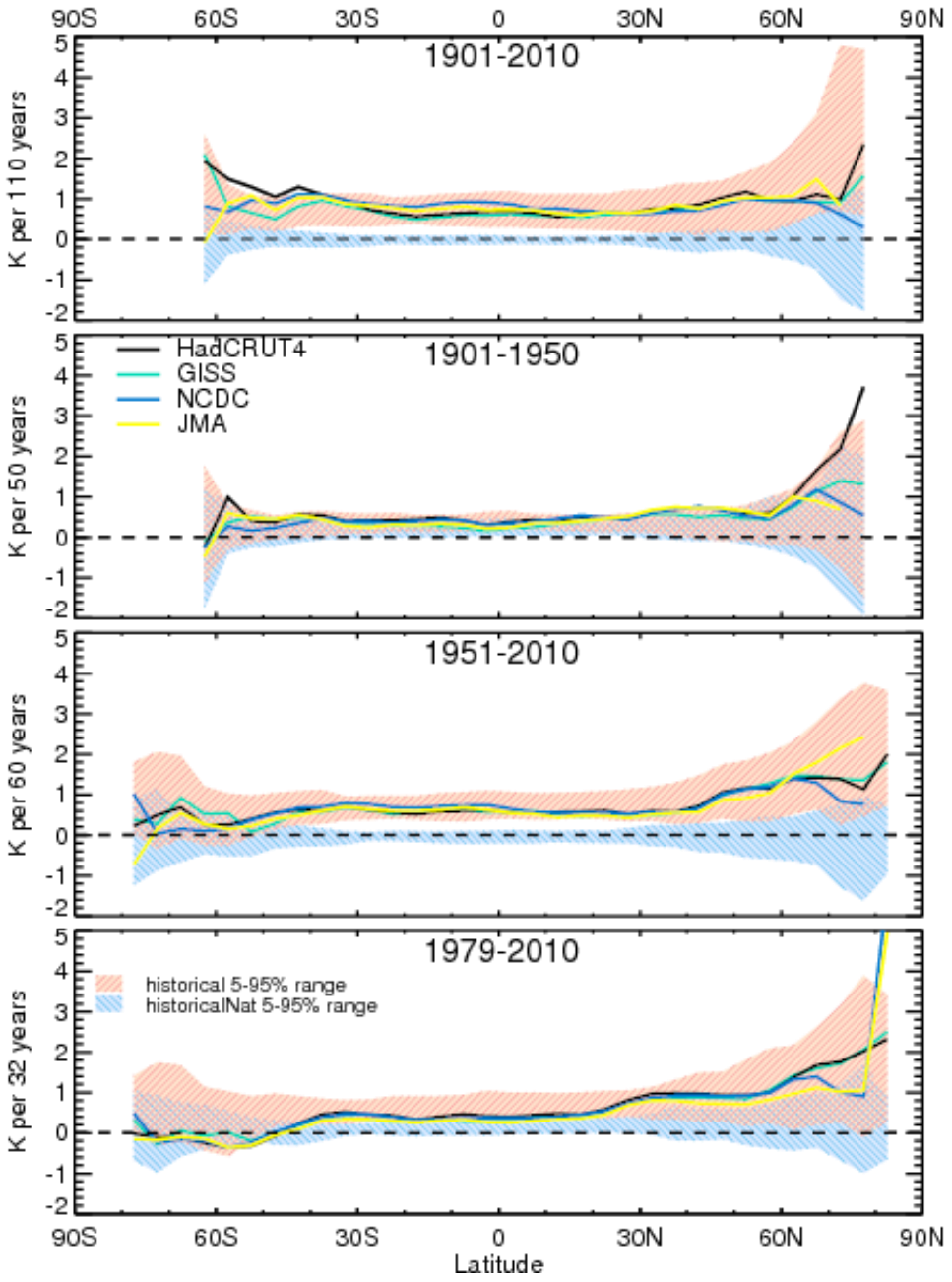

Figure 10.3: Zonal mean temperature trends per period shown. Solid lines show HadCRUT4 (black), GISTEMP (green), NCDC (blue), JMA (yellow) observational datasets, red shading represents the 90% central range of simulations with anthropogenic and natural forcings, blue shading represents the 90% central range of simulations with natural forcings only. All model and observations data are masked to have the same coverage as HadCRUT4.

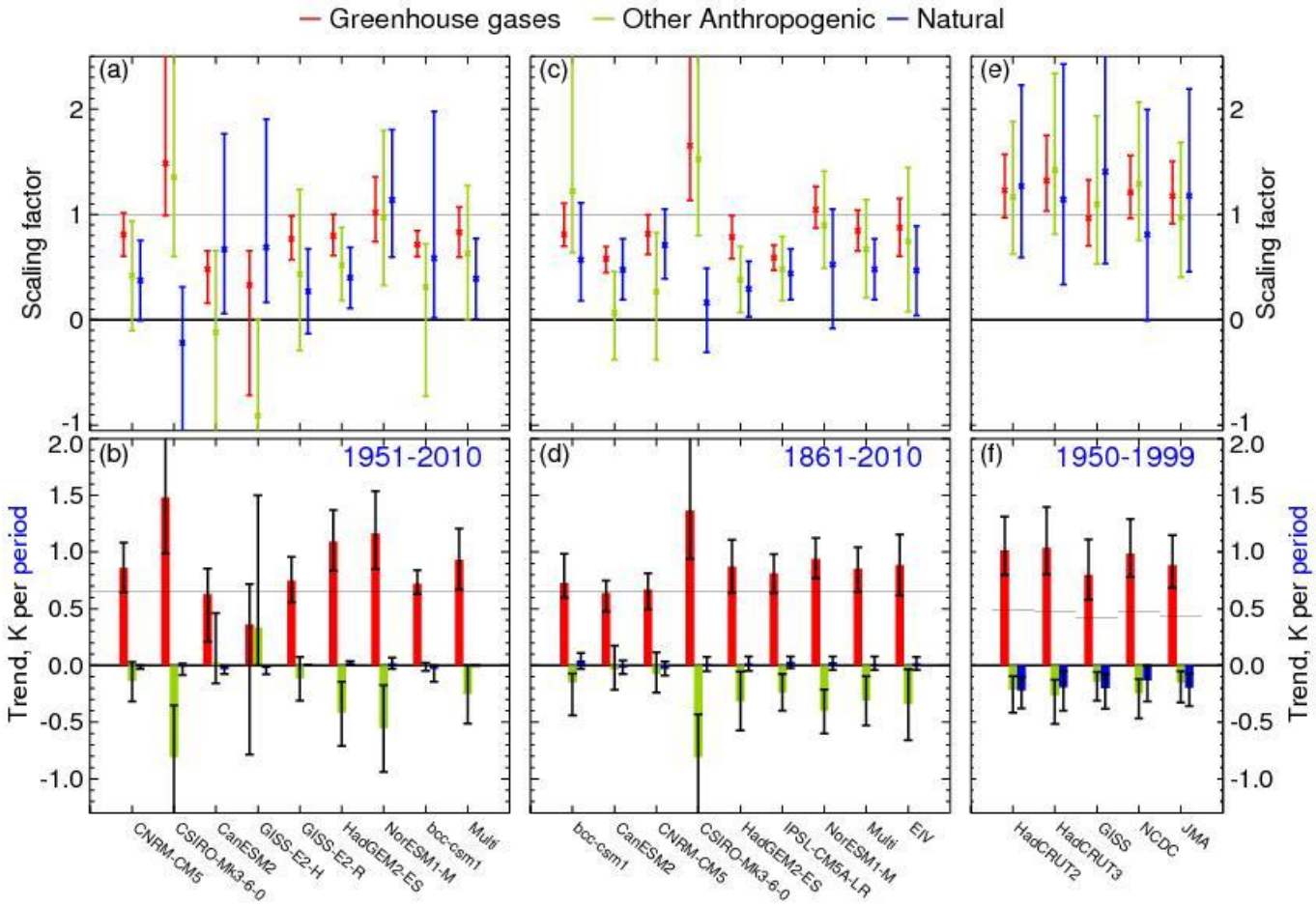

Figure 10.4: Estimated contributions from greenhouse gas (red), other anthropogenic (green) and natural (blue) components to observed global surface temperature changes a) from HadCRUT4 (Morice et al., 2011) showing 5–95% uncertainty limits on scaling factors estimated using eight climate models and a multi-model average (multi) and based on an analysis over the 1951–2010 period and b) The corresponding estimated contributions of forced changes to temperature trends over the 1951–2010 period (Jones et al., 2012). c) and d) As for a) and b) but estimated using seven climate models, a multi-model average (multi), and an estimate taking account of model uncertainty (eiv; Huntingford et al., 2006) based on an analysis over 1861–2010 period (Gillett et al., 2012b) e) and f) as for a) and b) but for the 1900–1999 period, for the HadCM3 model and for five different observational datasets; (HadCRUT2v, HadCRUT3v, GISTEMP, NCDC, JMA. (Jones and Stott, 2011).

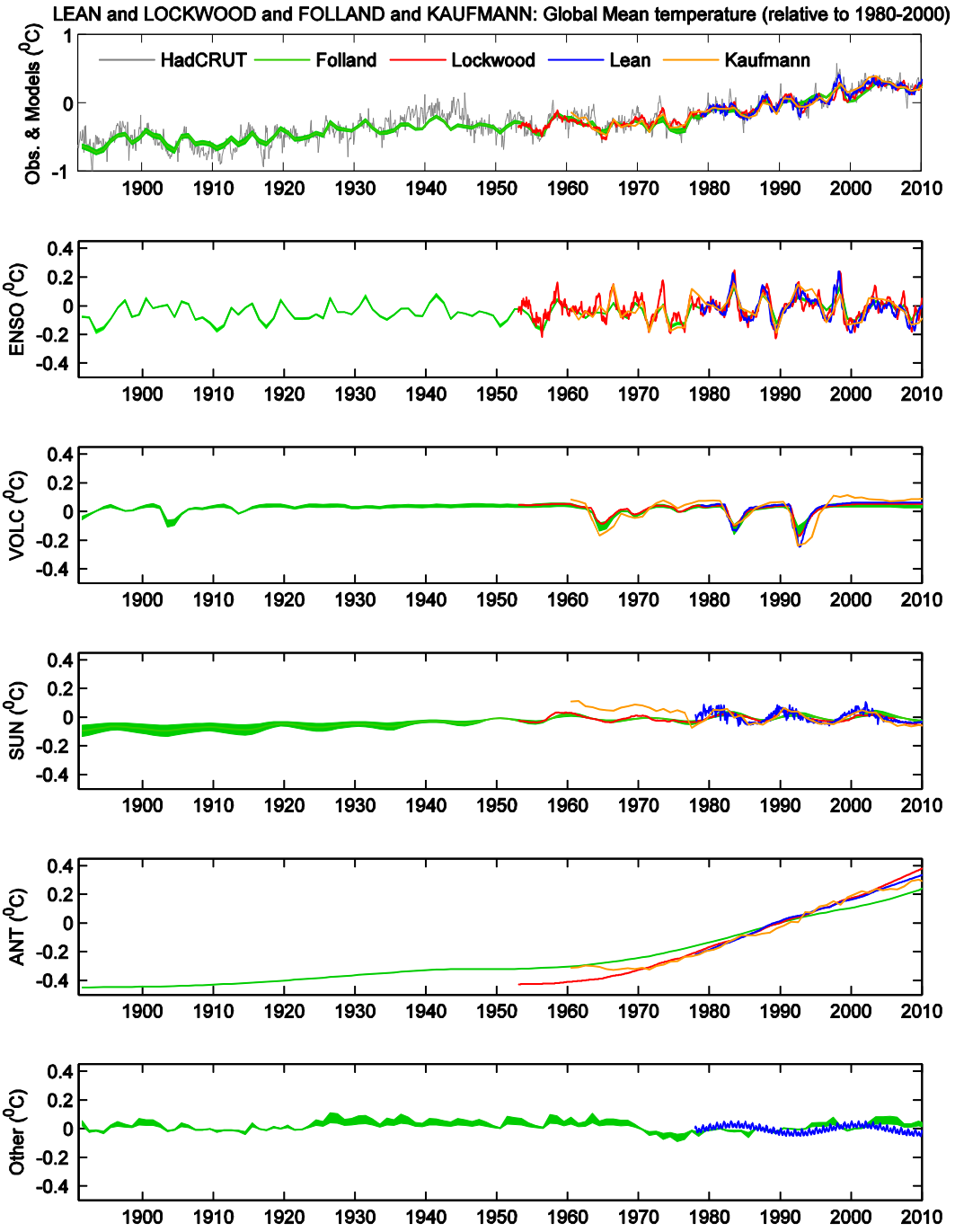

Figure 10.5: Top: the variations of the observed global mean air surface temperature anomaly from HadRCUT3 (grey line) and the best multivariate fits using the method of Lean (blue line) Lockwood (red line), Folland (green line) and Kaufmann (orange line). Below: the contributions to the fit from a) ENSO, b) volcanoes, c) solar contribution, d) anthropogenic contribution and e) other factors (AMO for Folland and a 17.5 year cycle, SAO, and AO from Lean). From Lockwood (2008) Lean and Rind (2009), Folland et al. (2011) and Kaufmann et al. (2011).

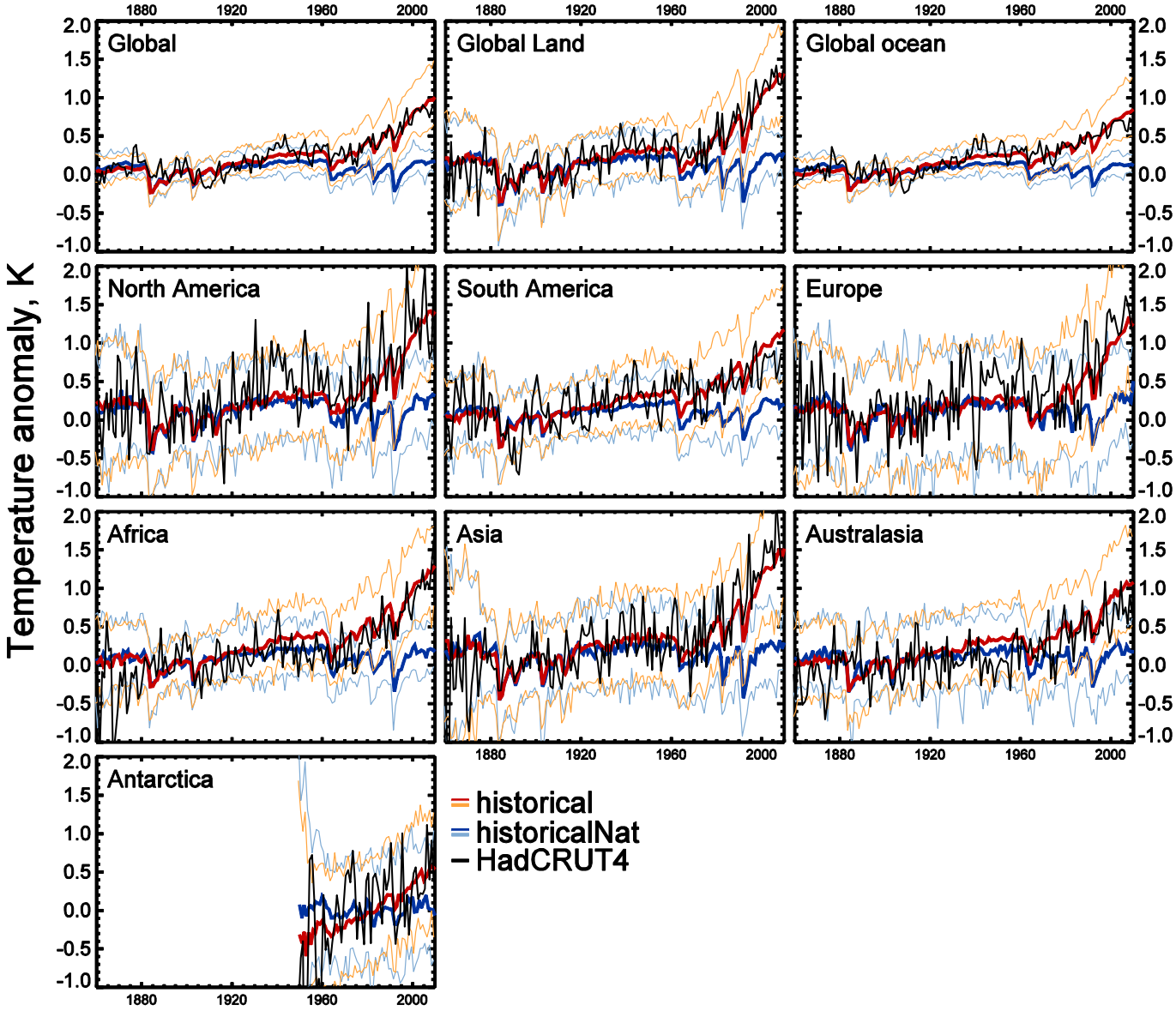

Figure 10.6: Global, land, ocean and continental annual mean temperatures for CMIP3 and CMIP5 historical (red) and historicalNat (blue) simulations (multi-model means shown as thick lines, and 5-95% ranges shown as thin light lines) and for HadCRUT4 (black) for six continental sized regions formed from combining the sub-continental scale regions defned by Seneviratne et al. (2012). Temperatures shown with respect to 1880–1919 apart for Antarctica where temperatures are shown with respect to 1950–2010. From Jones et al. (2012).

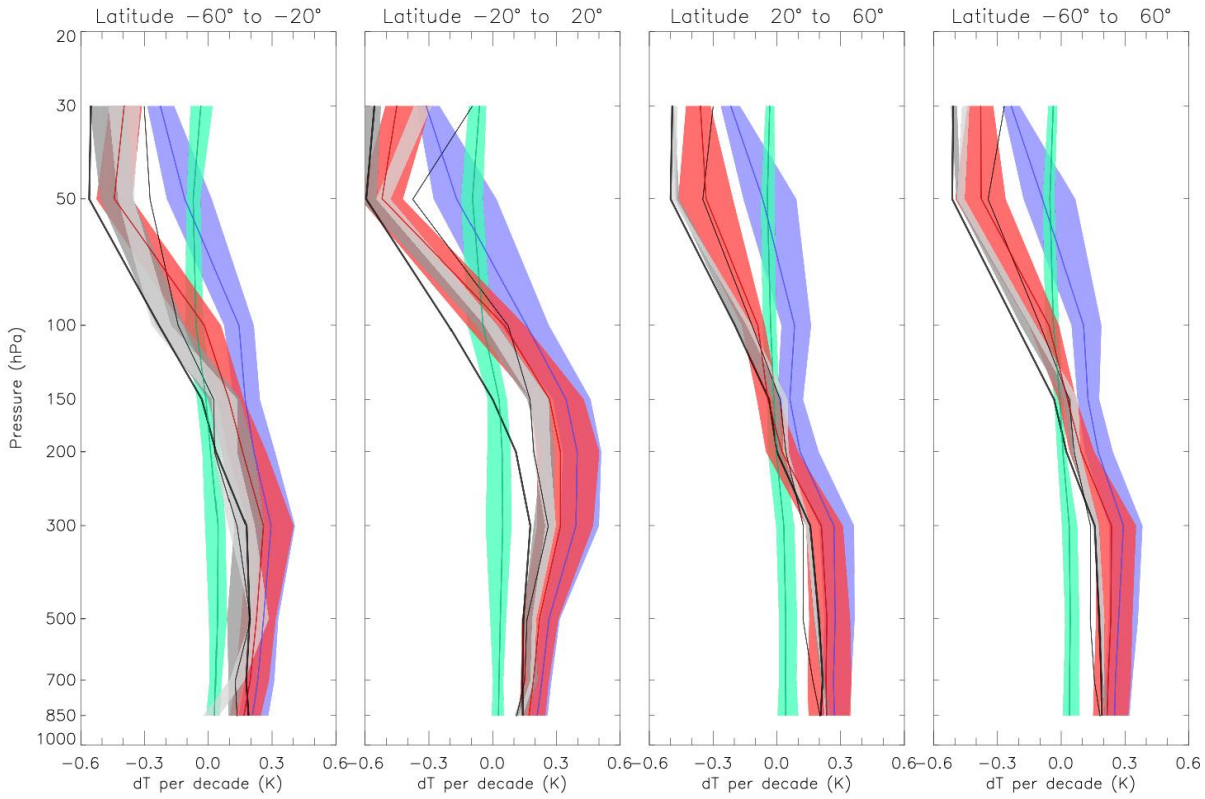

Figure 10.7: Observed and simulated zonal mean temperatures trends from 1961 to 2010 for CMIP5 simulations containing both anthropogenic and natural forcings (red), natural forcings only (green) and greenhouse gas forcing only (blue) where the 5 to 95 percentile ranges of the ensembles are shown. Three radiosonde observations are shown (thick black line: HadAT2, thin black line: RAOBCORE 1.5, dark grey band : RICH-obs 1.5 ensemble and light grey: RICH- τ 1.5 ensemble. After (Lott et al., 2012).

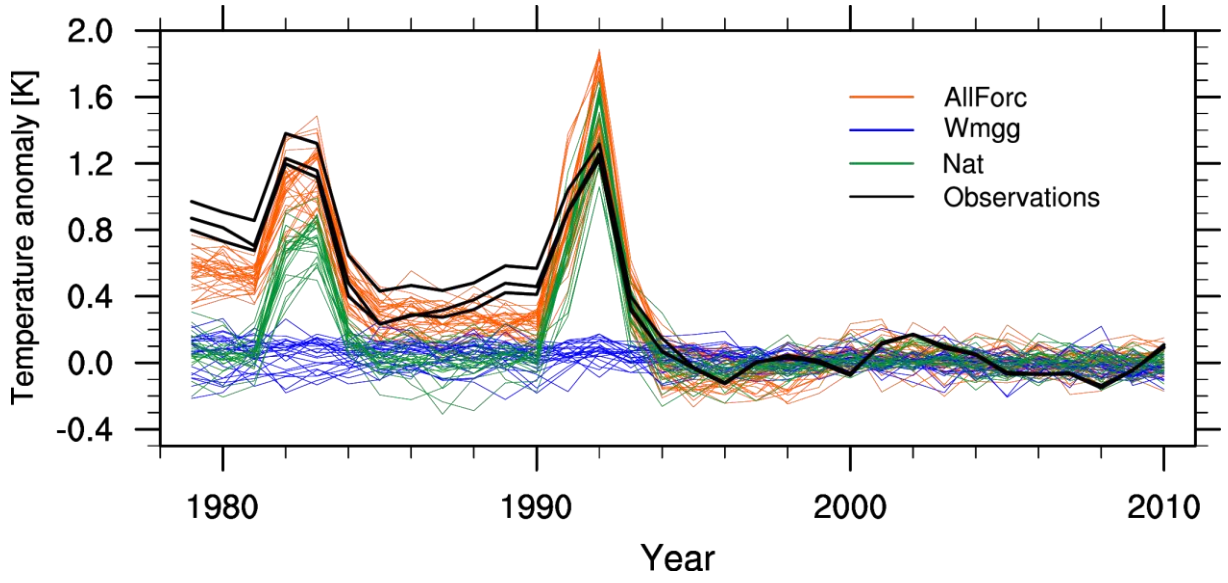

Figure 10.8: Time series (1979–2010) of observed (black) and simulated global mean (82.5°S–82.5°N) MSU lower stratosphere temperature anomalies in a subset of six CMIP5 simulations (Simulations with both anthropogenic and natural forcings (red: Allforc), simulations with increases in well mixed greenhouse gases (blue: Wmghg), simulations with natural forcings (green: Nat) . Anomalies are calculated relative to 1996–2010. Adapted from Ramaswamy et al. (2006).

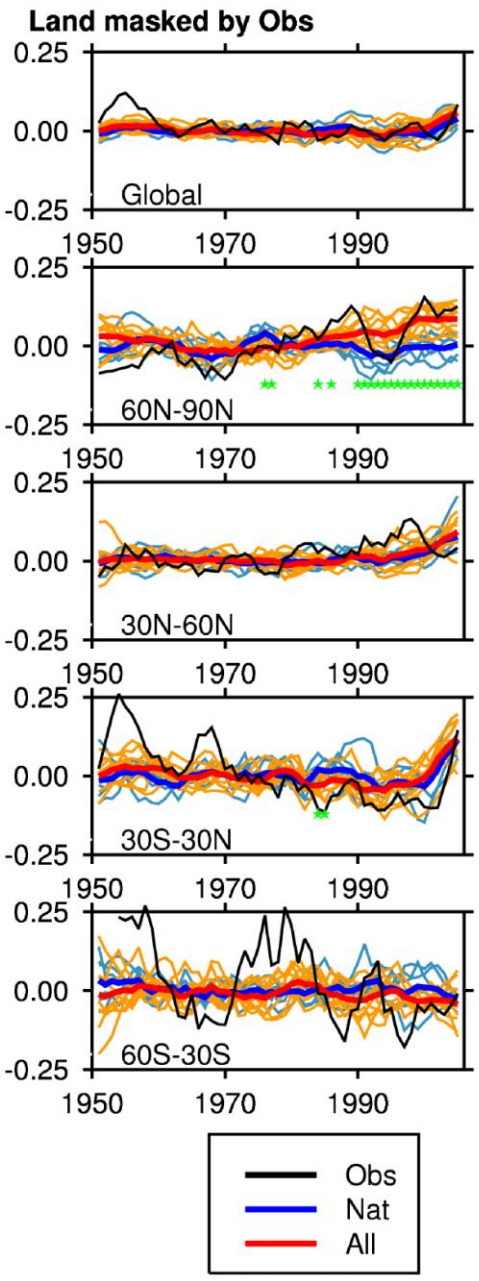

Figure 10.9: Global and zonal changes in annual mean precipitation (mm/day) over areas of land where there are observations, expressed relative to the baseline period of 1961-90, simulated by CMIP5 models forced with both anthropogenic and natural forcings (red lines) and natural forcings only (blue lines) for the global mean and for four latitude bands. Multi-model means are shown in thick solid lines and observations are in black solid line. A 5-year running mean is applied to both simulations and observations. Green stars show statistically significant changes at 5% level (p value <0.05) between the ensemble of runs with both anthropogenic and natural forcings (red lines) and the ensemble of runs with just natural forcings (blue lines) using a two-sample two-tailed t-test for the last 30 years of the time series. From (Balani Sarojini et al., 2012).

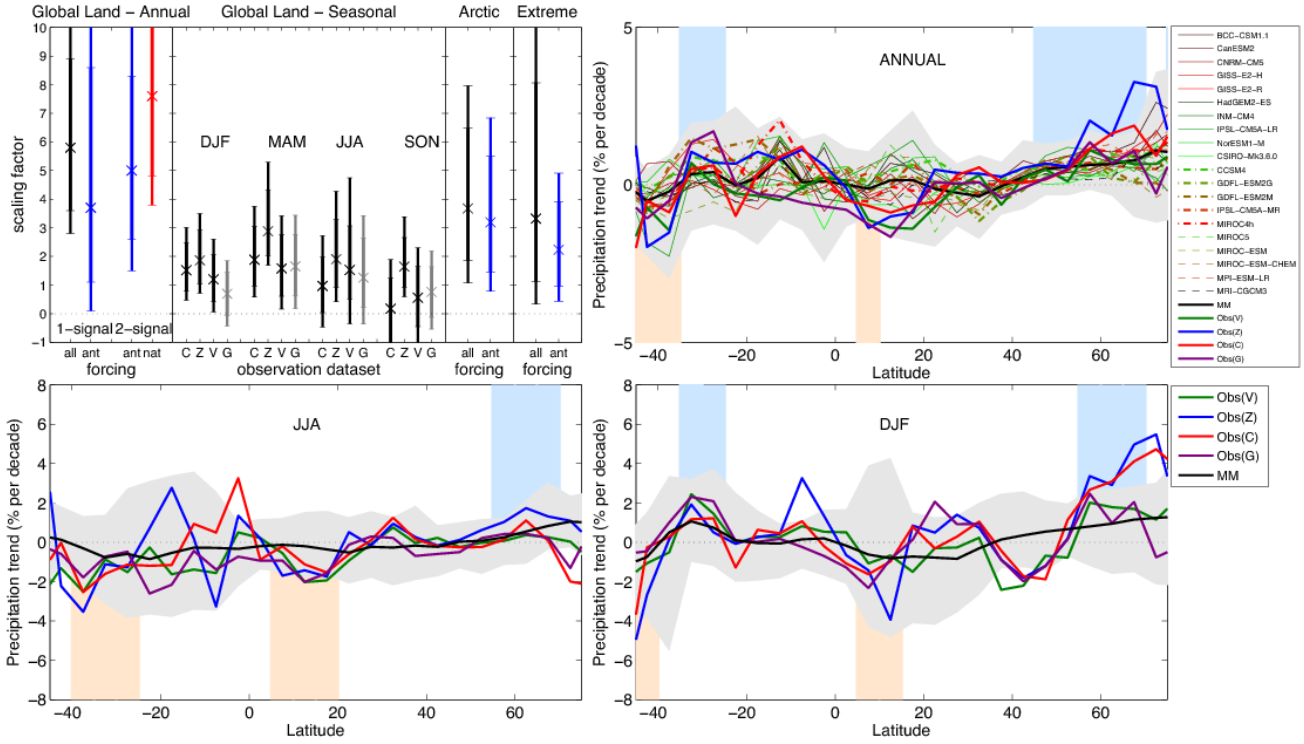

Figure 10.10: Detection and attribution results for precipitation trends in the second half of the 20th century (1951–2005), adapted from Noake et al. (2012), Polson et al. (2012), and for Northern high latitude precipitation (1950–1999) from Min et al. (2008b) and Northern hemisphere land extreme precipitation (1951–1999) from Min et al. (2011). TOP LEFT: Scaling factors for precipitation changes. Crosses show the best-guess scaling factor for the multi-model mean, thick lines are the 5–95% uncertainty range for the raw variance added as noise, and thin lines are the 5–95% uncertainty range for double the variance. In each panel the black bars indicate estimated response to all forcings, red bars to natural forcing and blue bars to anthropogenic-only forcing. Panel labelled "Global land-Annual" shows scaling factors for both single fingerprint and two fingerprint results. Panel labelled "Global land-Seasonal" shows scaling factors resulting from single-fingerprint analyses for zonally and seasonally averaged precipitation, using four different datasets to estimate observed trends. Detectable results are found at the 5% significant level for the three datasets depicted by black bars. Panel labelled "Arctic" shows scaling factors for spatial pattern of Arctic precipitation trends. Panel labelled "Extreme" shows scaling factors for changes of a global-wide intense precipitation index. TOP RIGHT: Thick solid colored lines show observed trends [% per decade] in annual average precipitation relative to climatological means from four observational datasets, as a function of latitude for land points only. The best guess scaled multimodel mean ensemble is shown as a black solid line. Corresponding results from ensembles of 20 different climate models are shown as dashed and thin solid lines. Model results are derived from land points only, masked to match the spatial and temporal coverage of the GPCC dataset (denoted 'G' in the seasonal scaling factor panel). Grey area represents the individual simulations' 5–95% range; vertical shaded bands show where 75% of models yield positive and negative trends, respectively. BOTTOM LEFT, RIGHT: Thick solid colored lines show observed trends [% per decade] relative to climatological means from four observational datasets for JJA (left) and DJF (right) seasons, compared to the range of model simulations (grey shading) with the best guess scaled multimodel mean shown as a black solid line. Blue and orange vertical shaded bands indicate latitude ranges where all observational datasets and the multimodel mean indicate trends with the same sign (positive blue, negative orange).

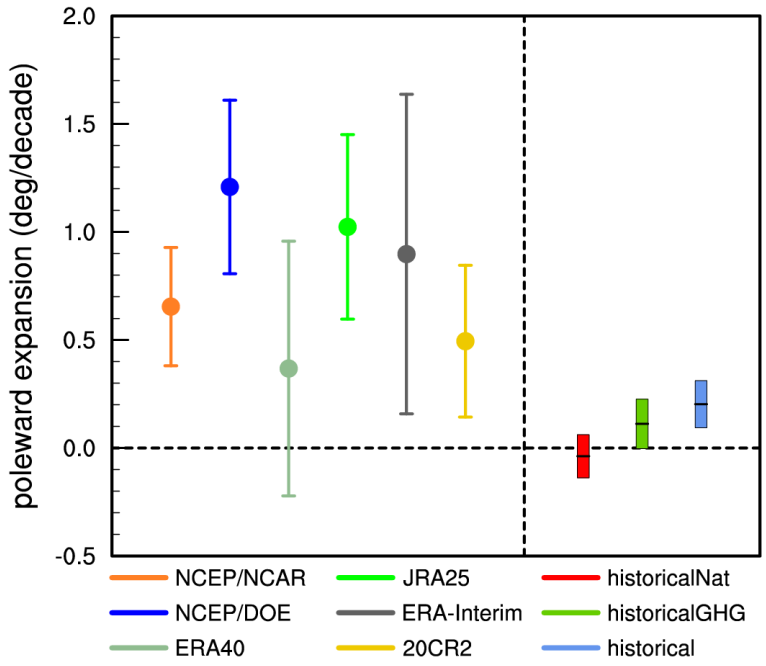

Figure 10.11: December-February mean change of southern border of Hadley. Unit is degree in latitude per decade. Reanalysis datasets are marked with different colors. Trends are all calculated over the period of 1979–2005, except for ERA40 over 1979–2001 and ERA-interim over 1989–2005. According to CMIP5, historicalNAT, historicalGHG, and historical denote historical simulations with natural forcing, observed increasing GHG forcing, and all forcings, respectively. Adapted from Hu et al. (2012).

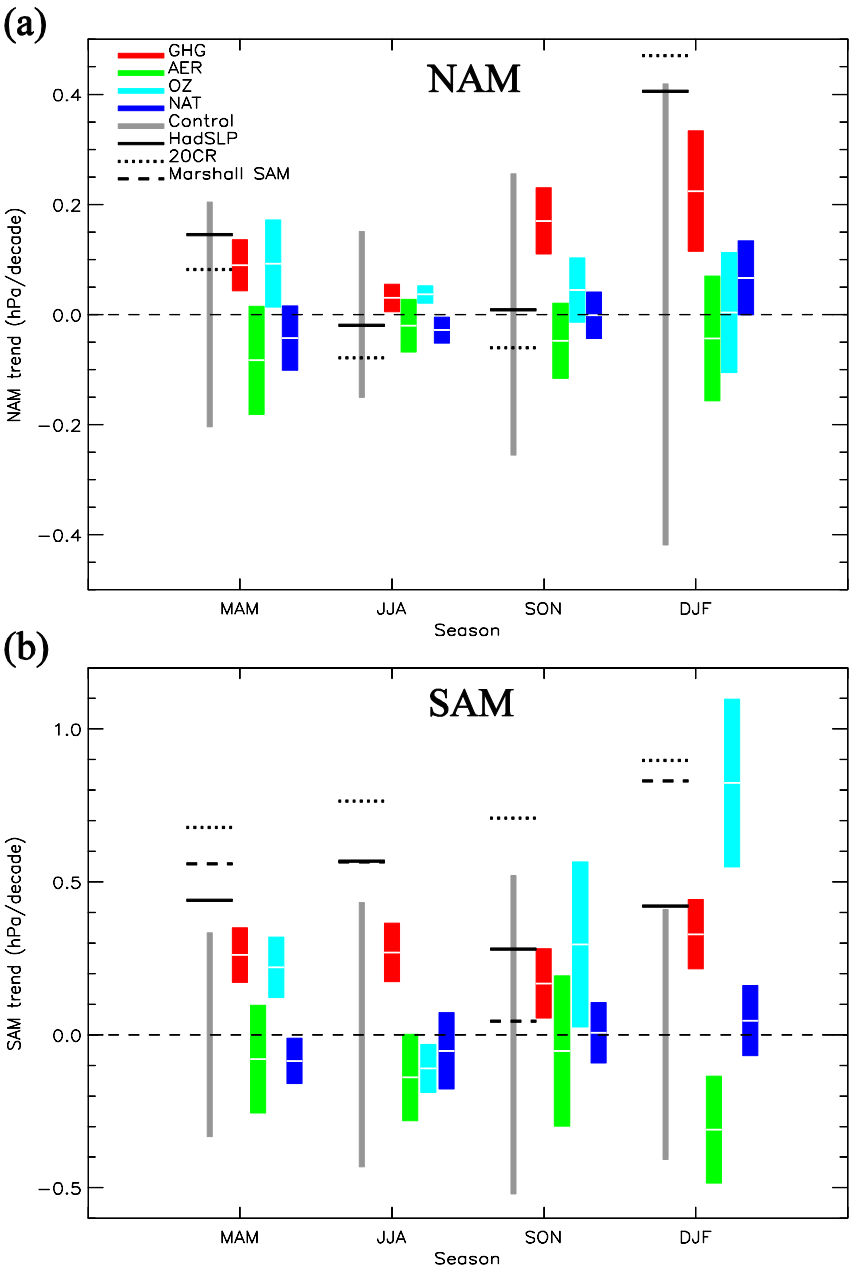

Figure 10.12: Simulated and observed 1951–2011 trends in the Northern Annular Mode (NAM) index (a) and Southern Annular Mode (SAM) index (b) by season. The NAM is a Li and Wang (Li and Wang, 2003) index based on the difference between zonal mean SLP at 35°N and 65°N. and the, and the SAM index is a difference between mean SLP at stations located at close to 40°S and stations located close to 65°S (Marshall, 2003). Both indices are defined without normalisation, so that the magnitudes of simulated and observed trends can be compared. Black lines show observed trends from the HadSLP2r dataset (Allan and Ansell, 2006) (solid), the 20th Century Reanalysis (Compo et al., 2011) (dotted) and the Marshall (2003) SAM index (dashed). While the synthetic Marshall indices have data present from 1951, the Marshall (2003) index itself begins in 1957. Grey bars show approximate 5th-95th percentile ranges of control trends, and coloured bars show 5–95% significance ranges for ensemble mean trends in response to greenhouse gas (red), aerosols (green), ozone (light blue) and natural (dark blue) forcings, based on CMIP5 individual forcing simulations. Taken from Gillett and Fyfe (2012).

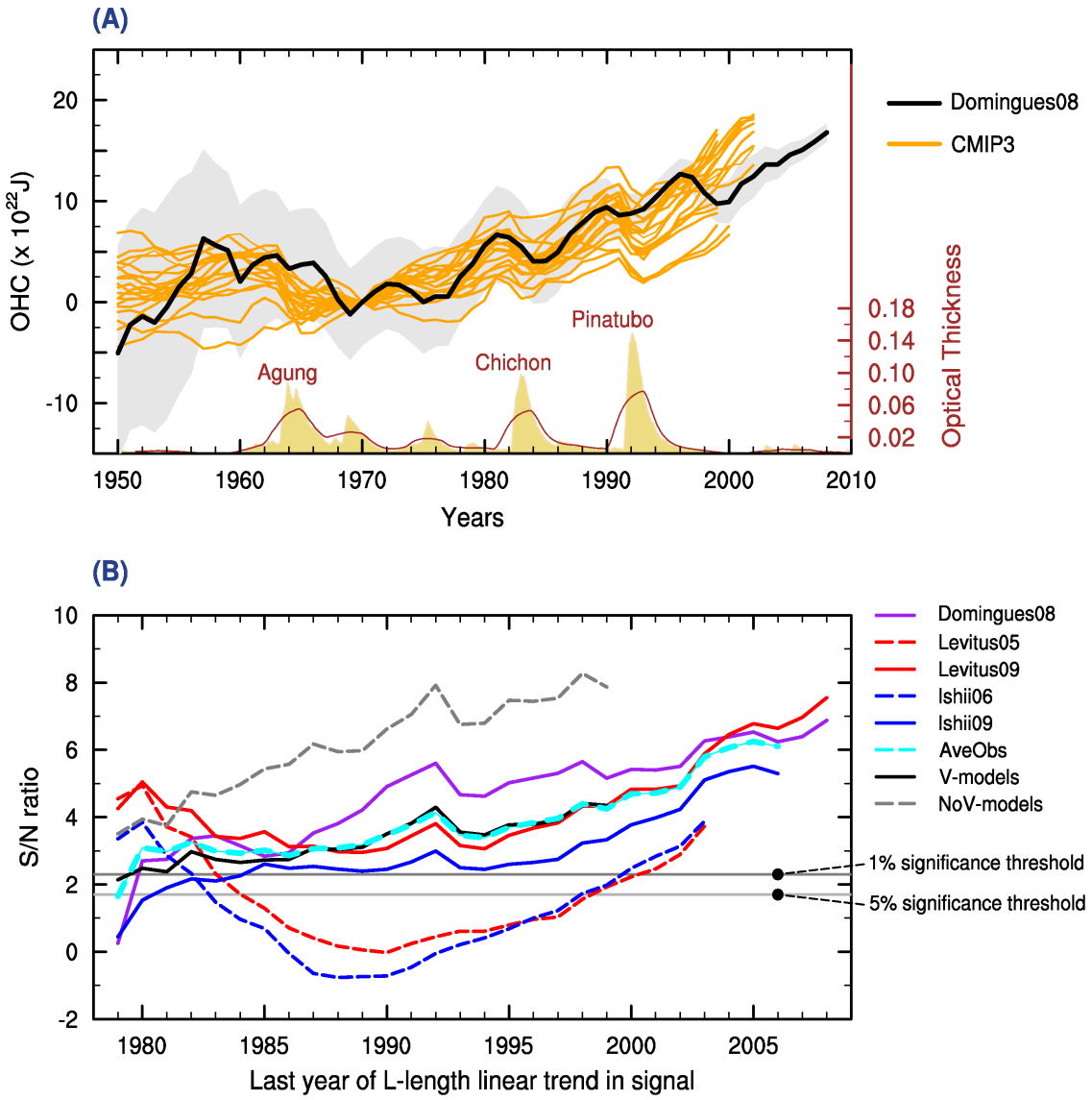

Figure 10.13: A) Comparison of observed global ocean heat content for the upper 700 m with simulations from six CMIP3 models that included anthropogenic and natural (solar and volcanic) forcings. The timing of volcanic eruptions and associated aerosol loadings are shown at base of panel (Domingues et al., 2008), B) Signal-to-noise (S/N) ratio (plotted as a function of increasing trend length L) of basin-scale changes in volume averaged temperature of newer, XBT-corrected data (solid red, orange and blue lines), older, uncorrected data (dashed red and orange lines); the average of the three corrected observational sets (AveObs; dashed purple line); and V and NoV models (black and grey solid lines respectively). The 1% and 5% significance thresholds are shown (as horizontal grey lines) and assume a Gaussian distribution of noise trends in the V-models control-run pseudo-principal components. The detection time is defined as the year at which S/N exceeds and remains above a stipulated significance threshold (Gleckler et al., 2012).

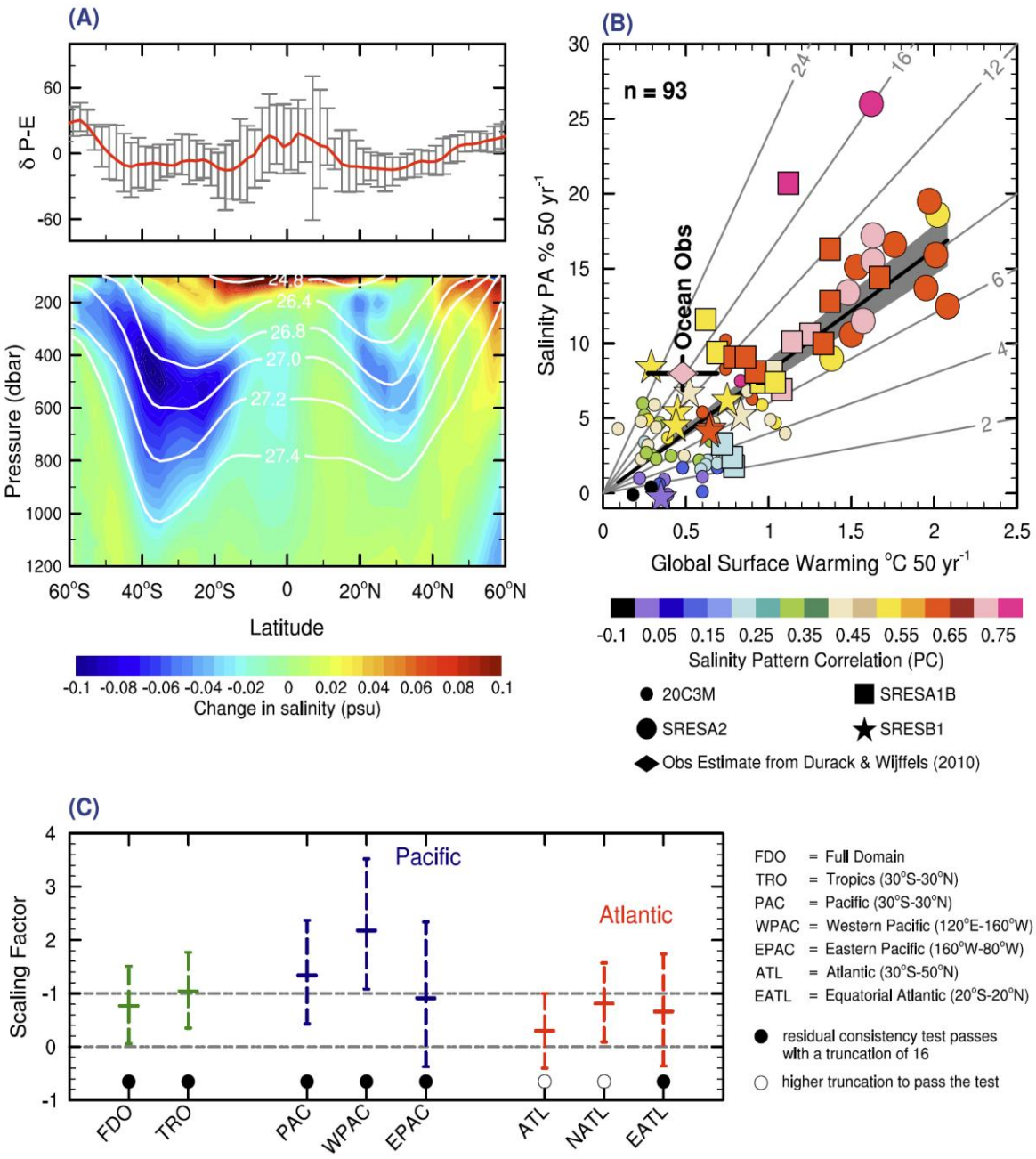

Figure 10.14: Ocean salinity change and hydrologic cycle. (A) Ocean salinity change observed in the interior of the ocean (A, lower panel) and comparison with 10 CMIP3 model projections of precipitation minus evaporation for the same period as the observed changes (1970 to 1990's) (A, top panel). (B) The amplification of the current surface salinity pattern over a 50 year period as a function of global temperature change. Ocean surface salinity pattern amplification has an 8% increase for the 1950 to 2000 period, and a correlation with surface salinity climatology of 0.7 (see text, and Section 3.3). Also on this panel coupled CMIP3 AOGCM with all forcings emission scenarios and from 20th and 21st century simulations. A total of 93 simulations have been used. The colours filling the simulation symbols indicate the correlation between the surface salinity change and the surface salinity climatology. Dark red is a correlation of 0.8 and dark blue is 0.0. (C) Regional detection and attribution in the equatorial Pacific and Atlantic Oceans for 1970 to 2002. Scaling factors for all forcings (anthropogenic) fingerprint are show (see Box 10.1) with their 5–95% uncertainty range, estimated using the total least square approach. Full domain (FDO, 30°S–50°N), Tropics (TRO, 30°S–30°N), Pacific (PAC, 30°S–30°N), west Pacific (WPAC, 120°E–160°W), east Pacific (EPAC, 160°W–80°W), Atlantic (ATL, 30°S–50°N), subtropical north

Atlantic (NATL, 20°N–40°N) and equatorial Atlantic (EATL, 20°S–20°N) factors are shown. Black filled dots indicate when the residual consistency test passes with a truncation of 16 whereas empty circles indicate a needed higher truncation to pass the test. (A, B and C) are from (Helm et al., 2010), (Durack et al., 2012) and (Terray et al., 2011), respectively.

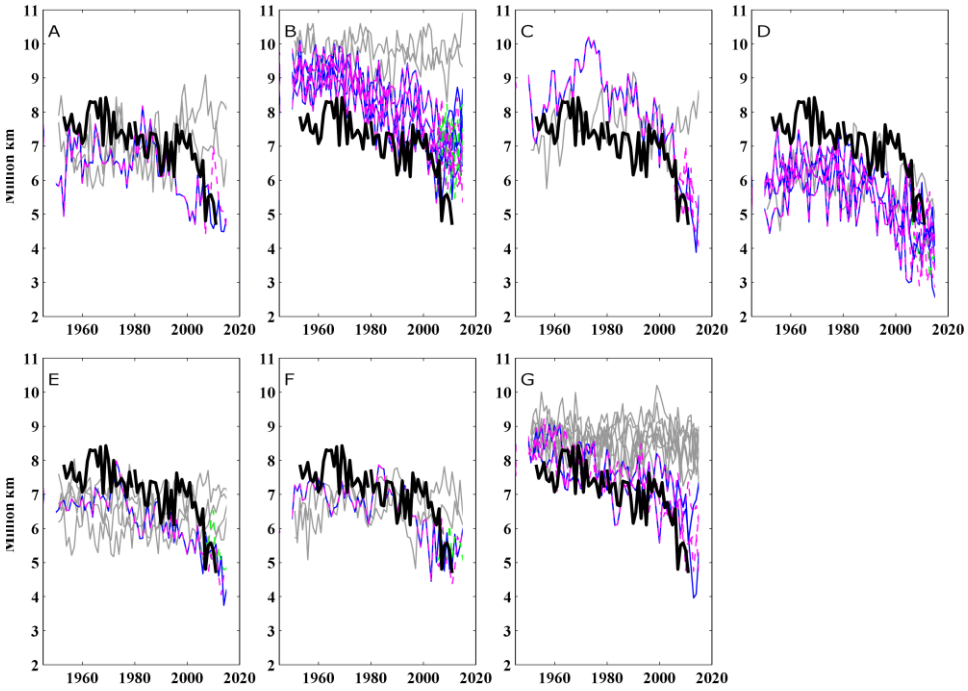

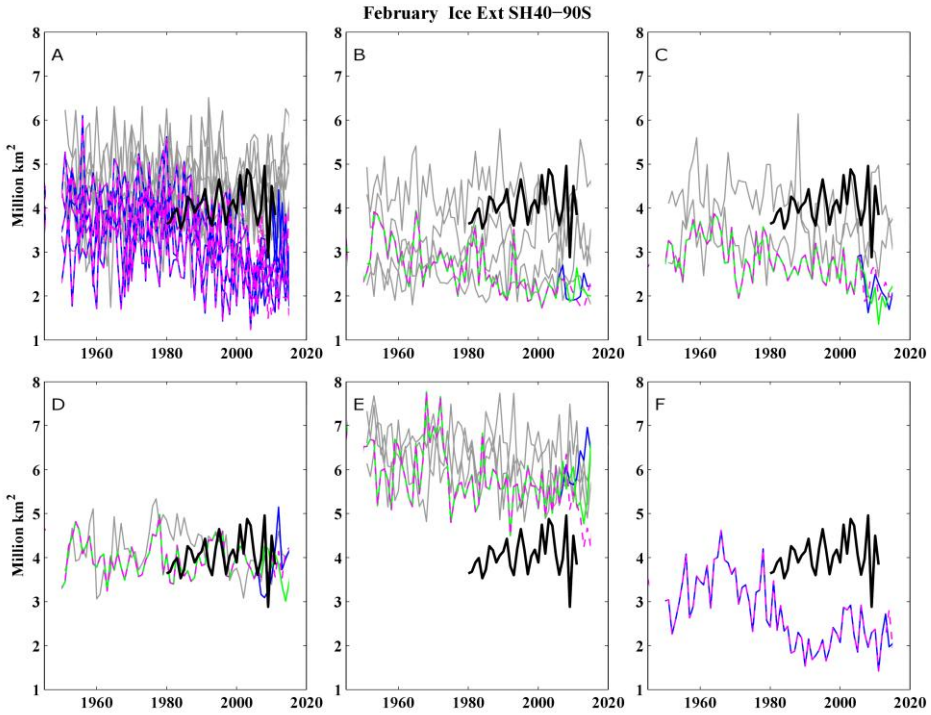

Figure 10.15: a) Northern Hemisphere September sea ice extent (>15% ice concentration) simulated by the seven CMIP5 models that matched the mean minimum and seasonality with less than 20% error compared with observations. The thin grey lines are based on pre-industrial control simulations (piControl). The coloured lines are historical runs (1950–2005) together with forced simulations (blue for RCP4.5, green for RCP6.0, and magenta for RCP8.5 emissions scenarios for the period 2006–2015). The thick black line is base on Hadley sea ice analysis (HadleyISST_ice). Panels A-G are models:

CCSM4, HadGEM2CC, HadGEM2ES, MIROC−ESM, MIROC−ESMC, MPI−ESM−lr, and ACCESS1. **b)** Similar to a) but for the Southern Hemisphere. Panels A-F are models: CanESM2, MIROC-ESM, MIROC-ESMC, MRI-CGCM3, NorESM1 and BCC-CSM1. For Antarctic sea ice we show results for two models that passed the same selection criteria as for the Northern Hemisphere and the next four models with lowest error scores. Note that the presented models are different for the Northern and Southern Hemisphere based on the selection criteria.

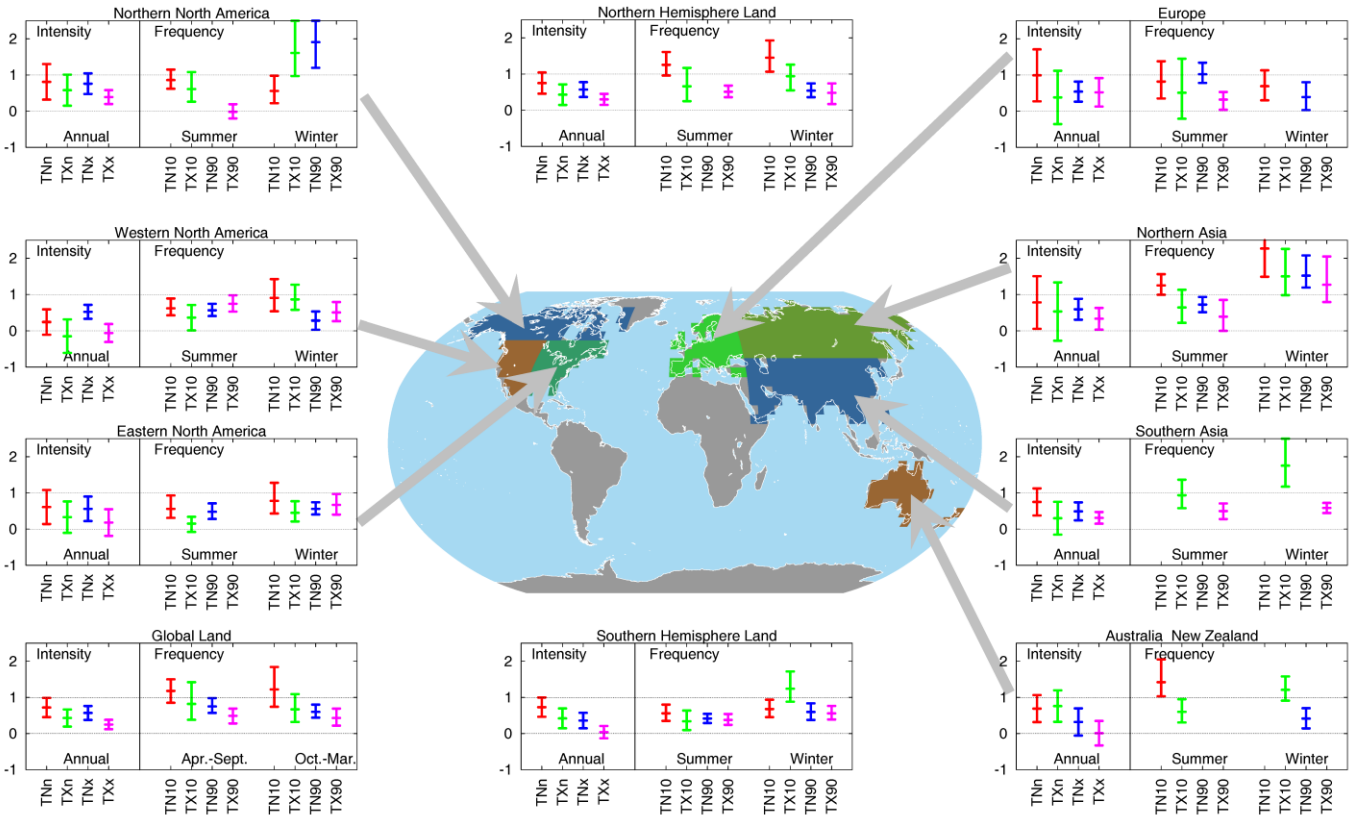

Figure 10.16: Detection results for changes in intensity and frequency of extreme events. Left side of each panel show scaling factors and their 90% confidence intervals for intensity of annual extreme temperatures in response to external forcings for the period 1951–2000. TNn and TXn represent annual minimum daily minimum and maximum temperatures, respectively, while TNx and TXx represent annual maximum daily minimum and maximum temperatures (updated from (Zwiers et al., 2011), fingerprints are based on simulations of CanESM2 with both anthropogenic and natural forcings). Right hand sides of each panel show scaling factors and their 90% confidence intervals for changes in thefrequency of temperature extremes for winter (October-March for Northern Hemisphere and April-September for Southern Hemisphere), and summer half years. TN10, TX10 are respectively the frequency for daily minimum and daily maximum temperatures falling below their 10th percentiles for the base period 1961–1990. TN90 and TX90 are the frequency of the occurrence of daily minimum and daily maximum temperatures above their respective 90th percentiles calculated for the 1961–1990 base period (Morak et al., 2012), fingerprints are based on simulations of HadGEM1 with both anthropogenic and natural forcings). Detection is claimed at the 10% significance level if the 90% confidence interval of a scaling factor is above zero line.

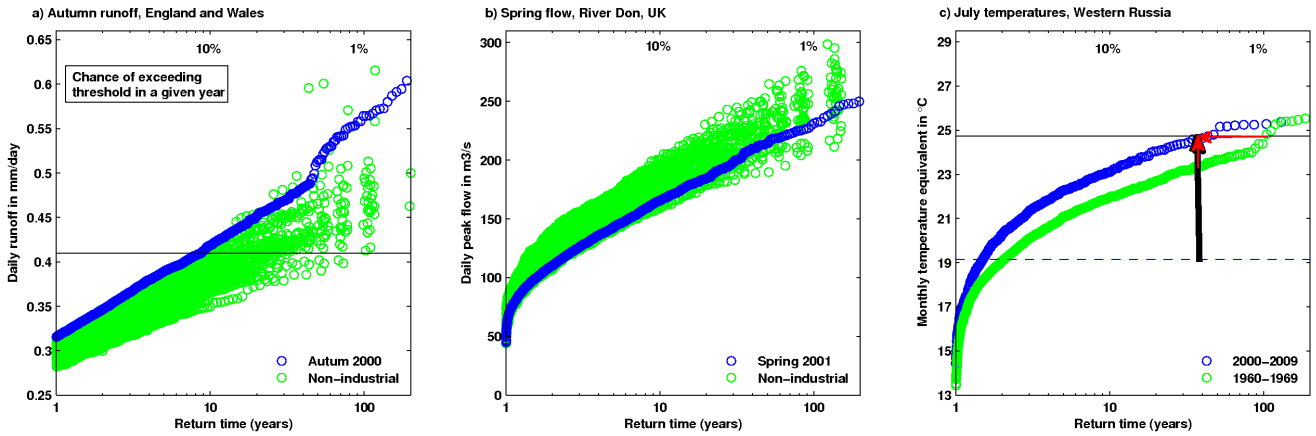

Figure 10.17: Return times for precipitation-induced floods aggregated over England and Wales for (a) conditions corresponding to October to December 2000 with boundary conditions as observed (blue) and under a range of simulations of the conditions that would have obtained in the absence of anthropogenic greenhouse warming over the 20th century – colours correspond to different AOGCMs used to define the greenhouse signal, black horizontal line to the threshold exceeded in autumn 2000 – from Pall et al. (2011); (b) corresponding to January to March 2001 with boundary conditions as observed (blue) and under a range of simulations of the condition that would have obtained in the absence of anthropogenic greenhouse warming over the 20th century (green; adapted from Kay et al., (2011b)); (c) return periods of temperature-geopotential height conditions in the model for the 1960s (green) and the 2000s (blue). The vertical black arrow shows the anomaly of the Russian heatwave 2010 (black horizontal line) compared to the July mean temperatures of the 1960s (dashed line). The vertical red arrow gives the increase in temperature for the event whereas the horizontal red arrow shows the change in the return period.

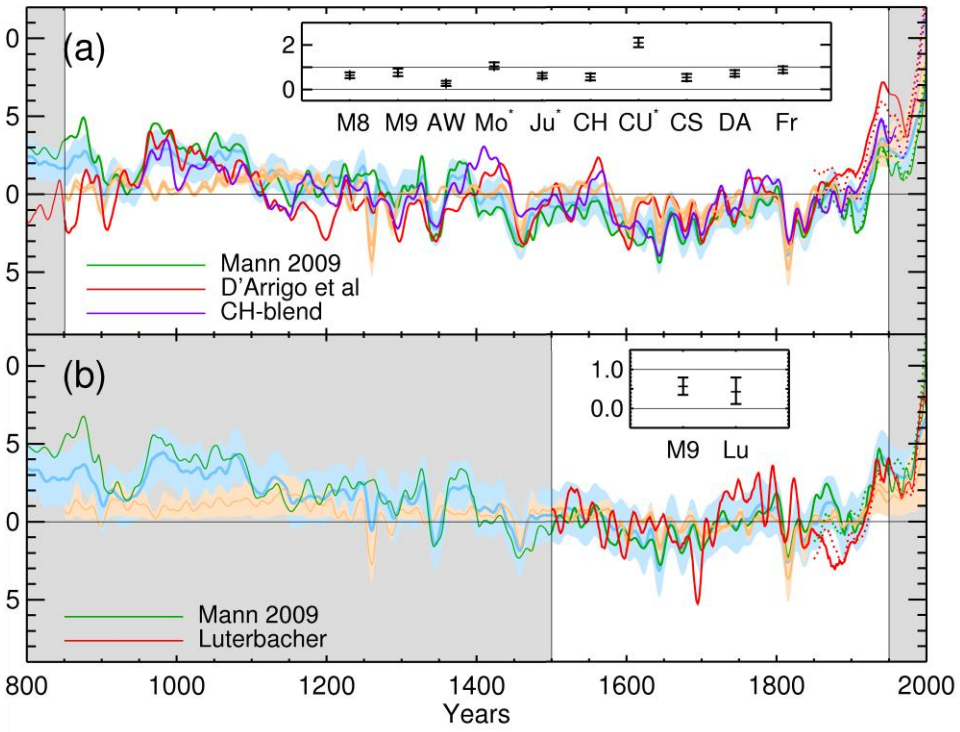

Figure 10.18: The top panel compares the mean annual Northern hemisphere surface air temperature from a multi-model ensemble to several NH temperature reconstructions, CH-blend from Hegerl et al. (2007a) in purple, which is a reconstruction of 30°N–90°N land only, Mann et al. (2009), plotted for the region 30°N–90°N land and sea (green) and D'Arrigo et al. (2006) in red, which is a reconstruction of 20°N–90°N land only. All results are shown with respect to the reference period 850–1950 (or for a shorter period depending on the maximum range of the reconstruction). The multi-model mean for the relevant region is scaled to fit each reconstruction in turn, using a total least squares (TLS) method (see e.g., Allen and Stott, 2003), with a 5–95% error range in scaling shown in orange with light orange shading. The best fit scaling values for each reconstruction are given in the insert as well as the scaling range for sixth other reconstructions (M8 – (Mann et al., 2008; Mann et al., 2009); AW – (Ammann and Wahl, 2007); Mo - (Moberg et al., 2005); Ju - (Juckes et al., 2007); CH – (Hegerl et al., 2007a); CL – (Christiansen and Ljungqvist, 2011) and inverse regressed onto the instrumental record CS; DA – (D'Arrigo et al., 2006); (Frank et al., 2007; Frank et al., 2010). An asterisk next to the reconstruction name indicates that the residuals (over the more robustly reconstructed period 1401–1950) are inconsistent with the internal variability generated by the control simulations of every climate model investigated (for details see Schurer et al., 2012) Also included on this plot are the NH temperature anomalies calculated in Goosse et al. (2012b) using a data-assimilation technique constrained by the Mann et al. (2009) temperature reconstruction using data from 30°N–90°N. This is plotted in blue, for the region 30°N–90°N land and sea, with the error range shown in light blue shading. The second panel is similar to the top panel, but showing the European region. The TLS scaling factors are calculated only for the period 1500–1950 for two reconstructions: (Luterbacher et al., 2004) for the region 35°N–60°N,-25°E–40°E, land only in red and labelled Lu in the insert and (Mann et al., 2009) averaged over the region 25°N–65°N, 0°–60°E, land and sea, in green and labelled M9 in the insert. The dotted coloured lines show the corresponding instrumental data. Also shown is the simulation from Goosse et al. (2012a) with data-assimilation constrained by the Mann et al. (2009) reconstruction. This is plotted in blue for the region 25°N–65°N, 0°–60°E, land and sea, with the error range shown in light blue shading.

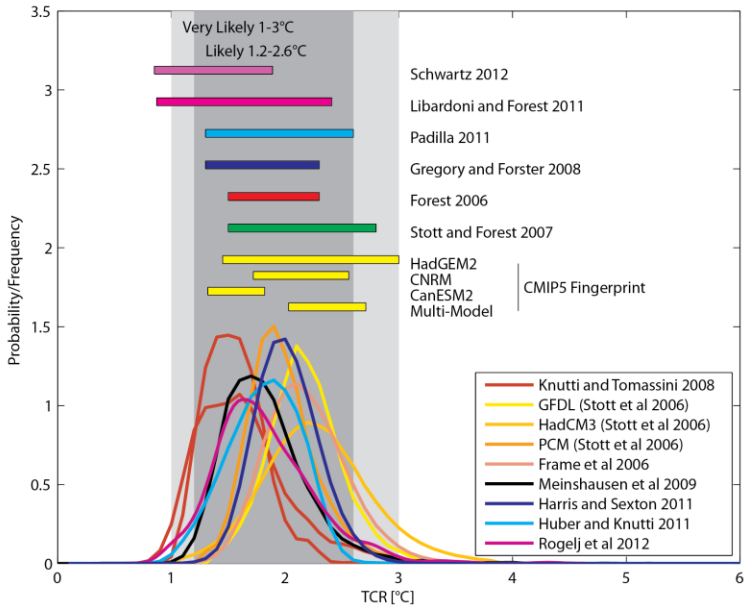

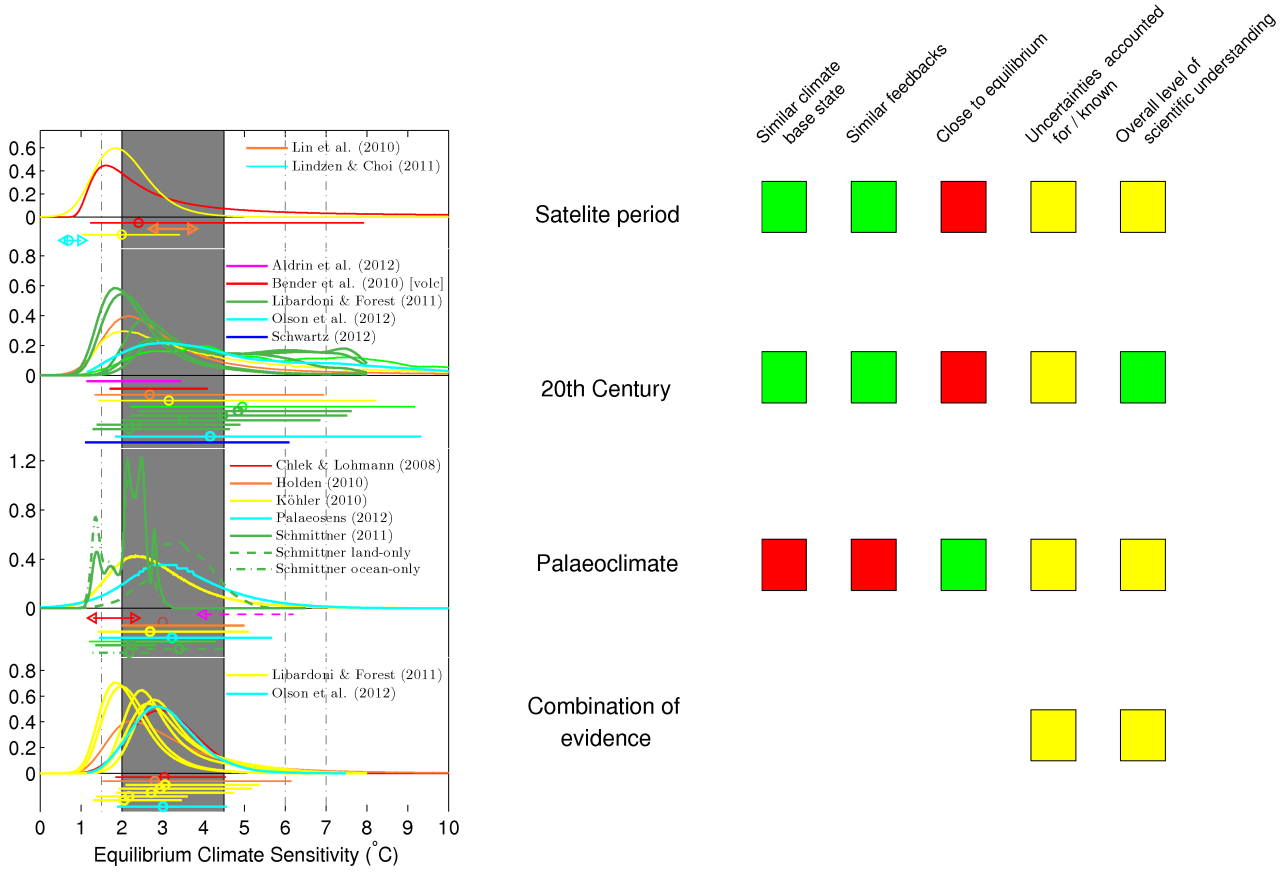

Figure 10.19: Top: Distributions of the transient climate response (TCR, top) and the equilibrium climate sensitivity (bottom). PDFs and ranges (5–95%) for the transient climate response estimated by different studies (see text). The grey shaded range marks the very likely range of 1°C–3°C for TCR as assessed in this section. Bottom: Estimates of equilibrium climate sensitivity from observed / reconstructed changes in climate compared to overall assessed likely range (grey). The figure compares some selected old estimates used in AR4 (no labels) with new estimates available since (labelled).

Distributions are shown where available, together with 5–95% ranges. Ranges that have been queried in the literature or have problematic assumptions are labelled by arrows at the border. Estimates are based on top-of the atmosphere radiative balance (top row), instrumental changes including surface temperature (2nd row); changes from palaeoclimatic data (3rd row), and studies using nonuniform priors or combining evidence (for details of studies, see text; fourth row). The boxes on the right hand side indicate limitations and strengths of each line of evidence given in a separate panel, for example, if a period has a similar climatic base state, if feedbacks are similar to those operating under CO_2 doubling, if the observed change is close to equlibrium, if, between all lines of evidence plotted, uncertainty is accounted for relatively completely, and summarizes the level of scientific understanding of this line of evidence overall. Green marks indicate an overall line of evidence that is well understood, has small uncertainty, or many studies and overall high confidence. Yellow indicates medium and red low confidence (i.e., poorly understood, very few studies, poor agreement, unknown limitations). After Knutti and Hegerl (2008). The data shown is as follows. Satellite period: (orange) (Lin et al., 2010a) (cyan) (Lindzen and Choi, 2011) (yellow) (Forster and Gregory, 2006), using a uniform prior on feedbacks and (red) using a uniform prior on ECS; 20th Century: (pink) (Aldrin et al., 2012), using different assumptions and priors,, (dark green) (Libardoni and Forest, 2011), based on 5 observational datasets, (cyan) Olson et al., (2012), (dark blue) (Schwartz, 2012), (green) Knutti et al, 2002; (yellow) Gregory et al., 2002; (orange) Frame et al., 2005; (red) (Bender et al., 2010) Palaeoclimate: (red) (Chylek and Lohmann, 2008b), (orange) (Holden et al., 2010) (yellow) (Koehler et al., 2010) (cyan) (Paleosens Members (E.J. Rohling and R.S.W. van de Wal, 2012) (green solid) Schmittner et al, 2011, land-and-ocean; (green dashed) (Schmittner et al., 2011),land-only; and dash dotted, ocean-only; (purple dashed) Annan LGM, 2005. Combination of evidence: (yellow) (Libardoni and Forest, 2011) using different datasets, cyan (Olsen et al.,) compared to (red) (Annan and Hargreaves, 2006) and orange, Hegerl et al., 2006.

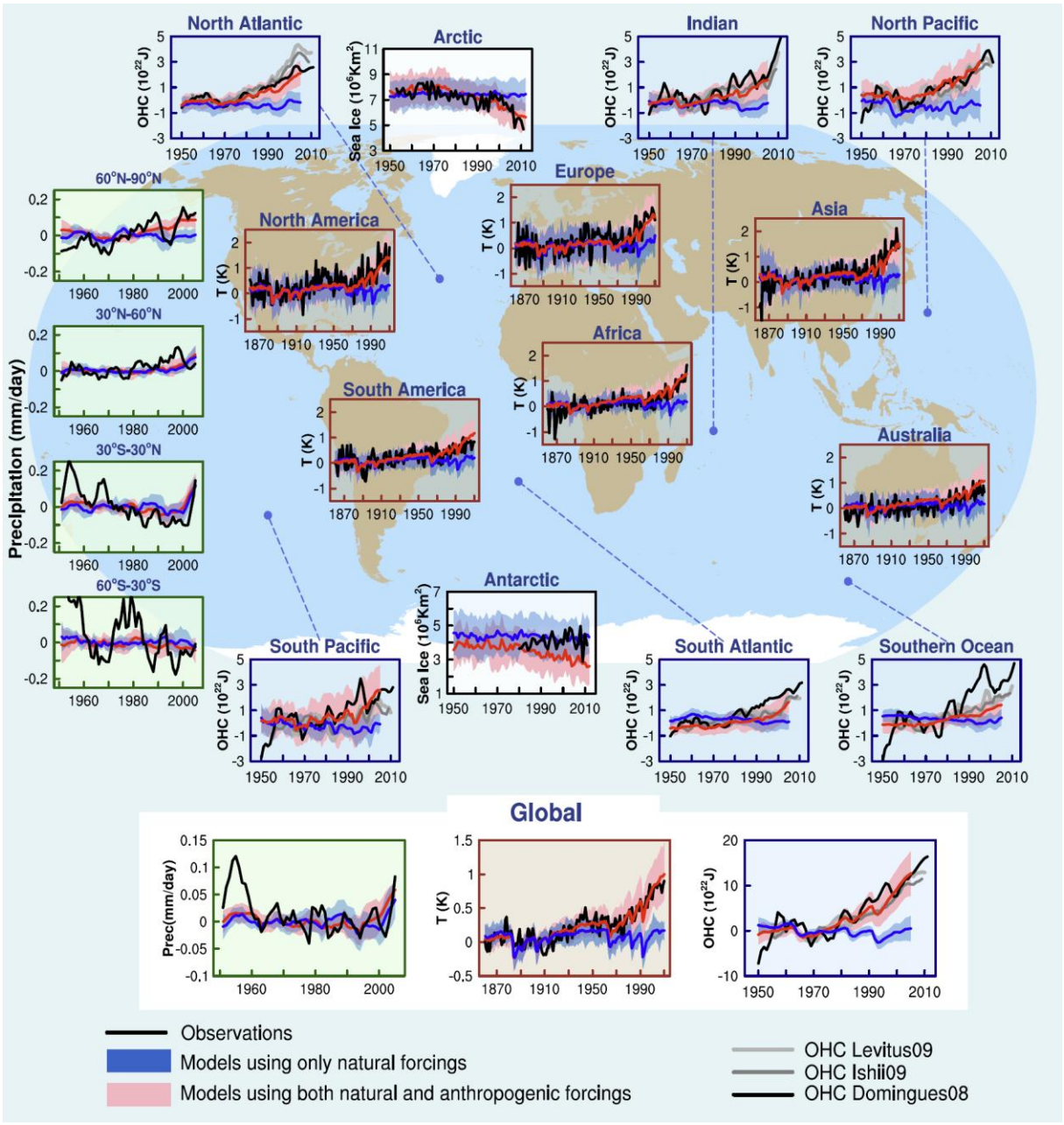

Figure 10.20: Detection and attribution signals in some elements of the climate system. Brown panels are land surface temperature time series, green panels are precipitation time series, blue panels are ocean heat content time series, and white panels are sea-ice time series. On each panel is observations (shown in black or black and shades of grey as in ocean heat content). Blue shading is the model time series for natural forcing simulations and red shading is the natural and anthropogenic forcings. The dark blue and dark red lines are the ensemble means from simulations. For surface temperature the 5 to 95% interval is plotted and is based on the Jones et al. (2012) (and Figure 10.1). The observed surface temperature is from HadCRUT4. For precipitation data the mean and one standard deviation shading of the simulations is plotted. Observed precipitation is from Zhang et al. (2007c). For Ocean Heat Content the mean and one standard deviation shading is plotted for an ensemble of CMIP5 models. Three observed records of OHC are shown. The sea ice extents simulations and observations are the same as in Figure 10.15. More details are in the Supplementary Material (Appendix 10.A).

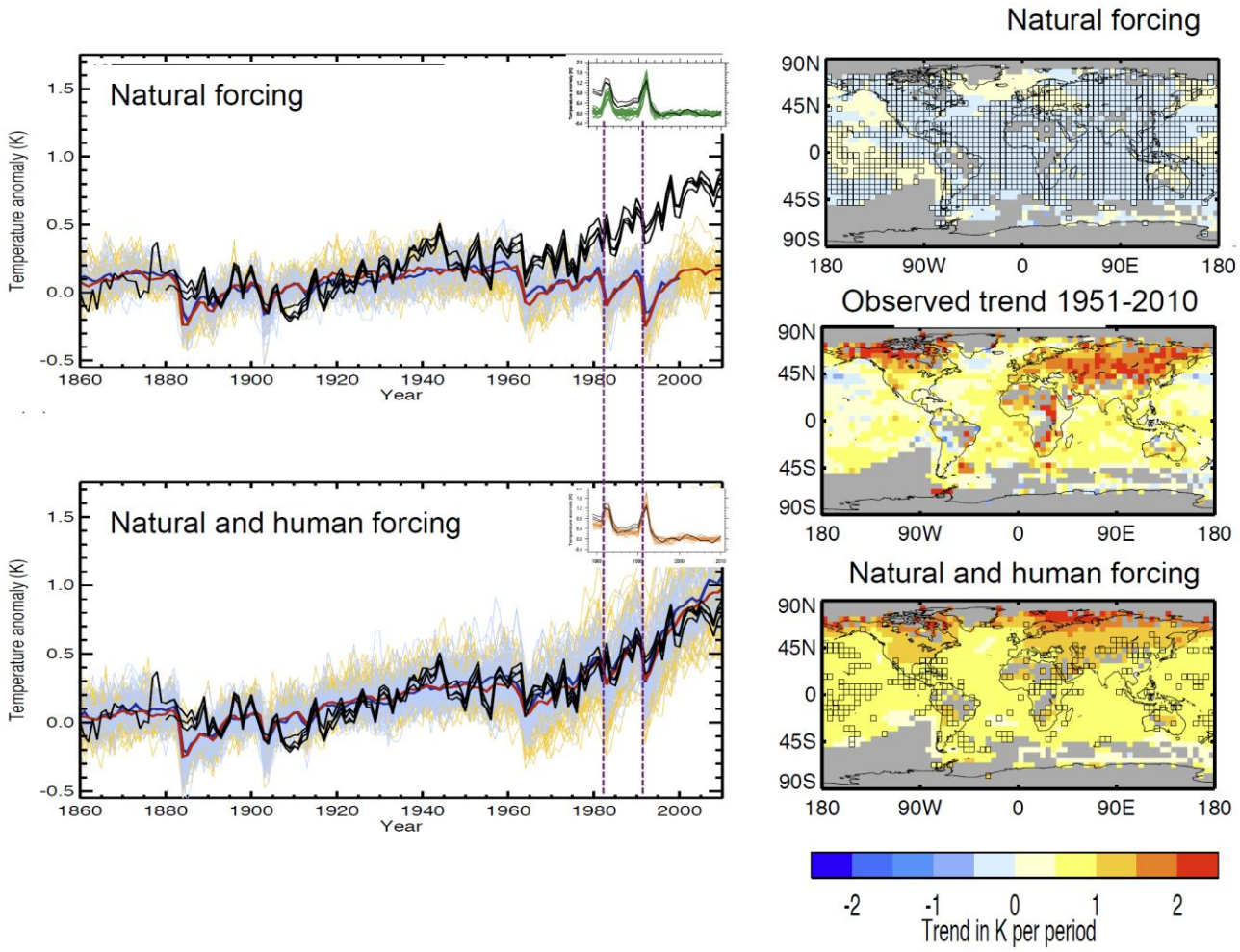

FAQ 10.1, Figure 1: Left: Time series of global and annual-average surface temperature change from 1860 to 2010. The top panel shows results from two ensemble of climate models driven with just natural forcings, shown as blue and yellow lines. The lower panel shows simulations by the same models, but driven with both natural forcing and human-induced changes in greenhouse gases and aerosols. The black lines in each panel show different estimates of global and annual-averaged observed temperature change. Small inset panels show global stratospheric temperature time series from 1981–2010. Observations are shown as black lines; green lines in the upper inset panel show simulations driven by natural forcing only, and orange lines in the lower inset panel show simulations driven by natural+human forcings. Vertical dashed lines denote major volcanic eruptions in 1982 and 1992. Right: Spatial patterns of local surface temperature trends from 1951–2010. The upper panel shows the pattern of trends from a large ensemble of simulations driven with just natural forcings. The bottom panel shows trends from a corresponding ensemble driven with natural+human forcings. The middle panel shows the pattern of observed trends during this period.

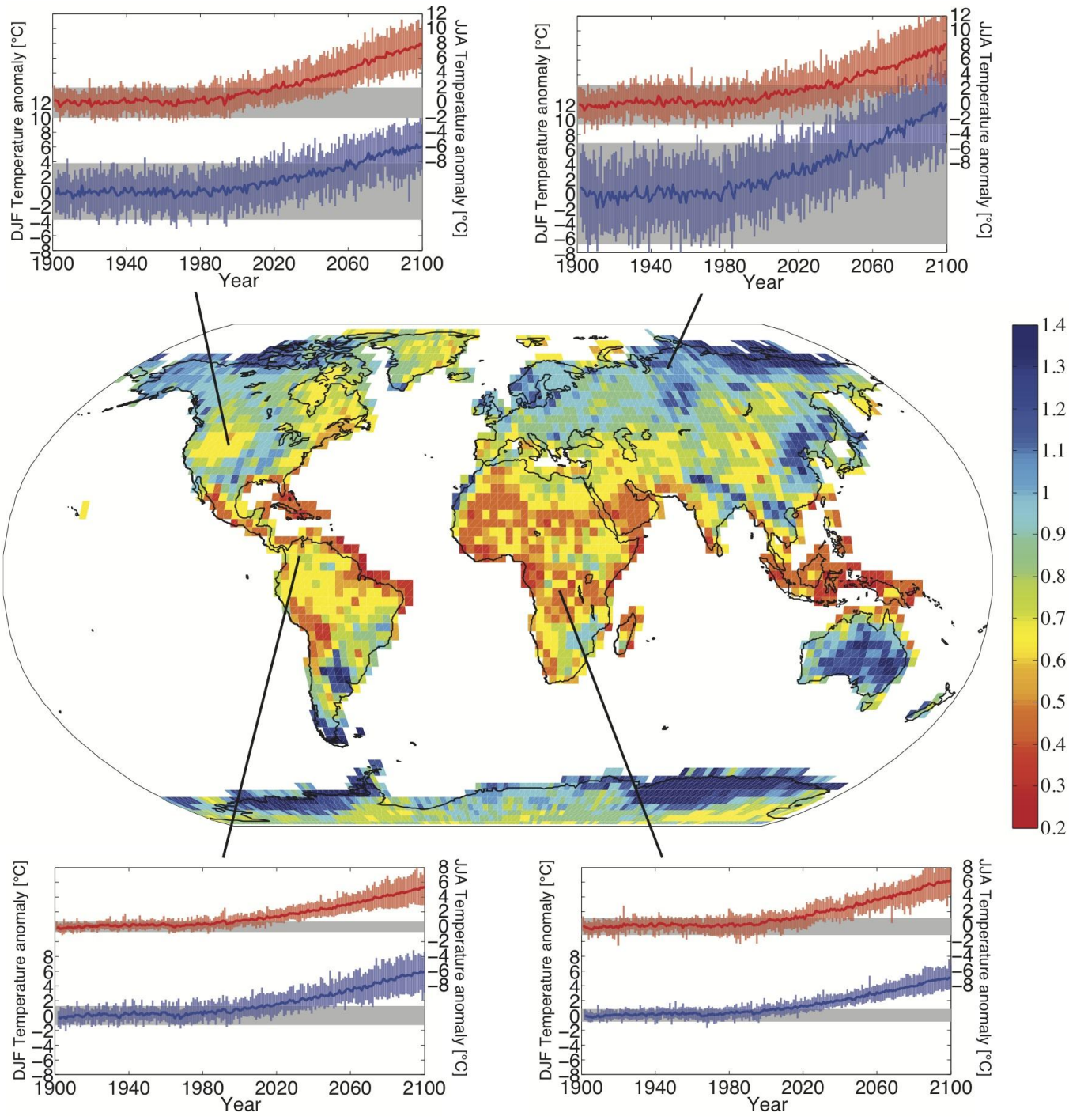

FAQ 10.2, Figure 1: Time series of projected temperature change shown at four representative locations for summer (red) and winter (blue). Each time series is surrounded by an envelope of projected changes (pink for summer, blue for winter) yielded by 24 different model simulations, emerging from a gray envelope of natural local variability simulated by the models using early 20th century conditions. The warming signal emerges first in the tropics during summer. The central map shows the global temperature increase (°C) needed for a temperatures in summer at individual locations to emerge from the envelope of early 20th century variability. All calculations are based on CMIP5 global climate model simulations forced by the RCP8.5 emissions scenario. Envelopes of projected change and natural variability are defined as ±2 standard deviations. Adapted and updated from Mahlstein et al. (2011).